UNIVERSITÉ de HAUTE ALSACE

P H D T H E S I S

to obtain the title of

PhD of Science

of the Université de Haute-Alsace

Speciality : Control theory

Defended by

Gaétan Pouly

Analysis and synthesis of advanced control laws for vehicle ground guidance.

Thesis Advisors: Jean-Philippe Lauffenburger and Michel Basset

prepared at the Laboratoire MIPS équipe MIAM defended on December 11th, 2009

Jury :

Reviewers :	J. Bokor	-	Budapest University (Hungary)
	S.Mammar	-	Université d'Evry Val-d'Essonne
Examinators :	Y. Chamaillard	-	Université d'Orleans
	O. Sename	-	Institut National Polytechnique de Grenoble
Invited :	J.-P. Garcia	-	Messier-Bugatti
Advisors :	M. Basset	-	Université de Haute-Alsace
	J.-P. Lauffenburger	-	Université de Haute-Alsace

À mon père.

Notations

The following table describes the different mathematical notations used in this manuscript.

Mathematic notations	**Description of the mathematics notations**
$\mathbb{C}$	Complex values set
$\mathbb{R}$	Real values set
A^*	Transpose conjugate of $A \in \mathbb{C}$
A^T	Transpose of $A \in \mathbb{R}$
λ	Eigenvalues
σ	Singular values
σ^H	Hankel singular values
$\Re$	Real part
$\Im$	Imaginary part

Table 1: Notations for the mathematical tools

The following table describes the different acronyms used in this manuscript.

Acronym	Description of the acronym
A/C	Aircraft
ACC	Adaptive Cruise Control
ADAS	Advanced Driver Assistance Systems
ADASRP	Advanced Driver Assistance Systems Research Platform
ANN	Artificial Neural Network
B&B	Branch and Bound
BS	Braking System
CAN	Controller Area Network
CC	Cruise Control
CG	Centre of Gravity
DC	Direct Current
DGPS	Differential Global Positioning System
FC	Follow the Carrot
FSM	Finite State Machine
GA	Genetic Algorithm
GPS	Global Positioning System
HIFOO	$\mathcal{H}_\infty$ Fixed-Order Optimization
I/O	Input/Output
ITS	Intelligent Transportation Systems
LoLG	Lateral or Longitudinal guidance
LaLG	Lateral and Longitudinal guidance
LAD	Look Ahead Distance
LFT	Linear Fractional Transformation
LTI	Linear Time Invariant
LPV	Linear Parameter Variant
LTV	Linear Time Variant
MIMO	Multi-Input/Multi-Output
MLD	Mixed Logical Dynamical
MOR	Model Order Reduction
MPC	Model Predictive Control
NLG	Nose Landing Gear
MLG	Main Landing Gear
NMPC	Non-linear Model Predictive Control
NN	Neural Network
NNMPC	Neural Network Model Predictive Control
ODE	Ordinary Differential Equations
PID	Proportional Integral Derivative

Acronym	Description of the acronym
PWA	Piecewise Affine
QP	Quadratic Programming
RMS	Root Mean Square
SDP	Semi Definite Programming
SISO	Single Input single Output
SPR	Strictly Positive Real
W/R	Wheel/Road

Table 2: Notations for the acronyms

The following table describes the different parameters used in this manuscript.

Notation	**Definition**	**Unit**
F	force	$[N]$
M	moment	$[N.m]$
θ_t	turning tube angle	$[rad]$
θ_w	wheel angle around the vertical axis	$[rad]$
$\dot{\theta}_w$	wheel speed around the vertical axis	$[rad.s^{-1}]$
θ_m	motor angle	$[rad]$
J_1	turning tube inertia	$[kg.m^2]$
J_2	sliding tube inertia	$[kg.m^2]$
J_{total}	sum of J_1 and J_2	$[kg.m^2]$
J_m	motor inertia	$[kg.m^2]$
T_r	resistive torque at the W/R interface	$[N.m]$
T_{leg}	torque at the leg level	$[N.m]$
T_{em}	electromechanical torque	$[N.m]$
N_c	first reduction ratio	[]
N_w	second reduction ratio	[]
K	actuator stiffness	$[N.rad^{-1}]$
e	caster length	$[m]$
V_x	longitudinal speed	$[m.s^{-1}]$
F_z	vertical load	$[N]$
β_{NW}	nose wheel tyre slip angle	$[rad]$
F_y	lateral force	$[N]$
M_z	self-aligning torque	$[N.m]$
k	stiffness	$[N.rad^{-1}]$
c	damping coefficient	$[N.rad^{-1}.s]$
V_y	lateral speed	$[m.s^{-1}]$
r	yaw rate	$[rad.s^{-1}]$
ψ	yaw angle	$[rad]$
L_{NW}	distance between the NLG and the CG	$[m]$
L_{MW}	distance between the MLG and the CG	$[m]$
γ_L	longitudinal acceleration	$[m.s^{-2}]$
γ_T	lateral accleration	$[m.s^{-2}]$

Table 3: Different used parameters

Introduction

Context of the work

Despite a slight decrease in air traffic during the last 10 months, mainly due to the global economic crisis, the number of passengers aboard aircraft is still enormous. Indeed, the aircraft has carried more than 2.4 billion of passengers in 2008, according to the International Air Transport Association (IATA). Moreover, according to the European Organisation for the Safety of Air Navigation (Eurocontrol), nearly 280,000 aircraft have departed from the Charles-De-Gaulle airport in Paris, during the year 2008. This figure corresponds to approximately one take off every two minutes. Also according to the IATA, a forecast of 2.75 billion of air passengers is planned for 2011, which corresponds to a rise of 29% compared with 2006. Due to this rapid increase in global air traffic, several issues must be raised [1] :

- **reducing the environmental impact of aviation:**
  Air transport has an impact on the environment, insofar as aviation produces around 2% of the world's manmade emissions of carbon dioxide (CO_2), according to the United Nations Intergovernmental Panel on Climate Change (IPCC). Moreover, 80 % of aviation's greenhouse gas emissions are related to passenger flights exceeding 1,500 km, for which there is no transportation alternative, according to Pulles J.W. et al[2]. To address these environmental problems, funding are made available for different research and development projects (Clean Sky[3] or SESAR[4] (Single European Sky Air Traffic Management Research)). Likewise, airliners contribute to limite the climate changes. For instance, Air France opts for lighter cabin equipment, rolley weight diminishes of 6kg, glass tray weight diminishes of 500g and drawer weight diminishes of 300g; allowing a CO_2 reduction emission of 19400 tons per year.

- **increasing the satisfaction of the aircraft passengers:**
  Outside the cost of aircraft tickets which is very important for the passengers, the satisfaction of these latter is likewise due to the minimization of the travel time. Ground traffic management, that means taxi time and ground waiting time must be improved. Moreover, important efforts are made to minimize flight delays. For example, low visibility conditions prevent the aircraft from moving freely on the runway and engender important delays. For

[1] These three items do not constitue an exhaustive descritpion of the problems encountered in the field of aeronautics. Moreover, no link can be made between the order of different items and the importance of them.

[2] AERO modelling system, Pulles J.W. et al., 2004

[3] www.cleansky.eu

[4] www.sesarju.eu

instance, according to Eurocontrol, in 2008, at the London Heathrow airport, 28 % of the delays were caused by bad weather.

- **minimising the cost for the airliners:**
  Different solutions are contemplated to minimize the cost for the airliners and for instance the fuel costs. In this way, energy efficiency of air operations has improved by 20% for 10 years, according to the IATA. Moreover, benefits can be done by limiting the turn-around time, that means the time needed to complete turn-around operation at the airport (refuelling, baggage handling, boarding and deplanning of passengers, etc). In this area, Airbus[5] works hardly on galley configuration (that means the kitchenette arrangement) or the Embraer 170/190 family jets[6] includes two main passenger entrances, resulting on a minimization of aircraft turn-around time. This latter could be improved as well, by favorising easier maintenance operations of the different onboard systems.

Faced with these problems, the Distributed and Redundant Electro-mechanical Nose Gear Steering System (DRESS) European project seeks to contribute to improved aircraft.

The DRESS European project and the "more electric" aircraft

The DRESS FP6 STREP European project, which brings together a total of 13 European actors of the aeronautic industry (Messier-Bugatti, Messier-Dowty, Airbus UK, SAAB, etc) and of academic research area (University de Haute-Alsace, INSA Toulouse, Budapest University of Technology and Economics etc), provides solutions for the development of a more electric aircraft.

Indeed, since the beginning of the aviation history, electric power is increasingly present in systems. Gradually, the different stages that lead to the "more electric" aircraft have been passed through. In the fifties, due to the increase of the electric power demand, the aircraft available voltage has evolved from 28V DC to 115V AC. In the eighties, with the advent of the Airbus A320, the aircraft electric flight control system appeared. The emergence of faster digital processors helps to develop controlled systems which are designed to directly drive the movement of the aircraft according to the different flight conditions. The action of the pilot on the tiller[7] does not act directly on the rudders[8] and ailerons[9]. Recently, on the Airbus A380, more and more electro hydrostatic actuators replace electro-hydraulic servo control systems.

In the following years, many electrical systems that are currently in the research area will appear. Among the various electrical systems that will be integrated on aircraft, we can mention the electrical braking system, the engine starter and the more interesting in the frame of this thesis, the electromechanical actuator of the nose landing gear. Considering the electrical braking system, the electronic control units and the electrical wiring replace the hydraulic lines and equipment and the braking torque resulting from the friction between the rotors and the stators

[5] www.airbus.com
[6] www.embraer.com
[7] A lever which gives the possibility to turn the rudder.
[8] A rudder is a control surface, attached to the upright tail of the A/C which allows the pilot to control the aircraft in the yaw axis.
[9] The ailerons are hinged control surfaces attached to the trailing edge of the wing of a fixed-wing aircraft and used to control the aircraft in roll.

of electrical motors, when they are subjected to a pressure produced by a set of motors and gears. When ice appears on the wings, it is especially dangerous during take-off, because a sheet of ice can reduce lift by more than 25%. Ice accumulation is a serious safety hazard for aircraft. Then, some deicing systems are proposed and old systems which employ the hot air from the engine could be replaced by electrical resistors glued to the wing surface. Finally, the steering of the aircraft which is actually based on an hydraulic actuator may be managed by an electromechanical one.

To conclude in this field, the future issue is to find a solution to meet the ever increasing demands of electrical energy. Several unanswered questions remain about the structure of new networks. What could be the solutions to produce and store the energy ? How will the power resources be managed ?

Scientific and technical objectives of the DRESS project

The goal of the DRESS project is to develop and validate a distributed and redundant electrical steering system for an aircraft landing gear, improving aircraft safety and competitiveness.

Currently, during the ground manoeuvres, the pilot controls the aircraft by orientating the nose landing gear wheel using a small control wheel (tiller), located on both side of the cockpit. The nose landing wheels are orientated by hydraulic actuators supplied by the aircraft hydraulic systems. Moreover, during automatic landing or automatic braking, the steering system is controlled by flight control computers which aim at keeping the aircraft on the runway centreline whatever the disturbances are (cross wind, asymmetric braking, deflated tyres, etc). Nevertheless, automated systems are limited and at the end of the runway, pilots have to regain the manual control of the aircraft insofar as no automatic ground guidance systems on taxiways exist today.

Thus, the DRESS European project focuses on three main objectives during the development of the new electromechanical steering actuator:

- **reducing the system weight at the aircraft level, by replacing the current hydraulic actuation by an electrical actuation:**
  As it is well-known, overall aircraft weight reduction is directly linked with the minimisation of the fuel consumption and the limitation of the impact of the aircraft on the environment. Thus, the proposed electro-mechanical actuator will help to achieve weight reduction insofar as the hydraulic components, such as valves, electrohydraulic servovalves, accumulators, swivel fittings, ... dedicated to the steering system will be removed on the nose landing gear.

- **improving aircraft safety by providing higher reliability and higher efficiency:**
  The electromechanical actuator is composed of two separated paths which could be potentially disengaged by the use of a clutch. Indeed, the two components work on the same time for normal cases, but when one path is defective, the system is always able to function for limited operation. Then, a modular architecture will improve safety and fault tolerance thanks to the digital bus reconfiguration capabilities. Finally, a greater efficiency is obtained with an electromechanical system than with an hydraulic one, better energy

management is also possible (if an actuator fails, switching to another actuator is easy) and the system is easier to maintain insofar as the monitoring of the electrical circuit is more reliable than finding a leak.

- **investigating the integration of the electrical actuator in a future fully automated aircraft ground guidance system:**

  The improvements in terms of safety will permit to integrate the electromechanical actuator in a fully automated guidance system. This will give the possibility to operate the airports in "all weather" conditions, corresponding to the Cat IIIC conditions[10], not currently authorized.

Finally, during the whole project, particular attention is focused on the modelling aspect, considering multi domain co-simulations at each level (mechanical, thermal, power electronics, system architecture, control laws, etc). Moreover, the last step is to build and assemble the complete electromechanical steering system and to integrate it on a nose landing gear to perform validation tests.

Contribution of the thesis

This thesis has been performed in the "Modélisation Intelligence Processus Systèmes" (MIPS) laboratoy, in the "Modélisation et Identification en Automatique et en Mécanique" (MIAM) team. During three years from September 2006 to September 2009, under the supervision of Jean-Philippe Lauffenburger (Assistant Professor) and Michel Basset (Professor) at the Université de Haute-Alsace, projects in aeronautical and automotive domains, concerning control laws development, have been performed.

In the aeronautical domain, control laws have been developed, in order to give the possibility to integrate the new electromechanical steering actuator on future aircraft.

- Solutions have been proposed to **control the actuator which steers the nose landing gear**. They help to **consider the non-linear behaviour of the system** by the **use of LPV gain scheduling techniques**. Particular **methodologies are proposed to enhance the controllers**, by considering the defined specifications and constraints. **Experimental results**, with the test bench developed in the frame of the DRESS project, help to validate the proposed solutions.

- An initiatory study has been performed, in simulation, concerning active shimmy damping (the damping of unstable oscillations which appear on the nose landing gear). Control solutions based on **fuzzy adaptive controllers**, developed in collaboration with Thai-Hoang Huynh from the Ho Chi Minh University, have shown that it was possible **to cancel these oscillations** using active solutions.

- **Automatic guidance algorithms** have been developed and tested **by simulation for A/C applications**. Then, they have been **validated through real tests in the automotive domain**. Indeed, similarities exist between aeronautic and automotive problematic. **Models used for these two systems are similar**. Thus, is possible **to transpose**

[10] defined by the International Civil Aviation Organization (ICAO)

algorithms from the aeronautic to the automotive fields and **to validate the proposed solutions through the available test vehicle**.

In the automotive domain, different control laws have been developed to favourite the development of automated vehicles. The proposed control solutions have been validated through experimental results with a passenger car, insofar as the possibilities to test the control algorithms on a real aircraft were very limited. The different objectives were to:

- **Improve car vehicle speed control:**
  In collaboration with other members of the laboratory, a new solution based on information provided by **a GPS system** helps to control the speed of the vehicle. The main contribution of this project was to define **an appropriate vehicle speed order**, taking account of **the road profile and the vehicle dynamics**. The control solution has been **implemented and validated on the test vehicle**.

- **Develop control strategies for lateral dynamics control:**
  Control solutions which permit **to follow a path** have been proposed. Based on **predictive control algorithms**, **non-linearities of the vehicle dynamics** are considered, contributing to the fully automated vehicle. The control solutions have been **implemented and validated on the test vehicle**.

Organization of the document

This thesis is divided in five chapters. If the two first chapters are dedicated to theoretical definitions, the three others present the context of the study and the different developments in aeronautical and automotive domains.

Chapter 1 presents the notions of systems and models. The attention is focused on the different possibilities to model a system (linear or non-linear model based on LTI, LTV, fuzzy or neural network formulations) and under what conditions each model is more appropriate. Then, after the modelling step, different solutions available in the literature that help to identify parameters of models are presented. Finally, tools to reduce the size of models (particularly the truncation methods) are studied.

Chapter 2 is dedicated to the presentation of different control solutions. Firstly, the robust $\mathcal{H}_\infty$ control theory is introduced. A dedicated section concentrates on the gain scheduling and particularly on the polytopic approaches. Secondly, adaptive control solutions based on fuzzy approximators are described. On the one hand, state feedback solutions based on direct and indirect approach are suggested. On the other hand , output feedback strategies are presented. Thirdly, the model predictive control strategy is detailed. This control solution is based on a problematic on-line optimization and solutions to cope with the use of non-linear prediction models are studied.

Chapter 3 has two main objectives. Primarily, the framework of the applications is presented: different control loops are described and the existing approaches are presented. Then, different models (aircraft model, nose landing gear model and shimmy model) which will be used for simulation purposes or controller synthesis are introduced.

Chapter 4 talks about the control of the DRESS electromechanical actuator developed in the frame of the European project. Firstly, the steering application based on a $\mathcal{H}_\infty$ gain scheduling approach is presented. The proposed control solutions are validated on the DRESS test bench. Secondly, active shimmy damping based on fuzzy adaptive solutions is detailed.

Chapter 5 is dedicated to applications developed in the automotive domain. Firstly, an open road speed assistant solution, based on navigation for the generation of a speed profile is presented. Secondly, different algorithms (Follow the carrot, LPV predictive control or neural predictive control), which give the possibility to develop road following applications are described. The different developed solutions are validated based on experimental tests made with the fully equipped vehicle, of the laboratory.

Publication list

International journal papers

1. G. Pouly, J.P. Lauffenburger, A. Birouche and M. Basset, "*Gain scheduling $\mathcal{H}_\infty$ controllers for Aircraft Nose Landing Gear steering using LPV techniques*", **IEEE Transactions on Control Systems Technology** (submitted, under review).

2. G. Pouly, T.-H. Huynh, J.-P. Lauffenburger and M. Basset, "*State feedback fuzzy adaptive control for active shimmy damping*", **European Journal of Control**, (submitted, under review).

International conference papers with proceedings

1. G. Pouly, J.-P. Lauffenburger, M. Basset and T. Wissart, "*Correlation between objective tire parameters and subjective test driver evaluation*", **5th IFAC Symposium on Advances in Automotive Control (AAC)**, Seascape resort, USA, August 20-22, 2006.

2. G. Pouly, T.-H. Huynh, J.-P. Lauffenburger and M. Basset, "*Indirect fuzzy adaptive control for active shimmy damping*", **17th IFAC World Congress**, Seoul, South Korea, July 6-11, 2008.

3. T.-H. Huynh, G. Pouly, J.-P. Lauffenburger and M. Basset, "*Active Shimmy Damping Using Direct Adaptive Fuzzy Control*", **17th IFAC World Congress**, Seoul, South Korea, July 6-11, 2008.

4. G. Pouly, J.-P. Lauffenburger, M. Basset and D. Ould Abdeslam "*Etude de robustesse d'une commande adaptative floue pour le contrôle de shimmy*", **5ème Conférence Internationale Francophone d'Automatique (CIFA)**, Bucarest, Roumania, September 3-5, 2008.

5. G. Pouly, T.-H. Huynh, J.-P. Lauffenburger and M. Basset, "*Active Shimmy Damping Using Fuzzy Adaptive Output Feedback Control*", **10th International Conference on Control, Automation, Robotics and Vision (ICARCV)**, Hanoi, Vietnam, December 17-20, 2008.

6. G. Pouly, J.-P. Lauffenburger and M. Basset, "*Reduced order $\mathcal{H}_\infty$ control design of a Nose Landing Gear steering system*", **12th IFAC Symposium on Control in Transportation Systems**, Redondo Beach, California, USA, September 2-4, 2009.

7. J. Daniel, G. Pouly, A. Birouche, J.-P. Lauffenburger and M. Basset, "*Navigation-based speed profile generation for an open road speed assistant*", **12th IFAC Symposium on Control in Transportation Systems**, Redondo Beach, California, USA, September 2-4, 2009.

Patents

1. G. Pouly, J.-P. Lauffenburger and M. Basset, "*Procédé de gestion de la commande d'orientation d'un atterrisseur d'aéronef*", Ref : 8F-2384 case 376 BP (submitted, under review)

Contents

Ce qui est affirmé sans preuve peut être nié sans preuve.

Euclide

Chapter 1

Which model for which system?

Contents

1.1 Introduction

As mentioned by the title of this chapter, the objective consists in trying to give an answer to the question "Which model for which system?". Section 1.2 will begin with a clarification about the vocabulary proposed in the previous question; the notions of system and model are

presented. This helps to express the link between these two notions and to clarify the modelling step. The different control solutions proposed in this manuscript deal with different formulations and types of models. Section 1.3 aims at giving an overview of the used notations. As soon as a model of the system is chosen, an important step introduced in Section 1.4 consists in identifying the parameters of the model. On the one hand, the general concept of model identification is introduced. On the other hand, the tools appropriated for the different model formulations are presented. Finally, Section C proposes some basic tools to reduce the complexity of models. Indeed, very complex models are sometimes obtained and the reduction of their orders is required to facilitate their use.

1.2 Relation between system and model

1.2.1 Definition of a system

A *system* ($\mathcal{S}$) is an object that is activated by different stimuli. These stimuli act on the various states that constitute the object and engender its reaction. The stimuli are partitioned in two different kinds of signals. The first one are the inputs named u; these external signals are generally manipulated by an operator. The others are the perturbations and are divided into two categories: the measured disturbances w and the unknown disturbances v. The reaction of the object is characterized by the output signals y that depend on the initial situation of the system and the different stimuli applied to it. Figure 1.1 presents these notions. Despite the nature of the chosen model, the identification step is required and Section 1.4 presents the needed steps which help to estimate the parameters of the model.

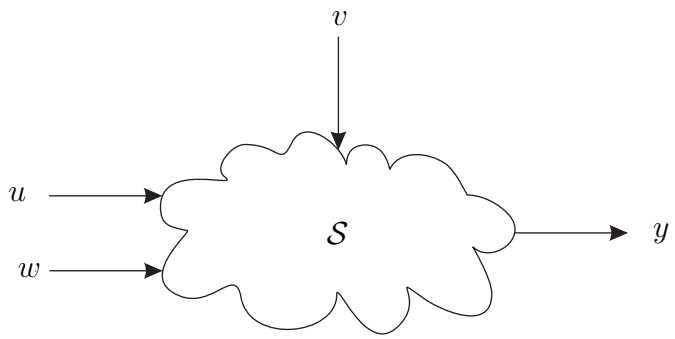

Figure 1.1: Description of the system

In the nature, many systems surround us. Among these various systems and considering the subject of this study, the "vehicle" is a well used system that involves several domains and gives the possibility to clarify the notions introduced before. This mixed-domain system is composed of mechanical variables (the wheel speed, the steering wheel angle, ...), electrical variables (the electricity produced at the spark plug level) or thermal variables (the pressure and the temperature of the air fuel mixture in the combustion chamber, ...). The driver acts on the system using different inputs (the steering-wheel, the acceleration pedal, ...) and the vehicle moves following the desired trajectory with the expected speed. When the pilot drives its vehicle, he is able to status on the tyre-ground interface. For example, ice on road can be visually detected by an expert or an inexperienced driver who will adapt his driving to prevent

from an eventual slide of the vehicle. As a consequence, the tyre-ground interface acts as an external event that can be detected and understood by the driver: it is a measured disturbance. The system is, as well, affected by the wind, which can induce dangerous situation when the driver has to counteract with the hand-wheel if the vehicle has to go in a straight line. The wind is only be observed through its influence on the vehicle direction, so it acts as unknown disturbance.

1.2.2 Definition of a model

A *model* ($\mathcal{M}$) is a formalism used to grasp a system. It can be defined as a representation of the system that helps to define some concepts concerning the relation between the various variables of the system. Similarly to the system, different kind of signals permit to activate the model: the inputs u and the measured disturbances w, while the response of the model is characterized by its outputs y. Figure 1.2 presents the different components of the model.

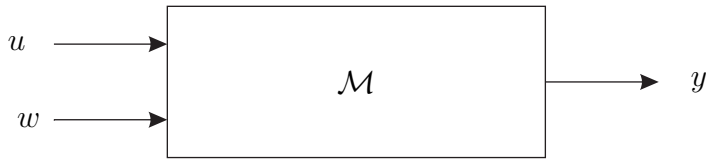

Figure 1.2: Description of a model

The term model is very large. Indeed, different points of view are available in the literature [Ljung, 1999]:

- mental model: a basic and daily life representation of a system;
- graphical model: a representation that uses numerical tables and plots;
- mathematical model: a description of the relation between the different variables of the system. The relations are expressed in terms of mathematical expressions such as differential equations.

The mathematical models are the principal representation used in the field of control theory and for this reason, our attention is focused here on such a representation. A model can be of different type or nature: it can be discrete-time or continuous-time, linear or non-linear, ...

1.2.3 Choice of a model structure: the modelling step

The notions of system ($\mathcal{S}$) and model ($\mathcal{M}$), are linked together [Pronzato, 2005]. The characteristics of the model clearly depend on the considered system. The first question to be answered during the modelling of a system is the selection of the mathematical model type (see Section 1.3.1). For example, it seems natural to describe a system that includes a lot of non-linearities by using a model structure that incorporates these non-linearities. Moreover, the conditions in which the model will evolve or its expected performances will define its level of description. For example, in the automotive domain, if an application of road following in conventional driving conditions is developed, the vehicle and particularly the tyre can be described by a linear model

[Cole et al., 2006]. Nevertheless, an application that aims at performing a double lane change at high speed has to consider different dynamics. In this case, an improved vehicle model that notably includes tyre non-linearities must be considered [Falcone et al., 2007b]. Generally, the complexity of the model depends on the application and the system to be described. A trade-off between simplicity and accuracy must be performed. Then, if the parameters of the model are not known, their identification is required. Finally, based on the available data and considering the identified model, it is important to consider the validity conditions of the model: how reliable is the obtained model with respect to the goal to be achieved?

The next section of this chapter will introduce definitions required in this manuscript. The identification procedure that permits to obtain the model parameters will be discussed. The MOR methods, required to reduce the order of the model, are finally presented. Considering our project, Chapter 5 will present the identification results of a vehicle model. It will be shown that based on the identification tools presented in this chapter, two models will be proposed. In the following, Chapter 4 which notably considers the control of the Nose Landing Gear (NLG) based on $\mathcal{H}_\infty$ theory, will use the notion of model reduction to obtain low order controllers.

1.3 Solutions to model a system

1.3.1 Types of the model

There are three main types of model that characterize the knowledge of a system:

- a black box model;
- a white box model;
- a grey box model.

A black box model is viewed in term of its input/output relationship considering that the knowledge of its internal working is not taken into account. These types of models are obtained by experimental measurements of the inputs and outputs and give the possibility to reproduce a behaviour that has been learned. They consider that an *a priori* knowledge of the system is not required and they are especially useful for control purposes. They give the possibility to obtain models with very simple structure which is an advantage for real time implementation. However, this simplicity makes that these models are not flexible, if a slightly difference has to be introduced in the model, an important work could be necessary to calibrate the new model. These types of models are not suitable to help the comprehension of the system insofar as they do not have physical meanings. For example, artificial neural networks (ANN) are one of the well-known black box models.

A white box model is characterized by the use of physical laws to describe the behaviour of the system it represents. Indeed, based on an *a priori* knowledge of the system, a set of equations is obtained. These types of models are based on physical parameters such as masses, stiffnesses, ... and help to obtain detailed and realistic models. The introduction of these physical parameters is a real advantage when flexible models are required: changing the value of one parameter can lead to another physical model. However, this accuracy and this flexibility

introduce two important drawbacks: these types of models introduce a higher complexity level and are computer demanding.

A grey box model is an hybridation of white and black box models. Grey models are based on a compromise between the introduction of physical expressions when an *a priori* knowledge is available and experimental measurements. Based on the hybridation, they can get advantages of both black and white models. The compromise helps to have a physical and flexible representation that can keep a simple structure and permits real-time implementation.

As a conclusion, the choice of the model type depends on the aim of this model, on the cost to obtain the model and the data available for its identification. Most of the time, the grey box models are chosen, insofar as they keep the advantages of the two other types.

The reader can find more details about the types of models and their uses in [Ljung, 1999], [Richalet, 1991] and [Schmitt, 1999].

1.3.2 State Space formulation

1.3.2.1 Linear model

The modelling of a system using a Linear Time Invariant (LTI) representation is the first and commonly used representation in the control engineering domain. The system is described by linear equations which are generally composed of a set of Ordinary Differential Equations (ODE). For a non-linear model, these equations can be obtained after the linearisation of the non-linear system behaviour around a local point. This approach helps to obtain a model that is validated around an operating point.

Definition 1 *Linear Time Invariant (LTI) model*

Considering the matrices $A \in \mathbb{R}^{n \times n}$ (the dynamic matrix), $B \in \mathbb{R}^{n \times n_u}$ (the control matrix), $C \in \mathbb{R}^{n_y \times n}$ (the output matrix) and $D \in \mathbb{R}^{n_y \times n_u}$ (the input/output matrix), a system can be described by a Linear Time Invariant (LTI) model $\mathcal{M}_{LTI}$ such that:

$$\mathcal{M}_{LTI} : \begin{cases} \dot{x}(t) &= A\,x(t) + B\,u(t), \\ y(t) &= C\,x(t) + D\,u(t), \end{cases} \tag{1.1}$$

where $x(t) \in \mathbb{R}^n$, $u(t) \in \mathbb{R}^{n_u}$ and $y(t) \in \mathbb{R}^{n_y}$ are respectively the state vector, the input vector and the output vector of the model.

Comment: The matrices A, B, C, D constitute a particular realization of the state space model. It is obvious that this realization is not unique. Among the various possible realizations, there is a special interest in the minimal realization (computationally less demanding and easy to use realization). Similarly, it exists different minimal realizations. These latter have the particularity to be realizations with the smallest dimension of the dynamic matrix A. In the case of minimal realizations, the dimension of the matrix A which indicates the "complexity" of the state space model, is commonly named the McMillan degree of the state space model. The methods which help to obtain the minimal realizations are proposed in [Gilbert, 1963] and [Kalman, 1963].

1.3.2.2 Structural properties of the linear state space model

This section gives some definitions linked to the state space model.

Firstly, the properties of observability, controllability, detectability and stabilizability are introduced. These notions are well-known properties which are primordial when a control solution or an observer have to be synthesized. For example, as it could be read in Section 2.2, in the frame of $\mathcal{H}_\infty$ control theory, the algorithm which helps to synthesize the controller needs some hypothesis. Indeed, when the system is stabilizable and detectable, the algorithm could find a solution.

Secondly, the definition of the singular values is proposed. This is required for the MOR tools. As it is detailed in Section C.2, Hankel singular values help to define the balanced realization which is recognized for its good numerical properties.

Thirdly, the norm of signals and models are given. These definitions are required for two main purposes. On the one hand, in the frame of MOR, the $\|\|\|_\infty$ norm is used to compare the initial model and the reduced model. On the other hand, when robust controllers are developed, the aim of the optimisation algorithm is to minimize the $\|\|\|_\infty$ norm of a closed-loop transfer function. Finally, the notion of Lyapunov stability is briefly reminded. This notion is primordial insofar as stability is the first required property of a closed loop system.

Controllability and observability

This paragraph presents the properties of observability and controllability of linear state space models. These concepts respectively deal with the possibility to reconstruct the state from inputs and outputs and the possibility to influence the state by manipulating the inputs. They are commonly used to characterize the stability of closed-loop systems (see for example the requirements for obtaining an $\mathcal{H}_\infty$ controller in Section 2.2).

The observability matrix $\mathcal{O}$ and the controllability matrix $\mathcal{C}$ are defined by:

Definition 2 *Observability matrix*

The observability matrix is $\mathcal{O} = \begin{bmatrix} C \\ CA \\ \cdots \\ CA^{n-1} \end{bmatrix}$

Definition 3 *Controllability matrix*

The controllability matrix is $\mathcal{C} = \begin{bmatrix} B & AB & \cdots & A^{n-1}B \end{bmatrix}$

The observability gramian W_o and the controllability gramian W_c are defined by:

Definition 4 *Observability gramian*

$W_o = \int_0^\infty e^{At} C C^T e^{A^T t} dt$ *is the solution of the Lyapunov equation:*

$$AW_o + W_o^T = -CC^T \tag{1.2}$$

Definition 5 *Controllability gramian*

$W_c = \int_0^\infty e^{At} B B^T e^{A^T t} dt$ *is the solution of the Lyapunov equation:*

$$AW_c + W_c^T = -BB^T \tag{1.3}$$

Generally, the Kalman criteria are used to define the notions of observability and controllability [Kalman and Bucy, 1961].

Definition 6 *Kalman observability*

Considering the matrices (A,B,C,D) that describe the system by using a LTI representation, the model is observable if and only if $rank(\mathcal{O}) = rank\left(\begin{bmatrix} C \\ CA \\ \cdots \\ CA^{n-1} \end{bmatrix}\right) = n$ *with n the dimension of the state vector x.*

Definition 7 *Kalman controllability*

Considering the matrices (A,B,C,D) that describe the system by using a LTI representation, the model is controllable if and only if $rank(\mathcal{C}) = rank\left(\begin{bmatrix} B & AB & \cdots & A^{n-1}B \end{bmatrix}\right) = n$ *with n the dimension of the state vector x.*

Moreover, it is important to distinguish the states, modes or dynamics which are not observable or controllable. Then, an alternative characterisation, which is sometimes called Popov-Belevitch-Hautus (PBH) test, presents an equivalent condition in terms of the eigenmodes of the model [Robert and Douglas, 2007]. This characterisation gives the possibility to define the notions of stabilizability which consider the asymptotic stability of uncontrollable and unobservable models.

The representation of the system $\mathcal{S}$ by the model $\mathcal{M}$ is observable if the state vector can be reconstructed from the inputs and outputs.

Definition 8 *Observability*

Considering the matrices (A,B,C,D) that describe the system by using a LTI representation and λ *the eigenvalues of A, the model is observable if* $rank\left(\begin{bmatrix} A - \lambda I \\ C \end{bmatrix}\right) = n, \forall \lambda \in \mathbb{C}$ *with I the identity matrix in appropriate dimension and n the system order.*

The representation of the system $\mathcal{S}$ by the model $\mathcal{M}$ is detectable if the unobservable states are stable.

Definition 9 *Detectability*

Considering the matrices (A,B,C,D) that describe the system by using a LTI representation and λ *the eigenvalues of A, the model is detectable if* $rank\left(\begin{bmatrix} A - \lambda I \\ C \end{bmatrix}\right) = n, \forall \lambda \in \mathbb{C} : \Re[\lambda] \geq 0$ *with I the identity matrix in appropriate dimension and n the system order.*

The representation of the system $\mathcal{S}$ by the model $\mathcal{M}$ is controllable if, starting from an arbitrary initial state x_0, any other state x_i can be reached in finite time by choosing an appropriate input sequence.

Definition 10 *Controllability*

Considering the matrices (A,B,C,D) that describe the system by using a LTI representation and λ *the eigenvalues of A, the model is controllable if* $rank\left([A - \lambda I, B]\right) = n, \forall \lambda \in \mathbb{C}$ *with I the identity matrix in appropriate dimension and n the system order.*

The representation of the system $\mathcal{S}$ by the model $\mathcal{M}$ is stabilizable if the uncontrollable states are stable.

Definition 11 *Stabilizability*

Considering the matrices (A,B,C,D) that describe the system by using a LTI representation and λ the eigenvalues of A, the model is stabilizable if $rank\,([A-\lambda I, B]) = n, \forall \lambda \in \mathbb{C} : \Re[\lambda] \geq 0$ *with I the identity matrix in appropriate dimension and n the system order.*

Singular values

In the field of MOR and when the norm of models are used (for example in $\mathcal{H}_\infty$ control theory), the notions of singular values and Hankel singular values are required.

Definition 12 *Singular values*

Considering the matrix $M \in \mathbb{R}^{m\times n}$, there are unitary matrices

$$U = [u_1, u_2, \cdots, u_m] \in \mathbb{R}^{m\times m} \tag{1.4}$$

$$V = [v_1, v_2, \cdots, v_n] \in \mathbb{R}^{n\times n} \tag{1.5}$$

such that,

$$M = U\Sigma V^T \tag{1.6}$$

where,

$$\begin{gathered} \Sigma = \begin{bmatrix} \Sigma_1 & 0 \\ 0 & 0 \end{bmatrix} \\ \Sigma_1 = diag(\sigma_1, \cdots, \sigma_p) \\ \sigma_1 \geq \sigma_2 \geq \cdots \geq \sigma_p \geq 0,\ p = min(m,n) \end{gathered} \tag{1.7}$$

$(\sigma_1, \cdots, \sigma_p)$ are called the singular values of M.

Definition 13 *Hankel singular values*

The Hankel singular values $(\sigma_1^H, \cdots, \sigma_p^H)$ are calculated as the square roots of the eigenvalues $(\lambda_1, \cdots, \lambda_p)$ for the product of the observability gramian W_o and the controllability gramian W_c, then

$$\sigma_i^H = \sqrt{\lambda_i(W_c W_o)} \tag{1.8}$$

Norm of the model

Definition 14 $\mathcal{H}_2$ *norm*

The norm $\mathcal{L}_2$ of a signal $x(t)$ which characterize its energy is defined by:

$$\|x(t))\|_2 = \sqrt{\int_0^{+\infty} x(t)^T x(t) dt} \tag{1.9}$$

Definition 15 $\mathcal{H}_\infty$ *norm*

The $\mathcal{H}_\infty$ norm of a LTI model characterized by its transfer function $G(jw)$ (if $G(s)$ is analytically in $\mathbb{C}$), its input $u(t)$ and its output $y(t)$ is defined by:

$$\|G(jw)\|_\infty = \sup_{u(t)} \frac{\|y\|_2}{\|u\|_2} = \sup_{w\in\mathbb{R}} \overline{\sigma}\left(G(jw)\right) \tag{1.10}$$

with u is square-integrable.

Commentary This norm is mainly used to define controllers in the case of robust $\mathcal{H}_\infty$ control theory and it helps to compare model in the field of MOR.

For SISO models, it represents the maximal peak value on the Bode magnitude plot of $G(jw)$.

Lyapunov stability

An informal definition of stability considers that an equilibrium state is stable if, whenever the initial state is near this equilibrium state, the state remains near or perhaps tends to the equilibrium state. The notion of stability and particularly the Lyapunov stability is described by the following definition:

Definition 16 *Lyapunov stability*

Considering the matrices (A,B,C,D) that describe the system by using a LTI representation the model is stable in the sense of Lyapunov if and only if the eigenvalues of A have strictly negative real parts.

1.3.2.3 Linear Varying model

LTI models considers that the parameters are invariant. However, these parameters can change according to a trajectory and the LTI model becomes a Linear Varying model. Linear Varying models can be viewed as a combination of LTI models where a linear structure is maintained. This structure permits to obtain a non-linear behaviour keeping a linear structure. In order to take into consideration these parameter non-linearities, different modellings are given in the literature [Biannic, 1996]:

- Linear Time Varying (LTV) models are defined by the time-dependence of the state-space matrices. The dependencies are known a priori. For example, an electrical thermal model may be characterized by a LTV model where the resistance depends on time $R(t)$.
- Linear Parameter Varying (LPV) models are defined by state-space matrices that are dependent on a set of varying parameters. The variations of the parameters depend only on time. For example, a longitudinal speed dependent bicycle model is a LPV model, because the matrices depends on the longitudinal speed V_x.
- Quasi Linear Parameter Varying (q-LPV) models are defined by state-space matrices that are dependent on a set of varying parameters. The variations of the parameters depend on both the time and the measured outputs of the system. For instance, a simple spring/mass system may be modelled by a q-LPV model considering that the spring stiffness depends on the deflection.

These three types of models which permit to describe the NLG dynamics or the vehicles dynamics are defined afterwards.

Definition 17 *Linear Time Varying (LTV) model*

Considering the matrices $A(t) \in \mathbb{R}^{n\times n}$, $B(t) \in \mathbb{R}^{n\times n_u}$, $C(t) \in \mathbb{R}^{n_y\times n}$, $D(t) \in \mathbb{R}^{n_y\times n_u}$, *the system can be described by the Linear Time Varying (LTV) model* $\mathcal{M}_{LTV}$ *such that:*

$$\mathcal{M}_{LTV} : \left\{ \begin{array}{rcl} \dot{x}(t) & = & A(t)\, x(t) + B(t)\, u(t), \\ y(t) & = & C(t)\, x(t) + D(t)\, u(t), \end{array} \right. \tag{1.11}$$

Definition 18 *Linear Parameter Varying (LPV) model*

Considering the matrices $A(\rho_t(t)) \in \mathbb{R}^{n\times n}$, $B(\rho_t(t)) \in \mathbb{R}^{n\times n_u}$, $C(\rho_t(t)) \in \mathbb{R}^{n_y\times n}$, $D(\rho_t(t)) \in \mathbb{R}^{n_y\times n_u}$ *and the time varying parameter* $\rho_t \in \Gamma \subset \mathbb{R}^p$ *where* Γ *is a compact set. The system can be described by the Linear Parameter Varying (LPV) model* $\mathcal{M}_{LPV}$ *such that:*

$$\mathcal{M}_{LPV} : \left\{ \begin{array}{rcl} \dot{x}(t) & = & A(\rho_t(t))\, x(t) + B(\rho_t(t))\, u(t), \\ y(t) & = & C(\rho_t(t))\, x(t) + D(\rho_t(t))\, u(t), \end{array} \right. \tag{1.12}$$

Definition 19 *Quasi Linear Parameter Varying (q-LPV) model*

Considering the matrices $A(\rho_x(x), \rho_t(t)) \in \mathbb{R}^{n\times n}$, $B(\rho_x(x), \rho_t(t)) \in \mathbb{R}^{n\times n_u}$, $C(\rho_x(x), \rho_t(t)) \in \mathbb{R}^{n_y\times n}$, $D(\rho_x(x), \rho_t(t)) \in \mathbb{R}^{n_y\times n_u}$ *and the time varying parameter* $(\rho_x, \rho_t) \in \Gamma \subset \mathbb{R}^p$ *where* Γ *is a compact set. The system can be described by the quasi Linear Parameter Varying (q-LPV) model* $\mathcal{M}_{q-LPV}$ *such that:*

$$\mathcal{M}_{q-LPV} : \left\{ \begin{array}{rcl} \dot{x}(t) & = & A(\rho_x(x), \rho_t(t))\, x(t) + B(\rho_x(x), \rho_t(t))\, u(t), \\ y(t) & = & C(\rho_x(x), \rho_t(t))\, x(t) + D(\rho_x(x), \rho_t(t))\, u(t), \end{array} \right. \tag{1.13}$$

The LPV and q-LPV formulations consider that the state space matrices depend on the varying parameters. However, there are different types of dependencies: the LPV-A dependency, the LPV-R dependency or the Linear Fractional Transformation (LFT). The LPV-A dependency which means affine parameter dependency considers that the state matrix A is given by $A(t) = A_0 + A_1\rho_1(t) + \cdots + A_n\rho_n(t)$. Similarly, the LPV-R dependency has the form of a rational function expressed by $A(t) = [A_{n0} + A_{n1}\rho_{n1}(t) + \cdots + A_{nn}\rho_{nn}(t)]\,[A_{d0} + A_{d1}\rho_{d1}(t) + \cdots + A_{dn}\rho_{dn}(t)]^{-1}$. Finally, the LFT dependency is based on the transformation of the parameter dependent system into an uncertain system. Here, attention is focused on another dependency type which is the polytopic one. This last type of dependency is interesting insofar as a lot of tools, adapted for polytopic system, are available in the literature. Moreover, this kind of dependency will be used in Chapter 4, where solutions for the control of the NLG based on gain scheduling polytopic approaches are proposed.

Definition 20 *Polytopic LPV or q-LPV model*

The LPV or q-LPV models are considered as polytopic when ρ *evolves in the polytope* $P = \boldsymbol{Co}\{w_1, \cdots, w_N\}$ *formed by the vertices* w_i *and when the state space matrices of the model have a linear dependency in the parameter* ρ *such that:*

$$\left[\begin{array}{cc} A(\rho) & B(\rho) \\ C(\rho) & D(\rho) \end{array} \right] = \sum_{i=1}^{N} \alpha_i(\rho) \left[\begin{array}{cc} A(w_i) & B(w_i) \\ C(w_i) & D(w_i) \end{array} \right] \tag{1.14}$$

where $\left[\begin{array}{cc} A(\rho) & B(\rho) \\ C(\rho) & D(\rho) \end{array} \right] \in \boldsymbol{Co}\left\{ \left[\begin{array}{cc} A(w_1) & B(w_1) \\ C(w_1) & D(w_1) \end{array} \right] \cdots \left[\begin{array}{cc} A(w_N) & B(w_N) \\ C(w_N) & D(w_N) \end{array} \right] \right\}$ *formed by the evaluation of the state space matrices at each vertices of* P *and where* $\alpha_i \geq 0\ \forall i$ *and* $\sum_{i=1}^{N} \alpha_i = 1$.

1.3.2.4 Piecewise Affine Model

A different way to approximate a smooth non-linear system with keeping a linear formulation of the model is to introduce the notion of Piecewise Affine (PWA) models. They are defined by series of affine linear models where the states evolution is governed by invariant transitions from one affine linear model to another. The state-input space is partitioned in region $\mathcal{X}_i$ with $i = 1, \cdots, s$ and every dynamics is defined in this region. For example, such model formulation is very interesting when the dynamics of a car vehicle and notably the tyre contributions must be considered. This latter can be modelled by the well-known non-linear Pacejka tyre model [Pacejka, 2006] (cf. Appendix A.3.3) but a linear model versus a non-linear model is easier to use from a control theory point of view. Then, the non-linear function describing the lateral tyre force (F_y) versus the slip angle (β) from the Pacejka model could be replaced by a PWA representation as presented in Figure 1.3.

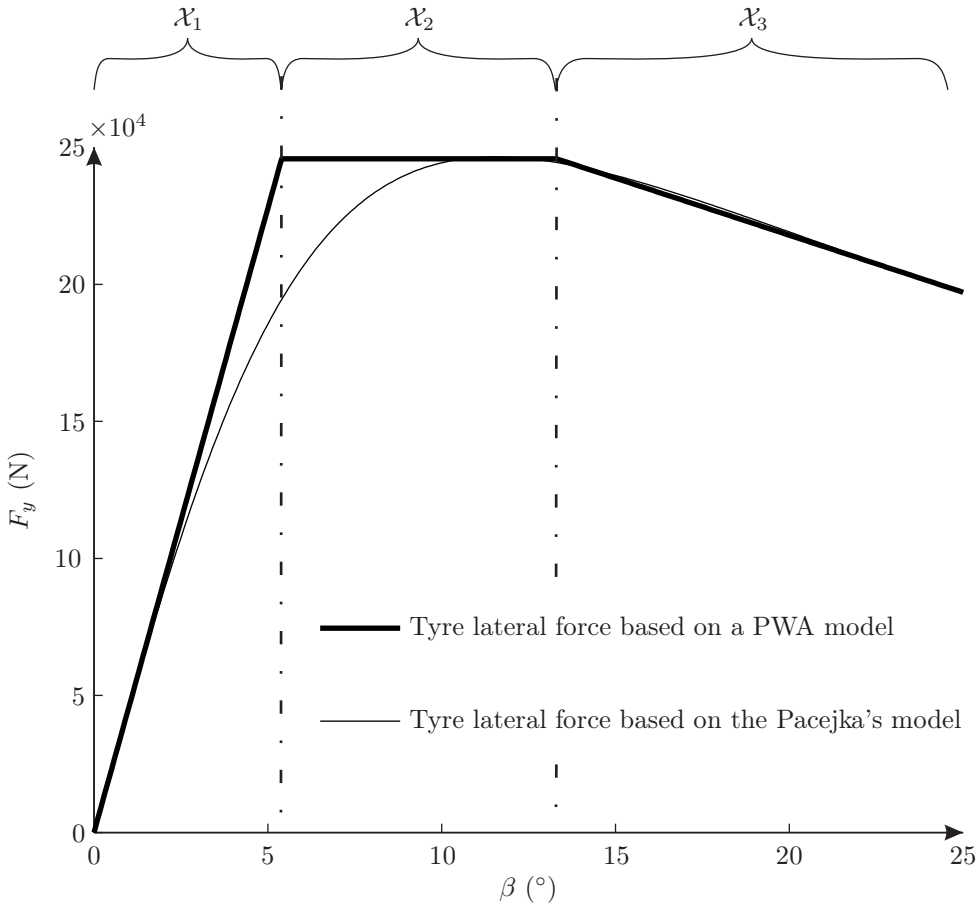

Figure 1.3: Approximation of the tyre lateral force by a PWA model

Definition 21 *Piecewise affine (PWA) model*

Considering the matrices and the vectors $A_i \in \mathbb{R}^{n \times n}$, $B_i \in \mathbb{R}^{n \times n_u}$, $C_i \in \mathbb{R}^{n_y \times n}$, $D_i \in \mathbb{R}^{n_y \times n_u}$, $f_i \in \mathbb{R}^{n_u}$ *and* $g_i \in \mathbb{R}^{n_y}$*; the system can be described by the Piecewise Affine (PWA) model* $\mathcal{M}_{PWA}$ *such that:*

$$\mathcal{M}_{PWA} : \begin{cases} \dot{x}(t) &= A_i(t)\, x(t) + B_i(t)\, u(t) + f_i, \\ y(t) &= C_i(t)\, x(t) + D_i(t)\, u(t) + g_i, \end{cases} \text{for } [x(t)^T, u(t)^T]^T \in \mathcal{X}_i \tag{1.15}$$

where $x(t)$, $u(t)$ and $y(t)$ are respectively the state vector, the input vector and the output vector of the system and $\mathcal{X}_i$, $i \in 1, 2, ..., s$ is a polyhedral partition of the state-input space such that:

- $\mathcal{X}_i \cap \mathcal{X}_j = \emptyset$
- $[x(t)^T, u(t)^T]^T \in \mathcal{X}_i$ *if* $E_i x(t) + E_i u(t) < E_i$
- $\bigcup_{i=1}^{s} \mathcal{X}_i = \mathbb{X}$ *with* $\mathbb{X}$ *the global state-input space.*

1.3.2.5 Non-linear model

LTI or Linear Varying models are restrictive insofar a lot of real systems include non-linearities. In this case, it is easy to understand that a non-linear model will be more appropriate than a linear one, giving a better approximation of the considered system. However, in terms of model identification, dynamics observation or controller synthesis, the use of a non-linear representation engenders an important complexity.

Definition 22 *Non-linear model*

Considering the non-linear functions $f : \mathbb{R}^n \times \mathbb{R}^{n_u} \rightarrow \mathbb{R}^n$ and $g : \mathbb{R}^n \times \mathbb{R}^{n_u} \rightarrow \mathbb{R}^{n_y}$ the system can be described by the non-linear model $\mathcal{M}_{Non-linear}$ such that:

$$\mathcal{M}_{Non-linear} : \begin{cases} \dot{x}(t) &= f(x(t), u(t)), \\ y(t) &= g(x(t), u(t)), \end{cases} \tag{1.16}$$

where x(t), u(t) and y(t) are respectively the state vector, the input vector and the output vector of the system.

Commentary The notions of observability, detectability, controllability, stabilizability and stability are expressed previously in the case of particular linear state space models. It is obvious that the extension to linear varying models, PWA models or non-linear models is possible [Hermann and Krener, 1977] [Lyapunov, 1992].

1.3.3 Artificial Neural Network (ANN) formulation

Chapter 5 will deal with automatic guidance and in this field, a control architecture based on ANN and Model Predictive Control (MPC) is proposed. It will be shown that the ANN modelling tool eliminates the limitations of common linear models that are based on a fixed structure. Then, this current section introduces the basic notions of ANN, required to understand the following applications.

An ANN model aims at reproducing the behaviour of a brain-like system [Fuller, 1995]. These kinds of models function are parallel distributed computing networks and they are able to learn and generalize the behaviour of the systems. An ANN model is characterized by its architecture (the number of inputs and outputs, the number of hidden layers, ...), the method that permits to obtain the parameters of the network ($w^{j,k}$ and W^k in Figure 1.4) and the activation function, the mathematical function that gives the output based on the inputs that can be a threshold function, a sigmoidal function or a tangent hyperbolic function [Fausett, 1994]. The following

just reminds the notations used in this manuscript. An improved description of the ANN can be found in [Fausett, 1994], [Fuller, 1995] or [Abdeslam, 2005].

The ANN model uses n inputs, nCC neurons in the hidden layer and one output; it is presented in Figure 1.4.

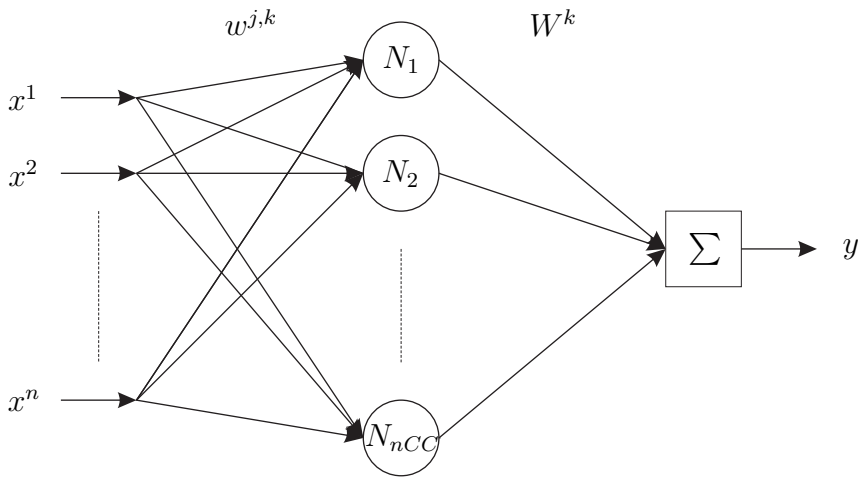

Figure 1.4: Multi layer Neural Network

The ANN model uses the following variables:

- o^k: with $k \in [1, \cdots, nCC]$ is the input of the hidden layer k,
- o: the [nCC, 1] vector of o^k values,
- O^k with $k \in [1, \cdots, nCC]$ is the output of the hidden layer k,
- O: the [nCC, 1] vector of O^k values,
- $w^{j,k}$ with $j \in [1, \cdots, n]$ and $k \in [1, \cdots, nCC]$ is the weight of the input layer,
- w: the [n,nCC] vector of $w^{j,k}$ values,
- W^k with $k \in [1, \cdots, nCC]$ is the weight of the output layer,
- W: the [nCC,1] vector of W^k values.

The output of the system is defined by:

$$y = \sum_{k=1}^{nCC} W^k O^k = W^T O. \tag{1.17}$$

The activation function of the hidden layer is equal to:

$$\frac{1}{1 + exp(-X)}, \tag{1.18}$$

then, the output of the hidden layer is obtained by:

$$O^k = \frac{1}{1 + exp(-o^k)}, \tag{1.19}$$

The input of the hidden layer is obtained with:

$$o^k = \sum_{j=1}^{n} w^{j,k} x^j = w^T x. \tag{1.20}$$

Different activation functions are available in the literature. The sigmoid has been chosen insofar as it has the property of being similar to the step function, but with the addition of a region of uncertainty. Then, sigmoid functions are very similar to the input-output relationships of biological neurons.

1.3.4 Fuzzy Logic formulation

Chapter 4 will focus on NLG shimmy control and in this field, fuzzy adaptive control solutions are proposed. In this particular control application, a fuzzy system helps to identify in real-time the dynamics of the NLG. These latter will be used to compute the control signal. Then, this section introduces the basic notions of fuzzy logic which will be required to understand the following application. To find more details about fuzzy logic, the reader may consider the work of [Zadeh, 1965], [Passino and Yurkovich, 1998] and [Kosko, 1993].

Fuzzy systems are one of the most useful approaches for the integration of expert knowledge. This solution is generally used for plants that are mathematically poorly modelled and where the experience of an operator is needed. The approximation based on a fuzzy system features four main components, namely fuzzification, fuzzy rule base, inference and defuzzification (see Figure 1.5):

- Fuzzification is the stage in which the input crisp values (inputs have real number values) are transformed into fuzzy set (a set whose elements have degrees of membership);
- Fuzzy rule base, which consists of a set of linguistic rules in the form "IF a set of conditions are satisfied, THEN a set of consequences are inferred", is then performed;
- Inference is the procedure whereby the values of the fuzzy variables are inferred from the fuzzy rule base, generating a fuzzy value for the output variables;
- In the final stage, the defuzzification aims at transforming these output fuzzy values into crisp data that can be used for the following parts of the control algorithm.

A representation of a fuzzy system is shown in figure 1.5.

Several standard fuzzy systems based on the previous four main components are introduced in the literature. Particularly, the three algorithms developed for the NLG shimmy control (see Sections 4.3.3 and 4.3.4) are based on the Takagi-Sugeno fuzzy system [Takagi and Sugeno, 1985]. It is a MISO (multi input, single output) fuzzy logic system mapping from an input vector $x = [x_1, x_2, ..., x_n]^T \in \mathbb{R}^n$ to an output $y = f(x) \in \mathbb{R}$. First, the universe of discourse (that means the set of all possible values) of each input of the fuzzy system is studied and this universe is decomposed into one or more fuzzy subsets. Furthermore, the fuzzy model consists of p fuzzy rules (corresponding to all combinations of the inputs). Generally, the output consequences of each fuzzy rule is a function of the state. In the approach proposed for the NLG control, the

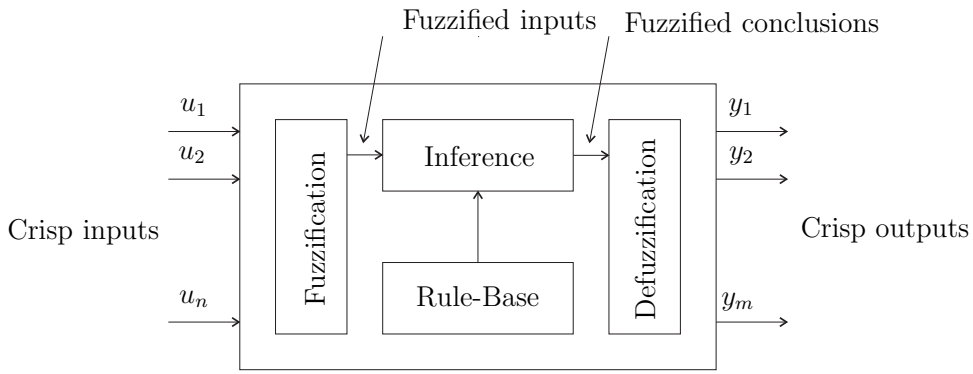

Figure 1.5: Fuzzy system

output consequences are considered as constant from θ_1 to θ_p. The fuzzy rules have the following form:

$$\begin{aligned} R_1: &\quad \textbf{If } (x_1 \text{ is } F_1^1 \textbf{ and } \cdots \textbf{and } x_n \text{ is } F_1^n) \textbf{ Then } y^1 = \theta_1 \\ &\qquad\qquad \vdots \\ R_p: &\quad \textbf{If } (x_1 \text{ is } F_k^1 \textbf{ and } \cdots \textbf{and } x_n \text{ is } F_l^n) \textbf{ Then } y^p = \theta_p \end{aligned} \tag{1.21}$$

where F_i^j is the ith fuzzy set (a part of discourse universe) for the state variable j ($i = 1 \dots k$ for the state x_1 or $i = 1 \dots l$ for the state x_n, $j = 1 \dots n$). For each fuzzy set F_i^j, a membership function μ such that $\mu_{F_i^j} \in [0, 1]$ is defined. This membership function enables to quantify how well an input state x_i belongs to the subset F_i^j. Several standard membership functions exist in the literature and the Gaussian membership function has been retained for the controllers proposed in Section 2.3.

1.4 Model identification

1.4.1 General concept

The process of determining the numerical values of the different parameters of the model representation is known as model identification. This step is fundamental for the implementation of a competitive control strategy [Landau and Besançon-Voda, 2001]. For example, a $\mathcal{H}_\infty$ control strategy needs a model to synthesize the optimal controller, or the Model Predictive Control (MPC) requires a model to predict the plant behaviour and obtain the optimal control signal. These control strategies depend on the model defined during the model identification procedure. This section helps to understand the results of the identification procedure of LPV and ANN models dedicated to control purposes and presented in Sections 4 and 5.

Considering a system $\mathcal{S}$ and a model $\mathcal{M}(p_i)$ that depends on several parameters p_i, the identification process aims at obtaining these parameters so that the system and the model have similar input-output behaviour. The parameters p_i may be physical parameters like the mass or the stiffness for a white box model or parameters without physical meaning in the case of a black box model. The same input signal u is used to activate the system and the model and their respective outputs y and $\hat{y}$ are compared. Finally the output error criteria $e = y - \hat{y}$ is used to optimally adjust the values of the parameters p_i. Figure 1.6 presents these different

contributions.

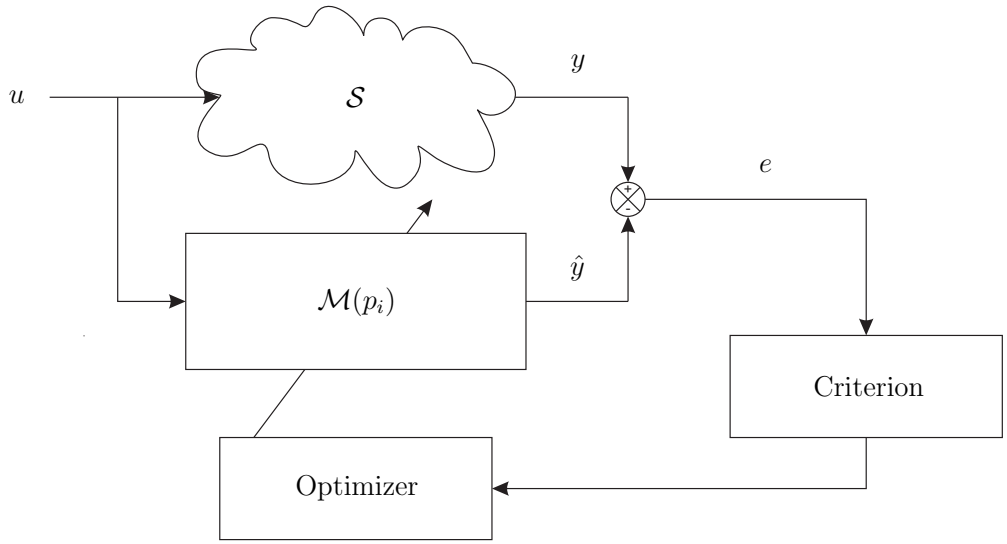

Figure 1.6: Identification procedure based on output error criteria

The identification of model parameters is always divided in four steps [Caroux, 2007]:

- protocol definition,
- cost criterion definition,
- parameter estimation,
- validation process.

The protocol definition aims at preparing the different sensors that should be used to measure the input and output signals. In this step, the properties of the measures are studied: what is the suitable sample time, what are the required filters, ...? Then, the choice of the input signals is performed, taking account of the model to be obtained: what are the frequencies that must be excited? Finally, it is important to evaluate the constraints linked to the input signals. For example, considering the identification of the vehicle model parameters, it is obvious that the commonly used identification signal (PRBS: Pseudo Random Binary Sequence) cannot be used: this signal is not feasible and a signal that takes account of the driver limitations must be considered.

The cost criterion is used to describe the difference between the system to be identified and the model. The commonly used cost criteria are the absolute error and the quadratic error. The identification results presented in the following chapters are based on the quadratic criterion J. This cost criterion is easier to implement but it is sensitive to "mad points". It is defined by:

$$J = e^T Q e \tag{1.22}$$

such that Q is a weighting matrix which weights the different outputs and the error $e = y - \hat{y}$ as presented in Figure 1.6

The parameter estimation uses an optimization algorithm aiming at reducing the difference between the output of the system y and the output of the model $\hat{y}$ and at providing step by

step an appropriate value to the model parameters. Considering $\hat{p}(k)$ the estimation of the parameters, the value of $\hat{p}$ at the next step is obtained by:

$$\hat{p}(k+1) = \hat{p}(k) + \alpha(k)d(k) \tag{1.23}$$

with d(k) the direction of the research and $\alpha(k)$ the adaptation gain which characterizes the evolution speed. This general formulation permits to regroup different optimization methods. First, the direct methods as the simplex method ([Dantzig, 1963]) or the Gauss method do not require the calculation of the derivative criterion. Secondly, first order methods as the gradient descent methods [Snyman, 2005]) use the first derivative and are slow methods. Finally, the Newton, Gauss-Newton or Levenberg-Marquardt methods ([Björck, 1996] and [Levenberg, 1944]) use the first and second derivative.

The last step of the identification process consists in the validation of the obtained parameters and the behaviour of the identified model. This step is divided into two phases. When white or grey box models are identified, the physical meaning of the obtained parameters is studied. For example, a model that considers an identified negative mass could not be accepted. Then, a validation input sequence, different from the identification input signal, is created. The response of the system using this new input signal is compared with the response of the model. If the two responses are similar, considering an acceptable residual error, the identified model is validated.

1.4.2 Identification considering a LPV model

Identification of LPV models is the subject of recent interest [Nemani et al., 1995] [Previdi and Lovera, 1999] [Ljung, 2008]. Two approaches are distinguished in the literature:

- the global approach, where a single experiment helps to directly obtain a parameter-dependent model;
- the local approach that aims at using multiple experiments to obtain many LTI models that will be interpolated

The identification of the LPV model used in this project is based on the local approach (see Section 5.4).

The identification method is divided into three steps. First, the space of the varying parameter is gridded. Secondly, the identification of the model parameters, using the method defined in Section 1.4.1, is made for each values of the varying parameter. Finally, the different obtained values are interpolated.

1.4.3 Identification considering a PWA model

Identification of a PWA models can be separated in two different cases. On the one hand, this task can be an easy problem when the polyhedral partition is known. In this case, it is an ordinary least square problem. On the other hand, it can become a hard problem when the polyhedral partition is unknown. In this case, non-convex optimization problems are generally obtained [Bemporad et al., 2003] [Ferrari-Trecate et al., 2003].

1.4.4 Identification considering an Artificial Neural Network model

In the literature, different methods concerning the identification of multi-layer ANN models are described [Abdeslam, 2005]. Basically, it is possible to distinguish on-line and off-line methods. On-line approaches are interesting when a lot of perturbations are applied on the system whereas off-line approaches are better to reduce the complexity notably when the ANN model is used for control purposes. Then, the learning phase can be a direct identification or an inverse identification. On the one hand, the difference between the system output and the model output helps to obtain the parameters of the ANN model. On the other hand, the input of the system is compared with the output of the ANN model. The ANN model, used in Section 5, is identified using an off-line method with the direct solution.

Identification method, called backpropagation method, adapt the weights of the input and output layers w^k and W^k to minimize the squared error of the output provided by the network. The commonly used method for the weighting adaptation is the gradient descent method. Considering an input/output training pattern (u(t),y(t)) the error measurement between the system and the ANN model permits to define the quadratic error:

$$E = \frac{1}{2}(y - \hat{y})^2. \tag{1.24}$$

Then, the adaptation which minimizes the quadratic error function uses the following iteration process:

$$W = W - \eta \frac{\partial E}{\partial W} \tag{1.25}$$

$$w = w - \eta \frac{\partial E}{\partial w} \tag{1.26}$$

Then, the cost functions $J_W = \dfrac{\partial E}{\partial W}$ and $J_w = \dfrac{\partial E}{\partial w}$ are defined by:

$$\begin{aligned} J_W &= \frac{1}{2}\frac{\partial}{\partial W}(y - \hat{y})^2 \\ &= \frac{1}{2}\frac{\partial}{\partial W}(y - W^T O)^2 \\ &= (y - W^T O)\frac{\partial}{\partial W}(y - W^T O) \\ &= -(y - W^T O)O \\ &= -eO \end{aligned} \tag{1.27}$$

and

$$
\begin{aligned}
J_w &= \frac{1}{2}\frac{\partial}{\partial w}(y-\hat{y})^2 \\
&= \frac{1}{2}\frac{\partial}{\partial w}(y-\frac{W^T}{1+exp(-w^Tx)})^2 \\
&= (y-\frac{W^T}{1+exp(-w^Tx)})\frac{\partial}{\partial w}(y-\frac{W^T}{1+exp(-w^Tx)}) \\
&= -(y-\frac{W^T}{1+exp(-w^Tx)})\frac{xexp(-w^Tx)}{(1+exp(-w^Tx))^2}W^T \\
&= -(y-\frac{W^T}{1+exp(-w^Tx)})xO^T(1-O)W^T \\
&= -(y-W^TO)xO^T(1-O)W^T \\
&= -exO^T(1-O)W^T
\end{aligned} \tag{1.28}
$$

1.5 Conclusion

In this chapter, the presentation of the system $\mathcal{S}$ (see Section 1.2.1) and the model $\mathcal{M}$ (see Section 1.2.2) has been done. These different notions are summarized in Figure 1.7. First, the

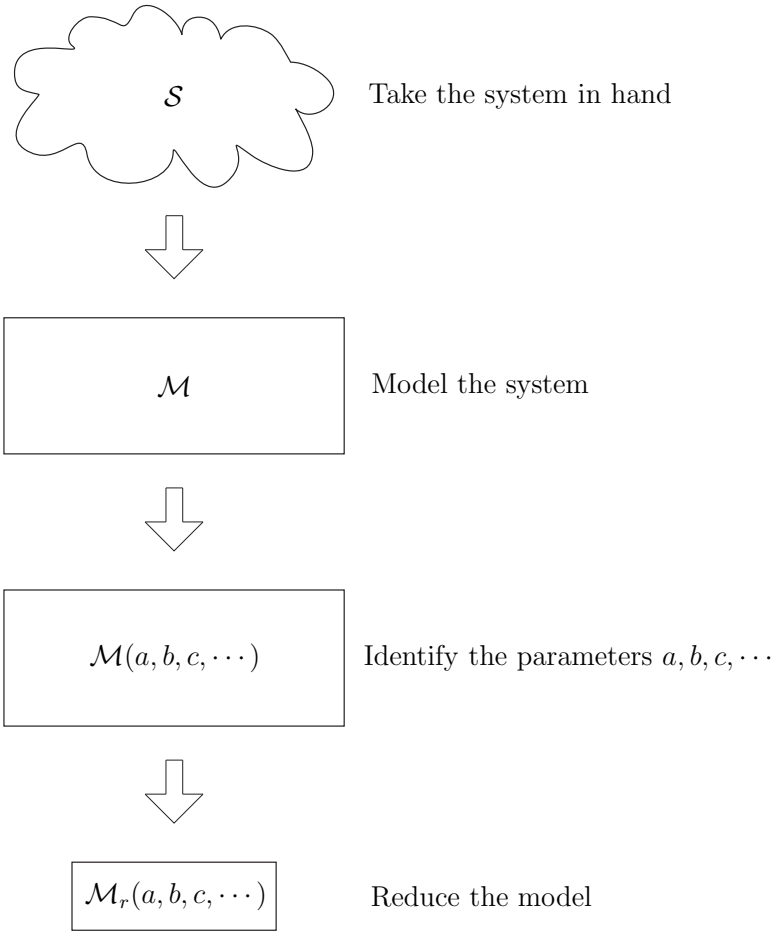

Figure 1.7: Notions presented in Chapter 1

system must be studied to define all its components. Then, the modelling step starts (see Section

1.3) and following the chosen structure of the model, its parameters are identified (see Section 1.4). Finally, when low order models are required, model reduction tools presented in Appendix C may be used.

The different model formulations which have been introduced in this chapter will be used in the following. For instance, it will be shown in Chapter 3 that the NLG could be described with an LPV formulation, the shimmy phenomenon uses a non-linear model and finally the vehicle dynamics are modelled with an ANN model. Then, identification tools have been proposed and Chapter 5 will present some results based on LPV model and ANN model identification. Finally, model order reduction techniques have been detailed. It will be shown in Chapter 4 that such tools will be used for high order controller reduction.

As a conclusion, the chapter has tried to answer the question "Which model for which system?". It has been shown that state space formulation is adapted for linear model when the physical description of the system is known. Indeed, the state space matrices are directly defined based on the parameters of the system. Moreover, when some non-linearities are detected in the system, it is interesting to be in favour of LPV models, insofar as efficient control tools are available with such modelling. Furthermore, it is sometimes required to consider a non-linear model. In consequence of hard non-linearities of the system, the modelling step is constrained by the use of non-linear model, despite the well-known difficulties which will be encountered with such solutions. Finally, when no experience of the model or when difficulties are encountered during the modelling step, it is possible to opt for black box models such as ANN or fuzzy models.

After describing the system with an appropriated model, it is possible to control this system. For this task, different tools are available in the literature and it could shown in the following chapter that the choice of the control solution frequently depends on the nature of the model. As a consequence, Chapter 2 will try to answer the question "Which control law for which model?"

La théorie, c'est quand on sait tout et que rien ne fonctionne. La pratique, c'est quand tout fonctionne et que personne ne sait pourquoi. Ici, nous avons réuni théorie et pratique : Rien ne fonctionne... et personne ne sait pourquoi !

Albert Einstein

Chapter 2

Which control law for which model?

Contents

2.1 Introduction

Chapter 1 presented the link between the system and the model. This chapter aims at discussing the relation between the model and the control law. It could be seen that depending on the model formulation, some solutions are more suitable.

Firstly, it is well-known that the model is an imperfect representation of the system. A robust control solution can help to consider, in the design of the controller, the unmodeled dynamics, the perturbations and/or the noise affecting the signals [Doyle et al., 1990]. Then, Section 2.2 introduces the theoretical aspect of $\mathcal{H}_\infty$ synthesis [Doyle et al., 1990]. A particular interest focuses on the solutions adapted to LPV models [Apkarian and Gahinet, 1995]. Secondly, a control solution well-suited for non-linear models is presented in Section 2.3. The provided solutions are based on feedback linearisation [Khalil, 2002] which is a common approach for such non-linear models. It consists in transforming the non-linear model into an equivalent linear one through a change of variables and the determination of a suitable control input. Moreover, in case of poor knowledge of the system behaviour, which is the case here, the control solutions integrate a real time identification of the system dynamics allowing the adaptation of the control law. Thus, Section 2.3 presents two states feedback and one output feedback fuzzy adaptive control solutions [Spooner and Passino, 1996] [Calise et al., 2001]. Thirdly, MPC, a control solution that requires the resolution of an on-line optimization algorithm is introduced [Garcia and Morari, 1989]. A trade off between the complexity of the model and the system dynamics has to be considered when using such a solution. Indeed, due to the on-line optimization, a complex model (a non-linear model for instance) must have low dynamics as the chemical systems, to ensure the optimization resolution. As a conclusion, Section 2.4 presents the theoretical aspects of MPC by considering both a state space [Maciejowski, 2000] formulation and an ANN formulation [Norgaard et al., 1999]. A particular attention will be paid on constrained optimization.

The control solutions presented in this chapter will be used in the applications presented in Chapters 4 and 5. The $\mathcal{H}_\infty$ synthesis permits to control the NLG in order to respond to the wheel angle demand from the pilot or the automatic guidance system. A non-linear adaptive control solution is used to damp shimmy oscillations of the NLG. Finally, the automatic guidance, applied in simulation on an A/C model and in real experiments on a passenger vehicle, is made possible through MPC

2.2 $\mathcal{H}_\infty$ synthesis: theoretical aspects

2.2.1 Introduction

Based on Chapter 1, it has been explained that models do not represent precisely the behaviour of the system. However, model-based controllers do not be influenced by an imperfect representation of the reality. Thus, the robustness of the control solution must be taken into account. Considering the required characteristics of the closed-loop system in terms of performances or stability, a controller $\mathcal{K}$ is robust when the considered characteristics are respected despite the difference between the model and the reality. Two robust properties are frequently examined: the robust stability and the robust performance. A controller $\mathcal{K}$ provides robust stability when it provides internal stability despite the difference between the model and the reality. Similarly,

a controller provides robust performance when the performances that must be reached by the closed-loop system are not degraded by the imperfect model. In the guideline of robustness, the controllers developed in the $\mathcal{H}_\infty$ framework are well-suited.

The synthesis of $\mathcal{H}_\infty$ controllers helps to include the inaccuracies of the model and the perturbations acting on the system. To provide the required closed-loop system, the $\mathcal{H}_\infty$ control solution proposes to describe the specifications to be reached in terms of mathematical criteria. Then, an optimization algorithm is required to obtain the state space representation of the controller. This control solution is adapted for Multi-Input/Multi-Output (MIMO) systems and the synthesis helps to obtain a linear controller. Nevertheless, it is possible to extend this formalism to LPV systems to obtain non-linear controllers by keeping a linear structure. This formalism is detailed in this section.

Currently, $\mathcal{H}_\infty$ formalism is employed in various areas: medical applications [Cuvillon et al., 2005], [Ruiz-Velázqueza et al., 2004]; aeronautic and spacecraft applications [Liu et al., 2003], [Ballois and Duc, 1996] ; vehicle applications [Wang et al., 2007], [Palladino et al., 2006] ; industrial applications [Knittel et al., 2007], etc.

2.2.2 $\mathcal{H}_\infty$ synthesis for LTI models

2.2.2.1 Introduction

$\mathcal{H}_\infty$ control theory helps to synthesize an optimal controller respecting performance criteria. These criteria are based on frequency concepts and are represented by weighting filters. The latter enables to generate error signals so as to characterize the performances that the system must reach.

This control strategy is based on the general control configuration presented in Figure 2.1:

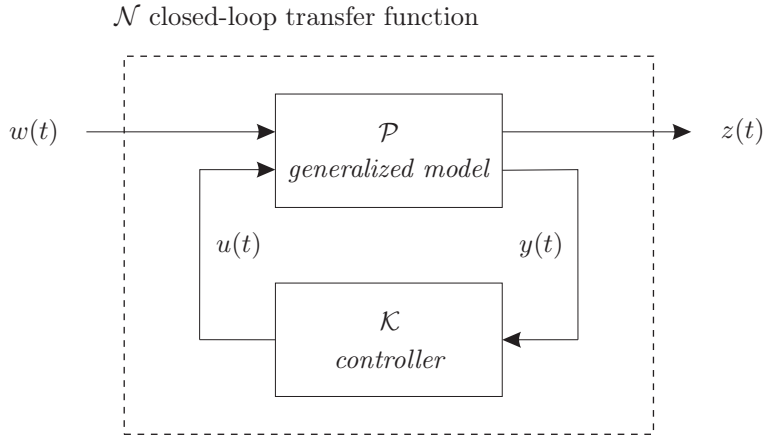

Figure 2.1: General control configuration (standard form)

Here, $w(t)$ represents the disturbances, the noise signals and the reference inputs, $u(t)$ denotes the control inputs, $z(t)$ is the error signal to be minimized and $y(t)$ denotes the measurements. The *"generalized model"*, represented by $\mathcal{P}$ in Figure 2.1 is an input/output inter-connection matrix, which contains the generally so called "system" as well as the weighting filters. Finally, the block $\mathcal{K}$ is the controller to be designed and is intended to minimize the impact of $w(t)$ to $z(t)$.

Figure 2.2 details the generalized model $\mathcal{P}$ mentioned in Figure 2.1. Indeed, $\mathcal{P}$ is composed

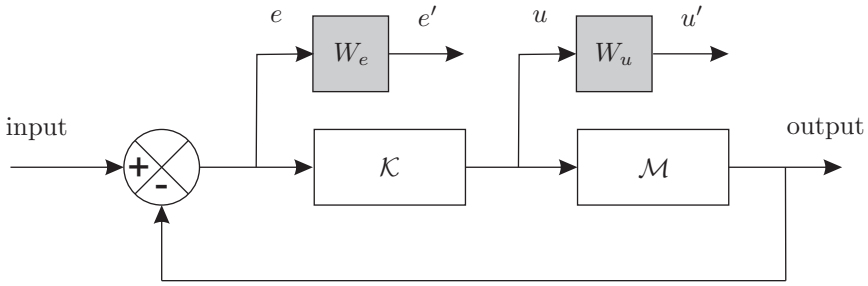

Figure 2.2: Presentation of the generalized model

of the weighting filters (W_e and W_u in the proposed structure) and the model of the system $\mathcal{M}$. By simplification, we can write that $\mathcal{P} = \mathcal{M} + W_e + W_u$. The choice of the weighing filters W_e and W_u is an important task for the design of $\mathcal{H}_\infty$ controllers and Section 4.2.2 is dedicated to the description of the existing methods.

Consider the Linear Time Invariant (LTI) plant $\mathcal{P}$ given by:

$$\mathcal{P} : \begin{cases} \dot{x}(t) &= A\,x(t) + B_1\,w(t) + B_2\,u(t), \\ z(t) &= C_1\,x(t) + D_{11}\,w(t) + D_{12}\,u(t), \\ y(t) &= C_2\,x(t) + D_{21}\,w(t), \end{cases} \tag{2.1}$$

where $x \in \mathbb{R}^n$ corresponds to the state vector. The matrices A, B_1, B_2, C_1, C_2, D_{11}, D_{12} and D_{21} have appropriated dimensions.

Consider $\mathcal{K}$, the dynamic controller is given by:

$$\mathcal{K} : \begin{cases} \dot{x}_K(t) &= A_K\,x_K(t) + B_K\,y(t), \\ u(t) &= C_K\,x_K(t) + D_K\,y(t), \end{cases} \tag{2.2}$$

where $x_K \in \mathbb{R}^n$ corresponds to the state vector of the controller. The matrices A_K, B_K, C_K et D_K have appropriated dimensions.

It is important to notice that the dimension of $x(t)$ matches the one of $x_K(t)$. This implies several implementation problems when dimensions are too important. Then, this major $\mathcal{H}_\infty$ drawback will be discussed in Chapter 4 when control implementation will be discussed.

Using $\mathcal{P}$ and $\mathcal{K}$ defined previously, the closed-loop transfer function $\mathcal{N}$ linking $w(t)$ and $z(t)$ is defined by:

$$\mathcal{N} : \begin{cases} \dot{x}_{cl}(t) &= \mathbf{A}\,x_{cl}(t) + \mathbf{B}\,w(t), \\ z(t) &= \mathbf{C}\,x_{cl}(t) + \mathbf{D}\,w(t), \end{cases} \tag{2.3}$$

where $x_{cl}^T = [x^T x_K^T]^T$ and

$$\begin{cases} \mathbf{A} &= \begin{pmatrix} A + B_2 D_K C_2 & B_2 C_K \\ B_K C_2 & A_K \end{pmatrix}, \\ \mathbf{B} &= \begin{pmatrix} B_1 + B_2 D_K D_{21} \\ B_K D_{21} \end{pmatrix}, \\ \mathbf{C} &= \begin{pmatrix} C_1 + D_{12} D_K C_2 & D_{12} C_K \end{pmatrix}, \\ \mathbf{D} &= D_{11} + D_{12} D_K D_{21}. \end{cases}$$

The $\mathcal{H}_\infty$ control problem consists in synthesizing a controller $\mathcal{K}$ that stabilizes the system and minimizes the $\mathcal{H}_\infty$ norm of the closed-loop transfer function $\mathcal{N}$.

The controller synthesis needs the distinction of two problems: the optimal $\mathcal{H}_\infty$ problem and the suboptimal $\mathcal{H}_\infty$ problem. The optimal problem aims at finding a controller that minimizes $\|\mathcal{N}\|_\infty$. This resolution is challenging and is not effectively required; thus, a suboptimal resolution is generally preferred. Consider a constant $\gamma > 0$, the aim of the suboptimal problem is to find a controller such that $\|\mathcal{N}\|_\infty < \gamma$.

2.2.2.2 Resolution method based on LMI equations

The optimization problem, obtained for the synthesis of the $\mathcal{H}_\infty$ controller can be solved using two different approaches. On the one hand, the first historical resolution method is based on Riccati's equations [Doyle et al., 1989]. On the other hand, the resolution based on Linear Matrix Inequalities (LMI) appeared in the nineties [Scherer et al., 1997], [Gahinet and Apkarian, 1994]. Thanks to recent advances in Semi-Definite Positive (SDP) programming [Vandenberghet and Boyd, 1996], the LMI becomes a very powerful tool appreciated by the control community due to the interesting possibility to solve many control problems [Boyd et al., 1994], [Herrmann et al., 2005]. Particularly, this tool gives the possibility to extend the $\mathcal{H}_\infty$ synthesis based on LTI models to LPV models. Moreover, the hypothesis required by the resolution based on the Riccati's equations are strict and the resolution based on LMI helps to relax these hypothesis. For example, hypotheses in relation with the rank of particular matrices are required when the resolution is based on Riccati's method. These different hypotheses and their utilities are clearly mentioned in [Zin, 2005]. As a conclusion, the synthesized $\mathcal{H}_\infty$ controllers are commonly obtained with the LMI resolution and the following presents this resolution method.

Definition 23 *Linear matrix inequalities*

A Linear Matrix Inequality has the form:

$$F(l) = F_0 + \sum_{i=1}^{m} l_i F_i > 0$$

where $l = (l_1, ..., l_m) \in \mathbb{R}^m$ is the vector with m variables and $F_i = F_i^T \in \mathbb{R}^{n \times n}$ $(i = 0, ..., m)$ are positive-definite symmetric matrices.

Definition 24 *Positive-definite matrix*

A matrix X is positive-definite if and only if:

$$\forall u \in \mathbb{R}^{n^\star},\ u^T X u > 0.$$

The resolution is based on the use of the bounded-real lemma [Scherer, 1990] and has to respect the following hypothesis:

- (A, B_2) is stabilizable;
- (C_2, A) is detectable.

This lemma demonstrates that the closed-loop system $\mathcal{N}$ is stable and the $\mathcal{H}_\infty$ norm of $\mathcal{N}$ is smaller than γ if there exists a symmetric matrix P such that:

$$\begin{pmatrix} \mathbf{A}^T\mathsf{P}+\mathsf{P}\mathbf{A} & \mathsf{P}\mathbf{B} & \mathbf{C}^T \\ \mathbf{B}^T\mathsf{P} & -\gamma I & \mathbf{D}^T \\ \mathbf{C} & \mathbf{D} & -\gamma I \end{pmatrix} < 0,\ \mathsf{P} > 0 \tag{2.4}$$

Based on the closed-loop system (2.3), it is easily outstanding that the first matrix inequality of (2.4) is not affine in the parameters and the convex optimization algorithm can not be used. A variable change, proposed in [Scherer et al., 1997], is required to obtain a LMI. Thus, the bounded-real lemma using the intermediate variables $\hat{A}, \hat{B}, \hat{C}, \hat{D}, X, Y$ is expressed by [Scherer et al., 1997]:

$$\begin{cases} \begin{pmatrix} M_{11} & * & * & * \\ M_{21} & M_{22} & * & * \\ M_{31} & M_{32} & -\gamma I & * \\ M_{41} & M_{42} & M_{43} & -\gamma I \end{pmatrix} < 0, \\ \begin{pmatrix} X & I \\ I & Y \end{pmatrix} > 0, \end{cases} \tag{2.5}$$

where $*$ denotes the blocks obtained by symmetry and transpose, and

$$\begin{cases} M_{11} = AX + XA^T + B_2\hat{C} + (B_2\hat{C})^T, \\ M_{21} = \hat{A} + (A + B_2\hat{D}C_2)^T, \\ M_{22} = A^TY + YA + \hat{B}C_2 + (\hat{B}C_2)^T, \\ M_{31} = (B_1 + B_2\hat{D}D_{21})^T, \\ M_{32} = (YB_1 + \hat{B}D_{21})^T, \\ M_{41} = C_1X + D_{12}\hat{C}, \\ M_{42} = C_1 + D_{12}\hat{D}C_2, \\ M_{43} = D_{11} + D_{12}\hat{D}D_{21}. \end{cases} \tag{2.6}$$

After solving the LMI, non singular matrices M and N are defined such that $MN^T = I - XY$. Then, the parameters of the controller are expressed as functions of the intermediate variables such that:

$$\begin{cases} D_K &= \hat{D}, \\ C_K &= (\hat{C} - D_kC_2X)M^T, \\ B_K &= N^{-1}(\hat{B} - YB_2D_K), \\ A_K &= N^{-1}(\hat{A} - NB_KC_2X - YB_2C_KM^T - \\ & \quad -Y(A + B_2D_KC_2)X)M^{-T}. \end{cases} \tag{2.7}$$

2.2.3 $\mathcal{H}_\infty$ synthesis for LPV models: the gain scheduling approach

The use of fixed-gain control solutions is not suitable for the systems whose parameters vary widely. Then, control solutions based on gain scheduling are required. It is an acknowledged technique and numerous different design notions are referred to this term [Rugh and Shamma, 2000]. Here, two kinds of gain scheduling controllers are considered:

- classic gain scheduling approach,

- modern gain scheduling approach.

The classic approach aims at defining a number of LTI models to describe the dynamics of the system; these models are used to synthesize a number of controllers. The control law is obtained by interpolating the output of these controllers. Different interpolation methods are proposed in [Theodoulis, 2008] (controller switching, controller blending, ZPK interpolation, state space matrices interpolation, ...) and the author suggests that controller blending is well-suited for MIMO use (the computational complexity is minimal and no limitation on the controller order or structure is detected).

The modern approach aims at using a LPV model to synthesize the controller. Two different approaches are available in the literature, the LFT formulation [Packard, 1994], [Apkarian and Gahinet, 1995] which considers the varying dynamics as perturbations, and the polytopic formulation [Apkarian et al., 1995] which is appropriate when the parameter dependency enters the LPV model in a linear way. The latter formulation is considered in this project, insofar as the linear dependency hypothesis is respected by the different models studied.

2.2.3.1 Classic gain scheduling approach and $\mathcal{H}_\infty$ synthesis

The classic gain scheduling technique and more particularly controller blending is presented in this section. This technique aims at synthesizing an LTI controller for each LTI model which grids the varying space. Then, the outputs of the adjacent controllers are blended (a weighted sum of the outputs is done) to provide the control signal to be applied on the system.

Consider for simplicity, an LPV model with two varying parameters ρ_1 and ρ_2 evolving inside a fixed operating region such that $\rho_1 \in [\rho_1^{min}, \rho_1^{max}]$ and $\rho_2 \in [\rho_2^{min}, \rho_2^{max}]$. The region is gridded with $m \times n$ points $P_{i,j}$ with $i \in [1, m]$ and $j \in [1, n]$. To each point corresponds a LTI model $\mathcal{P}_{i,j}(\rho_1^i, \rho_2^j)$ and a controller $\mathcal{K}_{i,j}$ is synthesized based on the $\mathcal{H}_\infty$ theory previously presented. At time t, the varying parameters defined by $\rho(t) = [\rho_1(t), \rho_2(t)]$ are located inside a square defined by four points $P_{i,j}$, $P_{i+1,j}$, $P_{i,j+1}$ and $P_{i+1,j+1}$ characterized by their respective LTI model and $\mathcal{H}_\infty$ controller. Then, the two distances d_i^t and d_j^t presented in Figure 2.3 which describe the proximity between the varying parameter and the vertex of the square, are defined by:

$$d_i^t = \frac{\rho_1(t) - \rho_1^i}{\rho_1^{i+1} - \rho_1^i} \tag{2.8}$$

$$d_j^t = \frac{\rho_2(t) - \rho_2^j}{\rho_2^{j+1} - \rho_2^j} \tag{2.9}$$

Finally, the control signal $u(t)$ applied on the system at time t is a combination of the four controller outputs $u_{i,j}$, $u_{i+1,j}$, $u_{i,j+1}$ and $u_{i+1,j+1}$ of the controllers $\mathcal{K}_{i,j}$, $\mathcal{K}_{i+1,j}$, $\mathcal{K}_{i,j+1}$ and $\mathcal{K}_{i+1,j+1}$ such that:

$$u(t) = (1 - d_i^t)\left[(1 - d_j^t) \cdot u_{i,j} + d_j^t \cdot u_{i,j+1}\right] + d_i^t\left[(1 - d_j^t) \cdot u_{i+1,j} + d_i^t \cdot u_{i+1,j+1}\right] \tag{2.10}$$

Nevertheless, numerous LPV models present a particularity insofar as the varying parameters evolve on a fixed trajectory. For example, considering an LPV model with two varying parameters ρ_1 and ρ_2, a constrained function f describes the relation between the two varying parameters

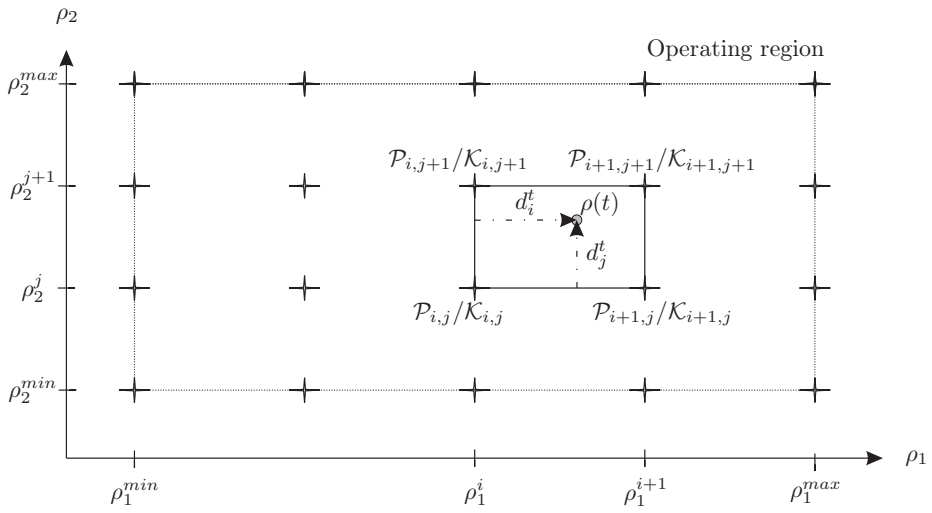

Figure 2.3: General controller blending technique

such that $\rho_2 = f(\rho_1)$ and defines a trajectory $\mathcal{T}$. The latter is gridded such that m points P_i are defined and m LTI models $\mathcal{P}_i(\rho_1^i, \rho_2^i)$ are distributed on the trajectory. For each LTI model, a controller $\mathcal{K}_i$ is synthesized based on the $\mathcal{H}_\infty$ theory. At time t, the varying parameters are on the trajectory between two adjacent points P_i and P_{i+1}. Then, three distances are calculated: D_i corresponds to the distance between P_i and P_{i+1}, d_i^t corresponds to the distance between P_i and the parameter $\rho(t)$ and d_{i+1}^t corresponds to the distance between P_{i+1} and the parameter $\rho(t)$. These different notions are illustrated in Figure 2.4. Finally, the control signal $u(t)$ applied on the system at time t is a combination of the two controller outputs u_i and u_{i+1} of the controllers $\mathcal{K}_i$ and $\mathcal{K}_{i+1}$ such that:

$$u(t) = d_{i+1}^t \cdot u_i + d_i^t \cdot u_{i+1} \tag{2.11}$$

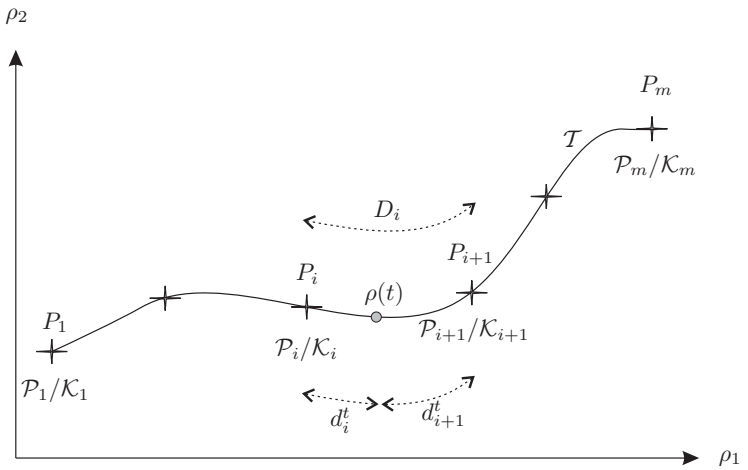

Figure 2.4: Controller blending technique considering a fixed trajectory

Commentary The classic gain scheduling solution is interesting insofar as only the output of the controller is processed and no matrix operation is required (the operation is done directly on the output signals and the state space matrices are, in this case, not taken into account). Moreover, controllers with different structures may be considered because only the outputs are summed. Thus, the well-known drawback of the $\mathcal{H}_\infty$ solutions which synthesize high order controllers is not important: the different controllers are reduced separately. However, this gain scheduling method presents two main drawbacks. On the one hand, numerous controllers must be synthesized to follow the dynamics of the system correctly (the varying space has to be gridded considering a small distance between the different points). On the other hand, just a few results concerning the stability of classic gain scheduling solutions are available in the literature.

2.2.3.2 Modern gain scheduling approach and $\mathcal{H}_\infty$ synthesis

The modern gain scheduling technique is presented in this section. Firstly, the difficulty to synthesise a controller encountered with the general formulation of an LPV system (cf. equations (1.11), (1.12) and (1.13)) is introduced. Secondly, the approach based on a polytopic formulation which helps to move from an infinite formulation to finite formulation is presented.

The $\mathcal{H}_\infty$ synthesis for LTI systems has been presented in Section 2.2.2. It is possible to extend the $\mathcal{H}_\infty$ synthesis to LPV or q-LPV systems. Let ρ being the set of varying parameters (that means ρ for a LPV system and ρ_x, ρ for a q-LPV system), the state-space model of equation (2.1) is described for LPV or q-LPV models by:

$$\mathcal{P}(\rho) : \left\{ \begin{array}{rcl} \dot{x}(t) & = & A(\rho)\, x(t) + B_1(\rho)\, w(t) + B_2(\rho)\, u(t), \\ z(t) & = & C_1(\rho)\, x(t) + D_{11}(\rho)\, w(t) + D_{12}(\rho)\, u(t), \\ y(t) & = & C_2(\rho)\, x(t) + D_{21}(\rho)\, w(t), \end{array} \right. \tag{2.12}$$

where $x \in \mathbb{R}^n$ corresponds to the state vector of the considered system. The matrices $A(\rho)$, $B_1(\rho)$, $B_2(\rho)$, $C_1(\rho)$, $C_2(\rho)$, $D_{11}(\rho)$, $D_{12}(\rho)$ and $D_{21}(\rho)$ depend on ρ and have appropriated dimensions.

Consider $\mathcal{K}$, the dynamic controller for the LPV system given by:

$$\mathcal{K}(\rho) : \left\{ \begin{array}{rcl} \dot{x}_K(t) & = & A_K(\rho)\, x_K(t) + B_K(\rho)\, y(t), \\ u(t) & = & C_K(\rho)\, x_K(t) + D_K(\rho)\, y(t), \end{array} \right. \tag{2.13}$$

where $x_K \in \mathbb{R}^n$ corresponds to the state vector of the controller, the matrices $A_K(\rho)$, $B_K(\rho)$, $C_K(\rho)$ et $D_K(\rho)$ depend on ρ and have appropriated dimensions.

Using $\mathcal{P}(\rho)$ and $\mathcal{K}(\rho)$ defined previously, the closed-loop transfer function $\mathcal{N}$ linking $w(t)$ and $z(t)$ is defined by:

$$\mathcal{N}(\rho) : \left\{ \begin{array}{rcl} \dot{x}_{cl}(t) & = & \mathbf{A}(\rho)\, x_{cl}(t) + \mathbf{B}(\rho)\, w(t), \\ z(t) & = & \mathbf{C}(\rho)\, x_{cl}(t) + \mathbf{D}(\rho)\, w(t), \end{array} \right. \tag{2.14}$$

$$\text{where: } \begin{cases} \mathbf{A}(\rho) &= \begin{pmatrix} A(\rho)+B_2(\rho)D_K(\rho)C_2(\rho) & B_2(\rho)C_K(\rho) \\ B_K(\rho)C_2\rho) & A_K(\rho) \end{pmatrix}, \\ \mathbf{B}(\rho) &= \begin{pmatrix} B_1(\rho)+B_2(\rho)D_K(\rho)D_{21}(\rho) \\ B_K(\rho)D_{21}(\rho) \end{pmatrix}, \\ \mathbf{C}(\rho) &= \begin{pmatrix} (C_1(\rho)+D_{12}(\rho)D_K(\rho)C_2(\rho) & D_{12}(\rho)C_K(\rho)) \end{pmatrix}, \\ \mathbf{D}(\rho) &= D_{11}(\rho)+D_{12}(\rho)D_K(\rho)D_{21}(\rho). \end{cases}$$

The synthesis for a LPV system is the same as for a LTI system and aims at finding a controller that minimizes $\|\mathcal{N}(\rho)\|_\infty$.

As previously, the bounded-real lemma is used to solve the problem. Then, $\mathcal{N}(\rho)$ is stable and the $\mathcal{H}_\infty$ norm of $\mathcal{N}(\rho)$ is smaller than γ if it exists a symmetric matrix P such that:

$$\begin{pmatrix} \mathbf{A}^T(\rho)\mathsf{P}+\mathsf{P}\mathbf{A}(\rho) & \mathsf{P}\mathbf{B}(\rho) & \mathbf{C}^T(\rho) \\ \mathbf{B}^T(\rho)\mathsf{P} & -\gamma I & \mathbf{D}^T(\rho) \\ \mathbf{C}(\rho) & \mathbf{D}(\rho) & -\gamma I \end{pmatrix} < 0,\ \mathsf{P} > 0 \tag{2.15}$$

Considering the fact that the first matrix inequality of (2.15) is not affine on the parameters, the convex optimization cannot be used and the variable change proposed in [Scherer et al., 1997] enables to come down to a LMI problem. Thus, the bounded-real lemma using the intermediate variables $\hat{A}(\rho)$, $\hat{B}(\rho)$, $\hat{C}(\rho)$, $\hat{D}(\rho)$, X and Y is expressed by:

$$\begin{cases} M_{11}(\rho) = A(\rho)X + XA^T(\rho) + B_2(\rho)\hat{C}(\rho) + (B_2(\rho)\hat{C}(\rho))^T, \\ M_{21}(\rho) = \hat{A}(\rho) + (A(\rho) + B_2(\rho)\hat{D}(\rho)C_2(\rho))^T, \\ M_{22}(\rho) = A^T(\rho)Y + YA(\rho) + \hat{B}(\rho)C_2(\rho) + (\hat{B}(\rho)C_2(\rho))^T, \\ M_{31}(\rho) = (B_1(\rho) + B_2(\rho)\hat{D}(\rho)D_{21}(\rho))^T, \\ M_{32}(\rho) = (YB_1(\rho) + \hat{B}(\rho)D_{21}(\rho))^T, \\ M_{41}(\rho) = C_1(\rho)X + D_{12}(\rho)\hat{C}(\rho), \\ M_{42}(\rho) = C_1(\rho) + D_{12}(\rho)\hat{D}(\rho)C_2(\rho), \\ M_{43}(\rho) = D_{11}(\rho) + D_{12}(\rho)\hat{D}(\rho)D_{21}(\rho). \end{cases} \tag{2.16}$$

The problem presented in equation (2.16) is an infinite dimension problem. Due to infinite values of the varying parameter ρ, an infinite number of LMI is obtained. Then, it is necessary to find a new formulation which permits to obtain a finite dimension problem. A usual method [Apkarian and Adams, 1998] is to consider the polytopic formulation of the LPV model.

The polytopic formulation of the LPV model requires two particular hypothesis. On the one hand, the state space matrices of the model (2.12) must have a linear dependency in the parameter ρ. On the other hand, the parameters of the vector ρ must be bounded such that $\rho(t) \in \mathcal{F}_\rho$ with $\mathcal{F}_\rho$ a compact set defined by $\mathcal{F}_\rho = \left\{\rho(.) \in \mathbb{R}^p : \underline{\rho_i} \leq \rho_i \leq \overline{\rho_i}, i = 1, \cdots, p\right\}$ where $\underline{\rho_i}$ and $\overline{\rho_i}$ are respectively the minimum and maximum allowable values.

Considering the polytopic LPV or q-LPV models, the system 2.12 can be expressed considering a polytopic approach by:

$$\mathcal{P}(\rho) = \sum_{i=1}^{N} \alpha_i(\rho) \begin{bmatrix} A(w_i) & B_1(w_i) & B_2(w_i) \\ C_1(w_i) & D_{11}(w_i) & B_{12}(w_i) \\ C_2(w_i) & D_{21}(w_i) & D_{22}(w_i) \end{bmatrix} \tag{2.17}$$

where w_i are the vertices of the polytope, N the number of vertices of the polytope and $\alpha_i \geq 0$ and $\sum_{i=1}^{N} \alpha_i = 1$. Then, a polytopic structure of the controller can be obtained such that:

$$\mathcal{K}(\rho) = \sum_{i=1}^{N} \alpha_i(\rho) \begin{bmatrix} A_K(w_i) & B_K(w_i) \\ C_K(w_i) & D_K(w_i) \end{bmatrix} \tag{2.18}$$

This formulation permits to obtain a finite dimension problem. The equation (2.5) is extended to LPV models on the polytopic form such that:

$$\begin{cases} \begin{pmatrix} M_{11}(w_i) & * & * & * \\ M_{21}(w_i) & M_{22}(w_i) & * & * \\ M_{31}(w_i) & M_{32}(w_i) & -\gamma I & * \\ M_{41}(w_i) & M_{42}(w_i) & M_{43}(w_i) & -\gamma I \end{pmatrix} < 0, \\ \begin{pmatrix} X & I \\ I & Y \end{pmatrix} > 0, \end{cases} \quad i = 1 \cdots N. \tag{2.19}$$

The different parameters of the controller are calculated such that the $N+1$ inequalities from (2.19) use the following definitions:

$$\begin{cases} M_{11}(w_i) = A(w_i)X + XA^T(w_i) + B_2(w_i)\hat{C}(w_i) + (B_2(w_i)\hat{C}(w_i))^T, \\ M_{21}(w_i) = \hat{A}(w_i) + (A(w_i) + B_2(w_i)\hat{D}(w_i)C_2(w_i))^T, \\ M_{22}(w_i) = A^T(w_i)Y + YA(w_i) + \hat{B}(w_i)C_2(w_i) + (\hat{B}(w_i)C_2(w_i))^T, \\ M_{31}(w_i) = (B_1(w_i) + B_2(w_i)\hat{D}(w_i)D_{21}(w_i))^T, \\ M_{32}(w_i) = (YB_1(w_i) + \hat{B}(w_i)D_{21}(w_i))^T, \\ M_{41}(w_i) = C_1(w_i)X + D_{12}(w_i)\hat{C}(w_i), \\ M_{42}(w_i) = C_1(w_i) + D_{12}(w_i)\hat{D}(w_i)C_2(w_i), \\ M_{43}(w_i) = D_{11}(w_i) + D_{12}(w_i)\hat{D}(w_i)D_{21}(w_i). \end{cases} \quad i = 1 \cdots N. \tag{2.20}$$

Finally, the N controllers expressed by the matrices at each vertex are defined by:

$$\begin{cases} D_K(w_i) &= \hat{D}(w_i), \\ C_K(w_i) &= (\hat{C}(w_i) - D_k(w_i)C_2(w_i)X)M^T, \\ B_K(w_i) &= N^{-1}(\hat{B}(w_i) - YB_2(w_i)D_K(w_i)), \\ A_K(w_i) &= N^{-1}(\hat{A}(w_i) - NB_K(w_i)C_2(w_i)X - YB_2(w_i)C_K(w_i)M^T - \cdots \\ & \quad \cdots - Y(A + B_2D_KC_2)X)M^{-T}. \end{cases} \tag{2.21}$$

Commentary The modern gain scheduling solution based on the polytopic formulation is a very powerful tool which helps to consider the non-linearities of the system in the control law. This technique allows to ensure internal stability of the control solution. Moreover, in this case, it is not required to grid the varying space but the choice of the polytope is very important. Its choice is a compromise between the number of vertices, which is directly linked to the number of $\mathcal{H}_\infty$ controllers and the way in which the polytope includes the parameter varying space: a bad polytope may introduce conservatism or the LMI solver cannot find a solution. The discussion concerning the definition of the polytope will be detailed in Chapter 4 through different examples.

2.2.4 Conclusion

This section presented the key notions which permit to apply, based on LMI, the $\mathcal{H}_\infty$ theory for LTI and LPV models . The application of this control theory is detailed in Chapter 4 through different examples where the NLG steering control is discussed.

Section 2.2 presented the design of robust controllers considering robust stability and robust performance notions. Indeed, this kind of controller is designed to cope with different operating points but it cannot always give satisfying results. To solve this problem, adaptive controllers are required such that their parameters may change with the changing operating conditions.

2.3 Adaptive control: theoretical aspects

2.3.1 Introduction

Since the sixties, there has been an exponential growth in adaptive control publications [Wang et al., 1995], [Astrom and Wittenmark, 1994] and [Sastry and Bodson, 1989]. A wide range of industrial and commercial systems need changing or updating feedback controllers $\mathcal{K}$ in order to adapt to the changing parameters of the system $\mathcal{S}$. Then, adaptive control aims at determining a suitable control law which is satisfactory over a wide range of operating points.

Adaptive control combines a priori knowledge of the system and an acquired on-line knowledge based on the observations of the system outputs. This knowledge helps to adjust automatically the parameters of the controller. There are two main approaches which help to design an adaptive controller:

- indirect adaptive approach,
- direct adaptive approach.

For the indirect solution, based on on-line observations or outputs measures, a model of the system is built and this model is then used to generate an appropriate controller. For the direct solution, the controller is built without the use of an intermediate model; the control law is estimated directly.

The more recent researches consider that the dynamics of the system are unknown and in this case, fuzzy systems or ANN models are used. An appropriate fuzzy system or an ANN which uses the inputs, the outputs and/or the states of the system gives the possibility to model the system. Then, the fuzzy or neural models are updated on-line and the controller is obtained based on an updated description of the system. Different kinds of controller structures are dealing with such considerations. For instance, several contributions consider fuzzy adaptive controllers based on backstepping [Yang et al., 2004], [Chen et al., 2007a] and [Chen et al., 2007b]. These solutions help to reduce the adapted on-line parameters and thus reduce the computation time of the algorithm. [Li and Tong, 2003] proposes an hybrid solution using $\mathcal{H}_\infty$ control to remove the influence of external disturbances. However, these solutions need a particular class of non-linear models (expressed in a strict feedback form), which is specific to particular systems. Finally, [Spooner and Passino, 1996] and [Calise et al., 2001] suggest fuzzy adaptive algorithms with no

restriction on the system structure. So, the ability of overcoming the uncertainties and time-varying dynamics of such an algorithm is well-suited for the shimmy phenomenon considered in Chapter 5.

The following sections present three different control solutions. The first two are based on state feedback solutions while the last has the advantage to be an output feedback solution. These different controllers will be used in Chapter 4 to damp the shimmy phenomenon. First, the two state feedback solutions, based on indirect and direct structures will be compared in Section 2.3.2. Then, considering the fact that the state feedback solutions are witnesses solutions, the obtained loss of performances with the output feedback solution presented in Section 2.3.3 is studied.

2.3.2 State feedback control

The considered model, in the frame of state feedback indirect and direct control theory is expressed by:

$$\begin{cases} \dot{x}(t) &= f(x) + g(x)u, \\ y(t) &= h(x), \end{cases} \tag{2.22}$$

where $x = [x_1, x_2, ..., x_n]^T \in \mathbb{R}^n$, $u \in \mathbb{R}$ and $y \in \mathbb{R}$ are respectively the system states, input and output; $f(x)$, $g(x)$ and $h(x)$ are smooth functions describing the dynamics of the system.

The common approach used with such model is the feedback linearisation ([Sastry and Bodson, 1989]) which aims at transforming a non-linear model into an equivalent linear one through a change of variables and the selection of a suitable control input. The non-linear model is converted such that the new states are the output y and its first derivatives. Thus, the concept of relative degree is used. For linear SISO model, the relative degree corresponds to the difference between the number of poles and zeros. For the considered non-linear model, "the model has relative degree r" means that the control input appears explicitly for the first time in the rth derivative of the output [Sonntag, 1998].

If the system has the relative degree of r ($r \leq n$), the first $r-1$ derivatives of the output y are independent of the input and its rth derivative can be expressed by:

$$y^{(r)} = a(x) + b(x)u \tag{2.23}$$

where $a(x) = L_f^r h(x)$ and $b(x) = L_g L_f^{r-1} h(x) \neq 0$ such that $L_f h(x) = \dfrac{dh(x)}{dx} f(x)$ is the Lie derivative of the function $h(x)$ with respect to $f(x)$ and $L_g h(x) = \dfrac{dh(x)}{dx} g(x)$ is the Lie derivative of the function $h(x)$ with respect to $g(x)$ [Sonntag, 1998].

For the particular case of the shimmy phenomenon, it could be seen in Section 3.3.3 that equation (2.23) can be simplified and written with a constant value $b(x) = B$ such that:

$$y^{(r)} = a(x) + Bu \tag{2.24}$$

2.3.2.1 Indirect fuzzy adaptive control

The block diagram of the indirect fuzzy adaptive controller, initially proposed in [Spooner and Passino, 1996] is presented in Figure 2.5.

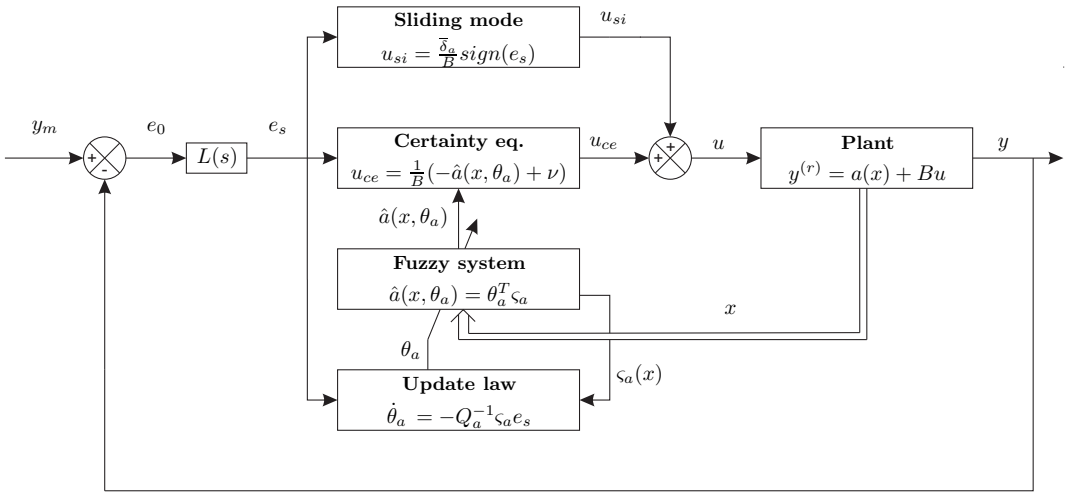

Figure 2.5: Indirect fuzzy adaptive control scheme

The plant is represented by equation (2.24). In this strategy, the states x of the system are used to estimate the dynamics $\hat{a}(x)$ through a fuzzy system in which the outputs of the rules θ_a is adapted using an update law. The control signal u is composed of the certainty equivalence control term u_{ce} based on the estimated system dynamics $\hat{a}(x)$ and the so called "sliding mode" term u_{si} [Khalil, 2002]. The latter helps to overcome the estimation error of the fuzzy system.

The certainty equivalence control term is used to estimate the feedback linearisation control term ; it is defined such that the output of the system follows the reference y_m and such that the error $e_0 = y_m - y$ decreases exponentially:

$$u_{ce} = \frac{1}{B}\left(-\hat{a}(x,\theta_a) + \nu\right) \tag{2.25}$$

where $\nu(t) := y_m^{(r)} + \eta e_s + \overline{e}_s$ and $\overline{e}_s := \dot{e}_s - e_o^{(r)}$. The tracking error e_s is defined as $e_s := k^T e$ with $e := [e_0\ \dot{e}_0\ \ldots\ e_0^{(r-1)}]$, $k := [k_0\ \ldots\ k_{r-2}\ 1]$.
The elements of k are chosen such that $L(s) := s^{r-1} + k_{r-2}s^{r-2} + \ldots + k_1 s + k_0$ is Hurwitz.

In this indirect fuzzy adaptive algorithm, $a(x)$ is an unknown non-linear function which must be estimated to calculate the feedback linearisation control law. In this situation, the fuzzy system helps to estimate this unknown function based on the following equation:

$$\hat{a}(x,\theta_a) = \theta_a^T \varsigma_a \tag{2.26}$$

where $\theta_a^T := \left[\theta_{a_1} \ldots \theta_{a_p}\right]$ and $\varsigma_a^T := \left[\mu_{a_1} \ldots \mu_{a_p}\right] / \left[\sum_{i=1}^{p} \mu_{a_i}\right]$. Moreover, the unknown function $a(x)$ can be formulated as follows:

$$a(x) = \theta_a^{*T} \varsigma_a + \delta_a(x) \tag{2.27}$$

where $\delta_a(x)$ is the optimal approximation error of $a(x)$ by the fuzzy system and θ_a^* is the best value of the parameter θ_a:

$$\theta_a^* := \arg\min_{\theta_a} \left[\sup_x \left|\theta_a^T \varsigma_a - a(x)\right|\right] \tag{2.28}$$

It is thus possible to prove that the fuzzy system can approximate a smooth non-linear function with arbitrary small error if the number of fuzzy rules is large enough [Kosko, 1994]. The

parameter error vector $\tilde{\theta}_a(t)$ represents the difference between the current estimated parameter and the best value of this parameter and is defined by:

$$\tilde{\theta}_a(t) = \theta_a(t) - \theta_a^*. \tag{2.29}$$

The estimation of the function $\hat{a}(x, \theta_a)$ in equation (4.3) needs to be updated in order to follow the system dynamics and the variations induced by external perturbations. Then, the parameter θ_a of the fuzzy system is updated such that:

$$\dot{\theta}_a = -Q_a^{-1} \varsigma_a e_s \tag{2.30}$$

with $Q_a \in \mathbb{R}^{p \times p}$ a square positive semi-definite matrix which helps to vary the adaptation speed of the fuzzy system. The sliding mode control term u_{si} is chosen to ensure the stability of the control law and is expressed by:

$$u_{si} = \frac{\overline{\delta}_a}{B} sign(e_s) \tag{2.31}$$

The constant $\overline{\delta}_a \in \mathbb{R}$ is defined such that the estimation error $\delta_a(x)$ is bounded:

$$|\delta_a(x)| \leq \overline{\delta}_a \tag{2.32}$$

In equation (2.32), $\overline{\delta}_a$ represents a known bound of the error estimation related to the fuzzy system. Since the fuzzy system is an universal approximator, it is considered that $\delta_a(x)$ remains arbitrarily small, if an appropriate fuzzy system with an arbitrarily large number of rules is chosen. Finally, $|\delta_a(x)|$ can be bounded by $\overline{\delta}_a$ and this term is used in this control law to counteract the modelling error between the real non-linear function $a(x)$ and its estimate $\hat{a}(x, \theta_a)$.

Considering the context of our project, aeronautical constraints are very strict and it is fundamental to ensure that the control solution is stable. The stability proof of the indirect state feedback controller can be found in [Spooner and Passino, 1996] and in Appendix B . The main properties of an indirect fuzzy adaptive controller are then presented in the following theorem.

Theorem 1 *Stability and tracking error results for the state feedback indirect fuzzy adaptive control solution:*
Considering the system defined in (2.22), the control signals defined in (2.25), (2.31) and assuming the following:

- ***A1****: the error estimation due to the fuzzy system is bounded (2.32).*

It can be concluded that:

- ***C1****: the plant output and its derivatives up to (r-1) order are bounded;*
- ***C2****: the control signal is bounded;*
- ***C3****: the output error e_0 will converge to zero.*

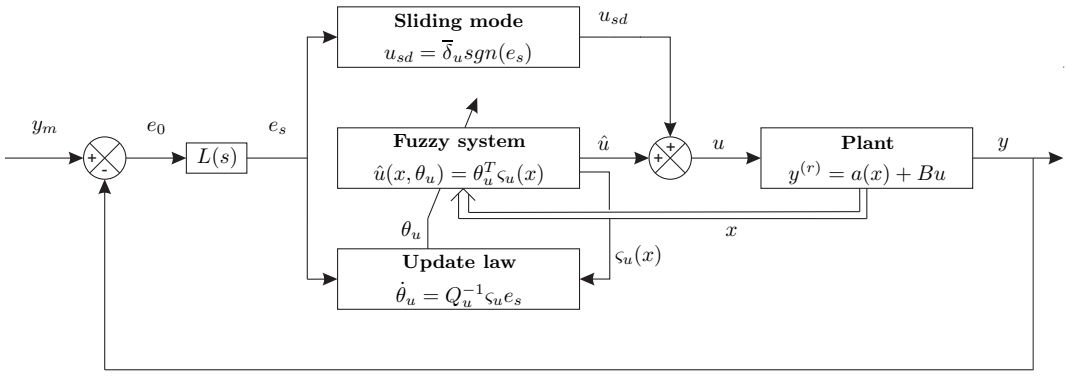

Figure 2.6: Direct fuzzy adaptive control scheme

2.3.2.2 Direct fuzzy adaptive control

The block diagram of the direct fuzzy adaptive controller, initially proposed in [Spooner and Passino, 1996] is presented in Figure 2.6.

In this strategy, there is no need to estimate the dynamics of the plant; the fuzzy system, adapted with an update law, is used to estimate the control signal $\hat{u}$ directly. As for the indirect solution, a sliding mode signal u_{sd} helps to overcome the estimation error of the fuzzy system. The control signal u is based on the estimated certainty equivalence control term $\hat{u}$ and the sliding mode term u_{sd} such that:

$$u = \hat{u} + u_{sd} \tag{2.33}$$

On the assumption that function $a(x)$ and constant B, describing the system dynamics are unknown, the ideal feedback linear control law cannot be implemented. Instead, this control term is approximated by a universal approximator, here a fuzzy system, of the following form:

$$\hat{u}(x, \theta_u) = \theta_u^T \varsigma_u \tag{2.34}$$

Moreover, the unknown function $u(x)$ can be formulated as follows:

$$u(x) = \theta_u^{*T} \varsigma_u + \delta_u(x) \tag{2.35}$$

where $\delta_u(x)$ is the optimal approximation error of $u(x)$ by the fuzzy system and θ_u^* is the best value of the parameter θ_u:

$$\theta_u^* := \arg \min_{\theta_u} \left[\sup_x \left| \theta_u^T \varsigma_u - u(x) \right| \right] \tag{2.36}$$

The parameter error vector $\tilde{\theta}_u(t)$ represents the difference between the current estimated parameter and the best value of this parameter and is defined by:

$$\tilde{\theta}_u(t) = \theta_u(t) - \theta_u^* \tag{2.37}$$

The estimation of the function $\hat{u}$ needs to be updated to take account of the possible changes in the system behavior due to time varying parameters. Then, the following fuzzy system update law is chosen:

$$\dot{\theta}_u = Q_u^{-1} \varsigma_u e_s \tag{2.38}$$

with $Q_u \in \mathbb{R}^{p \times p}$ a square positive semi-definite matrix.

The sliding mode control term which helps to overcome the approximation error of the fuzzy system and ensures the stability of the control loop, is expressed as:

$$u_{sd} = \overline{\delta}_u sign(e_s) \tag{2.39}$$

The constant $\overline{\delta}_u \in \mathbb{R}$ is defined such that:

$$|\delta_u(x)| \leq \overline{\delta}_u \tag{2.40}$$

It represents a known bound of the error estimation due to the fuzzy system.

The main properties of the direct fuzzy adaptive controller are presented in the following theorem and the stability proof can be found in [Spooner and Passino, 1996] and in Appendix B .

Theorem 2 *Stability and tracking error results for the state feedback direct fuzzy adaptive control solution:*
Considering the system defined in (2.22), the control signal defined in (2.33), (2.34), (2.39) and assuming the following:

- ***A1**: the error estimation due to the fuzzy system is bounded, so* $|\delta_u(x)| \leq \overline{\delta}_u$.

It can be concluded that:

- ***C1**: the plant output and its derivatives up to (r-1) order are bounded;*
- ***C2**: the control signal is bounded;*
- ***C3**: the output error* e_0 *will converge to zero.*

2.3.3 Output feedback control

The main drawback of state feedback controllers is the need to feedback all the states of the system, compared to output controllers, which only require the knowledge of the output. Then, this section proposes a fuzzy adaptive control solution which will be used to damp the shimmy oscillations in Section 4.3.4, based exclusively on the output measurements.

The block diagram of the output feedback control solution, initially proposed in [Calise et al., 2001] is presented in Figure 2.7. It can be shown that the plant is controlled based on an output feedback control signal which is produce by the use of the invert approximation of the plant dynamic. This latter requires as input the signal v and the system output y. v is obtained with the fuzzy approximation and its update law, with a linear compensator that produces v_{dc} and with the r derivative of the reference.

The considered model in the frame of output feedback control solutions is the non-linear model presented in equation (1.16). Then, the objective of the output feedback control solution is to design a feedback control law to drive the system output y tracking a reference output y_m.

Let $\hat{h}(y, u)$ be the best available approximation of the following function

$$y^{(r)} = h_r(x, u). \tag{2.41}$$

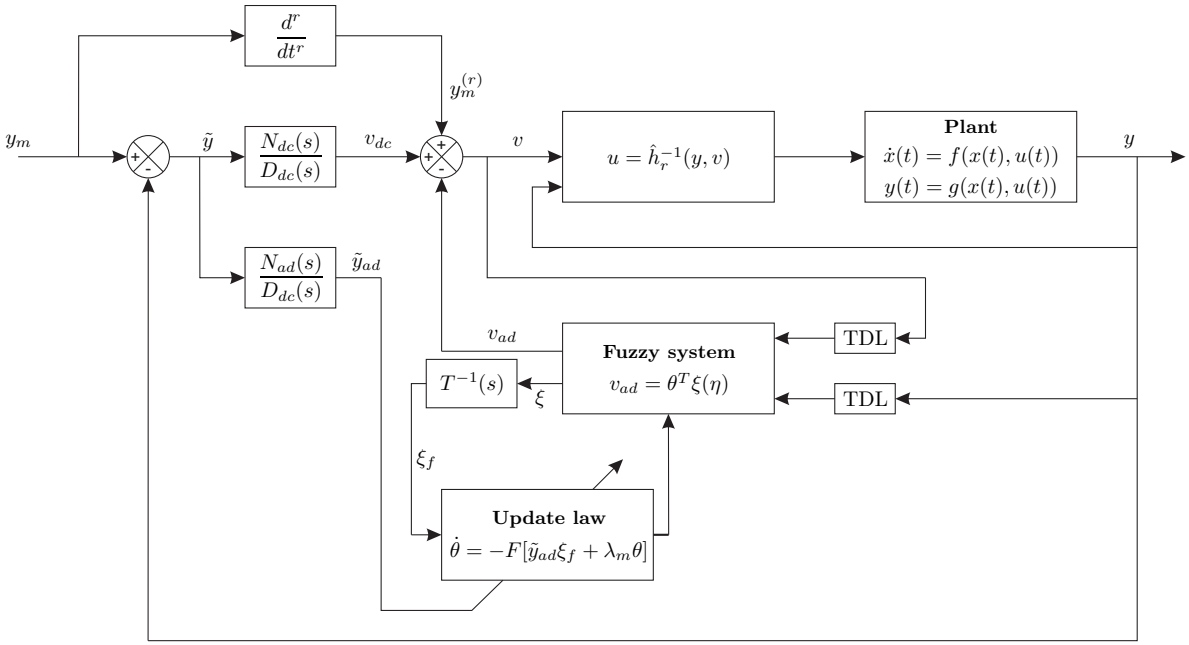

Figure 2.7: Fuzzy adaptive output feedback control diagram

Suppose that $\hat{h}(y, u)$ is invertible according to u. The feedback linearisation control law is:

$$u = \hat{h}_r^{-1}(y, v) \tag{2.42}$$

where v is commonly referred to a pseudo control. Substitute equation (2.42) into equation (2.41), it is possible to write:

$$y^{(r)} = v + \Delta \tag{2.43}$$

Where Δ is the approximation error:

$$\Delta(x, v) = h_r(x, \hat{h}_r^{-1}(y, v)) - \hat{h}_r(y, \hat{h}_r^{-1}(y, v)) \tag{2.44}$$

The pseudo control signal is chosen as [Calise et al., 2001]:

$$v = y_m^{(r)} + v_{dc} - v_{ad} \tag{2.45}$$

where $y_m^{(r)}$ is the rth derivative of the input signal, v_{dc} is the output of a linear compensator and v_{ad} is the adaptive control signal. Let $\tilde{y} = y_m - y$ be the output error, then the error dynamics of the closed-loop system can be written as

$$\tilde{y}^{(r)} = -v_{dc} + v_{ad} - \Delta \tag{2.46}$$

The adaptive term v_{ad} is designed to eliminate the approximation error δ, and the linear control term v_{dc} is designed such that the output error dynamics meets the performance requirement. The linear compensator presented in Figure 2.8 is defined as:

$$v_{dc}(s) = \frac{N_{dc}(s)}{D_{dc}(s)} \tilde{y}(s) \tag{2.47}$$

$$\tilde{y}_{ad}(s) = \frac{N_{ad}(s)}{D_{dc}(s)} \tilde{y}(s) \tag{2.48}$$

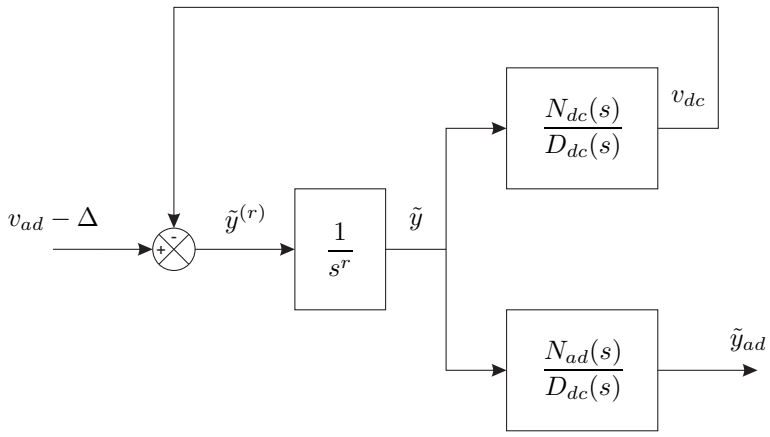

Figure 2.8: Linear compensator block diagram

where the polynomial $D_{dc}(s)$ is chosen such that all its roots are located in the open left half plane of the complex s-plane. The input-output relationship of the system shown in Figure 2.8 is:

$$\tilde{y}_{ad}(s) = G(s)(v_{ad} - \Delta)(s) \tag{2.49}$$

where G(s) is the closed-loop transfer function

$$G(s) = \frac{N_{ad}(s)}{s^r D_{dc}(s) + N_{dc}(s)} \tag{2.50}$$

Because $G(s)$ must be stable, the Routh-Hurwitz stability necessary criterion implies that the degree of the polynomials $N_{dc}(s)$ and $D_{dc}(s)$ must satisfy:

$$\deg(D_{dc}(s)) \geq \deg(N_{dc}(s)) \geq r - 1 \tag{2.51}$$

The adaptive term v_{ad} is implemented by a fuzzy system with tunable parameters in the conclusions. The input vector η of the fuzzy system consists of time delays (TDL) of the pseudo input $v(t)$ and the system output $y(t)$ as following:

$$\eta = [v(t), v(t-d), \ldots, v(t-(n_1-r-1)d), y(t), y(t-d), \ldots, y(t-(n_1-1)d)]^T \tag{2.52}$$

where n_1 is a constant satisfying $n_1 \geq n$ with n the dimension of the state vector x. The fuzzy system corresponds to the one presented in Section 1.3.4 and consists of fuzzy rules of the form:

$$\textbf{If } (\eta_1 \text{ is } \tilde{F}_{i1} \textbf{ and } \cdots \textbf{and } \eta_m \text{ is } \tilde{F}_{im}) \textbf{ Then } v_{ad} = \theta_i \tag{2.53}$$

where m is the number of input, $\tilde{F}_{ij}$ is the fuzzy set of input variable j used in rule i ($i = 1, \cdots, K$). The output of the fuzzy system can be expressed as:

$$v_{ad} = \theta^T \xi(\eta) \tag{2.54}$$

where $\xi(\eta)$ is the true degree of fuzzy rule's condition; θ consists of the parameters of the fuzzy rule's conclusion:

$$\theta = [\theta_1, \theta_2, \ldots, \theta_K]^T \tag{2.55}$$

$$\xi(\eta) = [\xi_1(\eta), \xi_2(\eta), \ldots, \xi_K(\eta)]^T \tag{2.56}$$

$$\xi_i(\eta) = \frac{\prod_{j=1}^{m} \mu_{ij}(\eta_j)}{\sum_{i=1}^{K} \prod_{j=1}^{m} \mu_{ij}(\eta_j)} \tag{2.57}$$

Since the function Δ is approximated by a fuzzy system with limited number of rules, an approximation error exists in general cases. Let $\xi_i(\eta)$ be the structure error, the function Δ can be expressed as follow:

$$\Delta = \theta^{*T}\xi(\eta) + \varepsilon(\eta) \tag{2.58}$$

Assume that the structure error is bounded, meaning that there is a constant ε^* such that:

$$|\varepsilon(\eta)| \leq \varepsilon^* \tag{2.59}$$

Substituting equations (2.54) and (2.58) into equation (2.49), $\tilde{y}_{ad}(s)$ becomes:

$$\tilde{y}_{ad}(s) = G(s)(\tilde{\theta}^T\xi - \varepsilon)(s) \tag{2.60}$$

where $\tilde{\theta} = \theta - \theta^*$ represents the difference between the current estimated parameter and the best value of this parameter. The filtered error $\tilde{y}_{ad}(s)$ is used in the adaptive rule as it will be seen latter in this section. For the adaptation rule to be realizable, i.e. dependent on available data only, the transfer function $G(s)$ must be strictly positive real (SPR). However, the relative degree of $G(s)$ is at least r. When the relative degree of $G(s)$ is one, it can be made SPR by a proper design of $N_{ad}(s)$. If $r > 1$, $G(s)$ cannot be SPR. To achieve SPR in the $r > 1$ case, a low pass filter $T^{-1}(s)$ is introduced into equation (2.60):

$$\tilde{y}_{ad}(s) = G(s)T(s)(\tilde{\theta}^T\xi_f + \delta - \varepsilon_f)(s) \tag{2.61}$$

Where ξ_f and ε_f are the signals ξ and ε, respectively, after being filtered through $T^{-1}(s)$, and δ is the mismatch term given by

$$\delta(s) = T^{-1}(s)(\tilde{\theta}^T\xi) - \tilde{\theta}^{T^T}\xi_f \tag{2.62}$$

that can be bounded as

$$\|\delta\| \leq c\left\|\tilde{W}\right\| \tag{2.63}$$

The polynomials $T(s)$ and $N_{ad}(s)$ are Hurwitz, they are chosen such that $\bar{G}(s) = G(s)T(s)$ is strictly positive real (SPR). Assume that $\bar{G}(s)$ can be expressed as:

$$\bar{G}(s) = \frac{N_{ad}(s)T(s)}{s^r D_{dc}(s) + N_{dc}(s)} = \frac{b_1 s^{p-1} + b_2 s^{p-2} + ... + b_p}{s^p + a_1 s^{p-1} + ... + a_p} \tag{2.64}$$

where $p = q + r$. A simple way to design $T(s)$ and $N_{ad}(s)$ ensuring the SPR property of $\bar{G}(s)$ is the zero placement approach. Since the polynomials $D_{dc}(s)$ and $N_{dc}(s)$ are chosen before, according to equation (2.64) the poles of $\bar{G}(s)$ are known. The polynomials $T(s)$ and $N_{ad}(s)$ are freely chosen such that the zeros of $\bar{G}(s)$ are placed interlacing with its poles to ensure that the Bode plot of $\bar{G}(s)$ is in the range ± 90. The adaptive rule is defined as:

$$\dot{\theta} = -F[\tilde{y}_{ad}\xi_f + \lambda_m\theta] \tag{2.65}$$

where F is a positive definite matrix and m is a positive constant.

The properties of the output feedback adaptive controller are presented in the following theorem and the stability proof can be found in [Calise et al., 2001].

Theorem 3 *Stability and tracking error results for the output feedback control solution: Considering the system defined in equation (1.16), the control signal defined in equation (2.42) and assuming the following:*

- ***A1**: the only measurement available for feedback is the output $y(t)$;*
- ***A2**: the reference output $y_m(t)$ and its derivatives up to the rth order are measurable and bounded;*
- ***A3**: the transfer function between the output error $\tilde{y}$ and the filtered output error $\tilde{y}_{ad}$ is stable.*

It can be concluded that:

- ***C1**: the described output feedback adaptive control system is stable;*
- ***C2**: the signal $\tilde{y}_{ad}$ and $\tilde{\theta}$ are uniform ultimate bounded;*
- ***C3**: $\tilde{y}$ is bounded.*

2.3.4 Conclusion

This section presented three control laws based on fuzzy adaptive control. While the two first proposed adaptive laws of Section 2.3.2 require the measure of all the states of the system, the last algorithm detailed in Section 2.3.3 has the advantage to exclusively takes account of the outputs of the system to built the control signal. These different control solutions will be used in Chapter 4, where it is shown that fuzzy adaptive control solutions give the possibility to damp the shimmy phenomenon.

2.4 Model predictive control (MPC): theoretical aspects

2.4.1 Introduction

In this section, a short introduction presenting the historical background of model predictive control (MPC) is done. Then, the general principle of MPC, divided in successive actions is described. Finally, the limits of non-linear predictive control are introduced and solutions to cope with are proposed.

Nowadays, the success of MPC is undeniable. Two main arguments may explain this success. On the one hand, the simplicity of the control strategy is an important advantage. The different steps that constitute an MPC are similar to a human decision taking. When a human takes a decision, he observes his environment to define an action and its effect. Then, by inverting this purpose, he is able to find the action required to obtain the desired behaviour. On the other hand, this control strategy gives the possibility to handle constraints and non-linearities in a rigorous way. Despite important calculation efforts, the non-linearities of the system are taken into account insofar as the description of the system evolution is used to obtain the optimal control input.

2.4.2 General principle of model predictive control

2.4.2.1 Steps of predictive control

The general principle of MPC is the resolution, at each sample-time, of a finite horizon open-loop optimal control problem to compute the control input. The optimization step helps to obtain an optimal control input sequence and the first value of this sequence is applied to the system. Then, the principle of MPC is based on five steps which are performed successively at each sample time:

- prediction of the system evolution,
- definition of the trajectory,
- definition of the cost criterion,
- minimization of the cost criterion,
- application of the first term of the optimal solution.

Prediction of the system evolution

The first step consists in predicting the system output using the knowledge of the system dynamics response. This knowledge helps to predict the future evolution of the system up to a limited prediction horizon N_p. The prediction may be done by using a linear or non-linear model; a black, grey or white box model.

Definition of the reference

The reference trajectory corresponds to the trajectory that must be followed by the system. Two solutions help to define this reference. On the one hand, if the trajectory is a priori defined, it is directly used as the reference trajectory. On the other hand, if only the final point is known, a smooth reference trajectory is built based on a reference model.

Definition of the cost criterion

The cost criterion is commonly composed of two terms. The first corresponds to the sum of the quadratic errors between the reference trajectory and the predicted outputs of the model. The second describes the limitation of the control signal. In the case of a SISO system, at time k, the cost criterion $J(k)$ is expressed by:

$$J(k) = Q \sum_{n=1}^{Np} (\hat{y}(k+n) - y_{ref}(k+n))^2 + R \sum_{n=0}^{Nc} u(k+n)^2 \tag{2.66}$$

with Q and R the weighting factors on the output error and the control input, $\hat{y}$ the predicted output, y_{ref} the reference trajectory, u the control signal, N_p the prediction horizon and N_c the control horizon. N_c is defined such that $N_c \leq N_p$ and beyond N_c, $u(k+n)$ is constant and is defined by $u(k+n) = u(k+N_c)$.

Minimization of the cost criterion

The minimization of the criterion $J(k)$ gives the optimal control input sequence. Without constraint and considering a prediction based on a linear model, it is possible to solve the optimization problem analytically by using a QR decomposition [Maciejowski, 2000]. For the general case, the minimization is described by:

$$\begin{aligned} &\min_{U} J(k) \\ &\text{respecting } \mathscr{C} \end{aligned} \tag{2.67}$$

with the constraints $\mathscr{C}$ defined by:

$$\mathscr{C} : \begin{cases} u_{min} \leq u(k+n) \leq u_{max} \ \forall k \in [1, N_c] \\ \hat{y}_{min} \leq \hat{y}(k+n) \leq \hat{y}_{max} \ \forall k \in [1, N_p] \\ \hat{x}_{min} \leq \hat{x}(k+n) \leq \hat{x}_{max} \ \forall k \in [1, N_p] \end{cases} \tag{2.68}$$

such that $\hat{x}$ corresponds to the estimated state of the system.

Application of the first term of the optimal solution

The first term of the optimal control sequence is applied on the system.

Finally the different signals which are involved in the frame of MPC are detailed in Figure 2.9.

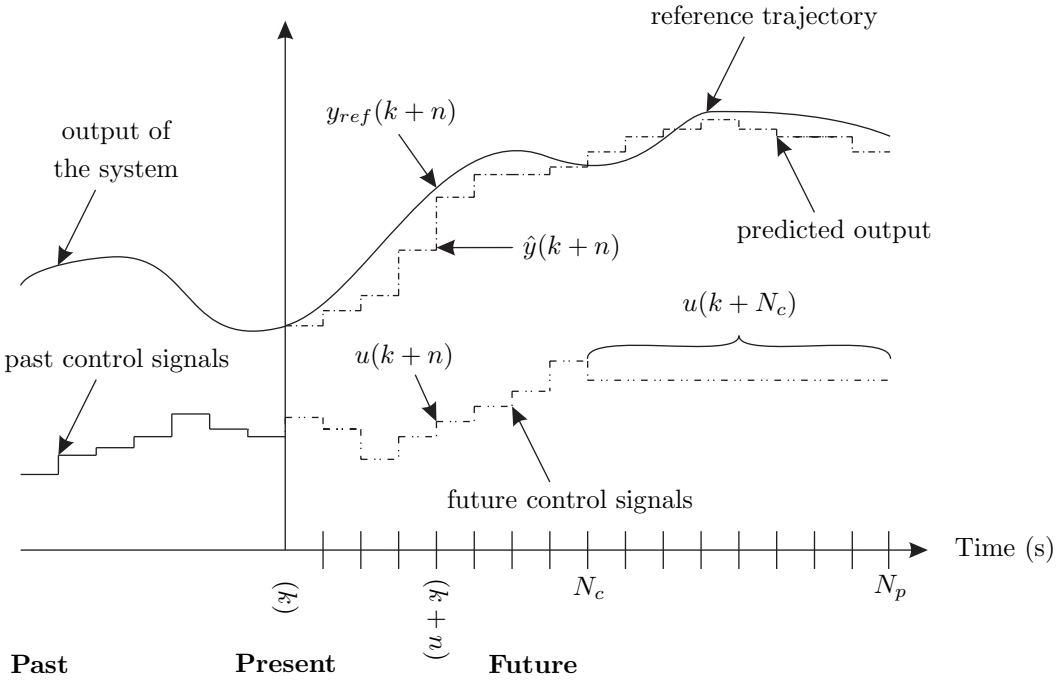

Figure 2.9: Definition of the signals used for MPC

2.4.2.2 Tuning of MPC parameters

The tuning of the parameters is an important task for the development of the control solution. Similarly to other control solutions, just few methods in the literature help to find the most

appropriate parameters. For example, [Han et al., 2006] and [Kawai et al., 2007] propose an automatic tuning for MPC. The aim of this section is to present the parameters that could be tuned and their influence on the closed loop behaviour.

The main parameters that are used for the tuning of the control solution are:

- N_p, the prediction horizon. This tuning parameter represents the number of future controlled variables involved in the performance objective. A large value of N_p leads to the improvement of the stability and the robustness of the closed-loop, but sacrifices the rapidity. N_p is chosen in relation to the response time of the system such that sufficient information is included in the cost criteria and no excessive and useless information increase the calculation time.

- N_c, the control horizon. This tuning parameter determines the number of control actions that are calculated in the optimization step. A large value of N_c induces excessive control action while a small value of N_c smooths the control action. Moreover, computational effort is reduced when the value of the control horizon is small.

- R, the weighting on the control input. This tuning parameter helps to scale the acceptable error. If R is small, the control signal will be very important and instability of the control law may appear. If R is important, only small control signals will be obtained.

- Q, the weighting on the output error. This tuning parameter has the opposite effect than the weighting on the control. For the tuning of the control solution, it seems interesting to fix one of the two weights and let the other vaies.

- $\mathscr{C}$, the constraint that the control law has to respect. Three main constraints are available. The constraint on the output estimation ($\hat{y}_{min}$ and $\hat{y}_{max}$), the constraint on the input (u_{min} and u_{max}) and the constraint on the estimated states ($\hat{x}_{min}$ and $\hat{x}_{max}$). For instance, in the case of trajectory tracking, the constraint on the input permits to limit the maximum value of the wheel angle and to prevent from mechanical damages of the steering column. Moreover, in the case of A/C applications, it could be possible to limit the nose landing gear slip angle by including constraints on the estimated states of the system.

- T_e, the sample time. The sample time limits the calculation time. For calculation aspects, it is preferable to work with a long sample time. However, this choice has to respect the Shannon theorem.

Chapter 5, which is dedicated to the application of the MPC for trajectory tracking underlines the importance of the different parameters. A trial error method has been used to find the most acceptable values for the proposed parameters. Particularly, it will be seen that the value of the weighting on the input R is very important.

2.4.3 NMPC limitations and solutions to cope with

When the system is subjected to strong non-linearities, it is well-known that non-linear control offers distinct advantages. In these cases, the use of Non-linear Model Predictive Control (NMPC)

is significant enough. Currently, this control strategy has been applied for a lot of applications ([Santos et al., 2001], [Qin and Badgwell, 2000], ...) but many drawbacks make it difficult to use:

- a detailed description of the system is needed to apply the NMPC and the identification of non-linear models is still difficult to obtain;
- the algorithm which helps to determine the optimal control sequence is very complex for the case of non-linear systems and despite significant computation infrastructure, the solution can be computationally intensive for on-line implementation [Borrelli et al., 2005];
- stability results are difficult to obtain, an infinite prediction horizon or a terminal state constraint are required [Qin and Badgwell, 2003].

Considering the limits of the NMPC, three main solutions help to integrate a non-linear behaviour of the controller:

- MPC based on LTV models,
- successive linearisation of non-linear models [Colin et al., 2007],
- approximation of non-linear systems by PWA models [Pena et al., 2005], [Schutter and Boom, 2004].

2.4.3.1 MPC based on LTV model

This section presents the possibility to introduce a non-linear behaviour of the MPC strategy by using an LTV model for the prediction. It is obvious that the proposed strategy may be easily adapted for LPV or q-LPV models. Considering the LTV model presented in equation (1.11), its discretisation with the assumption that the matrix $D = 0$, is expressed with the realization $(A_d,\, B_d,\, C_d)$ by:

$$\left\{ \begin{array}{rcl} x(k+1) & = & A_d(k)\, x(k) + B_d(k)\, u(k), \\ y(k) & = & C_d(k)\, x(k), \end{array} \right. \tag{2.69}$$

At each sample time k, the predictions are expressed by the use of the state space matrices. In other words, the estimation of the outputs $\hat{Y}(k) = [\hat{y}(k+1), \hat{y}(k+2), \cdots, \hat{y}(k+N_p)]$ is obtained with the three matrices $A_d(k)$, $B_d(k)$ and $C_d(k)$. Then, the vector of output estimations is described by the use of $x(k)$ and the vector of inputs $U = [u(k), u(k+1), \cdots, u(k+N_p-1)]$:

$$\hat{Y}(k) = \Psi(k)x(k) + \Theta(k)U \tag{2.70}$$

such that:

$$\Psi(k) = \left[\begin{array}{c} C_d(k)A_d(k) \\ C_d(k)A_d(k)^2 \\ \vdots \\ C_d(k)A_d(k)^{N_p} \end{array} \right] \tag{2.71}$$

and

$$\Theta(k) = \begin{bmatrix} C_d(k)B_d(k) & 0 & \dots & 0 \\ C_d(k)A_d(k)B_d(k) & C_d(k)B_d(k) & 0 & \vdots \\ \vdots & C_d(k)A_d(k)B_d(k) & \ddots & \vdots \\ \vdots & \vdots & \ddots & \vdots \\ C_d(k)A_d(k)^{N_u-1}B_d(k) & \cdots & \cdots & C_d(k)B_d(k) \\ \vdots & \vdots & \vdots & \vdots \\ C_d(k)A_d(k)^{N_p-1}B_d(k) & \cdots & \cdots & C_d(k)\sum_{i=0}^{N_p-N_u} A_d(k)^i B_d(k) \end{bmatrix} \tag{2.72}$$

Then, the cost criterion can be written as:

$$J(k) = (\hat{Y}(k) - Y_{ref})^T Q(\hat{Y}(k) - Y_{ref}) + U^T R U \tag{2.73}$$

with $Y_{ref} = [y_{ref}(k+1), y_{ref}(k+2), \cdots, y_{ref}(k+N_p)]$.

Thus, the minimization problem becomes:

$$\min_U U^T(\Theta(k)^T S_Q^T + S_R^T)(S_Q\Theta(k) + S_R)U + (x(k)^T\Psi(k)^T - Y_{ref}^T)Q(\Psi(k)x(k) - Y_{ref}) \quad \text{respecting } \mathscr{C} \tag{2.74}$$

such that $S_Q^T S_Q = Q$ and $S_R^T S_R = R$.

2.4.3.2 MPC based on successive linearisation

Considering a non-linear model of the system described by the equation (1.16). This model is difficult to use in the frame of MPC. Then, the simplest way to deal with it, is to perform successive linearisation around an operating point. The local linearisation helps to obtain a linear formulation which can be solved by the use of Quadratic Programming (QP) techniques.

The non-linear model presented in equation (1.16) or the ANN described in Section 1.3.3 which are used for the prediction of the system evolution can be both described by their output such that:

$$\hat{y}(k+1) = f(y(k), u(k)) \tag{2.75}$$

Around an operating point O defined by $O = (y_0, u_0)$, the output is linearised such that

$$\hat{y}(k+1) = a_0(k) + b_0(k)y(k) + c_0(k)u(k) \tag{2.76}$$

with:

$$\begin{cases} a_0(k) = f|_0 - \left.\dfrac{\partial f}{\partial y(k)}\right|_0 y_0 - \left.\dfrac{\partial f}{\partial u(k)}\right|_0 u_0 \\ b_0(k) = \left.\dfrac{\partial f}{\partial y(k)}\right|_0 \\ c_0(k) = \left.\dfrac{\partial f}{\partial u(k)}\right|_0 \end{cases} \tag{2.77}$$

At each sample time k, the predictions are expressed by the use of the state space matrices. In other words, the estimation of the outputs $\hat{Y}(k) = [\hat{y}(k+1), \hat{y}(k+2), \cdots, \hat{y}(k+N_p)]$ are obtained

with the three expressions $a_0(k)$, $b_0(k)$ and $c_0(k)$. Then, the vector of output estimations is described by the use of the $y(k)$ and the vector of inputs $U = [u(k), u(k+1), \cdots, u(k+N_p-1)]$:

$$\hat{Y}(k) = \Psi(k) + \Gamma(k)y(k) + \Theta(k)U \tag{2.78}$$

such that:

$$\Psi(k) = \begin{bmatrix} a_0(k) \\ a_0(k) + a_0(k)b_0(k) \\ \vdots \\ a_0(k) + \sum_{i=0}^{N_p-1} b_0(k)^j \end{bmatrix} \tag{2.79}$$

$$\Gamma(k) = \begin{bmatrix} b_0(k) \\ b_0(k)^2 \\ \vdots \\ b_0(k)^{N_p} \end{bmatrix} \tag{2.80}$$

and

$$\Theta(k) = \begin{bmatrix} c_0(k) & 0 & . & 0 \\ b_0(k)c_0(k) & c_0(k) & 0 & . \\ \vdots & \ddots & \ddots & 0 \\ \vdots & \ddots & \ddots & 0 \\ b_0(k)^{N_p-1} & \cdots & b_0(k)c_0(k) & c_0(k) \end{bmatrix} \tag{2.81}$$

Similarly to equation (2.73), the cost criterion can be written as:

$$J(k) = (\hat{Y}(k) - Y_{ref})^T Q(\hat{Y}(k) - Y_{ref}) + U^T RU \tag{2.82}$$

Thus, the minimisation problem becomes:

$$\begin{gathered} \min_U U^T(\Theta(k)^T S_Q^T + S_R^T)(S_Q\Theta(k) + S_R)U + \cdots \\ (\Psi(k)^T + y(k)^T\Gamma(k)^T - Y_{ref}^T)Q(\Psi(k) + \Gamma(k)y(k) - Y_{ref}) \\ \text{respecting } \mathscr{C} \end{gathered} \tag{2.83}$$

such that $S_Q^T S_Q = Q$ and $S_R^T S_R = R$.

2.4.3.3 MPC based on PWA model

The main drawback of the two previous MPC solutions (MPC based on LTV model and MPC based on successive linearisation) is the fact that the prediction uses a linear modelling of the system. The non-linear characteristic of the control law is obtained by changing from one linear modelling to another at each sample time. Considering a long prediction horizon or a non-linear system that is not particularly smooth, it could be required to take account of the non-linear evolution of the system during the prediction step. For this purpose, MPC based on PWA model is an interesting compromise. The prediction is based on a set of linear model and the optimization step is still performed by the use of QP programming coupling with a particular

strategy which considers the possible evolution of the model in the polyhedral partition of the state-input space.

Considering the PWA model description presented in Section 1.3.2.4, the estimation of the outputs $\hat{Y}(k) = [\hat{y}(k+1), \hat{y}(k+2), \cdots, \hat{y}(k+N_p)]$ can be expressed by several solutions. For example, the states of the system at time k is known but at time $k+1$, different expressions can appear according to the possible models of the polyhedral partition. Then, the output can be expressed as:

$$\begin{aligned} &\hat{y}(k+1) = C_j\ x(k+1) = C_j A_i\ x(k) + C_j B_i\ u(k) + C_j f_i \\ &\text{or} \\ &\hat{y}(k+1) = C_l\ x(k+1) = C_l A_i\ x(k) + C_l B_i\ u(k) + C_l f_i \end{aligned} \tag{2.84}$$

The sequence of subsystems $I_j = [I_k, I_{k+1}, ..., I_{k+N_p-1}]$ which is obtained with successive models from the polyhedral regions $[\mathcal{X}_k, \mathcal{X}_{k+1}, ..., \mathcal{X}_{k+N_p-1}]$ is considered. Then, the estimation of the outputs $\hat{Y}_{I_j}(k)$ which corresponds to a particular sequence of subsystems is defined by:

$$\hat{Y}_{I_j}(k) = \Psi_{I_j} + \Gamma_{I_j} x(k) + \Theta_{I_j} U \tag{2.85}$$

with

$$\Psi_{I_j} = \begin{bmatrix} C_{k+1} f_k \\ C_{k+2} A_{k+1} f_k + C_{k+2} f_{k+1} \\ \vdots \\ C_{k+N_p} A_{k+N_p-1} \cdots A_{k+1} f_k + \cdots + C_{k+N_p} f_{k+N_p-1} \end{bmatrix} \tag{2.86}$$

$$\Gamma_{I_j} = \begin{bmatrix} C_{k+1} A_k \\ C_{k+2} A_{k+1} A_k \\ \vdots \\ C_{k+N_p} A_{k+N_p-1} \cdots A_k \end{bmatrix} \tag{2.87}$$

$$\Theta_{I_j} = \begin{bmatrix} C_{k+1} B_k & 0 & \dots & 0 \\ C_{k+2} A_{k+1} B_k & C_{k+2} B_{k+1} & 0 & \vdots \\ \vdots & C_{k+3} A_{k+2} B_{k+1} & \ddots & \vdots \\ \vdots & \vdots & \ddots & \vdots \\ C_{k+N_u} A_{k+N_u-1} \cdots A_{k+1} B_k & \cdots & \cdots & C_{k+N_u} B_{k+N_u-1} \\ \vdots & \vdots & \vdots & \vdots \\ C_{k+N_p} A_{k+N_p-1} \cdots A_{k+1} B_k & \cdots & \cdots & \Theta_{I_j}(N_p, N_u) \end{bmatrix} \tag{2.88}$$

with

$$\Theta_{I_j}(N_p, N_u) = C_{k+N_p} B_{k+N_u-1} + C_{k+N_p} \sum_{i=1}^{N_p-N_u} \prod_{j=1}^{i} A_{k+N_p-j} B_{k+N_u-1} \tag{2.89}$$

and A_k, B_k, C_k and f_k which corresponds respectively to the matrices of the PWA model in the polyhedral region $\mathcal{X}_k$.

I corresponds to the set of all the sequences of subsystems such that $\hat{Y}(k)_I = \Psi_I + \Gamma_I x(k) + \Theta_I U$ represents all the possible predictions. Then, the MPC based on PWA model is based on

the following minimization problem:

$$\begin{aligned} &\min_{I,U} U^T(\Theta_I^T S_Q^T + S_R^T)(S_Q\Theta_I + S_R)U + \cdots \\ &(\Psi_I^T + y(k)^T\Gamma_I^T - Y_{ref}^T)Q(\Psi_I + \Gamma_I y(k) - Y_{ref}) \\ &\text{respecting } \mathscr{C} \end{aligned} \tag{2.90}$$

The application of MPC based on PWA model requires to solve a QP which is able to take account of the different sequences of subsystems. For this purpose, [Pena et al., 2005] propose to use a Branch and Bound (B&B) algorithm to obtain the optimal input sequence. The B&B method is a structured search technique and a representation of this method is shown in Figure 2.10 such that $\mathcal{X}_i^{j/k}$ corresponds to a particular element of the B&B structure (i is the region of the

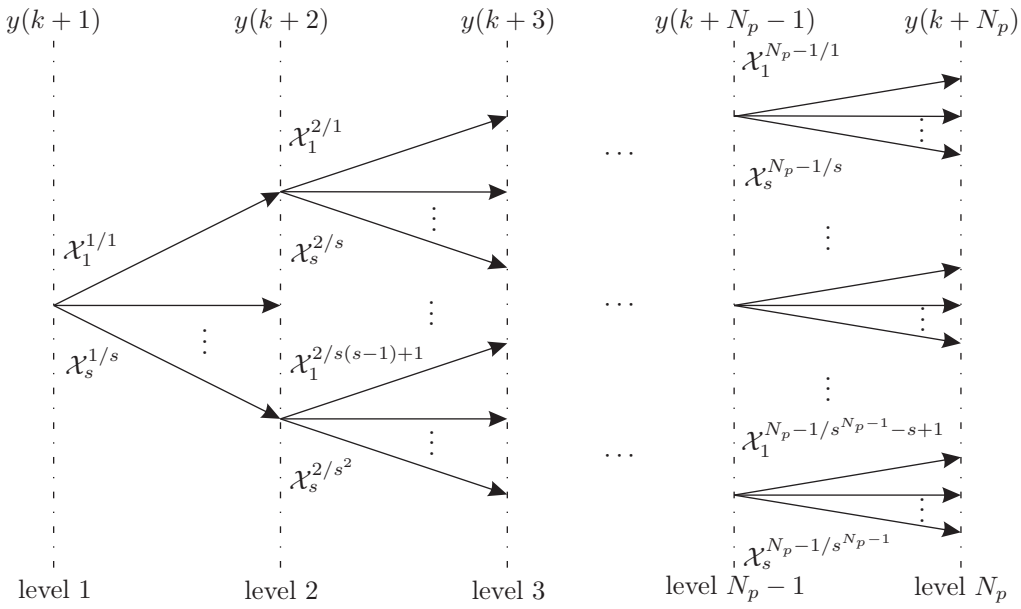

Figure 2.10: Branch and Bound (B&B) algorithm

polyhedral partition , j is the number of the level and k is the number of the particular sequence in the level j). However, it is possible to reduce the number of combinations. Considering the example presented in Figure 1.3, when the sample time is sufficiently low, it is not possible to go directly from the region $\mathcal{X}_1$ directly to the region $\mathcal{X}_3$. This simplification helps to reduce the time required for the optimization step. Another possibilities consist in using an hybrid automate which gives the possibility to have a finite number of transition or on transforming the system into an Mixed Logical Dynamical (MLD) system where mixed optimisation algorithms are available [Bemporad and Morari, 1999].

2.4.4 Conclusion

This section has presented some theoretical points concerning MPC. After a short introduction, the different steps which are involved in this control strategy have been detailed. Then, the main drawback of NMPC has been introduced and some solutions which help to cope with have been proposed. Indeed, because of the optimisation algorithm required at each sample time, non-linear and fast systems are difficult to manipulate. As shown in Section 2.4.3, solutions

based on LTV and PWA models or successive linearisations give the possibility to integrate non-linear behaviour of MPC algorithm. As it could be read in Section 3.2.3.4, MPC is particularly adapted for path following applications. In Chapter 5, some control solutions based on MPC are implemented and tested on an instrumented test vehicle.

2.5 Conclusion

This chapter gave theoretical explanations concerning different control strategies which will be used in Chapters 4 and 5:

- $\mathcal{H}_\infty$ control theory and particularly the gain scheduling solution based on a polytopic approach,
- fuzzy adaptive control considering state feedback and output feedback control solutions,
- model predictive control (MPC).

Section 2.2 presented the theoretical aspects of $\mathcal{H}_\infty$ control solution. First, the equations based on LTI models have been presented and a particular attention is focused on the LMI formulation [Scherer et al., 1997]. Then, due to the limitations of linear models and the possibility to describe non-linear behaviours with LPV models, $\mathcal{H}_\infty$ control solution has been extended for LPV models. Thus, classic gain scheduling [Theodoulis, 2008] and modern gain scheduling based on polytopic approaches [Poussot-Vassal et al., 2008] have been introduced.

Section 2.3 is dedicated to adaptive control solutions. These latter consider an on-line knowledge based on the observations of the system which helps to adjust automatically the parameters of the controller. Particularly, the three control solutions proposed here are based on a fuzzy approximator that permits to adjust the controller in real-time. On the one hand, two state feedback control solutions based on indirect and direct structures are proposed in Section 2.3.2. While the first solution uses the fuzzy approximator to identify the dynamics of the system which will subsequently be used to adapt the control law, the second directly adjust the control signal. On the other hand, an output feedback solution is detailed in Section 2.3.3. This last control solution just requires a limited number of measures which seems more realistic considering aeronautical constraints. Indeed, this solution considers the delayed outputs and inputs of the system to adjust the control signal by the use of a fuzzy system [Calise et al., 2001].

Section 2.4 deals with model predictive control. Firstly, the different steps required for the obtaining of the control signal are detailed. It is important to notice that MPC requires a real-time optimisation which is the major constraint of this solution. Secondly, due to the difficulties encountered when the optimisation is performed based on a non-linear model, solutions which permit to cope with are proposed. Indeed, LTV models, successive linearisations and PWA models are different propositions which give the possibility to confront the difficulties engendered by the optimization step when non-linear models are considered.

The application of these different control strategies can be found in the following chapters. Firstly, robust $\mathcal{H}_\infty$ control solutions are used in Section 4.2 which is dedicated to the control of the nose landing gear. Secondly, the state feedback and output feedback fuzzy adaptive control solutions are applied to damp the shimmy phenomenon in Section 4.3. Thirdly, the automatic

guidance algorithms, presented in Section 5.6 and validated on real tests, illustrate the advantages of MPC.

Finally, the following chapter presents the context in which different control laws will be implemented. Thus, the low level loop which is used to control the different actuators and the high-level loop which aims at controlling the displacement of the rolling system are presented. Moreover, a section which details the different required models is proposed.

Rien ne vaut la recherche lorsqu'on veut trouver quelque chose.

J. R. R. Tolkien, extrait de Bilbo le Hobbit

Chapter 3

Aircraft on ground automatic guidance: from actuator control to path following

Contents

3.1 Introduction

The two previous chapters give theoretical aspect on systems, models and control theories. Now, this chapter aims at presenting the framework of the applications in which the introduced theoretical tools will be applied and at giving the equations of the models used to synthesize the controllers and to perform the simulations.

Firstly, in Section 3.2 the problematic of automatic guidance, from actuator control to path following is introduced. Particularly, two different loops of the control structure are defined:

- the low-level loop (cf. Section 3.2.2), which aims at controlling the actuators,
- the high-level loop (cf. Section 3.2.3), which defines the strategy to obtain an automated rolling system.

For the low-level loop, two applications are detailed. On the one hand, the steering of the nose landing gear with the presentation of the DRESS electromechanical actuator is proposed. On the other hand, the presentation of the shimmy phenomenon (an unstable oscillation of the landing gear) [Besselink, 2000] and the existing control solutions which are proposed in the literature to damp these oscillations [Goodwine and Stépán, 2000] [Fallah et al., 2008] are suggested.

For the high-level loop, the attention is focused on control solutions based on geometrical approaches (cf. Section 3.2.3.3) or model-based approaches (cf. Section 3.2.3.4) which help to automatically guide a rolling system (a car vehicle, an A/C, ...). This section gives the possibility to point up three control strategies ("Follow the carrot", MPC and NNMPC), particularly adapted for the current application, which will be studied in detail in Chapter 5.

Secondly, mathematical equations of models used in Chapters 4 and 5 used to synthesize the controllers and to perform the simulations are detailed. Three classes of models are presented:

- A/C on ground models (cf. Section 3.3.1,
- nose landing gear steering models (cf. Section 3.3.2),
- shimmy model (cf. Section 3.3.3).

3.2 Presentation of the thesis framework

3.2.1 Introduction

The purpose of automatic guidance is to drive a rolling system (a car vehicle, an A/C, ...) from a point A to a point B by following a particular path or trajectory. Some examples in the literature suggest different solutions for different rolling systems: mobile robots [Peng et al., 2007], car vehicles [Falcone et al., 2007b], agriculture vehicles [Fang et al., 2005], motorcycle [Rowell et al., 2007].

From these approaches, it is possible to identify three distinguishable strategies for the purpose of automatic guidance: the "Lateral guidance (LG)", the "Lateral or Longitudinal guidance (LoLG)" and the "Lateral and Longitudinal guidance (LaLG)". For the LG, the rolling system is generally driving at constant speed and the aim is to generate a steering input such that the system follows the path [Chaib et al., 2004], [Cole et al., 2006]. With regard to the LoLG, the

strategy is divided in two different parts; the first part aims at steering the rolling system and the second one aims at cruising the system. The particularity of this strategy is the decoupling of the longitudinal control and the lateral control and the fact that only one control action (longitudinal or lateral) may be performed. For the LaLG, the objective is similar to the preceding case, however the longitudinal and lateral dynamics are handled at the same time by a unique controller [Gu and Hu, 2002, Maalouf et al., 2006] [Beji and Bestaoui, 2005].

Considering the three previous presented strategies (LoLG, LaLG and LG), the control structure could be the same. It consists of two loops, a low-level loop (for steering and/or speed control purpose) and a high level loop (for path following or trajectory tracking). These loops are presented in Figure 3.1 which represents the proposed control structure.

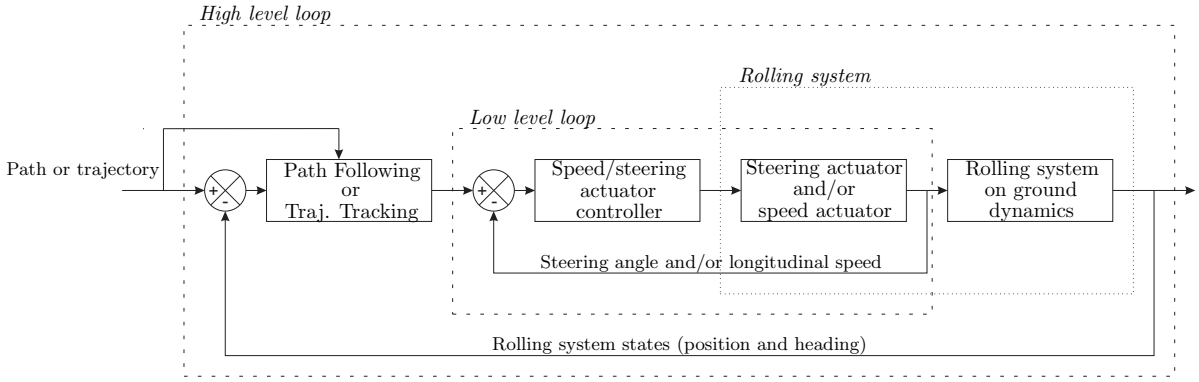

Figure 3.1: Guidance control structure

The low-level controller goal is to take the instructions given by the high level controller and to generate an appropriate signal to adapt the lateral and/or longitudinal dynamics of the rolling system. In this manuscript, the low-level loop corresponds to the control of the electromechanical NLG actuator (cf. Chapter 4). The high level controller responsibility is to assimilate the current rolling system configuration and the path or trajectory specificities to generate the different inputs that will be applied to the rolling system. Control algorithms dedicated to the high-level loop, are detailed in Chapter 5 and implemented for car vehicles.

3.2.2 Low-level control loop

Two main applications are treated in the low-level control loop. On the one hand, the steering of the landing gear is discussed. This consists in introducing the different solutions which help to rotate the wheel and consequently permit the lateral displacement of the A/C. On the other hand, the shimmy phenomenon is discussed. This phenomenon, manifested by unstable oscillations of the landing gear, is clearly explained and the solutions to cope with are introduced.

3.2.2.1 Steering of the nose landing gear

This section aims at presenting different systems used to steer the nose landing gear. Firstly, a state of art, which presents existing actuation solutions and their control units is proposed. Secondly, the new electromechanical steering actuator developed in the frame of the DRESS project is introduced. Moreover, specifications which have to be respected by the control algorithms,

presented in section 4.2 are detailed.

State of art on nose gear steering system and control unit

The NLG system is composed of the "upper part" (the electromechanical actuator, that means the electric motor and its mechanical transmission) and the "lower part" (the turning tube, the sliding tube and the wheel). Figures 3.2 and 3.3 give the details of the subsystems composing the NLG system.

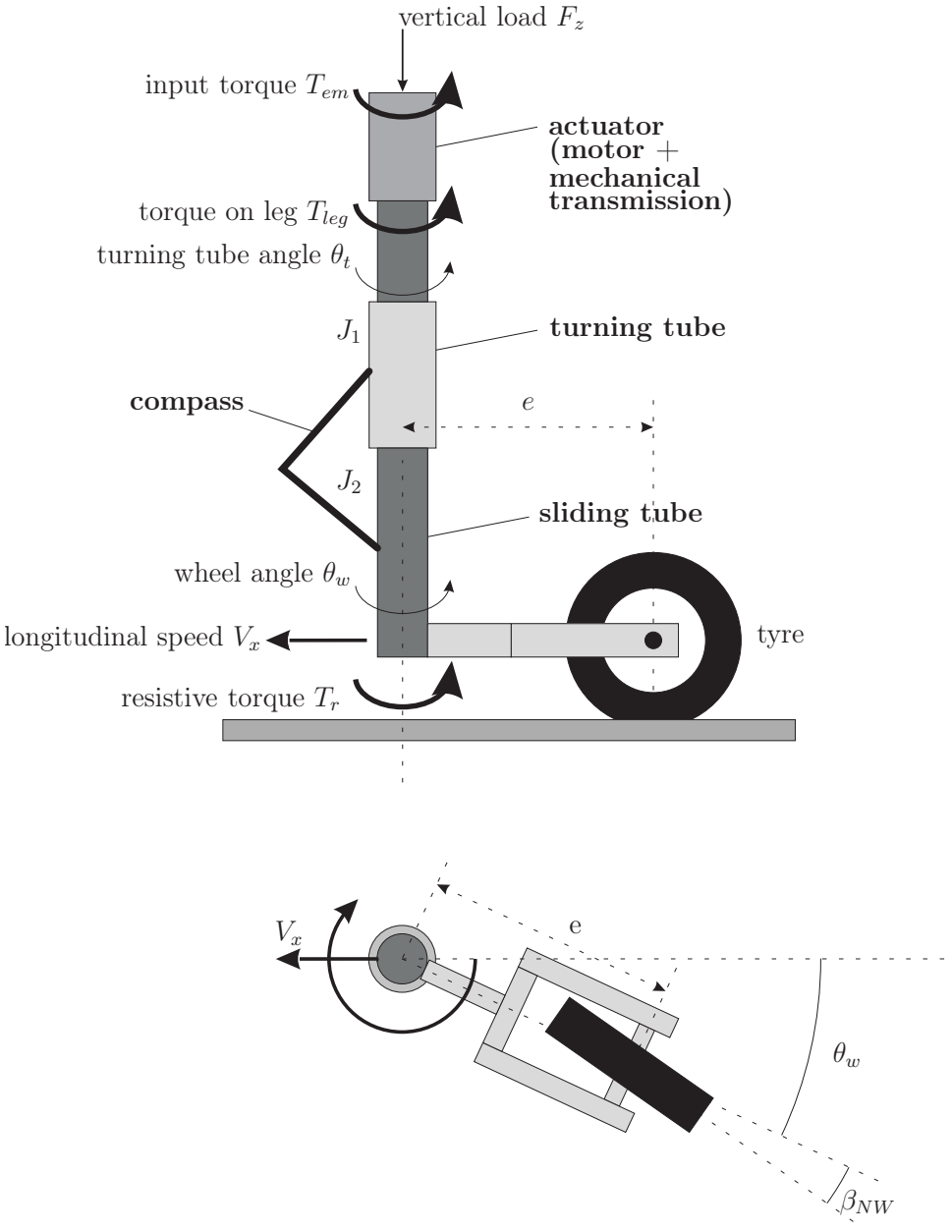

Figure 3.2: Nose Landing Gear

Functions of a nose landing gear (cf. Figure 3.3) are duplicated:

- absorb a small share of the A/C landing energy, insofar as the major energy is received by the main landing gears,

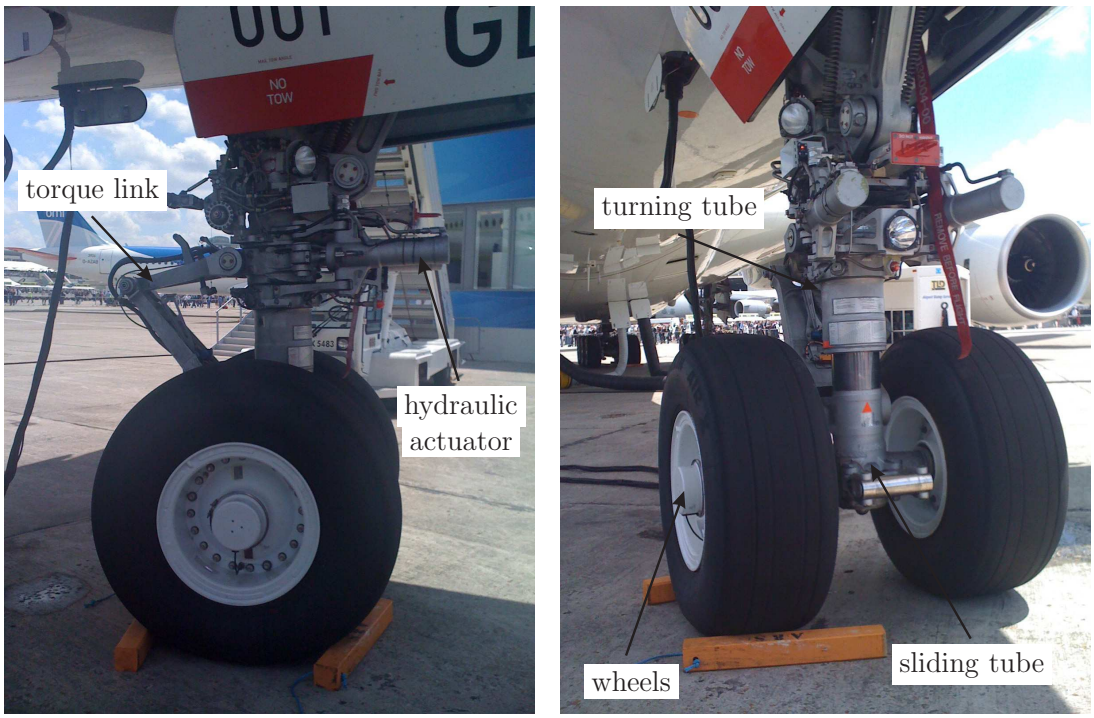

side view front view

Figure 3.3: A nose landing gear

- perform ground manoeuvre of the A/C.

For the last purpose, the lower part of the NLG to which the wheels are attached, can rotate around the vertical axis. This rotation corresponding to a demanded angle, produces a lateral force on the wheels forcing the A/C to turn.

Currently, hydraulic actuators are used to rotate the NLG and then let the A/C following the desired path. Various design configurations are available:

- "rack and pinion" hydraulic actuator:
  the hydraulic fluid, introduced under pressure in one of the two opposite actuator chambers, moves the rack which rotates the pinion fixed on the landing gear turning tube. Then, through the landing gear torque link (also called compass), the lower part of the landing gear rotates. This type of assembly is complex, expensive and requires frequent adjustment of the gear system to control backlash (it corresponds to the amount of lost motion due to clearance or slackness when movement is reversed and contact is re-established, in a pair of gears for instance).

- "push/pull" hydraulic actuator:
  this system consists of two simple linear actuators. Steering of the nose wheel is effected by simultaneously pushing with one linear actuator and pulling with the other actuator. The system thus operates as a dual crank and crankshaft mechanism which translates the linear force of the actuators to a rotational torque applied on the landing gear. The disadvantage of this type of system is that the actuators must necessarily be designed to have excess power insofar as the torque is unevenly applied across its range of rotation.

Pilots control the orientation of the nose landing gear wheels using a small control wheel tiller located on both sides of the cockpit. Until the advent of the "steer by wire" technology, the link between the pilot's control tiller and the hydraulic control valve was made by a mechanical cable, which closed the loop by providing the control to the hydraulic valve as well as the feedback. A tiller demand actuated the hydraulic valve input which activated the actuator proportionally. Currently, "steer by wire" technology is embedded in A/C. Thus, an electric control signal which comes from the pilot's tiller sensor, is transmitted to an electronic control unit. This latter sends a control current to an electro-hydraulic servovalve which distributes the hydraulic pressure to the appropriate actuator chamber and let the lower part of the landing gear rotate. In the control unit, a comparison is done between the order given by the pilot and the current position of the wheels, measured by an electric sensor and a simple PID-type controller calculates the new order to be effectively transmitted to the electro-hydraulic servovalve.

In the frame of the DRESS project, a new electromechanical actuator which has the objective to increase the safety and reliability levels of the A/C ground steering system is developed. This new system will be compatible with future fully automatic ground guidance system requirements.

Electromechanical steering system

In the frame of the DRESS project, the new electrical nose wheel steering system which has been proposed, is based on a distributed architecture. This architecture is presented in Figure 3.4.

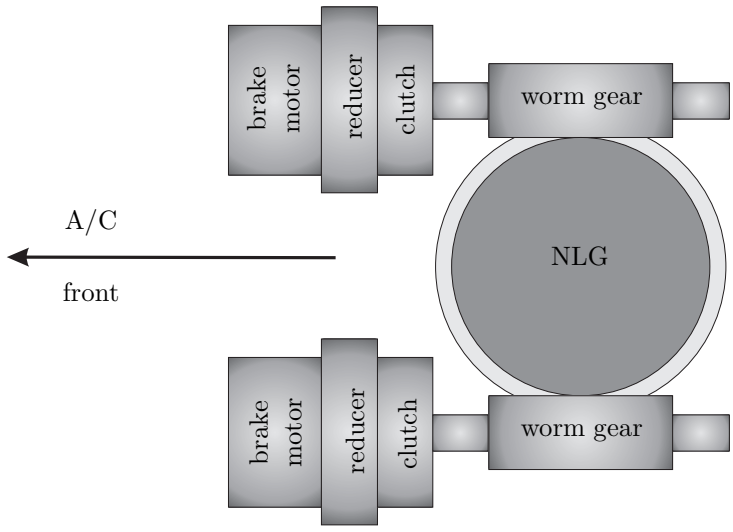

Figure 3.4: Architecture of the DRESS electromechanical actuator (from DRESS WP410)

A trade off considering safety, reliability, integration, mass, efficiency, conception and innovation has been performed to finally define the actuator's architecture. The redundant actuator is composed of two separate "paths" which could be potentially disengaged by the use of a clutch. It offers:

- a 50% - 50 % power capability in normal mode (when the two paths are ON),
- a 100% - 0% capability in reversionary mode (when only one path is ON); this configuration has thermal limitation at motor and control motor level,

- a torque summing duplex design,
- an overall reducer ratio of 845.5.

This actuator is composed of the following components:

- two motors: brushless DC / Permanent magnet synchronous motors which are recognized to have exceptional torque-to-volume and torque-to-weight performances,
- two brakes: electrically controlled, monostable brakes to lock the motor shaft in position,
- reducers: used to increase the torque and decrease the speed at the output of the motors with a ratio equal to 59,
- clutch: electrically controlled clutch which is normally declutched, to allow NLG free castoring[1] for the towing mode[2]. It helps to change the configuration of the actuator: active/active configuration in normal mode (the two paths operate) and active/passive configuration in degraded mode (one path is declutched when a problem is identified on one of the two paths),
- worm gear: to sum the torque at the output of the reducers,
- wheel gear: fixed to the NLG, in order to perform its rotation.

A picture of the DRESS electromechanical actuator is proposed in Figure 3.5.

Specifications

To be incorporated into future aircraft and to be compatible with future fully automatic ground guidance system requirements, strict specifications must be respected by the DRESS actuator as well as the closed-loop system. These specifications, provided by the A/C manufacturers, define the required responses of the system for particular input signals and its domain of validity. In the case of the DRESS actuator, beside all the constraints, two main specifications must be respected for the control point of view:

1. Specification 1: frequency response,

   considering the frequency response, the Bode diagram of the closed-loop, that means the Bode diagram between the wheel angle demand $\theta_{w\,ref}$ and the effective wheel angle θ_w must respect a plot similar to the one presented in Figure 3.6.

   The considered figure notably shows that at low frequency, just a 2 dB difference is tolerated between the wheel angle reference and the effective wheel angle. Then, the phase plot points out that just a $-12°$ delay is accepted. At higher frequency, around 5Hz, the bode characteristic drops off meaning that higher differences are allowed between the wheel angle reference and the effective wheel angle. Nevertheless, no overshoot, are permitted for these frequencies, the effective wheel angle has to be smaller than the reference angle. Similar comments can be done for the phase; for high frequencies, a more important delay is admitted.

1

2

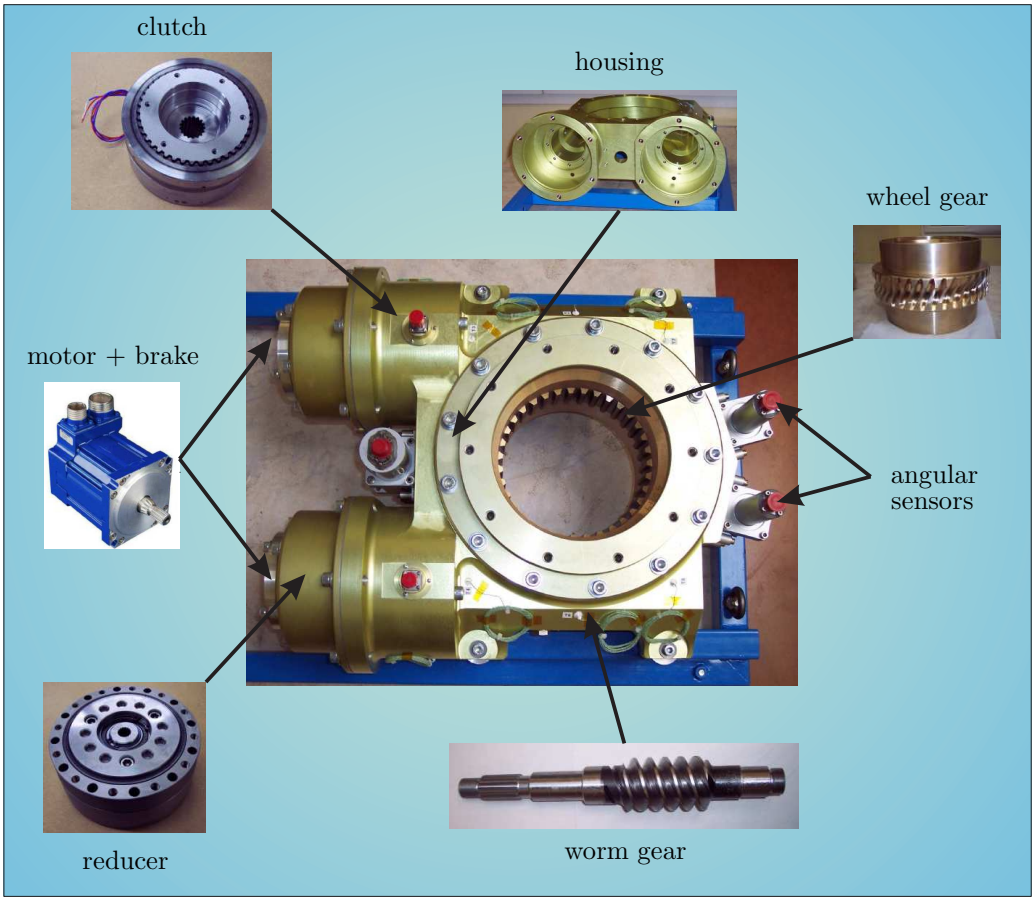

Figure 3.5: DRESS electromechanical steering actuator

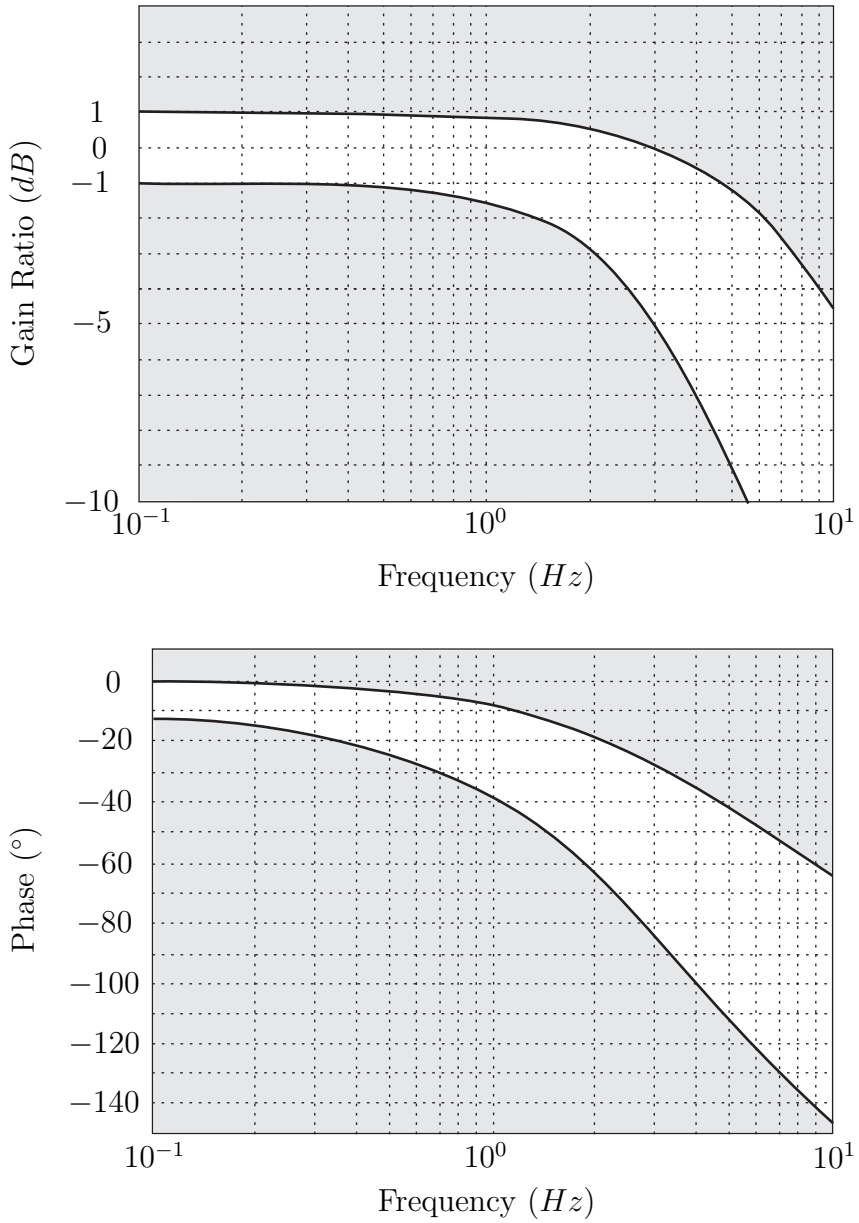

Figure 3.6: Specification 1: frequency response such that $G(s) = \dfrac{\theta_w(s)}{\theta_{w\,ref}(s)}$

2. Specification 2: velocity step response.

   considering the step response, a ramp in position is demanded such that the wheel speed demand $\dot{\theta}_{w\ demand}$ equals 10m/s. In this case, the wheel speed $\dot{\theta}_w$ is constrained as it is presented in Table 3.1 and Figure 3.7. The main particularities of this figure are that the response must be fast insofar as the rise-time from 0 to 64% is less than 155ms; the overshoot is limited because its maximum must not be beyond 10% and the final value has to be reached in only 300ms with a low error which must be less than 2%.

Symbol	Description	Value	Unit
w_0	Maximum allowable overshoot beyond $\dot{\theta}_{w\ demand}$ which is the nose wheel steering rate demand	10	%
w_A	Settling criteria, centred on $\dot{\theta}_{w\ demand}$	± 2	%
τ_d	Maximum allowable time delay (demand to response)	25	ms
τ_{1r}	Maximum allowable rise time from 0% to 64% if no overshoot	155	ms
τ_{2r}	Minimum allowable rise time from 10% to 90% in case of overshoot	120	ms
t_s	Maximum allowable time to achieve settling criteria (difference between steering rate and demand absolute value $\leq 2\%$)	300	ms

Table 3.1: Specification 2: step response

Commentary The two specifications detailed in this section are only related to control purposes. The frequency response and the step response describe the performances that the closed loop system must reach. Nevertheless, numerous other constraints have been defined in the frame of the DRESS project. For example, power constraints have been given insofar as 2 different power supplies, a low voltage supply (28V DC) and a high voltage supply (270V DC) are available. Environmental requirements have also been identified as for instance the fact that the landing gear must stand up from $-55°C$ to $70°C$.

3.2.2.2 Shimmy phenomenon

This section aims at introducing the shimmy phenomenon. On the one hand, a description of the shimmy is proposed; the different parts involved in the phenomenon are described, the issues related to the occurrence of this phenomenon are mentioned and the modelling of this phenomenon is discussed. On the other hand, the solutions which help to remedy the malfunctions due to the shimmy phenomenon are discussed and the solutions proposed in this work, based on fuzzy adaptive control are described.

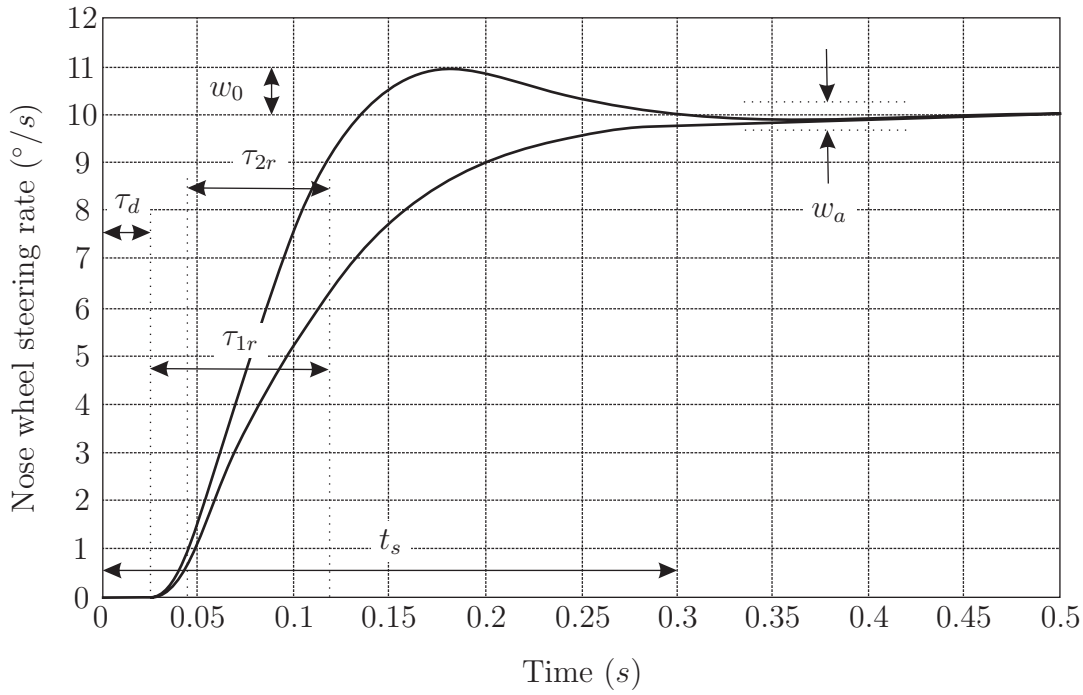

Figure 3.7: Specification 2: step response

What is shimmy?

The shimmy phenomenon is the self-excited oscillation of a wheel around its vertical axis, which may occur in many physical rolling systems such as aircraft nose wheels, automobiles, motorcycles... In the context of aircraft, shimmy is an unstable oscillatory phenomenon, which combines lateral and yaw motion of the landing gear, mainly due to the interaction between the ground, the tyre and the landing gear structural dynamics. A number of conditions such as low torsional stiffness, excessive free-play in the gear, wheel imbalance or worn parts may cause shimmy oscillations. Everything on the landing gear has an impact on the shimmy behaviour. The motion has a typical frequency in the range of 10 to 30Hz. This phenomenon may grow to an uncomfortable level of vibrations and can, in particular cases, result in severe damage to the landing gear. Figure 3.8 illustrates the consequence of the shimmy phenomenon observed on a A/C NLG during a rolling sequence.

Difficulties to model the shimmy phenomenon - literature review

Modelling and simulation of the shimmy phenomenon are primordial tasks in order to control it. Indoor testing is critic insofar as the considered energies are very important. In like manner, during the conception of a NLG, shimmy testing on an aircraft is very risky and dangerous because the system becomes unstable and may break out. Moreover, shimmy is a complex phenomenon which is influenced by many parameters and different sensitivity analysis available in the literature ([Somieski, 1997] [Besselink, 2000]) show that a thin variation of critical parameters may modify the characteristics of the system from a stable behaviour to an unstable one. Then, for this particular application, it is obvious that an accurate model description is essential.

The number of publications available in the literature appears to be relatively small, in spite

Figure 3.8: Shimmy phenomenon (from [Besselink, 2000])

of the fact that shimmy studies have a long history. Initially, the main focus was to obtain a good description of the tyre behaviour. Then, in the fifties, the tyre models of Von Schilippe [Schlippe and Dietrich, 1954], Moreland [Moreland, 1954] and Smiley [Smiley, 1957] were developed. The description of the tyre model was naturally followed by several works which concern the methodology to obtain accurate tyre parameters. In this way, [Smiley and Horne, 1960] furnished an overview of measurements for many different aircraft tyres and [Black, 1982] provided an approach to obtain the tyre parameters. Initially, the models that helped to study shimmy stability were linear and, little by little, non-linear models for both the tyre and the landing gear have been proposed. An accurate review of landing gear shimmy is available in [Besselink, 2000].

Currently, in the literature, different models help to describe and analyse shimmy [Goodwine and Stépán, 2000], [Sura and Suryanarayan, 2004], [Thota et al., 2008] and [Somieski, 1997]. [Goodwine and Stépán, 2000] proposes a model which is described by 3 non-linear equations. It considers the steering dynamics, that means the rotation around the vertical axis, the lateral displacement at the kingpin (connecting point between the leg and the body) and the wheel angle rotation. Two main drawbacks can be noticed with this model. On the one hand, some modelling simplifications are performed: the torsional characteristics of the landing gear are not taken into account and the elasticity is simply modelled by a spring. On the other hand, it can be shown that the linearised stability of the system around its zero position does not contain the A/C longitudinal speed which is a crucial parameter for the stability analysis. The model presented by [Sura and Suryanarayan, 2004] is quite similar to the one mentioned previously by considering the lateral displacement of the wheel and the rotation around the vertical axis. This model does not take account of the wheel angle rotation but the dynamics of the landing gears are considered and modelled by a non-linear stiffness. However,

the main drawback of this model lies in the modelling of the W/R interface. As it is mentioned in the literature, the tyre plays a very important part in the shimmy phenomenon and its modelling with a hard contribution (the lateral tyre is modelled by a positive or negative constant depending on the sign of the skid velocity which represents the velocity of the tyre contact point with respect to ground) seems to be not representative enough. A recent model has been developed by [Thota et al., 2008]. This mathematical model is described by a five dimensional system which considers two modes (torsional and lateral dynamics). It takes account of different geometrical characteristics of the landing gear [3] and models the W/R interface by the use of a non-linear tyre model. This model is accurate and considers a lot of contributions which are very important insofar as the shimmy phenomenon is due to the interaction of the different landing gear components. It seems that this kind of model is appropriate for the analysis of the shimmy phenomenon, when the importance and the contribution of each parameter is studied. However, in the case of control purposes, a compromise between the accuracy of the system description and the complexity of the obtained model has to be considered. Thus, considering the conclusions of [Thota et al., 2008] mentioning notably that the torsional mode is still dominant, it is possible to consider an intermediate model. The last shimmy description available in the literature is the one provided by [Somieski, 1997]. This model describes the more influencing contributions insofar as it considers the torsional dynamics of the landing gear and the non-linear W/R interface. Then, the sensitivity analysis proposed by the author helps to conclude on the contributions of the longitudinal speed, the caster length and the mechanical characteristics of the landing gear. As a conclusion, this model has been chosen as a reference model for the shimmy phenomenon description. This model which is well detailed in detail in Section 3.3.3, has been used to develop the presented active shimmy damping solutions.

Solutions for shimmy damping: passive vs active solutions

As mentioned previously, shimmy engenders malfunctioning or severe damages of the different parts of the NLG. Then, a solution which helps to damp the unstable oscillations of the shimmy phenomenon is required. A classical solution to avoid shimmy is to increase the global stiffness of the NLG by changing its material for instance and to increase the damping constant by using additional passive dampers. These passive damping solutions are proposed by [Besselink, 2000]. One of the main drawbacks of such shimmy passive damping solutions is that under changing load conditions or ground-tyre interfaces, they may not be efficient because of the fixed structural parameters of the NLG. Moreover, when it is chosen to oversize the NLG to prevent from shimmy, the high stiffness is achieved at the cost of a large mass. Then, considering the limitations of passive damping, active solutions may be investigated in order to take account of the changing conditions.

Today, active shimmy damping is made with hydraulic steering systems. The shimmy oscillations are damped by preventing the hydraulic fluid from travelling freely at high speeds without resistance from one actuator chamber to the opposite one. This is done by installing hydraulic restrictors on the actuator chambers or in the hydraulic control unit usually located close to the

[3] the rake angle that means the inclination of the landing gear around the vertical axis and the tilt angle that means the inclination of the wheel angle around the forward axle when a steering angle is applied

actuator. The restrictors are biased in order to oppose a high resistance when the fluid is leaving the chamber and a low resistance, to avoid cavitation, when the fluid is entering the chamber.

As it has been widely mentioned earlier, hydraulic actuators are currently replaced by electrical actuators. Due to the improvement of the embedded systems (microprocessor efficiency, field bus integration,...) electrically-based active shimmy damping control solutions are now conceivable. Several control solutions, proposed in the literature help to steer the electromechanical actuator and in parallel to damp actively the shimmy oscillations [Goodwine and Stépán, 2000], [Fallah et al., 2008].

[Goodwine and Stépán, 2000] proposed a shimmy damping solution which aims at transforming a non-linear system into a linear one through feedback linearisation. The main assumption of this control solution is the fact that the dynamics of the system are entirely known. Indeed, the controller takes account of these dynamics and cannot be adapted. When some external perturbations affect the system, the proposed solution cannot change its behaviour. For example, it is a major drawback when the W/R interface varies from wet to icy conditions.

[Fallah et al., 2008] developed a robust MPC solution which can effectively suppress the shimmy. The proposed control solution is based on a LPV model and constraints on the control signal and on the output are considered. The authors focus their works on the computational efficiency of the robust MPC algorithm. But, despite significant improvements over other similar approaches, the average computational time per loop of the algorithm is larger than the sampling interval. Such solution is not currently conceivable for real time application. Moreover, the LPV model which helps to synthesize the controller only considers variations of the A/C longitudinal speed. It could be interesting to take account of the variations of other parameters like the tyre lateral forces characteristics. Finally, the solution is based on state measurements and it is well-known that in the aeronautical domain measurements are difficult and expensive to obtain.

As a conclusion, the two active damping control solutions proposed overhead could not be conceivable for an A/C implementation. Then, in the frame of this thesis, control solutions, validated by simulations are proposed. Thus, Sections 4.3.3 and 4.3.4 present results obtained with fuzzy adaptive algorithms. The two first solutions are based on state feedback control solution while the last solution deals with output feedback control solution. The validation is obtained with three scenarios detailed in Section 4.3.2. Scenario 1 considers a constant ground speed and a pulse disturbance acting on the NLG. For scenario 2, the ground speed is always constant but the roughness of the runway is taken into account. Finally, Scenario 3 aims at studying the effect of varying ground speed on the control solution efficiencies.

3.2.3 High-level control loop

3.2.3.1 Introduction

It exists a lot of algorithms solving the problem of automatic guidance. Among all the existing solutions, it is possible to distinguish two main approaches. On the one hand, the algorithms based only on geometrical approaches consider Cartesian or polar representation of the road to be followed to produce the appropriated control signal. As it could be read in Section 3.2.3.3, the existing solutions are the “follow the carrot”, the “pure pursuit”, the “virtual vehicle” or the “vector pursuit”. On the other hand, the model-based approaches use some description of the

road to be followed but also considerations about the rolling system. In this second class of solutions, the approaches based on neural network, backstepping, adaptive control, fuzzy logic, MPC and NNMPC are detailed (see Section 3.2.3.4). All the solutions are described and their advantages and disadvantages are mentioned. Finally, the choice of the better solutions concludes this section.

3.2.3.2 State of art on automatic guidance in aeronautical domain

In the aeronautical domain, air transportation has increased a lot over the last decade. This leads to the congestion of the airports due to an unappropriated modus operandi. To remedy this problem, either infrastructure renovations and new airports must be considered or the management of the A/C on ground must be rethought. Here, discussions focus on solutions to improve the movement of the A/C on ground without changing the existing infrastructure. Two solutions help to reach more flexible A/C on ground displacements. On the one hand, ground traffic control has to be improved. Current solutions based on surface movement radar are limited due to an incomplete surveillance, the fact that the weather affects greatly the traffic... Recently, ground traffic control has been improved through the A-SMGCS (Advanced Surface Movement Guidance and Control System) project [Adamson, 2005]. The objectives of this A/C on ground movement control is multiple. It helps to supervise the real time situation of the traffic (A/C position, speed, destination ...). It gives the possibility to control the traffic and particularly it detects conflicts. Moreover, it enables the A/C routing, it defines the A/C road to follow and allows destination changing; the system is very adaptive. On the other hand, an automatic guidance system could be introduced. It aims at introducing a high level control loop which replaces the manual steering control [Duprez et al., 2004], [Duprez, 2004] , [Villaumé, 2002], [Roos and Biannic, 2006]. It gives the possibility to follow a trajectory or a path whatever the weather and the ground conditions are (dry, wet, icy, ...). Moreover, an automatic guidance system improves the flow of traffic because the A/C speed could increase and then taxiing time will reduce.

[Villaumé, 2002] suggests a new procedure for the automatic landing by acting on the longitudinal and the lateral A/C dynamics. During, the landing phase, an automatic deceleration profile is generated; the system aims to predict the reachability of the exit way and provides an optimal deceleration control. A solution to follow the runway axle is proposed, this is done by calculating the distance between the runway axis and the A/C and by providing a control of the A/C yaw angle. [Duprez, 2004] continued the Villaumé's works and developed speed control laws which use the braking system and the engine thrust. Then, lateral control solutions which takes account of the non-linear dynamics have been studied. Finally, [Roos and Biannic, 2006] proposed an aircraft-on-ground lateral control which has the particularity to consider the saturation of the system. The efficiency of the solution is notably due to its adaptive properties insofar as an on line procedure estimates the runway state (dry, wet or icy).

The studies available in the literature ([Villaumé, 2002], [Duprez, 2004] and [Roos and Biannic, 2006]) propose very interesting control solutions to act on the longitudinal and lateral dynamics of the A/C. These solutions have the advantage to consider different runway states (dry, wet or icy) or to take account of actuators saturations. Nevertheless, information provided by accurate positioning devices, like GPS for instance, are not considered

in this applications. Indeed, from the A-SMGCS system, it could be possible to define the road that the A/C must follow and using GPS information, control solutions can be developed to minimize the distance and the time to travel between the desired road and the A/C position.

3.2.3.3 Automatic guidance - geometrical approaches

This section aims at presenting a review of the different automatic guidance algorithms based on geometrical approaches. Four different strategies are presented and Table 3.2 describes the advantages and disadvantages of each.

Follow the carrot

A carrot point (i.e. an objective point), that is at a Look Ahead Distance (LAD) along the specified path, is defined. The aim of this algorithm is to join this changing point [Hellstöm and Ringdahl, 2006]. This is achieved by minimizing the orientation error between the vehicle and the carrot point. This angle is ε_{EO}. Then, the steering angle δ is obtained by a simple proportional control law:

$$\delta = k_p \times \varepsilon_{EO} \tag{3.1}$$

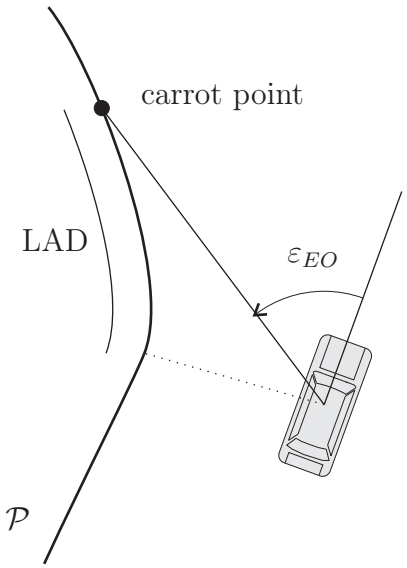

Figure 3.9: Follow the carrot

The LAD is the calculation of the distance on the path $\mathcal{P}$ as presented in Figure 3.9. To facilitate the calculation of this distance, it was chosen to define it as the distance between the rolling system centre of gravity and one point on the path.

This solution has some major drawbacks. The LAD is a very important parameter of the controller. This value must be chosen very carefully. A short LAD value implies that the rolling system will oscillate. A large LAD value implies that the rolling system will cut the corners. Then, the speed of the rolling system affects the results of the controller. A good tuning for a particular speed could be a bad tuning for another speed.

Some solutions could be used to solve this problem. First, to take into account the speed dependency of the system, a gain scheduling method can be applied. Then, the steering angle could also be a function of the speed. In other words, the two parameters LAD and k_p are speed dependent. Then, the choice of the two previous parameters is quite difficult and an optimization algorithm has to be used to find them precisely. The fitness function of the optimization algorithm evaluates the distance between the rolling system and the path for each iteration. Then, these values are summed. Moreover, it is possible to add an integral and a derivative contribution for the controller. The integral contribution enables to erase the static error and the derivative contribution erases the overshoot and the oscillations. Finally, the method could be improved by combining the orientation and perpendicular distance errors into the steering angle control law such that $\delta = k_p \times \varepsilon_{EO} + k_d \times d$ with d the perpendicular distance to the path.

Pure pursuit

An improvement of the "follow the carrot" method is the pure pursuit. The calculation of the future steering input is based on the calculation of the curvature necessary to reach the carrot point. The algorithm is divided in five parts [Putney, 2006] [Coulter, 1990]:

- determination of the current location of the vehicle,
- research of the closest path-point to the vehicle,
- research of the goal-point based on the LAD,
- calculation of the curvature,
- calculation of the steering angle.

The calculation of the curvature is based on geometrical aspects. Considering the path $\mathcal{P}$ in the vehicle coordinates, (x, y) is the carrot point, r is the radius of the arc that joins the origin of the referential to (x, y) and whose chord length is the LAD.

Then, the following geometrical equations are obtained:

$$\begin{cases} x^2 + y^2 = LAD^2, \\ x + d = r, \end{cases} \tag{3.2}$$

then with,

$$\begin{aligned} &d = r - x, \\ &(r - x)^2 + y^2 = r^2, \\ &r^2 - 2rx + x^2 + y^2 = r^2, \\ &LAD^2 = 2rx, \end{aligned} \tag{3.3}$$

the curvature is:

$$\gamma = \frac{2x}{LAD^2} \tag{3.4}$$

Finally the steering angle input applied to the system (considering the wheel base L of the rolling system) is:

$$\delta = \tan^{-1}(\gamma L) = \tan^{-1}\left(\frac{2xL}{LAD^2}\right). \tag{3.5}$$

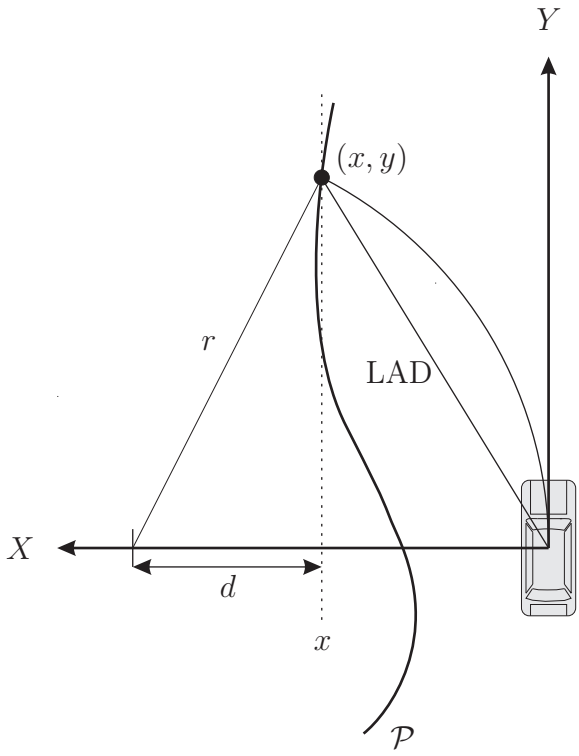

Figure 3.10: Pure pursuit

Virtual vehicle method

The virtual vehicle method [Egerstedt et al., 2001] uses the "follow the carrot approach", defining a target (the virtual vehicle) to be reached and it aims at limiting the distance between the road and the vehicle such that the equation $\lim_{t\to\infty} \sup \rho(t) \leq LAD$ with $\rho(t)$ the distance between the vehicle and the desired point, is respected. Furthermore, the motion of the desired point (the virtual vehicle) is governed by a differential equation containing error feedback. The target path is given by a curvilinear representation:

$$\begin{cases} x_d = p(s) \\ y_d = q(s) \end{cases} \tag{3.6}$$

then based on a differential equation:

$$\dot{\rho} - L\dot{A}D = -\gamma(\rho - LAD) \tag{3.7}$$

with ρ the distance between the rolling system and the carrot point and $\gamma = \frac{1}{LAD} v \cos(\psi_d - \psi_v)$. The algorithm is:

$$\begin{cases} \dot{s} &= \dfrac{1}{\sqrt{p'^2 + q'^2}\cos(\psi_d - \theta_r)}(2v\cos(\psi_d - \psi_v) - \gamma\rho) \\ \delta &= -k(\psi - \psi_d) \\ v &= \text{constant speed} \end{cases} \tag{3.8}$$

with ψ_d the desired orientation, ψ_v the velocity vector angle and θ_r the orientation angle of the tangent to the reference path at s. As a remark, it can be noticed that equation (3.8)

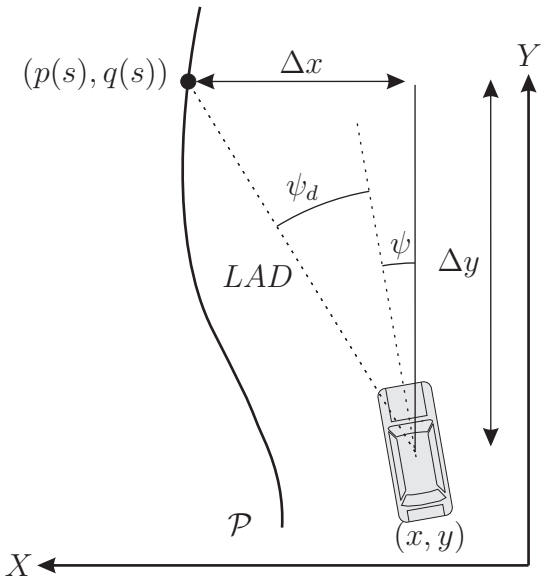

Figure 3.11: Virtual vehicle

uses two different notations to formulate the derivative. The first $\dot{s}$ represents a derivative with respect to time while the second p' or q' are derivatives with respect to the curvilinear variable s. The introduced notations are specified in Figure 3.11 relative to the virtual vehicle control solution.

The algorithm is based on a constant speed assumption, but [Egerstedt et al., 2001] present another algorithm which adds a longitudinal velocity control.

Vector pursuit

"Vector pursuit" is a path-tracking method that uses the theory of screws [Wit, 2000]; it is a way to express displacements, velocities, forces and torques in three dimensional space, combining both rotational and translational movements. This technique is similar to other geometric methods in that a LAD is used to define a current goal point, and then, geometry is used to determine the desired motion of the rolling system. On the other hand, it is different from current geometric path-tracking methods, such as "follow the carrot" or "pure pursuit", which do not use the orientation at the look-ahead point. This method adds the current position error multiplied by some gain to the current orientation error multiplied by some gain, and therefore becomes physically meaningless since terms with different units are added. Vector pursuit uses both the location and the orientation of the look-ahead point.

Conclusions for the geometrical approaches

These conclusions are summarized in Table 3.2 .

The first method based on a carrot point is the preferred geometrical approach. Its implementation is easy and the steps of this approach are quite similar to the behaviour of a driver. Indeed, a point in front of the vehicle is fixed and the steering order is given based on the vehicle status. Then, this control solution has been implemented in real time on the test vehicle and Section 5.6.2 presents the obtained results.

Method	Advantages	Drawbacks
Follow the carrot	easy to implement	oscillates around the target path for short look ahead distances, cuts corners
Pure pursuit	competitive for curved path	bad performances for straight path
Virtual vehicle	quite robust with respect to measurement errors and external disturbances	calculation load
Vector pursuit	good following with correct orientation and curvature	complexity

Table 3.2: Geometrical approaches comparison

3.2.3.4 Automatic guidance - model-based approaches

This section aims at giving a global overview of the different automatic guidance algorithms based on a model. Six different strategies are introduced (neural network, backstepping, adaptive control, fuzzy logic, MPC and NNMPC) and Table 3.3 ends this section by giving the advantages and disadvantages of each solution.

Neural network

Neural network control has been applied to solve the problem of trajectory tracking [Peng et al., 2007]. Here, the authors use a recurrent fuzzy cerebellar model articulation controller (RFCMAC) network structure to control the longitudinal and lateral dynamics of a particular rolling system, a mobile robot. The advantages of CMAC technique, compared with other neural networks are its excellent learning characteristics and its fast computation speed. The network presented in [Peng et al., 2007] is a recurrent network (i.e. with an internal feedback loop) and demonstrates good performances in the presence of parameter variations, external disturbances and unmodeled and non-linear dynamics. Then, a fuzzy layer is added to take into account the input uncertainties. Finally, the backpropagation is used to train the proposed RFCMAC network and simulations are made. However, this solution needs important memory requirement and based on simulation results, it can be shown that control signals provided to the real system have high dynamics (the controller engenders high fluctuations of the control signal). The control algorithm uses four inputs: the velocity error, its rate, the azimuth (or orientation angle) error and its rate. It helps to compute two outputs and these computed driving torques are used to control left and right wheels.

Backstepping

[Fang et al., 2005], [Fang et al., 2006] applied backstepping control theory to solve trajectory tracking problems. In these works, the longitudinal and lateral control are based on a backstepping algorithm which integrates a parameter adaptation technique. This technique provides a constructive systematic method to achieve globally stabilizing control laws. In other words, the

control signal is built step by step by considering successive virtual controls which stabilize a virtual increasing system until a global control law stabilizes the full system. A detailed explanation applied on a simple second order system is presented in [Fang et al., 2006]. Afterwards, the algorithm is applied on an agriculture vehicle which is modelled with a kinematic model combined with sliding. The particularity of this robust adaptive backstepping algorithm is to consider the sliding effect as an unknown constant contribution with time-varying bounded disturbances.

The previously cited papers show the design of two control signals (wheel rotating velocity and steering angle of the virtual front wheel) which guarantee that the longitudinal and lateral errors tend to zero and the orientation error is bounded. The different gains used for this algorithm should be tuned gradually to make an "optimal" compromise between transient characteristics and limited bandwidth of the steering system.

Unfortunately, the calculation of the control signals is quite difficult and the obtained expressions are usually complex. However, the authors present a simplified adaptive controller with projection mapping and the conclusions show that in particular cases, a simplified controller could be enough.

Adaptive control

The theory of adaptive control has been used by different authors [Beji and Bestaoui, 2001], [Beji and Bestaoui, 2005] and [Netto et al., 2004]. Generally, models used for the description of the rolling systems are highly non-linear. Moreover, uncertainties of the modelling are quite important, notably tyre/road contact parameters or other perturbations as wind forces. Then, considering authors conclusions, adaptive control seems well suited to solve this problem, insofar as the controller is based on linear structures which can be adapted to fit the non-linear behaviour of the system.

Fuzzy logic

Fuzzy control is an interesting method for constructing non-linear controllers acting as a "human-in-the-loop" controller for a system. Following these perspectives, it seems that these methods could be adapted for trajectory tracking. Then, this theory has been used for a few applications [Naranjo et al., 2003b], [Naranjo et al., 2005], [Naranjo et al., 2003a], [Hajjaji and Bentalba, 2003], [Maalouf et al., 2006] which aim at controlling longitudinal, lateral and combined longitudinal-lateral dynamics of rolling systems.

For example, [Naranjo et al., 2003b] use fuzzy control to perform a longitudinal control of a rolling system. The controller adjusts speed in order to maintain a proper distance or gap between vehicles. This fuzzy controller needs four inputs and one output is generated. The inputs are the "speed error" which is the difference between the current speed and the driver required speed, the "acceleration" which is approximated by the derivative of the speed at the instant t, the "time gap" which represents the time needed by the pursuiver to reach the point where the pursued vehicle is and finally the "derivative of time gap". The output of the fuzzy controller is the new accelerator pedal pressure. The controller uses five fuzzy rules to maintain the present speed and to keep a safe distance.

[Naranjo et al., 2005], [Naranjo et al., 2003a] use fuzzy logic for the automatic control of the

steering wheel of a vehicle. Only two input variables are needed to manage the steering wheel: the lateral error and the angular error. The lateral error is the deviation, in meters, of the front of the car from the reference trajectory, measured perpendicularly from it. The angular error is the angular deviation, in degrees, of the vehicle from the reference trajectory. The output of the controller is the steering angle. Two different operating modes are defined, one for straight road driving and the other for curve driving. Based on these two modes, different membership-functions are used. In fuzzy control, the shapes of these membership-functions could be difficult to identify and here, they are derived from verbal description of driver behaviour and refined experimentally. The four fuzzy rules are very intuitive and describe the behaviour of people when manoeuvring car, the aim of the rules is to mimic human behaviour. Finally, the test shows that the fuzzy control, with precise GPS map and positioning, can maintain a vehicle in its lane on the road.

[Hajjaji and Bentalba, 2003], [Maalouf et al., 2006] use fuzzy logic for trajectory tracking. Particularly, the objective of [Hajjaji and Bentalba, 2003] is to determine the control actions for the traction force or braking force and the steering angle of the front axle of a car vehicle to follow a trajectory defined by a reference vehicle. In other words, the objective is to make the vehicle follow a desired trajectory such that the longitudinal velocity and the lateral velocity of the real vehicle tend to the reference vehicle and the orientation error between both vehicles and the coordinates of the position error tends to zero. The particularity of this paper is the use of a Takagi-Sugeno model of a vehicle obtained by linearisation near different operating points and the stability analysis of the controller based on Lyapunov's method combined with the linear matrix inequalities (LMI) approaches. [Maalouf et al., 2006] choose to adapt the linear velocity and angular speed based on the look-ahead curvature to have a smooth and almost linear continuous behaviour.

Model Predictive Control (MPC)

In this section, several control solutions based on models are presented. These methods are based on classic MPC (the prediction consides a linear model), NMPC and NNMPC.

The problem of path following can be solved with MPC applied on linear systems and aims at controlling the lateral dynamics of the rolling system. [Cole et al., 2006] applied the MPC algorithm using the well-known yaw-sideslip "bicycle" model. In [Rowell et al., 2007], the aim is to demonstrate the applicability of MPC for the control of motorcycle on a simple lane change manoeuvre. The motion of the motorcycle is modelled by a non-linear model that is continually linearised at each iteration step.

The methodology based on linear MPC ([Cole et al., 2006]) is an unconstrained predictive control problem. This solution uses equations of motion that are derived with respect to axes fixed in and moving with the vehicle. Then, the used model is a state space model with four states, $v(t)$ the lateral velocity of vehicle in the direction of vehicle's lateral axis, $w(t)$ the yaw velocity of vehicle with respect to ground, $y(t)$ the lateral displacement of vehicle in ground-fixed axes, $\phi(t)$ the yaw angle of vehicle with respect to the ground. The input is the steering wheel angle $\delta(t)$ and the chosen outputs are the lateral displacement and yaw angle. [Cole et al., 2006], [Rowell et al., 2007] examined the problem of path-following control based on a linear model pre-

dictive control solution. However, a few systems are quite complicated and cannot be described by a linear model and some more complicated theories are necessary.

Some other solutions, [Borrelli et al., 2005], [Falcone et al., 2007b], based on MPC are using a non-linear model of the rolling system (NMPC). These algorithms focus on lateral control, the aim is to minimize deviations from their references to the heading and to the lateral distance. These algorithms using non-linear optimization give good results. However, MPC implementation requires significant computation infrastructure which might not be available on processes with fast sampling time and limited computational resources. The authors present some non linear solvers which can permit the resolution of the optimization problem. The solution of constrained non-linear optimization is a critical point, then it was proposed in [Borrelli et al., 2005], [Falcone et al., 2007a] and [Falcone et al., 2007d] to work with LTV and PWA models.

Some improvements of the LTV MPC can be found in [Falcone et al., 2007c]. The authors combine the brakes at the four wheels independently and the front steering systems to improve the efficiency of the controller. Moreover, [Seyr and Jakubek, 2005] decides to work with a NMPC solution but this implies a particular structure of the control function. In this case, the control function u has the following expression, $u(k) = A + B(1 - exp(-KT_s)$, with K a constant, T_s the sampling time. The aim of the optimization is simply the choice of the two variables A and B.

Neural Network Model Predictive Control (NNMPC)

The theory of NNMPC is very close to the theory of MPC and the application of this algorithm for automatic guidance is very new [Seyr et al., 2005], [Gu and Hu, 2002]. In this case, the only difference comes from the structure of the model. Here, the prediction is made with a NN and the following stages of the algorithm are the same ones as the traditional MPC. The algorithm is tested on mobile robot and the results seem very satisfying.

Conclusions for the model-based approaches

The different model-based approaches are summarized in Table 3.3, giving their advantages and drawbacks.

This bibliographic has studied presents the different model-based approaches used for path following. Two solutions have been retained, both are based on MPC. Indeed, MPC aims at defining a few points in front of the vehicle and calculating an optimal control signal which gives the possibility to come closer to the path. In the path following application, the future points of the road which must be reached are known, thus MPC which required a reference trajectory is an appropriated method. Then, the optimisation which helps to obtain the control signal requires a model of the system. In Sections 5.6.3 and 5.6.4, two different MPC solutions based on two different prediction models will be implemented and tested on the vehicle. On the one hand, a state space model will help to predict the system behaviour. On the other hand, a NN will be used in the MPC process.

Method	Advantages	Drawbacks
Neural network	Easy to implement, need a learning phase	Needs a lot of memory and no application in vehicle or aeronautic domain, only robot control applications
Backstepping	Gives good results at low speed, can be coupled with an adaptive part	The expression of the control law is very complex
Adaptive control	Takes into account the perturbations and the uncertainties	The impact of noise is very important, the assumptions for the stability are sometimes difficult to verify
Fuzzy logic	Able to take account of many parameters	Stability problems, difficulties to tune the controller in terms of membership functions
Model Predictive Control	Very adapted for trajectory tracking due to the prediction of the behaviour of the rolling system	Time needed for the optimization step could be a problem for real time implementation but solutions as LTV MPC or shape function could solve the problem, the application only deals with lateral control
Neutral Network Model Predictive Control	No accurate model of the rolling system is necessary and the model could be adapted at each sample time during the control stage	The model is not physical

Table 3.3: Model-based approaches comparison

3.2.4 Conclusion

The two previous sections described the general principles of automatic guidance. A review of the different control solutions adapted for low-level and high-level loops control have been presented. It can be shown that an important number of parameters are involved in the implementation of automatic guidance solutions. For example, the dynamics of the actuators have to be taken into account as well as the lateral and longitudinal behaviour of the rolling system. Then, it is important to define clearly the particularities of the study to obtain an appropriate control solution.

Based on the presented approaches, it can be noticed that the model of the system is very important. Indeed, the control algorithm highly depends on the model that is chosen. A lot of different models are used in the literature, kinematic models, dynamic linear or non-linear models, etc. A choice has to be done depending on the performances that must be reached.

Moreover, it seems that different control theories enable to solve the control issues raised in this manuscript. It seems important to be able to differentiate the results provided by these different control theories. Then, it is primordial to work with fixed test conditions (in term of trajectory, speed) in order to test the different algorithms and compare them. Thus, it could be interesting to follow the works of [Chaib et al., 2004] where an overview as well as a comparison of four controllers is proposed, to compare the different algorithms.

Finally, this section gives the possibility to point out three control strategies ("Follow the carrot", MPC and NNMPC), particularly adapted for the application which will be studied in detail in Chapter 5.

3.3 Models description

This section is dedicated to the presentation of the different models used in Chapters 4 and 5. These models will help to synthesize the proposed controllers or to perform simulations using the obtained controllers. The developped models are the following:

- A/C on ground models (cf. Section 3.3.1),
- nose landing gear steering models (cf. Section 3.3.2),
- shimmy model (cf. Section 3.3.3).

3.3.1 Aircraft on ground modelling

3.3.1.1 Introduction

This section focuses on the modelling of the A/C. These models are important insofar as they will be used for different purposes: synthesis of the controllers (MPC in Chapter 5), modelling of the NLG (this is clearly explained in Section 3.3.2) and for simulations purposes (for instance the validation of the NLG control laws). Three different models are presented in this section:

- a non-linear accurate model which presents a global structure of the A/C; it will be used to deduce simplified models (see Section 3.3.1.2)

- a non-linear model adapted for low speed; based on the previous model, it is used for simulation purposes (see Section 3.3.1.3)
- a simple LPV model, commonly called "bicycle model"; it is well-suited for controller synthesis (see Section 3.3.1.4)

3.3.1.2 Non-linear accurate A/C model

The non-linear aircraft on ground dynamic model presented in this section corresponds to a representation previously described in [Villaumé, 2002], [Jeanneau, 2007] and [Roos, 2007]. The general structure of the model is divided in three blocks described in Figure 3.12. The different variables which are introduced in this figure will be detailed in the following.

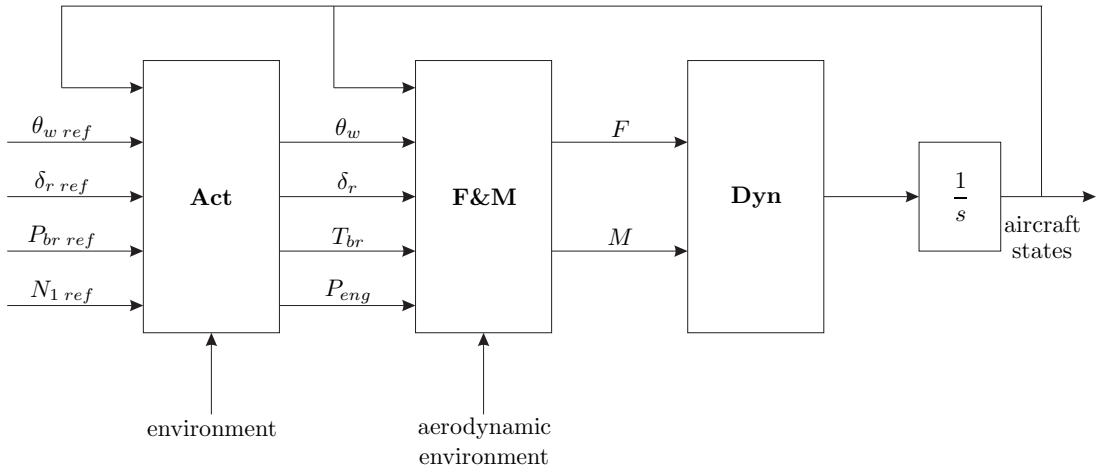

Figure 3.12: Architecture of the nonlinear A/C model (from [Roos, 2007])

- **Act**: corresponds to the different actuators (NLG, braking system, ...),
- **F&M**: corresponds to the description of the different forces and moments which act on the A/C,
- **Dyn**: corresponds to the evolution of the A/C (12 degrees of freedom).

The equations of the A/C on ground dynamic movement, described in block **Dyn**, consider the following 12 degrees of freedom:

- $V = [V_x, V_y, V_z]$: linear speed vector (longitudinal, lateral and vertical speeds) at the centre of gravity,
- $\Omega = [p, q, r]$: angular speed vector (roll, pitch and yaw speeds) at the CG,
- $\Lambda = [x, y, z]$: positioning vector of the CG,
- $\Xi = [\phi, \theta, \psi]$: angular vector (roll, pitch and yaw angles).

The evolution of the linear and angular speeds are obtained based on the Newton's law of motion applied at the A/C centre of gravity (CG) and are associated with the A/C axes presented in

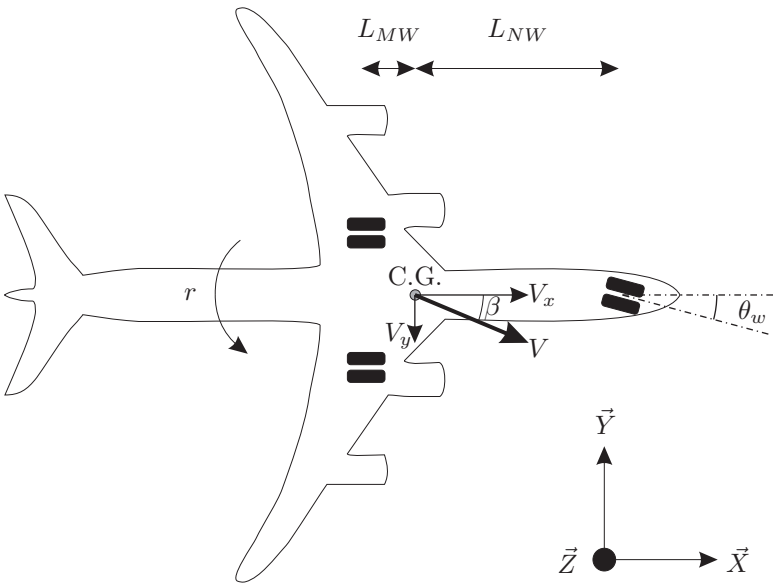

Figure 3.13: Schema of the A/C

Figure 3.13. This figure introduces the longitudinal and lateral speeds V_x and V_y at the CG, the yaw speed r which corresponds to the rotational speed around the vertical axis, the parameters L_{NW} and L_{MW} which characterize the distances respectively between the CG and the NLG and the CG and the MLG, the slip angle β at the CG defined by $\beta = atan\left(\frac{V_y}{V_x}\right)$ and the wheel angle rotation θ_w. Then, the equation of the movement helps to determine the position and the different angles of the A/C on the runway. These different contributions are summed up in the following equation:

$$\begin{bmatrix} \dot{V} \\ \dot{\Omega} \\ \dot{\Lambda} \\ \dot{\Xi} \end{bmatrix} = \begin{bmatrix} \frac{F}{M_{A/C}} - \Omega \wedge V \\ \frac{M}{\mathbf{J}} - \frac{\Omega \wedge \mathbf{J}\Omega}{\mathbf{J}} \\ T_\Lambda(\Lambda) \\ T_\Xi(\Xi) \end{bmatrix} \tag{3.9}$$

such that the forces F and moments M are provided by the block **F&M** , $M_{A/C}$ corresponds to the mass of the A/C and **J** is the matrix of inertia.

The block **F&M** details the forces and moments which act on the dynamics of the A/C on ground. These forces and moments can be divided in five main contributions: the aerodynamic effect, the gravity, the motor, the braking system and the wheel/road (W/R) interface. The expression of the forces is defined by the following equation:

$$\begin{bmatrix} F_x \\ F_y \\ F_z \end{bmatrix} = \frac{1}{2}\rho S V_a^2 \begin{bmatrix} -C_x \\ C_y \\ -C_z \end{bmatrix} + \begin{bmatrix} -M_{A/C} g sin(\theta) \\ M_{A/C} g sin(\psi) cos(\theta) \\ M_{A/C} g cos(\psi) sin(\theta) \end{bmatrix} + \begin{bmatrix} P_{eng} \\ 0 \\ 0 \end{bmatrix} + \begin{bmatrix} T_{br} \\ 0 \\ 0 \end{bmatrix} + F_{W/R} \tag{3.10}$$

The aerodynamic effects characterized by non-linear contributions depend on A/C shape. It is defined by ρ (density of air), S (reference surface), V_a (aerodynamic speed) and the aerodynamic coefficients C_x, C_y and C_z which depends on the rudder input θ_r. The modelling and the identification of this contribution is very complex and [Lavergne et al., 2004] proposes the use of

a NN to describe the aerodynamic effects. Thrust engines P_{eng} is obtained based on the reference engine speed $N_{1\,ref}$ [Yamane et al., 1997], [Duprez, 2004]. The braking torque T_{br} results from the friction between the rotors and the stators of the braking system when they are subject to a pressure $P_{br\,ref}$. This pressure effort may be produced by a hydraulic circuit, pistons and servo valve in the case of hydraulic braking system or by a set of motors and gears in the case of electric braking system [Jacquet, 2008]. The forces at the W/R interface corresponds to the forces generated by the tyres and the ground reactions. This contribution is very difficult to model due to non-linear dependencies in the nose wheel tyre slip angle β_{NW} and the main wheel tyre slip angle β_{MW}. Then, a lot of parameters act on the estimation of the W/R forces and moments like the vertical load F_z applied on the gears, the runway condition (dry, wet, frozen) or the longitudinal speed of the aircraft V_x. A detailed description of the different models and the parameters acting on the W/R forces and moments is presented in Appendix A.

3.3.1.3 Low speed non-linear lateral A/C model

The non-linear A/C model presented in the previous section describes a lot of contributions that are not specifically required for particular conditions discussed in the frame of this manuscript. Indeed, in this work, the required A/C model helps to simulate the trajectory tracking algorithm at low speed and will also be used as an observer for the NLG steering model (see Section 3.3.2.2). So, it is possible to neglect several phenomena and to obtain a model that is adapted for low speed manoeuvres (lower than 15m/s) like taxiing for instance. A two dimensional lateral simplified A/C model described in [Lemay, 2008] is then considered. This model, derived from the complete A/C model described in Section 3.3.1.2, is obtained by making the following hypothesis:

(H1): the runway is considered as horizontal then the position of the CG is fixed on the vertical axes and contributions V_z and $\dot{V}_z$ can be neglected,

(H2): the landing gear dampers are considered as rigid. This implies that the roll and pitch phenomena are not taken into account resulting in $p = 0$ and $q = 0$,

(H3): the limitation of the A/C longitudinal speed V_x helps to neglect the aerodynamic effects, indeed this contribution is minor compared to the W/R forces,

(H4): the actuator representations are neglected. For example the NLG wheel angle θ_w is an input of the model and the engine and braking systems are simplified and a virtual thrust drives the A/C longitudinal speed V_x.

This low speed non-linear lateral A/C model is obtained by applying the first Newton's law of motion on the $\vec{X}$ and $\vec{Y}$ axes and the second Newton's law of motion on the $\vec{Z}$ axis (cf. Figure 3.13). This model has the particularity to consider the load distribution due to centrifugal effects. The W/R is modelled by the use of the well-known Pacejka tyre model [Pacejka, 2006], presented in Appendix A; a non-linear representation of the forces generated by the tyre.

This model is well-suited for simulation purposes insofar as it is able to reproduce the A/C dynamics in the considered situations. However, synthesizing controllers from non-linear models is often a difficult task. That is why, the following section presents the equations of a simplified

A/C model. The proposed longitudinal speed dependent A/C LPV model is adapted for the synthesis of model-based controllers.

Finally, considering the fact that the A/C is composed of two wheels on the nose gear and two wheels on each main gears, the description of the low speed non-linear lateral A/C model is:

$$\begin{cases} \dot{V}_y = \dfrac{1}{M}\left(2 \cdot F_{y\,NW}(\beta_{NW}) + 4 \cdot F_{y\,MW}(\beta_{MW})\right) - V_x r \\ \\ \dot{r} = \dfrac{1}{J_{A/C}}\left(2 \cdot L_{NW} \cdot F_{y\,NW}(\beta_{NW}) - 4 \cdot L_{MW} \cdot F_{y\,MW}(\beta_{MW})\right) \end{cases} \tag{3.11}$$

with $F_{y\,NW}()$ and $F_{y\,MW}()$ the functions which describe the Pacejka model and the side slip angles β_{NW} and β_{MW} are expressed by:

$$\beta_{NW} = \theta_w - atan\left(\frac{V_y + r \cdot L_{NW}}{V_x}\right) \tag{3.12}$$

and

$$\beta_{MW} = -atan\left(\frac{V_y - r \cdot L_{MW}}{V_x}\right) \tag{3.13}$$

3.3.1.4 Bicycle model

The bicycle model is a well-known model mainly used in automotive and aircraft domains [Caroux, 2007] and [Duprez, 2004]. This model is based on the previously mentioned hypothesis (H1) to (H4) and is characterized by two more hypothesis:

> (H5): the aircraft is defined as symmetrical about its longitudinal axis, and a virtual wheel located at the middle of the rear axle is considered. In this way, the aircraft geometry is similar to that of a bicycle,
>
> (H6): only low slip angles are considered. This permits to make two major simplifications: the expression of the tyre slip angle is linearised and the linear contribution of the tyre forces are taken into account (cf. Appendix A).

Hypothesis (H5) can be done insofar as the roll dynamics, that means the movement around the lateral axis are relatively thin. Hypothesis (H6) related to tyre forces considers only low slip angle which is conceivable when the lateral dynamics are not larger than $3m/s^2$. Finally, based on the model presented in equation (3.11) and considering the two previous hypothesis (H5) and (H6), a LPV bicycle model is proposed.

Based on Appendix A and considering hypothesis (H6), the tyre slip angle is simplified such that:

$$\beta_{NW} = \theta_w - \left(\frac{V_y + r \cdot L_{NW}}{V_x}\right) \tag{3.14}$$

and

$$\beta_{MW} = -\left(\frac{V_y - r \cdot L_{MW}}{V_x}\right) \tag{3.15}$$

and the tyre contributions $F_{y\,NW}$ and $F_{y\,MW}$ are expressed by:

$$F_{y\,NW} = CS_{NW} \cdot \beta_{NW} \tag{3.16}$$

and

$$F_{y\,MW} = CS_{MW} \cdot \beta_{MW} \tag{3.17}$$

with CS_{NW} and CS_{MW} which correspond respectively to the cornering stiffness of the nose and main landing tyres. Finally, the aircraft bicycle model is described by:

$$\begin{cases} \dot{V}_y &= \dfrac{-(2 \cdot CS_{NW} + 4 \cdot CS_{MW})}{M \cdot V_x} V_y + \cdots \\ & \quad \cdots + \left(\dfrac{-(2L_{NW}CS_{NW} - 4 \cdot L_{MW}CS_{MW})}{M \cdot V_x} - V_x \right) r + \dfrac{2 \cdot CS_{NW}}{M} \theta_w \\ \dot{r} &= \dfrac{-(2 \cdot L_{NW}CS_{NW} - 4 \cdot L_{MW}CS_{MW})}{J_{A/C} \cdot V_x} V_y + \cdots \\ & \quad \cdots + \left(\dfrac{-(2 \cdot L_{NW}^2 CS_{NW} + 4 \cdot L_{MW}^2 CS_{MW})}{J_{A/C} \cdot V_x} \right) r + \dfrac{2 \cdot L_{NW}CS_{NW}}{J_{A/C}} \theta_w \end{cases} \tag{3.18}$$

The bicycle model will be used for two main purposed:

- the synthesis of $\mathcal{H}_\infty$ controllers for NLG steering purposes (see Section 4.2),
- the prediction of the MPC algorithms dedicated to path following (see Section 5.6)

3.3.2 Nose landing gear modelling

3.3.2.1 Introduction

This section deals with the modelling of the NLG. As it can be read in Section 4.2, the NLG control requires models for simulation purposes or for the synthesize of the controllers. Then, three models are used:

- a non-linear model integrating a non-linear A/C model (previously presented in Section 3.3.1.2) to describe the W/R interface. This model is presented in Section 3.3.2.2 and will be used for the simulation validation of the NLG control laws.
- a LPV model based on the A/C bicycle model from Section 3.3.1.4 to estimate the moment and forces and the W/R interface. This model is presented in Section 3.3.2.3 and will be used for the synthesis of $\mathcal{H}_\infty$ controllers.
- a simple LPV model which describes the W/R interface with a proportional relationship between the wheel angle and the resistive torque T_r; this helps to reduce the controller synthesis complexity. This model is presented in Section 3.3.2.4.

3.3.2.2 Non-linear NLG steering model based on an A/C model

The input of the NLG steering system is the electromechanical torque T_{em} and the output is the wheel angle θ_w around the vertical axis. The wheel angle will be considered to be equal to the sliding angle since the wheel can not rotate around its fixing axis. The "upper part", that means the electromechanical actuator is described by the following equation:

$$J_m \ddot{\theta}_m = T_{em} - \frac{1}{2N_c N_w} T_{leg} - T_{los}, \tag{3.19}$$

with T_{los} the mechanical losses of the actuator (friction torque in direct or inverse operating conditions). T_{leg} is defined by:

$$T_{leg} = 2N_w \left(\frac{\theta_m}{N_c} - N_w \theta_w \right) K. \tag{3.20}$$

with N_c and N_w two reduction ratios. Then, the "lower part" which integrates the turning tube, the sliding tube and the wheel is described by two rotating masses such that:

$$\begin{cases} \ddot{\theta}_t = \dfrac{1}{J_1} \left(T_{leg} - k(\theta_t - \theta_w) - c(\dot{\theta}_t - \dot{\theta}_w) \right) \\ \\ \ddot{\theta}_w = \dfrac{1}{J_2} \left(k(\theta_t - \theta_w) + c(\dot{\theta}_t - \dot{\theta}_w) + T_r \right) \end{cases} \tag{3.21}$$

The main problem of the NLG steering model lies in modelling the resistive torque T_r generated by the tyres at the W/R interface. In particular, the estimation of the nose wheel slip angle β_{NW} which is defined by the angle between the wheel direction and the wheel speed vector, is essential. It helps to calculate the forces and moments which create the resistive torque at the W/R interface. The proposed model is based on the estimation of the nose wheel slip angle using a non-linear A/C model which takes account of the non-linearities at the tyre/ground interface. This approach is presented in Figure 3.14.

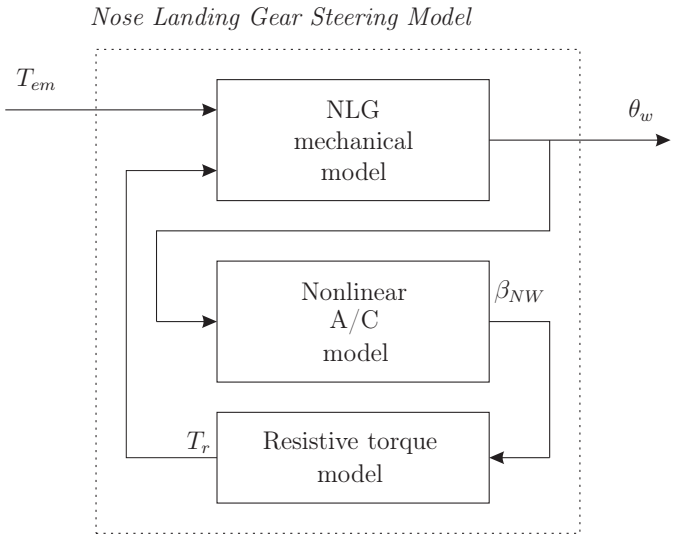

Figure 3.14: Structure of the NLG model integrating an A/C model

The non-linear A/C model, presented in Section 3.3.1.3, allows the estimation of the nose wheel slip angle β_{NW} as a function of the wheel angle θ_w. This estimation is then used as an input of the resistive torque model and helps to obtain the resistive torque T_r at the W/R interface.

Considering the fact that the NLG is composed of two tyres, the resistive torque is formulated by:

$$T_r = 2 \cdot M_{z\,NW}(\beta_{NW}) - 2 \cdot e \cdot F_{y\,NW}(\beta_{NW}). \tag{3.22}$$

This equation involves the tyre self-aligning moment $M_{z\,NW}$, the lateral tyre force $F_{y\,NW}$ and the caster length e which corresponds to the distance between the landing gear axle and the axle

which passes through the wheel centre. Both functions $M_{z\,NW}(.)$ and $F_{y\,NW}(.)$ are expressed using the well-known Pacejka tyre model [Pacejka, 2006] and need the knowledge of the slip angle β_{NW} on the nose wheel. β_{NW} is obtained with the states of the non-linear A/C model, V_y (the lateral speed at the A/C centre of gravity (C.G.)) and r (the vertical rotational speed) and V_x (the longitudinal speed at the C.G) which is the varying parameter. The expression of β_{NW}, based on the non-linear A/C model, presented in equation (3.11), has earlier been described in equation (3.12).

The obtained model is a non-linear NLG steering model. It considers an improved description of the electromagnetic behaviour of the motors. The mechanical transmission is described accurately considering its efficiency and the mechanical losses (cf. equation (3.19)). The resistive torque is obtained by an estimator which uses the non-linear A/C model presented in Section 3.3.1.3 and including non-linearities of the tyres thanks to a Pacejka tyre model. However, this non-linear model is incongruous for control laws synthesis because of its complexity; it is difficult to synthesize a controller when the synthesis model includes several non-linearities. Despite this drawback, this model is used for two main purposes:

- it is a reference and realistic model, permitting to test the proposed controllers during simulations,
- it helps to obtain the two LPV models used for the synthesis of the controllers which are presented in Sections 3.3.2.3 and 3.3.2.4.

The coming sections present two LPV models derived from this detailled NLG steering model. The first model is based on the structure presented in Figure 3.14, but the A/C and tyre non-linearities are neglected. This model estimates the resistive torque using an A/C LPV model which depends on the A/C longitudinal speed. The second model aims at reducing the structure presented in Figure 3.14 and notably the resistive torque estimation. Then, this model considers a simple proportional relation between the wheel angle and the resistive torque and thus neglects the effect of the wheel slip angle.

3.3.2.3 LPV NLG steering model based on an A/C model

Synthesizing controllers from non-linear models is often a difficult task. That is why, the equations of the actuator are simplified and a LPV model based on the estimation of the resistive torque using a longitudinal speed dependent A/C LPV model is developed. Then, this model is simplified insofar as some state variables and the non-linearities of the tyres are neglected.

Considering equation (3.19) which models the actuator, the non-linear contribution T_{los} is neglected and the simplified modelling of the electromechanical actuator becomes:

$$J_m\ddot{\theta}_m = T_{em} - \frac{1}{2N_cN_w}T_{leg} \tag{3.23}$$

with T_{leg} defined in equation (3.20). This simplification can be done insofar as T_{em} and $\frac{1}{2N_cN_w}T_{leg}$ are predominant compared with T_{los}.

Contrary to the shimmy phenomenon, where the dynamics of the compass have to be considered (cf. Section 3.3.3), for the steering application, the positions of the turning tube θ_t and the

wheel θ_w could be considered as similar. Then, equation (3.21) can be simplified and becomes:

$$\ddot{\theta}_w = \frac{1}{J_1 + J_2}\left(T_{leg} + T_r\right) \tag{3.24}$$

Then, the proposed LPV model is based on the structure defined in Figure 3.14. For the steering application, the non-linear A/C model and the non-linear resistive torque contribution are linearised as it has been done in Section 3.3.1.4. Indeed, the tyre contribution is frequently limited by its linear part when the slip angle β_{NW} is low ($< 5°$), which is the case for the considered application. Then, the two functions $M_{z\,NW}(.)$ and $F_{y\,NW}(.)$ of equation (3.22) are expressed using the self aligning stiffness SAS_{NW} and the cornering stiffness CS_{NW} such that:

$$T_r = 2 \cdot SAS_{NW} \cdot \beta_{NW} - 2 \cdot e \cdot CS_{NW} \cdot \beta_{NW} \tag{3.25}$$

Moreover, small slip angles can be considered and similarly to equations (3.14) and (3.17), the nonlinearities due to the *atan* function are neglected. The A/C model that results from this simplification is described in equation (3.18).

Finally, the obtained model has 1 input T_{em}, 6 states θ_w, $\dot{\theta}_w$, θ_m, $\dot{\theta}_m$, V_y and r and can be expressed as an LPV model with two varying parameters $\rho_1 = V_x$ and $\rho_2 = \dfrac{1}{V_x}$ such that:

$$\begin{cases} J_m\ddot{\theta}_m &= T_{em} - \dfrac{1}{N_c}\left(\dfrac{\theta_m}{N_c} - N_w\theta_w\right)K \\ (J_1+J_2)\ddot{\theta}_w &= 2N_w\left(\dfrac{\theta_m}{N_c} - N_w\theta_w\right)K + 2SAS_{NW}\left(\theta_w - \rho_2\left(V_y + rL_{NW}\right)\right) - \cdots \\ &\quad \cdots - 2eCS_{NW}\left(\theta_w - \rho_2\left(V_y + rL_{NW}\right)\right) \\ \dot{V}_y &= \dfrac{-\rho_2(2CS_{NW} + 4CS_{MW})}{M}V_y + \cdots \\ &\quad \cdots + \left(\dfrac{-\rho_2(2L_{NW}CS_{NW} - 4L_{MW}CS_{MW})}{M} - \rho_1\right)r + \dfrac{2CS_{NW}}{M}\theta_w \\ \dot{r} &= \dfrac{-\rho_2(2L_{NW}CS_{NW} - 4L_{MW}CS_{MW})}{J_{A/C}}V_y + \cdots \\ &\quad \cdots + \left(\dfrac{-\rho_2(2L_{NW}^2CS_{NW} + 4L_{MW}^2CS_{MW})}{J_{A/C}}\right)r + \dfrac{2L_{NW}CS_{NW}}{J_{A/C}}\theta_w \end{cases} \tag{3.26}$$

3.3.2.4 Simple LPV NLG steering model

The above presented LPV model is based on a complex structure. Indeed, the accurate estimation of the resistive torque at the W/R interface requires the use of an A/C model which must consider the contributions of the main landing gears. The two main drawbacks of such modelling are the required knowledge of the tyres on the main gear and the increase of the model order which is an important characteristic insofar as it is directly linked with the order of the synthesized controller in the case of $\mathcal{H}_\infty$ control theory. As a consequence, a simplified model is proposed. This simplified solution makes the realistic assumption of the conditions of its use that the

resistive torque T_r is only proportional to the wheel angle θ_w via a longitudinal speed dependent parameter $K_r(V_x)$ such that:

$$T_r = -K_r(V_x) \cdot \theta_w \tag{3.27}$$

As presented in Section 1.4.2, two approaches help to identify LPV models, the global approach and the local approach. The identification of the simple LPV NLG steering model is based on the local approach: $K_r(V_x)$ is obtained through simulations based on the reference model presented in Section 3.3.2.2. The identification method is divided into three steps: the gridding of the varying space V_x, the identification of the parameter K_r for each value of the varying parameter and finally an interpolation. The varying parameter V_x is gridded from $5m/s$ to $30m/s$ with a step of $5m/s$. Based on the detailed model, the parameter K_r is identified for each value of V_x. Finally, the different models are interpolated. Figure 3.15 presents the relation between V_x and K_r obtained by this approach. The interpolation is obtained with a second order

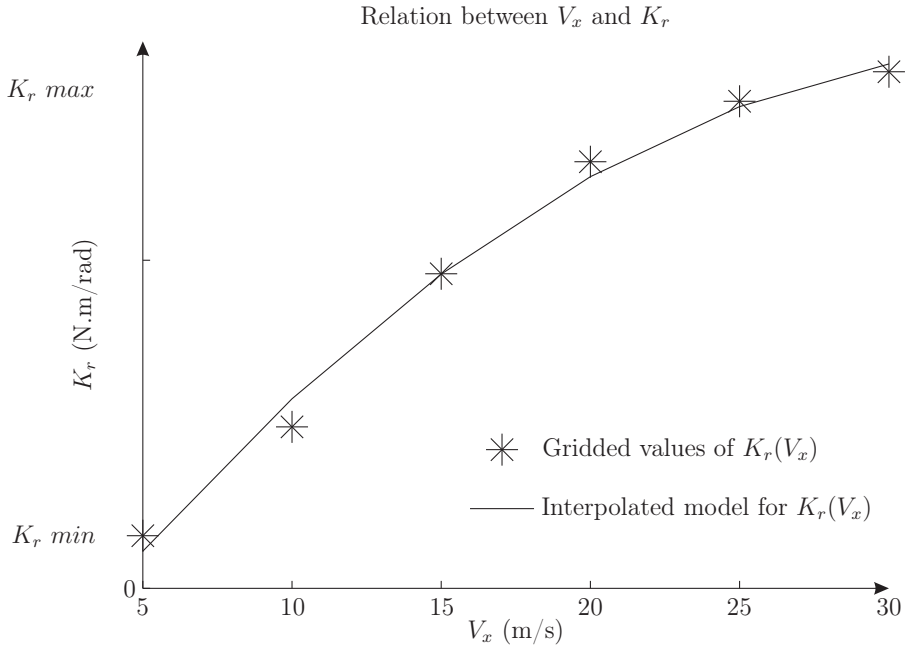

Figure 3.15: Interpolation results of the simple LPV model

polynomial such that:

$$K_r(V_x) = a_2 V_x^2 + a_1 V_x + a_0 \tag{3.28}$$

In this model, the actuator description is also simplified and the dynamics of the compass are not taken into account, similarly to the propositions made in Section 3.3.2.3. Finally, the simple model has 1 input T_{em}, 4 states θ_w, $\dot{\theta}_w$, θ_m, $\dot{\theta}_m$ and can be expressed as an LPV model with $\rho = K_r(V_x)$, the varying parameter. Based on equations (3.19), (3.20), (3.24) and (3.27), the equations of this simple LPV NLG steering model becomes:

$$\begin{cases} \ddot{\theta}_m = \dfrac{1}{J_m} T_{em} - \dfrac{K}{N_c^2 J_m} \theta_m + \dfrac{K N_w}{N_c J_m} \theta_w, \\ \ddot{\theta}_w = \dfrac{K}{N_c^2 (J_1 + J_2)} \theta_m - \left(\dfrac{\rho}{J_1 + J_2} + \dfrac{K N_w}{N_c (J_1 + J_2)} \right) \theta_w \end{cases} \tag{3.29}$$

3.3.3 Shimmy modelling

The description of the shimmy phenomenon has been done in Section 3.2.2.2. This section aims at presenting the equations of the model that permit to simulate the unstable oscillations characterising this phenomenon.

3.3.3.1 Description of Somieski's model

The input of the model is the control torque T_{em} which is provided by an electromechanical actuator here and the output of the model is the yaw angle of the wheel θ_w about its vertical rotating axis. It is important to insist on the fact that the study of the shimmy phenomenon, proposed in this manuscript, has been done as an initiatory study. The aim is not to validate the proposed control solutions, presented in Section 4.3, based on real tests. However, the objective is to study the feasibility of active shimmy damping (that means the damping of the shimmy oscillations with a controlled system). Then, the representation of the actuator considered for simulation purposes is based on a simple description. Indeed, the actuator developed in the frame of the DRESS project, presented in equation (3.19) is not taken into account. The link between the actuator and the turning tube is assumed to be rigid and the actuator dynamics only consider the viscous friction phenomena.

Based on the discussion about the actuator modelling and applying Newton's second law to the rotating movements of the actuator and the NLG, it is possible to leads to the following equations:

$$\begin{cases} J_1\ddot{\theta}_t = T_{em} - B_a\dot{\theta}_t - k(\theta_t - \theta_w) - c(\dot{\theta}_t - \dot{\theta}_w) \\ J_2\ddot{\theta}_w = k(\theta_t - \theta_w) + c(\dot{\theta}_t - \dot{\theta}_w) + M_3 + M_4 \end{cases} \tag{3.30}$$

where M_3 is the tyre moment caused by the lateral tyre deformations due to side slip and M_4 is the tyre damping moment related to the yaw rate, J_1 is the inertia of the turning tube plus the inertia of the actuator, J_2 is the inertia of the sliding tube and B_a is the viscous friction constant of the actuator. This landing gear description seems very close to the model presented in equation (3.21). Nevertheless, two main differences have to be noticed:

- the actuator description is simplified because its dynamics are not considered,
- the W/R interface is modified insofar as an important difference lies in the modelling of the tyre slip angle. The contribution of the tyre damping M_4 is considered because of its influence on the shimmy phenomenon.

Considering the tyre dynamics, the following equations summarize the non-linear characteristics of the tyre, which are discussed in [Somieski, 1997] and presented in details in Appendix A:

$$M_3 = 2M_{z\,NW}(\beta_{NW}) - 2eF_{y\,NW}(\beta_{NW}). \tag{3.31}$$

$$F_{y\,NW} = \begin{cases} c_F\beta_{NW}F_z & \text{for } |\beta_{NW}| \leq \delta \\ c_F\delta F_z sign(\beta_{NW}) & \text{for } |\beta_{NW}| > \delta \end{cases} \tag{3.32}$$

$$M_{z\,NW} = \begin{cases} c_M F_z \dfrac{\alpha_g}{180} \sin\left(\dfrac{180}{\alpha_g}\beta_{NW}\right) & \text{for } |\beta_{NW}| \leq \alpha_g \\ 0 & \text{for } |\beta_{NW}| > \alpha_g \end{cases} \tag{3.33}$$

$$M_4 = \frac{\kappa}{V_x}\dot{\theta}_w \tag{3.34}$$

$$\dot{y}_l + \frac{V_x}{\sigma} y_l = v\theta_w + (e-a)\dot{\theta}_w \tag{3.35}$$

$$atan(\beta_{NW}) \approx \beta_{NW} = \frac{y_l}{\sigma} \tag{3.36}$$

where M_z and F_y are respectively the self aligning torque and the lateral side force of the tyre, F_z is the vertical load applied on the NLG, V_x is the aircraft longitudinal speed, y_l is the lateral displacement of the tyre footprint. This lateral displacement is obtained using the elastic string theory defining the tyre lateral deformation as a stretched elastic string. Finally, β_{NW} is the slip angle of the tyre, e is the caster length, a is half of the contact length and c_{F_α}, c_{M_α}, κ, δ, α_g, σ are constants defined in [Somieski, 1997].

It is important to note that there are two non-linearities in the model, both related to the elasticity of the tyres. These non-linearities may cause limit cycles and instabilities. Therefore, the nose landing gear is rather difficult to control.

3.3.3.2 State space representation of Somieski's model

A state space representation of the NLG model is needed to design the adaptive damping controller. By choosing the state variables $x_1 = \theta_w$, $x_2 = \dot{\theta}_w$, $x_3 = y_l$, $x_4 = \theta_t$, $x_5 = \dot{\theta}_t$ and considering the control torque T_{em}, the non-linear dynamics presented above can be expressed as:

$$\begin{cases} \dot{x}_1 &= x_2 \\ \dot{x}_2 &= \dfrac{k(x_4-x_1)}{J_1} + \dfrac{c(x_5-x_2)}{J_2} + f_1(x_3) + f_2(x_2) \\ \dot{x}_3 &= V_x x_1 + (e-a)x_2 - \dfrac{v}{\sigma}x_3 \\ \dot{x}_4 &= x_5 \\ \dot{x}_5 &= -\dfrac{B_a x_5}{J_a} - \dfrac{k(x_4-x_1)}{J_a} - \dfrac{c(x_5-x_2)}{J_a} + \dfrac{1}{J_a}u \end{cases} \tag{3.37}$$

where:

$$f_1(x_3) = \frac{M_3(\alpha)}{J_2} = \frac{M_3(y_l/\sigma)}{J_2} \tag{3.38}$$

$$f_2(x_2) = \frac{M_4(\dot{\psi}_w/V_x)}{J_2} \tag{3.39}$$

The output of the system is $y = \theta_w = x_1$. Hence the third derivative of the output:

$$y^{(3)} = \ddot{x}_2 = \frac{k(\dot{x}_4-\dot{x}_1)}{J_1} + \frac{c(\dot{x}_5-\dot{x}_2)}{J_2} + \dot{f}_1(x_3)\dot{x}_3 + \dot{f}_2(x_2)\dot{x}_2 \tag{3.40}$$

Replacing the derivatives of the state variables (3.37) in (3.40), it is obvious that the input u appears on the right hand side of the result. This means that the system has the relative degree $r = 3$, and can be described by the following equation:

$$y^{(3)} = a(\mathbf{x}) + b(\mathbf{x})u \tag{3.41}$$

where $\mathbf{x} = [x_1, x_2, \ldots, x_5]^T$ is the system state vector, $a(\mathbf{x})$ and $b(\mathbf{x})$ are non-linear smooth functions. The explicit descriptions of these two non-linear functions can be obtained after some

mathematical manipulations. However, even if the exact expressions are calculated, they might not accurately describe the dynamics of the system when it is operating, because of time-varying parameters such as the vertical force F_z or tyre characteristics. For this reason, $a(\mathbf{x})$ and $b(\mathbf{x})$ are considered as unknown functions, and the adaptive control theory is adopted to cope with this uncertainty.

Nevertheless, by developing equation (3.40), it could be seen that the function $b(\mathbf{x})$ does not depend on the state variables $\mathbf{x}$. Then, this expression is simplified and $b(\mathbf{x})$ becomes B. Finally, equation (3.41) can be transformed into:

$$y^{(3)} = a(\mathbf{x}) + Bu \tag{3.42}$$

3.4 Conclusion

In the beginning of this chapter, the general purpose of guidance has been described and the structure of the global control strategy divided in two loops has been detailed. The low-level loop, presented in Section 3.2.2, is dedicated to the actuator control. This Section has presented the shimmy phenomenon and the specifications linked to the steering aspects. Then, the electromechanical steering actuator, developed in the frame of the DRESS project which replaces the hydraulic actuator has been described. The high level loop control, presented in Section 3.2.3 proposed through a detailed bibliography the different solutions which helps to automatically follow a path. Finally, based on the drawbacks and the advantages of the geometrical and model-based approaches, three solutions have been retained. These solutions will be developed and Chapter 5 presents the obtained results, based on real tests.

Later in this chapter, different models which will be used to develop the control solutions and to test them through simulations have been introduced. First, models which describe the A/C on ground dynamics have been detailed. Then, different modelling solutions, based on LPV descriptions, have been suggested for the description of the nose landing gear dynamics. Finally, a non-linear model has been proposed to represent the unstable oscillations which characterize the shimmy phenomenon. From Section 3.3.1 to Section 3.3.3, 7 models have been introduced. To understand the utility of each model, to show where the models will be used and to clarify the differences between the proposed models, a synthesis is presented in Table 3.4.

Model name	Purpose	Presented in Section	Used in Section	Utility	Particularity
Non-linear accurate A/C model	A/C dynamics description	3.3.1.2	⊘	Introduces all the phenomena that have an influence on the A/C on ground dynamics	Complex model
Low spedd non-linear lateral A/C model	A/C dynamics description	3.3.1.3	4.2	Simulations purposes	Obtain the nose wheel slip angle in the nose landing gear model

Model name	Purpose	Presented in Section	Used in Section	Utility	Particularity
Bicycle model	A/C dynamics description	3.3.1.4	3.3.2.3 - 5.6	• Build the nose landing gear model • Predict vehicle behaviour for MPC path following applications	Aeronautic and automotive applications
Non-linear NLG steering model based on an A/C model	Nose landing gear model	3.3.2.2	4.2	Simulations purposes	Non-linear model coupled with an A/C model to obtain the slip angle
NLG steering model based on an A/C model	Nose landing gear model	3.3.2.3	4.2	$\mathcal{H}_\infty$ controllers synthesis	LPV model with two varying parameters $\rho_1 = V_x$ and $\rho_2 = \frac{1}{V_x}$, integrating an A/C model to estimate the side slip angle
Simple NLG steering model	Nose landing gear model	3.3.2.4	4.2	$\mathcal{H}_\infty$ controllers synthesis	LPV model with one varying parameter (the resistive torque is proportional to the wheel angle)
Shimmy model	Shimmy modelling	3.3.3	4.3	Simulate the shimmy phenomenon	Improvement of the Somieski model

Table 3.4: Synthesis of the different models

J'ai inventé une lampe de poche qui fonctionne à l'énergie solaire, elle n'a qu'un dernier défaut, elle ne marche qu'en plein soleil.

André Franquin

Chapter 4

Control of the aircraft nose landing gear

Contents

4.1 Introduction

In Chapter 3, the context of the study has been presented, insofar as the low-level loop and the high-level loop are accurately described and the models required for control purposes are introduced. In this chapter, the low-level loop control and particularly the control of the NLG is detailed. Two main applications are described in this chapter:

- nose landing gear steering control (see Section 4.2);
- shimmy control (see Section 4.3).

On the one hand, in Section 4.2, the robust control solution which gives the possibility to steer the NLG is presented ([Pouly et al., 2009b], [Pouly et al., 2009d] and [Pouly et al., 2009c]).

Firstly, this section begins with the motivations for the choice of robust control theory. Indeed, based on the theoretical description of Section 2.2 and the different documents available in the literature notably [Scherer et al., 1997], [Gahinet and Apkarian, 1994], it seems that the synthesis based on $\mathcal{H}_\infty$ theory is adapted for the considered application of the aeronautic domain. This is clearly extended in Section 4.2.1.

Secondly, the particularity of $\mathcal{H}_\infty$ theory which needs the use of weighting filters to synthesize the controller is mentioned; their functions and the methods which help to obtain them are defined based on classic design rules [Ortega and Rubio, 2004] and [Hu et al., 2000]. Then, a tuning method which optimizes the choice of these weighting filters is proposed. Indeed, based on a genetic algorithm [Goldberg, 1989] and [Wang et al., 2003], it will be shown in Section 4.2.2 that this optimization methodology facilitates the design of the controller by decreasing the time required for the tuning step and by integrating for example specifications defined in the time domain.

Then, a discussion concerning the structure of the synthesis model is proposed in Section 4.2.3. Three structures respectively called "usual" structure (see Section 4.2.3.1), structure using an improved synthesis model (see Section 4.2.3.2) and structure using a synthesis model with 2 inputs (see Section 4.2.3.3) are proposed. These different structures are evaluated and compared to finally lead to a choice which corresponds to the only structure which helps to reach the specifications.

Next, simulation results based on gain scheduling and $\mathcal{H}_\infty$ theory are proposed. After the definition of the different test scenarios in Section 4.2.4.2, two gain scheduling techniques

([Theodoulis, 2008] and [Apkarian et al., 1995]) using each two synthesis models are presented. These different control solutions are based on the previously selected structure requiring 2 inputs (see Section 4.2.3.3) such that four different control solutions are synthesized and evaluated:

- Classic gain scheduling, based on an output blending approach (see Sections 4.2.4.3 and 4.2.4.4):
  - the synthesis model based on the LPV NLG steering representation which uses an A/C model (see Section 3.3.2.3),
  - the synthesis model that considers the NLG representation based on a proportional relation between the resistive torque and the wheel angle (see Section 3.3.2.4).
- Modern gain scheduling, based on a polytopic approach (see Sections 4.2.4.5 and 4.2.4.6):
  - the synthesis model based on the LPV NLG steering representation which uses an A/C model (see Section 3.3.2.3),
  - the synthesis model that considers the NLG representation based on a proportional relation between the resistive torque and the wheel angle (see Section 3.3.2.4).

Moreover, in Section 4.2.5, a discussion which aims at presenting the tools available for controller order reduction is proposed. Indeed, due to the well-known drawback of $\mathcal{H}_\infty$ theory which synthesizes high order controller, solutions to reduce the controller order are required. For this purpose two main solutions are discussed. On the one hand, the MOR tools, presented in Section C, such as balanced truncation tools, are applied to reduce the order of the controller synthesized in Section 4.2.4. On the other hand, a $\mathcal{H}_\infty$ synthesis algorithm which gives the possibility to consider the controller constraints (notably the dimension of the synthesized state space controller) during the synthesis step is studied [Burke et al., 2005].

Finally, in Section 4.2.6, the developed algorithms are tested on the test bench developed in the frame of the DRESS project. The difficulties, encountered during the transfer between the simulation step and the validation step on bench will be presented.

On the other hand, in Section 4.3, the control of the shimmy phenomenon is done through an initiatory study ([Pouly et al., 2009a], [Pouly et al., 2008b], [Huynh et al., 2008], [Pouly et al., 2008c] and [Pouly et al., 2008a]). The objective consist in analysing the impact of the new electrical steering system on the shimmy phenomenon and studying different methods for shimmy damping. The proposed solutions are limited to simulation validation and the algorithms are not implemented on the DRESS test bench for technical as well as for security reasons[1]. This section begins with the presentation of different scenarios for which the shimmy phenomenon appears. Then, three controllers, based on fuzzy adaptive theory, are presented and simulation tests are proposed. Firstly, Section 4.3.3 describes the design of two solutions based on state feedback and then presents the obtained simulation results. One solution considers a control law based on a direct structure which means that the fuzzy system is adjusted directly to ensure the control objectives while the second solution is based on an indirect structure where the fuzzy system helps to estimate the plant dynamics and then calculate the control law. Secondly, in Section 4.3.4, a control solution which only requires the measure of the wheel angle is

[1] It is quite difficult to simulate on a test bench the conditions of the shimmy phenomenon

detailed. After the description of the different values of the controller parameters, the results obtained with this output feedback control solution are presented. The main objectives of this section are:

- to test the feasibility of active shimmy control by using an electromechanical actuator,
- to evaluate if a control solution is able to actively damp the shimmy oscillations,
- to size the required actuator in term of bandwidth or amplitude if a control solution is satisfying.

4.2 Nose landing gear steering control

4.2.1 Motivations for the $\mathcal{H}_\infty$ synthesis choice

The choice of the theory used to synthesize the controller is an important step in the development of a control solution. In the literature, despite a lot of similitudes in the control solutions, the study of the specificities of each solutions has to be done. Indeed, it is possible to adapt the control solution to the particularities of the model as it was mentioned in Chapter 2. Here, the nose landing gear steering control is presented. Based on the NLG model presented in Section 3.3.2 and the objectives of the closed loop system described in Section 3.2.2.1, a control solution based on the $\mathcal{H}_\infty$ is adopted.

The $\mathcal{H}_\infty$ control solution has the advantage to consider the non-linearities of the plant. Particularly, using a polytopic formulation of the model, a non-linear controller is synthesized. Likewise, the obtained controller is on the polytopic form. This method gives the possibility to introduce the non-linearities in the control solution with simplicity.

In the early stages of the control solution development, it is important to keep in mind the objectives of the controller to be developed and the specificities of the system to be controlled. Indeed, the $\mathcal{H}_\infty$ method has the advantage to synthesise a simple controller expressed on the state space form. The implementation of such controller is very easy insofar as the tools which help to develop embedded software permit to implement these simple controller structures. The comparison of such a solution with the non-linear adaptive methods proposed in Section 2.3 shows clearly the interest of the industrial for such a simple structure. Moreover, this control solution is well adapted for systems with fast dynamics. The simple matrix operations, insofar as the size of those is not too high, can be implemented easily in real-time. In comparison with MPC, which needs a lot of calculation power to allow the on-line optimization, $\mathcal{H}_\infty$ helps to reduce the A/C on-board calculation equipment.

The consideration of the model of the system for the synthesis of the controller (frequently named as model-based control) is very interesting. On the one hand, it helps to have a precise formulation of the problem. Then, it is possible to consider stability and performance constraints based on a priori knowledge of the system. On the other hand, it facilitates the evolution of the control law for other systems close to the considered one. For instance, if a controller is developed for the NLG of an Airbus A320 A/C, when a similar electromechanical NLG actuator will be developed for an Airbus A350, it will be sufficient to model and identify the landing gear and the actuator systems and then use the obtained model to synthesize the controller.

Finally, considering the industrial interest, it is possible to develop an automatic tuning of the control solution. Based on the specifications, the controller can be synthesized, which means that an optimal structure of the synthesis model is obtained and the tuning parameters of the controller are adjusted. This clearly facilitates the time required for the tuning of the controller.

4.2.2 Optimal tuning of the $\mathcal{H}_\infty$ control solution

4.2.2.1 Introduction

The weighting filters used in $\mathcal{H}_\infty$ synthesis determine the controller. The design of appropriate weighting filters helps to satisfy the required specifications. For instance, considering the filter commonly named W_e which has the tracking error as an input, it enables to specify the acceptable error signal. Based on the definition of this weighting filter, the characteristics of the close loop system will evolve and particularly the error signal. If W_e is chosen large and broad (an important gain with a high cut-off frequency), the signal error will be small, but it is obvious that a compromise has to be reached.

The suitable selection of weighting filters which must incorporate stability and performance requirements is difficult to obtain. A basic method based on a trial and error process is often used. Despite the importance of the weighting filters, just a few references in the literature deal with the definition of design rules to obtain the weighting filters. [Hu et al., 2000] propose a basic form of performance weighting filters taking account of disturbances rejection and steady state error. For the control signal weighting filter, the position and rate constraints are considered by the use of characteristic responses of the actuator signal. [Ortega and Rubio, 2004] suggests a methodology for the case of S/T mixed sensitivity approach. This case aims at designing a controller which satisfies simultaneously performance and robustness specifications[2]. The properties of the weighting filter W_T, related to the transmission function, are suggested in particular by the nature of uncertainties. The design of the weighting filter W_S, which imposes the performances conditions to the system, is based on the required behaviour of the system. Finally, these methods give a first advice for the design but the trial and error process is required anyway.

In order to facilitate the design of $\mathcal{H}_\infty$ controllers, the tuning of the weighting filters could be formulated as an optimization problem [Sandou et al., 2008], [Sweriduk et al., 1998]. In this method, the weighting filters are expressed in terms of variable parameters and an optimization algorithm helps to identify these parameters. Based on this tuning, it is possible to define the controller and the augmented system structure. For instance, [Sandou et al., 2008] translates the performances to be reached, that means the frequency characteristics of the open-loop (bandwidth, gain margin, phase margin, module margin) or the classic temporal closed-loop requirements, into an optimization problem. Then, the particle swarm theory [Eberhart and Kennedy, 1995] is used to solve the optimization problem. The main drawback of such an approach is to compare the different specifications. In other words, a method is required to compare the frequency responses with the time responses. Here, the authors chose to use very hard penalty functions. Then, this consideration aims at requiring that all the specifications

[2]The sensibility transfer function $S(p)$ from the setting to the error and the transmission function $T(p)$ from the setting to the output are used in the frame of the S/T mixed sensitivity approach.

must be satisfied and no compromise is considered. In [Sweriduk et al., 1998], the authors decided to simply consider one temporal specification and use a genetic algorithm (GA) to obtain the optimal weighting filters. It has been decided to be in favour of the method proposed by [Sweriduk et al., 1998]. This choice is based on two main arguments:

- GA method is a well-known global search technique and the difficulties introduced by the use of the particle swarm theory are not necessary (notably the complex implementation compared with GA),
- two main specifications are required in the frame of the DRESS project (cf. Section 3.2.2.1) and the temporal one (Specification 2) is the most difficult to reach. If this specification is satisfied, the other is satisfied too.

4.2.2.2 Weighting filters tuning using Genetic Algorithms

GA [Goldberg, 1989], frequently used to solve control engineering problems [Wang et al., 2003], help to obtain optimal parameters to solve an optimization problem. The schematic of the working principle of a GA is presented in Fig. 4.1. The GA is based on a population composed of several individuals in a species, evolving in an environment following an iterative process. This population is designed to keep alive its species in its environment. To do this, it tries to adapt itself. In this case, each individual is more or less adequate to solve the problem of survival. The first step consists in initializing the population. In the frame of the considered application,

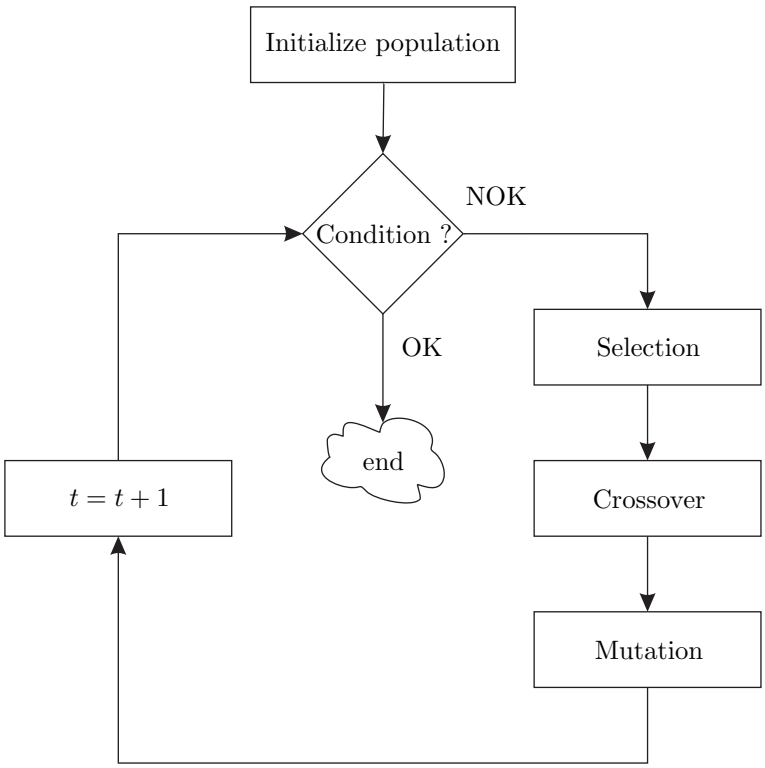

Figure 4.1: Working principle of a GA

it has been decided to create a population composed of 50 individuals (this values has been chosen after empiric tests). Each individual is composed of genes which correspond to different

parameters to optimize. Values of the genes are initialized randomly according to the definition spaces of the parameters to optimize. Individuals form a population which represents all the potential solutions to the optimization problem. The individuals in the population are evaluated according to a fitness function, a particular function which depends on the problem to solve. This function returns, based on one individual of the population, a single numerical fitness. This latter represents the ability of the individual to solve the optimization. The fitness function helps to rank the different member of the population. Then, as presented in Figure 4.1, a condition based on a termination criterion, is defined to let the population continue its evolution. If the termination criterion commonly based on a particular value of the fitness function or a process iteration number is validated, the process is stopped. In the application presented below, it has been decided to set the number of maximum process iteration number to 200. The iterative process is composed of three main steps, the selection, the crossover and the mutation. The selection aims at keeping a part of the existing population before building the new population. The selection step of the GA used to obtain the optimal weighting filters keeps only the best individual (one who has the best fitness value) and tries to improve the population by changing all the other individuals of the population. Two evolution mechanisms help to improve the population, the crossover and the mutation. The crossover is a sexual reproduction, it takes two individuals, cuts their genes at some randomly chosen position to produce two "head" parts and two "tail" parts. The "tail" parts are swapped over to produce two new individuals. This step is repeated for all the individuals which are not selected. This evolution mechanism which does not permit to create new genes is followed by the mutation. This latter is an asexual reproduction mechanism which aims at randomly altering one part of the gene. The crossover helps to explore rapidly a search space while the mutation provides a small amount of random search. Two parameters characterize the reproduction mechanism, the crossover probability and the mutation probability. The first defines the probability that a crossover will occur between two individuals and the second defines the probability that a mutation will occur in any given gene. Note that probability of the crossover is typically near 1 and 0.8 is chosen in the frame of the presented optimization problem. Concerning the mutation probability, the chosen value which corresponds to the typical value is 0.1.

Figure 4.2 presents the different steps of the optimization procedure developped for the obtaining of the weighting filters. The first point is to define the objective which must be

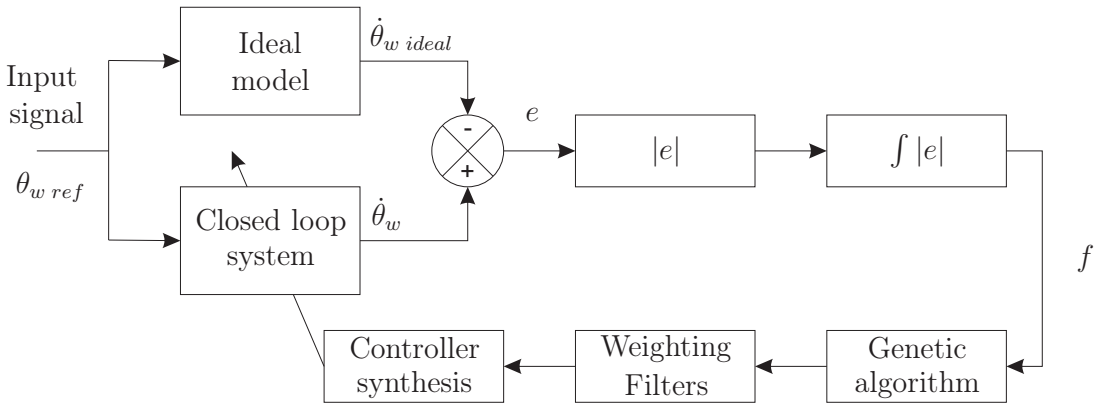

Figure 4.2: Weighting filters optimization technique

reached. This objective results in the description of the input signal ($\theta_{w\,ref}$) and the ideal model which helps to have $\dot{\theta}_{w\,ideal}$. In the frame of the presented application, based on the specifications provided by the A/C manufacturers, the input signal $\theta_{w\,ref}$ is a ramp in position and the ideal model is obtained by searching a transfer function which stays between the two lines of the template (cf. Specification 2 (3.2.2.1). Then, the input and the ideal model help to obtain the ideal response that the controlled system should reach. This output of the ideal model is compared with the output of the closed-loop system, giving the error signal e. The closed-loop system is composed of the system with the $\mathcal{H}_\infty$ controller. The synthesis of the controller is obtained by expressing the weighting filters in terms of free parameters K_i which must be optimized. For example, as it will be detailed further, the weighting filter W_e specifying the penalty on the control signal becomes $W_e = \dfrac{K_1 s + K_2}{K_3 s + K_4}$. To quantify the difference between the ideal model and the closed-loop system, the integral of the absolute error is calculated and used by the GA as a fitness function (f). Based on this fitness function, the optimization algorithm tries to provide suitable parameters K_i which reduce the fitness value. Finally, the free parameters are used to define the weighting filters and a new closed-loop system is obtained.

4.2.3 Nose Landing Gear steering control based on a LTI system

The optimal tuning of the $\mathcal{H}_\infty$ control solution based on a GA approach helps to obtain the optimal "generalized" model $\mathcal{P}$. This section presents three different "generalized" models $\mathcal{P}$, based on different structures of the weighting filters and the use of the model of the system $\mathcal{M}$ presented in Section 3.3.2.3. Thus, this optimization procedure has two main objectives:

- to define an optimal structure of the "generalized" model $\mathcal{P}$ (here, only structure of the weighting filters is optimized, the model of the system $\mathcal{M}$ is not changed in this section),
- to obtain the optimal definition of these weighting filters.

Particularly, the results presented in this section aim at identifying the value of two weighting filters, W_e for the acceptable error signal (the difference between the wheel angle reference $\theta_{w\,ref}$ and the wheel angle θ_w) and W_u for the penalty on the control signal. They are expressed in terms of free parameters such that $W_e = \dfrac{K_1 s + K_2}{K_3 s + K_4}$ and $W_u = \dfrac{K_5 s + K_6}{K_7 s + K_8}$. So, the GA must optimize the 8 parameters K_1 to K_8. To perform the optimization, the input signal (see $\theta_{w\,ref}$ in Figure 4.2) is a ramp in position, with a slope of $10°/s$, which corresponds to the specification 2 (cf. Section 3.2.2.1). The fitness function f is evaluated when the simulation ran for $1.5s$. The ideal model is defined in terms of a transfer function $\dfrac{\dot{\theta}_{w\,ideal}(s)}{\theta_{w(s)}}$ such that $G_{ideal}(s) = \dfrac{355.3s}{s^2 + 30.16s + 355.3}$. As mentioned previously, this ideal model has been identified based on the specification defined in Figure 3.7. Indeed, the response of $G_{ideal}(s)$ for a ramp stays between the maximum and minimum plots defined in the specification.

The following will present three different model synthesis structures. The structures have been developed successively. The drawbacks of each structure have been defined and solutions have been proposed to improve the results. Finally an optimal "generalized" model $\mathcal{P}$, to the extent it complies with the specifications, has been adopted.

Table 4.1 summarizes the different simulations which are performed in Sections 4.2.3.1, 4.2.3.2 and 4.2.3.3 and the conditions under which they are made.

Section	Structure	Model of the system $\mathcal{M}$	Fixed weighting parameters	Optimized weighting parameters
4.2.3.1	"Usual" 1-input structure	LPV NLG steering model based on an A/C model (cf. Section 3.3.2.3)	W_r	W_e, W_u
4.2.3.2	1-input structure with ideal model weighting filter	LPV NLG steering model based on an A/C model (cf. Section 3.3.2.3)	W_r, W_{mod}, W_{perf}	W_e, W_u
4.2.3.3	"Usual" 2-input structure	LPV NLG steering model based on an A/C model (cf. Section 3.3.2.3)	W_r	W_e, W_u

Table 4.1: Description of the studied structures

4.2.3.1 "Usual" 1-input structure

The $\mathcal{H}_\infty$ controller is synthesized using one input for the controller and three weighting filters: W_e and W_u, which must be optimized and $W_r = \dfrac{1.3}{0.05s+1}$, which helps to specify the reference signal $\theta_{w\,ref}$. Such weighting filters (W_r) are generally used when the control problem requires the tracking of a reference signal. It shapes the reference signal $\theta_{w\,ref}$ in terms of magnitude and frequency. So, it is obtained considering the maximum amplitude of the demanded angle and the maximum wheel speed defined by the technical specifications. Finally, the "generalized" model based on a commonly used structure is called "usual" 1-input structure and is presented in Figure 4.3.

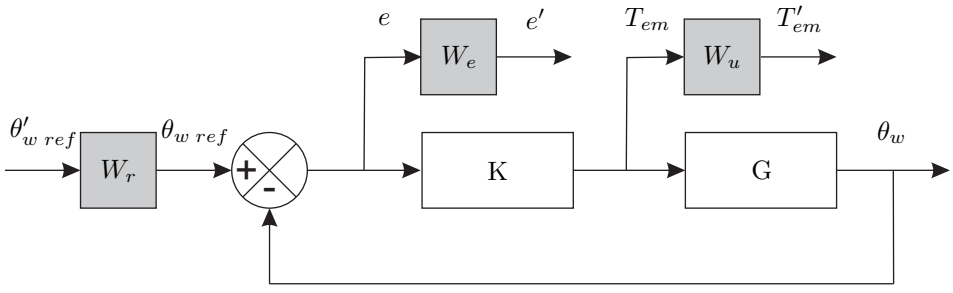

Figure 4.3: "Usual" 1-input structure

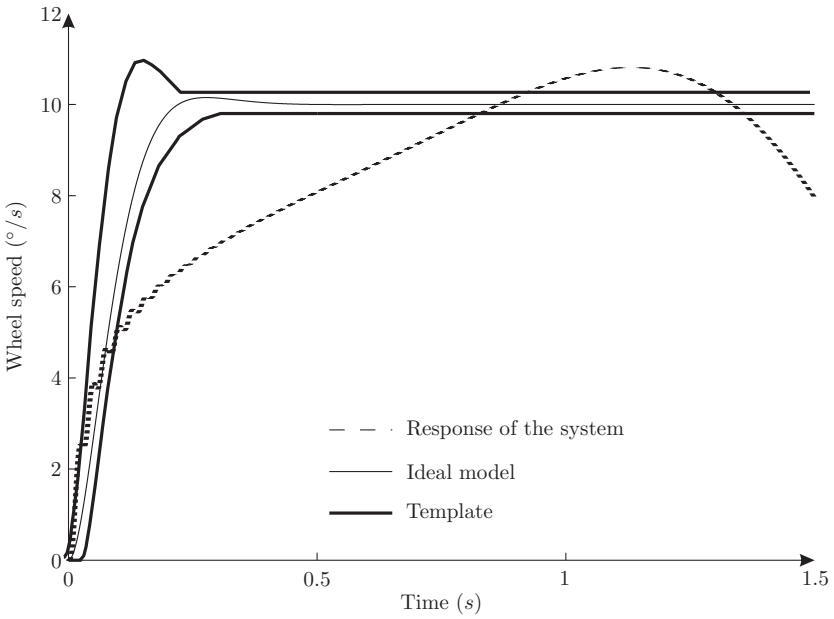

Figure 4.4: Results of the optimization based on the "usual" 1-input structure

Figure 4.4 presents the results of the closed-loop system when the optimal weighting filters are obtained. It can be seen that the specifications of the ramp position are not met: the response of the system is not within the defined template.

4.2.3.2 1-input structure with ideal model weighting filter

To improve the response for the ramp position, this structure also considers the wheel speed $\dot{\theta}_w$ for the controller synthesis. This quantity is not used as an additional input of the controller, which means that its real-time measurement is not required. Indeed, the wheel speed $\dot{\theta}_w$ is compared with the reference speed determined from the signal $\theta_{w\,ref}$ and the weighting filter W_{mod}. Finally, this structure considers that the controller has one input and five weighting filters: W_e and W_u, which must be optimized and $W_r = \dfrac{1.3}{0.05s+1}$, which helps to specify the reference signal $\theta_{w\,ref}$, $W_{mod} = \dfrac{355.3s}{s^2+30.16s+355.3}$, which characterizes the desired wheel speed response (this transfer function corresponds to the ideal model presented in Figure 4.2) and $W_{perf} = 20$ which weights the acceptable error between the wheel speed and the desired wheel speed.

Commentary It can be noticed that the same definitions are proposed for the ideal model G_{ideal} and the weighting filter W_{mod}. Nevertheless, these two components have two completely different objectives. G_{ideal} is used to define the closed-loop response that must be reached in the frame of the GA optimization process while W_{mod} is a weighting filter used for the synthesis of the $\mathcal{H}_\infty$ controller. Thus, both represent the expected behaviour of the system, they are acting for the same objective but they are not used at the same level.

This improved structure, called 1-input structure with ideal model weighting filter, is shown in Figure 4.5.

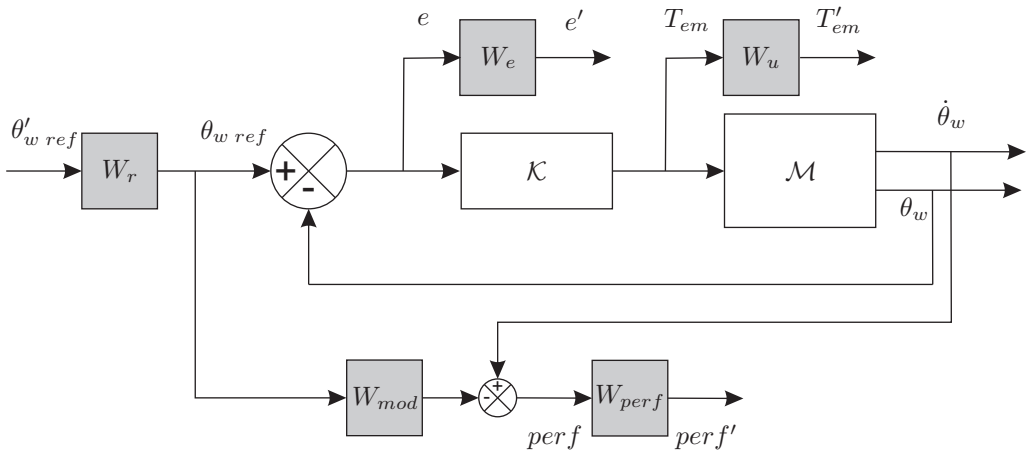

Figure 4.5: 1-input structure with ideal model weighting filter

This structure of the "generalized" model gives better results than the "usual" 1-input structure, as shown in Figure 4.6. Despite some oscillations, the response of the system remains close to the template (the maximum amplitude is $11.2°/s$). But, after 0.6s, the response signal does not fall within the specified template, this structure is not acceptable and must be improved.

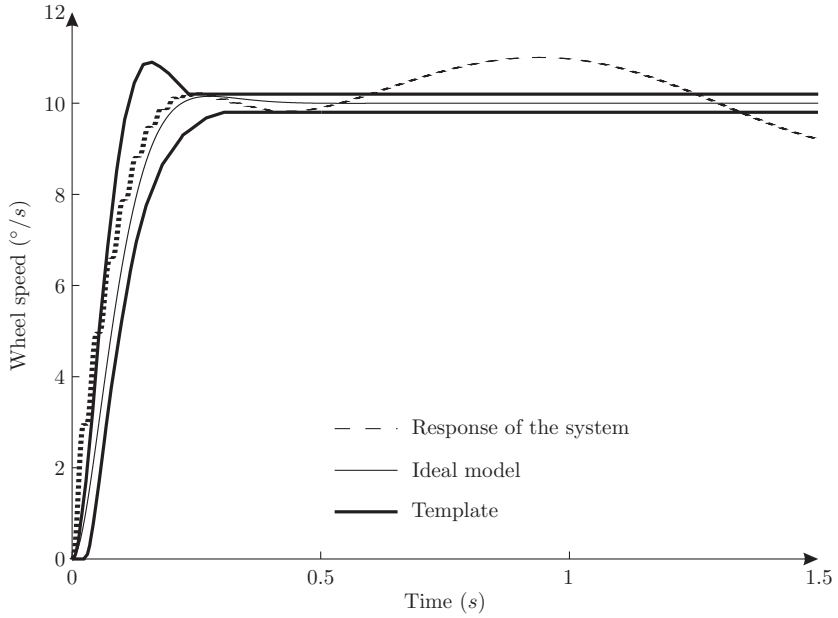

Figure 4.6: Results of the optimization based on the 1-input structure with ideal model weighting filter

4.2.3.3 "Usual" 2-input structure

The two previous structures give unsatisfactory results. The main reason is the lack of information received by the controller from the NLG system. Specifically, the controller knows the behaviour of the "lower part" of the system through the measurement of θ_w; however, the behaviour of the "upper part", i.e. the actuator, is not considered in the previous structures. From this observation, structure 3 proposes to use the motor speed $\dot{\theta}_m$ as an additional input of the

controller. The following reasons justify this choice:

- the motor speed $\dot{\theta}_m$ is easy to obtain, since it is still measured for the inner engine control loop,
- the input torque to be applied is directly linked to the motor speed.

The $\mathcal{H}_\infty$ controller is synthesized using two inputs for the controller and three weighting filters: W_e and W_u, which must be optimized and $W_r = \dfrac{1.3}{0.05s+1}$, which is similar to the other structures. This synthesis model is presented in Figure 4.7.

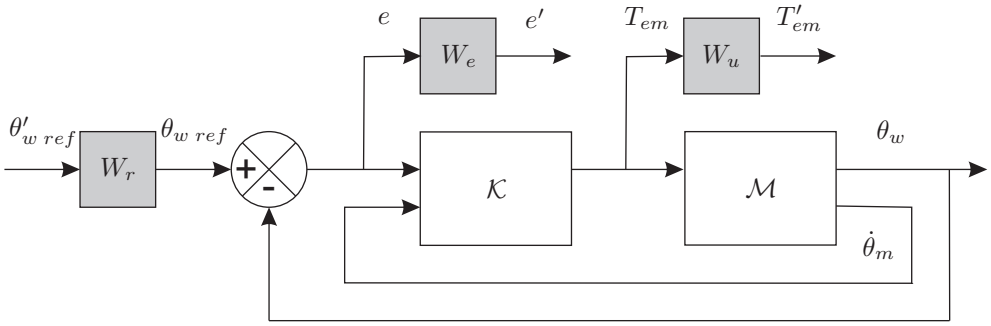

Figure 4.7: "Usual" 2-input structure

The results presented in Figure 4.8 show that the specifications are met, despite the fact that a slight overshoot can be noticed at time $t = 0.35s$. The response to a ramp position is suitable (cf. Figure 4.9); the response of the system with the proposed control solution is very close to the template (the maximum amplitude is $10.3°/s$ while the template authorizes $10.2°/s$). Moreover, Figure 4.9 presents the wheel angle response. A tracking error of $\approx 0.1°$ is observed, but the specifications defined in terms of wheel speed response are respected. Now, this strategy requires the measurement of two system states (θ_w and $\dot{\theta}_m$).

Commentary The "generalized" model, based on the "usual" 2-input structure gives the best results. As a consequence, the synthesis of the proposed controllers uses this structure. This methodology is well-suited from an industrial point of view. Indeed, it is possible to build the controller automatically, based on the aeronautical specifications and the model of the system. This method also helps to synthesize a controller when a new system is studied. Considering the development of a new actuator for a new NLG which has different performance characteristics, the $\mathcal{H}_\infty$ controller can be synthesized as soon as a model of the system is available.

This section presented an optimization principle which helps to define the structure of the $\mathcal{H}_\infty$ "generalized" model and to search the appropriate weighting filters. This principle is used and extended in section 4.2.4.

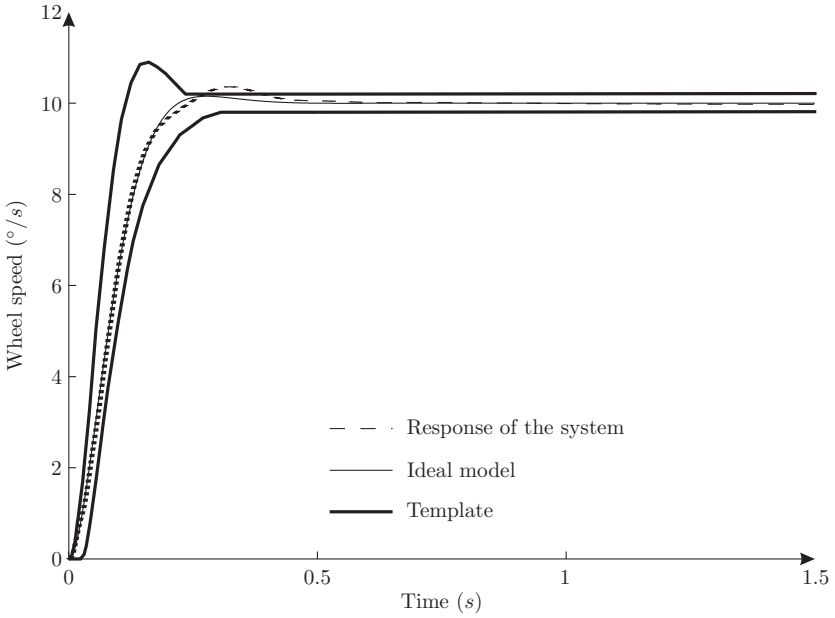

Figure 4.8: Results of the optimization based on the "usual" 2-input structure

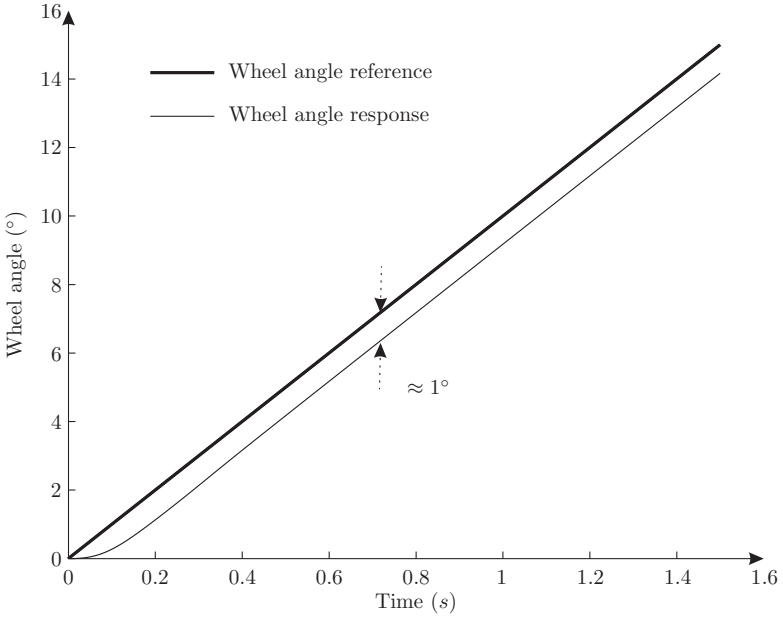

Figure 4.9: Obtained wheel angle response with the "usual" 2-input structure

4.2.4 Simulation results of the gain scheduling $\mathcal{H}_\infty$ solutions

4.2.4.1 Introduction

Section 4.2.3 presented an optimisation methodology which permits to define the "generalized" model, by obtaining an appropriated structure (the "usual" 2-input structure is adopted) and by defining an optimal definition of the weighting filters. This methodology has been applied for LTI models and it will be extended for LPV models and gain scheduling controllers in the frame of the current Section. Then, Section 4.2.4 is dedicated to the presentation of NLG steering simulation results by the use of different gain scheduling control solutions.

Firstly, Section 4.2.4.2 reminds the two test scenarios used for the simulations validation of the different gain scheduling control solutions. Secondly, Sections 4.2.4.3, 4.2.4.4, 4.2.4.5 and 4.2.4.6 present the different parameters required for the synthesis of the gain scheduling controllers, and the simulation results. Thirdly, Section 4.2.4.7 discusses the obtained results and tries to propose new approaches which may help to improve the closed-loop response of the system.

To apprehend the distinctness between the different gain scheduling control solutions, Table 4.2 proposes to summarize these solutions and to clarify their own specificities.

4.2.4.2 Definition of the test scenarios

The simulation step is a significant step in the development of the control laws. It is very important to test drastically the capacities of the closed-loop with numerous scenarios. These numerous simulations could give the possibility to apply the control solutions on the real test bench with more confidence and a better knowledge of the issues.

The results of the four proposed gain scheduling controllers (classic gain scheduling and modern gain scheduling, both synthesized with the previously described LPV models) are presented here using two different simulation scenarios:

- scenario 1: the simulation lasts $1.5s$, the longitudinal speed of the A/C is constant at $V_x = 17m/s$ and a ramp in position is demanded (this signal corresponds to Specification 2 (cf. Section 3.2.2.1)). The aim of this simulation is to examine the response of the closed-loop system for this restrictive specification,
- scenario 2: the simulation lasts $20s$, the longitudinal speed of the A/C varies from $5m/s$ to $25m/s$ and a sinusoidal angle with varying amplitudes is demanded. The aim of this simulation is to analyse the behaviour of the different gain scheduling controllers in varying parameters conditions.

4.2.4.3 Controller blending applied to the A/C-based NLG steering model

Classic gain scheduling requires the gridding of the varying parameter space. From $V_x = 5m/s$ to $V_x = 30m/s$, it has been decided to synthesize six $\mathcal{H}_\infty$ controllers. No method permits to fix the number of controllers which must be synthesized and a compromise between the complexity due to a large number of controllers and the efficient gridding of the varying space must be done. Then, the different distances D_i, d_i and d_{i+1} presented in Figure 2.4 are calculated numerically. The relation between the two varying parameters $\rho_1 = V_x$ and $\rho_2 = \dfrac{1}{V_x}$ helps to obtain these

Section	Model $\mathcal{M}$ used for the synthesis	Gain scheduling control solution	Specificities of the control solution
4.2.4.3	LPV NLG steering model based on an A/C model (cf. Section 3.3.2.3)	classic gain scheduling, blending output approach (theoretical aspects: Section 2.2.3.1)	• two varying parameters • gridded varying space • six interpolated LTI controllers
4.2.4.4	Simple LPV NLG steering model (cf. Section 3.3.2.4)	classic gain scheduling, blending output approach (theoretical aspects: Section 2.2.3.1)	• one varying parameter • gridded varying space • six interpolated LTI controllers
4.2.4.5	LPV NLG steering model based on an A/C model (cf. Section 3.3.2.3)	modern gain scheduling, polytopic approach (theoretical aspects: Section 2.2.3.2)	• two varying parameters • trapezoidal polytope with four vertices
4.2.4.6	Simple LPV NLG steering model (cf. Section 3.3.2.4)	modern gain scheduling, polytopic approach (theoretical aspects: Section 2.2.3.2)	• one varying parameter • polytope with two vertices

Table 4.2: Description of the different gain scheduling control solutions

calculations. Finally, the function $f = \frac{1}{x}$ leads to six different controllers. The weighting filters are the ones obtained in Section 4.2.3.3 and the six controllers are synthesized with similar weighting filters which are obtained using the optimal procedure based on GA.

The simulation results for each scenario are presented respectively in Figure 4.10 and Figure 4.11.

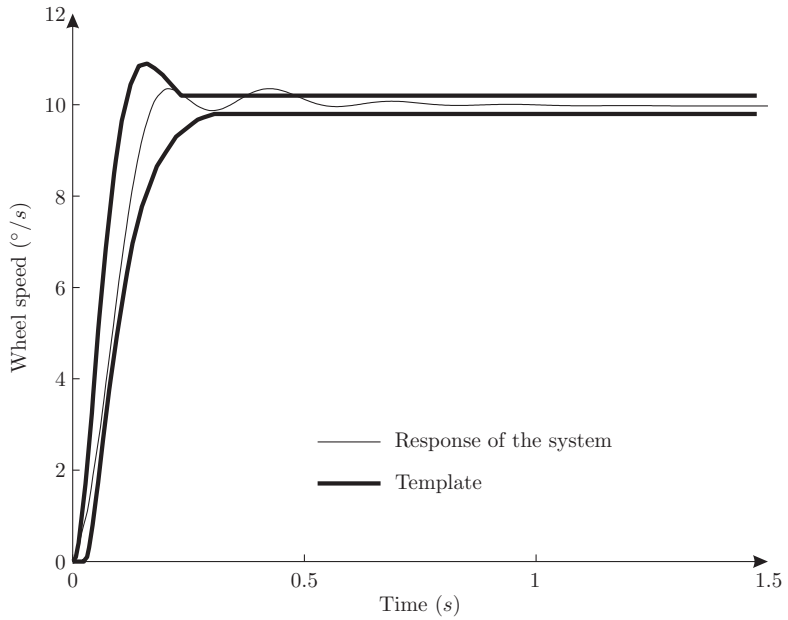

Figure 4.10: Scenario 1 for the classic gain scheduling based on the complex model

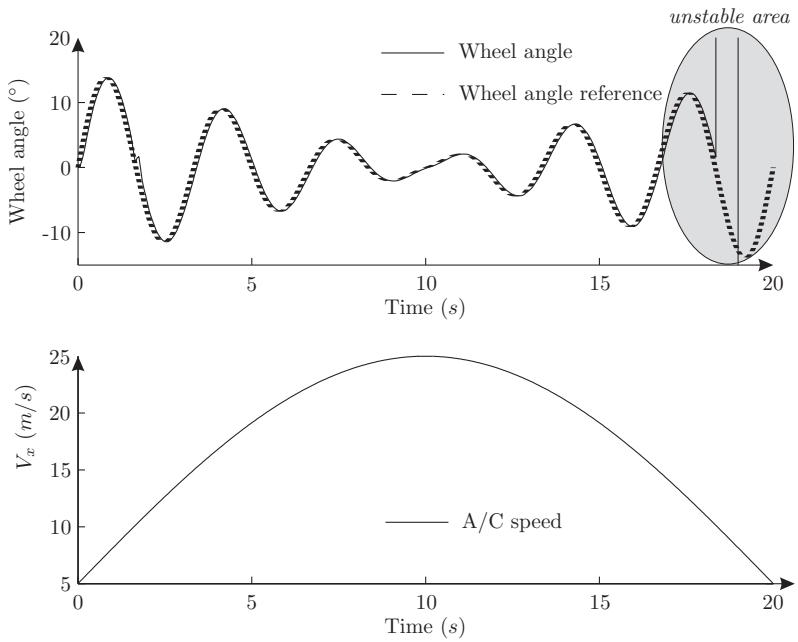

Figure 4.11: Scenario 2 for the classic gain scheduling based on the complex model

Classic gain scheduling based on the complex model gives satisfying results for scenario 1 (cf. Figure 4.10). Indeed, the response of the system oscillates slightly and stays close to the template. However, the response obtained for scenario 2 is not satisfactory (cf. Figure 4.11).

After $18s$, the wheel angle moves away from the wheel angle reference; an unstable area appears.

Indeed, the stability of such control solution cannot be proved. [Rugh and Shamma, 2000] explain that extensive simulations must be done for the evaluation of stability and performance. Typically, stability can be assured only locally when a slow variation of the varying parameter is considered and typically there are no performance guarantees. The authors insist on the fact that controller interpolations are not stabilizing at intermediate equilibria and this leads to situations in which instabilities in the closed-loop gain scheduled system appear. Moreover, [Liberzon and Morse, 1999] claim that the stability of all the individual subsystems is not sufficient to be sure that the global system is stable. Conversely, even if the independent subsystems are unstable, it is conceivable to find a particular path that stabilizes the overall system. The authors emphasize this topic when they show through an example that depending on a particular switching signal and from stable subsystem, the trajectories of the switched system may render to an asymptotically stable system or to an unstable one. Finally, [Narendra and Balakrishnan, 1997] add that stability is not assured for arbitrary switching schemes, since there may be controllers which destabilize the system. Nevertheless, it is mentioned that a large number of fixed models may be needed to assure stability and good steady-state performance. As a conclusion, if the number of LTI controllers increases, stability of the closed-loop system can be obtained. Yet, this large number of controllers could be harmful for real-time implementation.

4.2.4.4 Controller blending applied to the simple NLG steering model

Classic gain scheduling is here applied with the use of the simple NLG model which considers a proportional relation between the resistive torque T_r and the wheel angle θ_w. The proposed control solution requires six $\mathcal{H}_\infty$ controllers (as it has been chosen for the controller proposed in Section 4.2.4.3), synthesized for the values of K_r dependent on V_x using equation (3.28). These values vary between $K_{r\ min}$ and $K_{r\ max}$ and the different distances are defined by $d_i = K_r - K_{r\ i}$ and $d_{i+1} = K_{r\ i+1} - K_r$. The six controllers are synthesized with similar weighting filters. These latter are obtained using the optimization algorithm presented in Section 4.2.2 with structure 3.

The two simulation results are presented in Figure 4.12 and Figure 4.13.

The results obtained with the classic gain scheduling approach based on the proportional resistive torque calculation are not acceptable (cf. Figure 4.12). The controller does not give a response which remains close to the template. Moreover, the wheel angle obtained for scenario 2 is relevant at the beginning of the test (cf. Figure 4.13), but after $17s$, the response of the system moves away from the wheel angle reference; the control solution becomes unstable. Concerning the instability observed with this control solution, the problem has been encountered previously and a discussion has been proposed in Section 4.2.4.3.

4.2.4.5 Polytopic controllers applied to the A/C based NLG steering model

The LPV model based on an A/C model considers two varying parameters $\rho_1 = V_x$ and $\rho_2 = \dfrac{1}{V_x}$. Figure 4.14 shows the polytope used to obtain the gain scheduling controller. It is composed of four vertices (S_1, S_2, S_3, S_4) and the choice of the α_i is based on the parameter ρ_{inter}. Generally, the α_i are deduced from a system of equations. Yet, in the considered application,

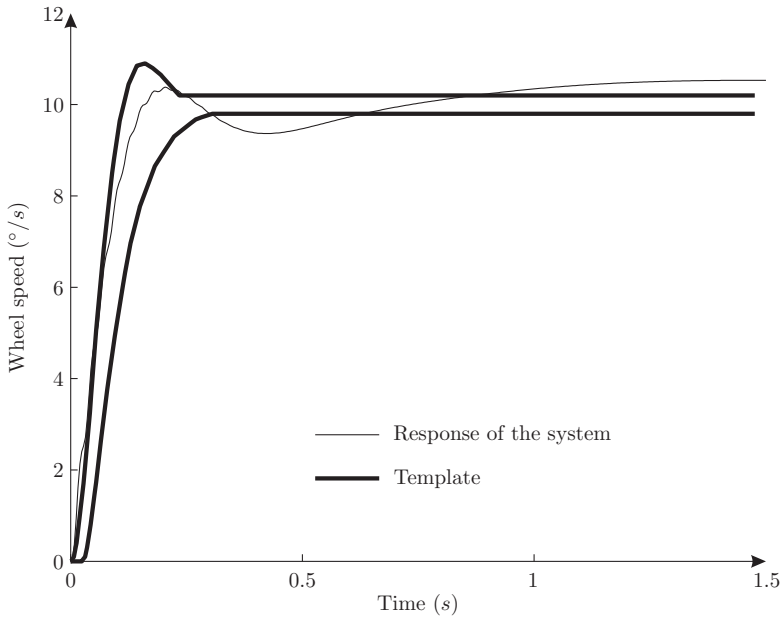

Figure 4.12: Scenario 1 for the classic gain scheduling based on the proportional resistive torque model

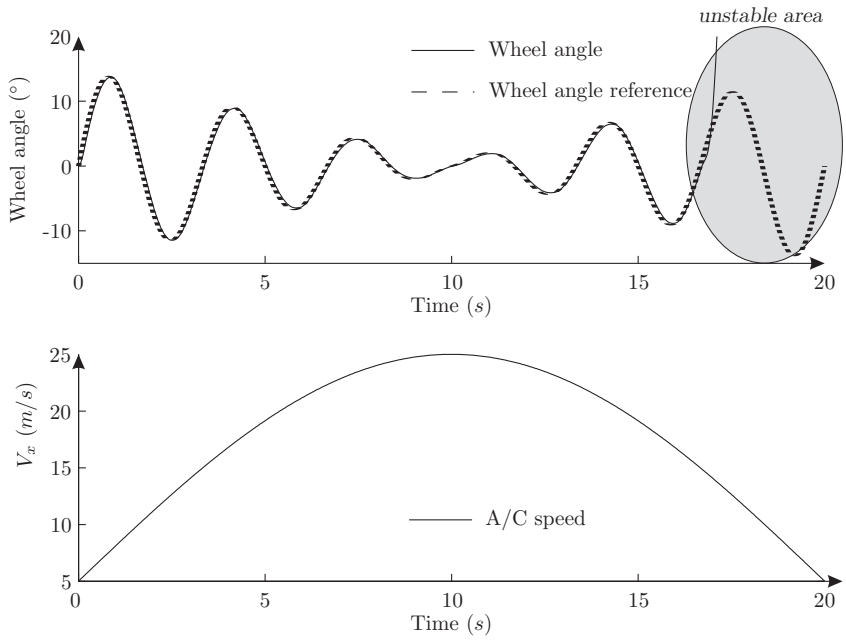

Figure 4.13: Scenario 2 for the classic gain scheduling based on the proportional resistive torque model

three equations are available and four parameters α_i have to be identified. Then, it is proposed to use the parameter ρ_{inter} to integrate a supplementary equation. This parameter is obtained by considering the intersection of the segment that passes through the two vertices S_2 and S_3 and the trajectory of the varying parameter represented by a bold curve in Figure 4.14. Then, when ρ_1 is larger than ρ_{inter}, the system is in the triangle polytope (S_2, S_3, S_4) and the parameter α_1 is null. In the other case, the system is in the polytope (S_1, S_2, S_3) and the parameter α_4 is null. This permits to obtain a system with the same number of equations and variables expressed by

the following equations:

if $\rho_1 < \rho_{inter}$ then

$$\begin{cases} \alpha_4 = 0 \\ \alpha_1\rho_1(S_1) + \alpha_2\rho_1(S_2) + \alpha_3\rho_1(S_3) = \rho_1 \\ \alpha_1\rho_2(S_1) + \alpha_2\rho_2(S_2) + \alpha_3\rho_2(S_3) = \rho_2 \\ \alpha_1 + \alpha_2 + \alpha_3 = 1 \end{cases}$$

if $\rho_1 > \rho_{inter}$ then

$$\begin{cases} \alpha_1 = 0 \\ \alpha_2\rho_1(S_2) + \alpha_3\rho_1(S_3) + \alpha_4\rho_1(S_4) = \rho_1 \\ \alpha_2\rho_2(S_2) + \alpha_3\rho_2(S_3) + \alpha_4\rho_2(S_4) = \rho_2 \\ \alpha_2 + \alpha_3 + \alpha_4 = 1 \end{cases}$$

such that $\rho_i(S_j)$ corresponds to the coordinates of the vertex S_j. The weighting filters are obtained using the optimization algorithm presented in Section 4.2.2 using the 2-input control structure.

Commentary It is important to notice that the weighting filters obtained in Section 4.2.3.3 are not adapted for the current structure. Indeed, the optimal weighting filters obtained with the A/C-based NLG steering model and considering an LTI control strategy do not permit to satisfy the specifications. This can be simply explained by the fact that the LMI system is different for the case of classic gain scheduling and for the case of modern gain scheduling. For the first, the system proposed in equation (2.7) is used while the second needs to solve the system of equation (2.19). The optimization procedure is performed again, by considering an inequality system adapted for the polytopic case.

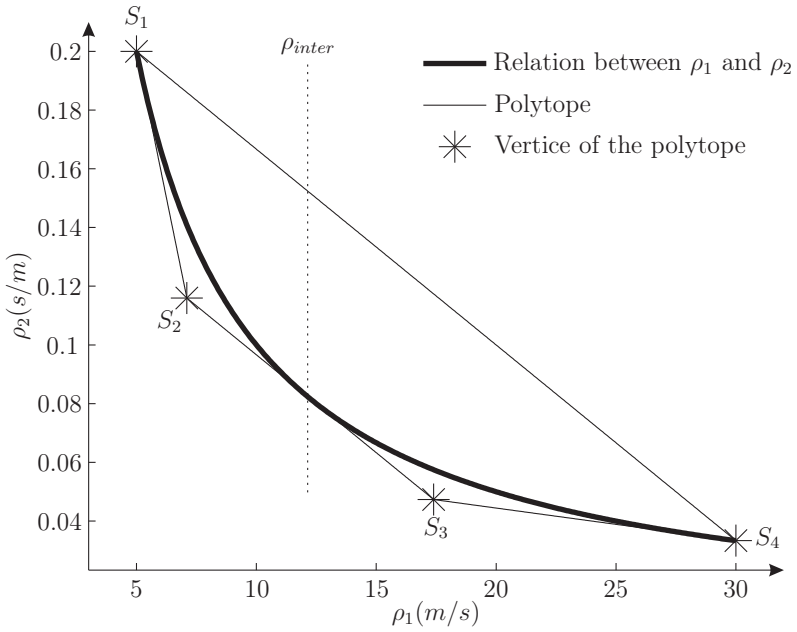

Figure 4.14: Polytope of the varying parameters

The two simulation results are presented in Figure 4.15 and Figure 4.16.

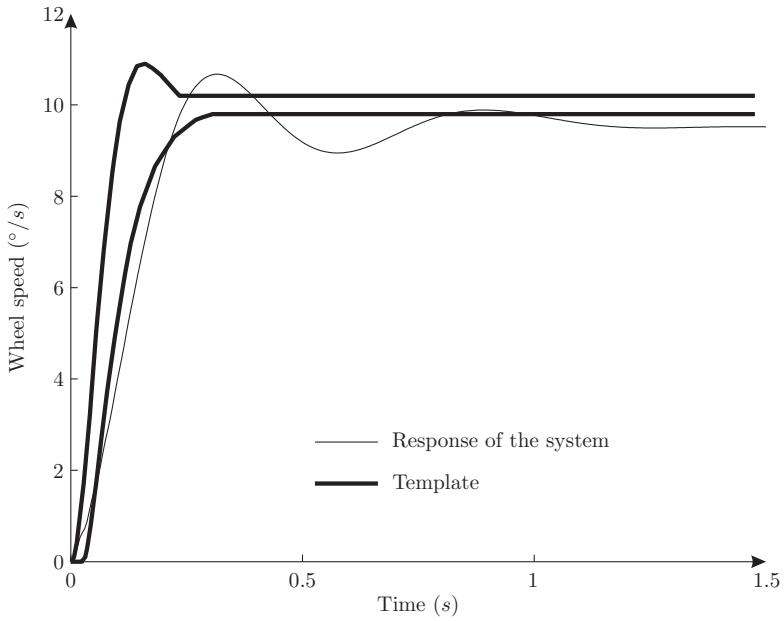

Figure 4.15: Scenario 1 for modern gain scheduling based on the A/C model torque model

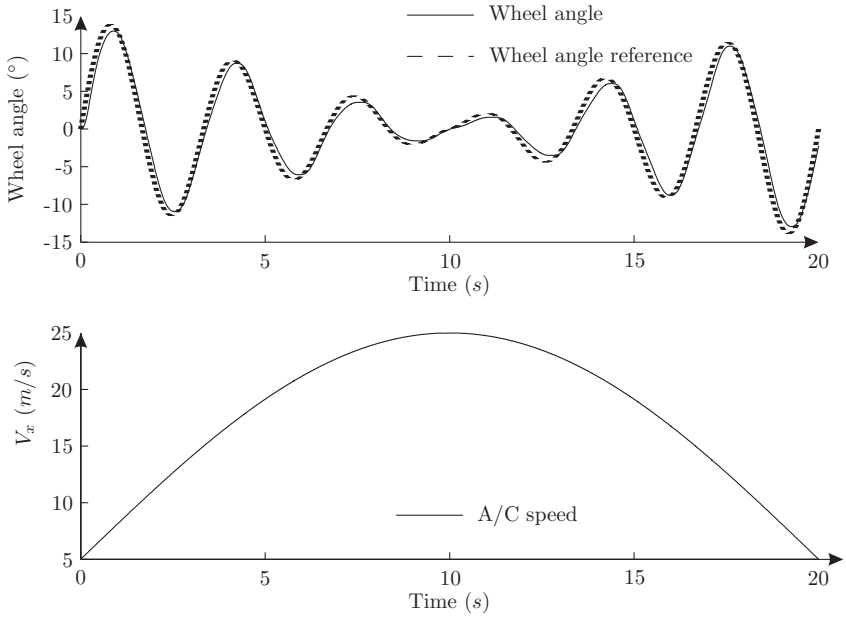

Figure 4.16: Scenario 2 for modern gain scheduling based on the A/C model resistive torque model

The results obtained with the modern gain scheduling based on the A/C model resistive torque calculation doest not respect the specifications (cf. Figure 4.15), insofar as important oscillations appear on the wheel speed signal. Concerning the response of scenario 2 (cf. Figure 4.16), the wheel angle and the wheel angle reference are quite similar, this response is satisfactory.

4.2.4.6 Polytopic controllers applied to the simple NLG steering model

The LPV model based on the proportional relationship between the resistive torque T_r and the wheel angle θ_w considers only one varying parameter $\rho = Kr(V_x)$. Then, the polytope is

composed of two vertices obtained for the extreme values of K_r which are $K_{r\ min}$ and $K_{r\ max}$. The weighting filters are obtained using the optimization algorithm presented in Section 4.2.2 using the last proposed control structure called "usual" 2-input structure.

The synthesis model which is used in this control strategy generates discussion compared to the LPV NLG steering model based on an A/C model. Indeed, the modelling of the NLG has been simplified and the obtained synthesis model does not represent the reality as accurately as the NLG steering model based on an A/C model. It seems obvious that, the more the model used for the synthesis of the controller corresponds to reality, the better the performances will be. But the simplification of the synthesis model helps to drastically simplify the control structure. On the one hand, the mathematical problem is easier insofar as the LMI formulation is relaxed. On the other hand, the implementation of the control strategy is simplified.

The two simulation results are presented in Figure 4.17 and Figure 4.18.

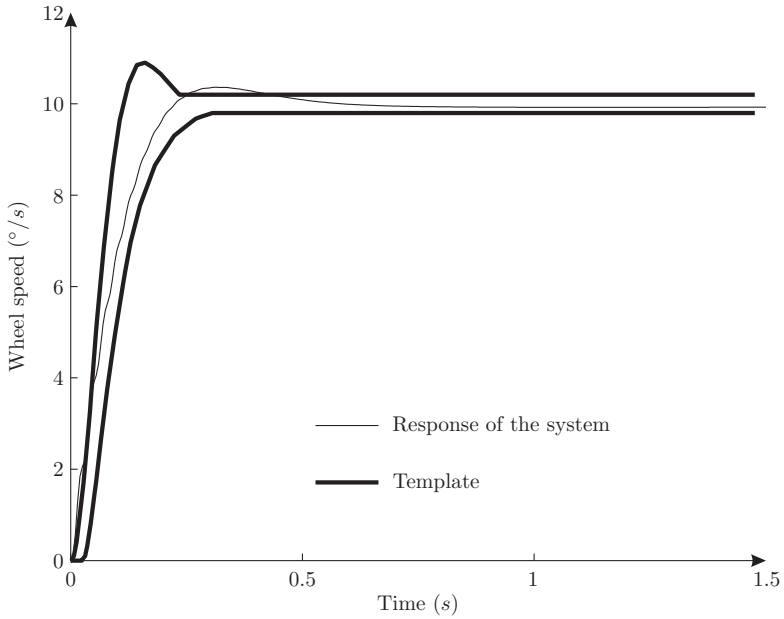

Figure 4.17: Scenario 1 for modern gain scheduling based on the proportional resistive torque model

The results obtained with the proportional resistive torque based model is satisfactory. Despite a slight overshoot at time $t \approx 0.25s$, the wheel speed signal remains inside the defined template (cf Figure 4.17). Besides, the response obtained for scenario 2 is satisfactory (cf Figure 4.18).

4.2.4.7 Discussion

Discussion about the classic gain scheduling results

Based on these different simulations, it can be concluded that the two classic gain scheduling solutions do not help to meet the specifications (particularly due to the instability observed after $17s$ for the solution based on the proportional resistive torque estimation and $18s$ for the solution based on the A/C model resistive torque estimation). Figure 4.11 and Figure 4.13 show that the wheel angle signal becomes unstable very rapidly with the two classic solutions. Moreover,

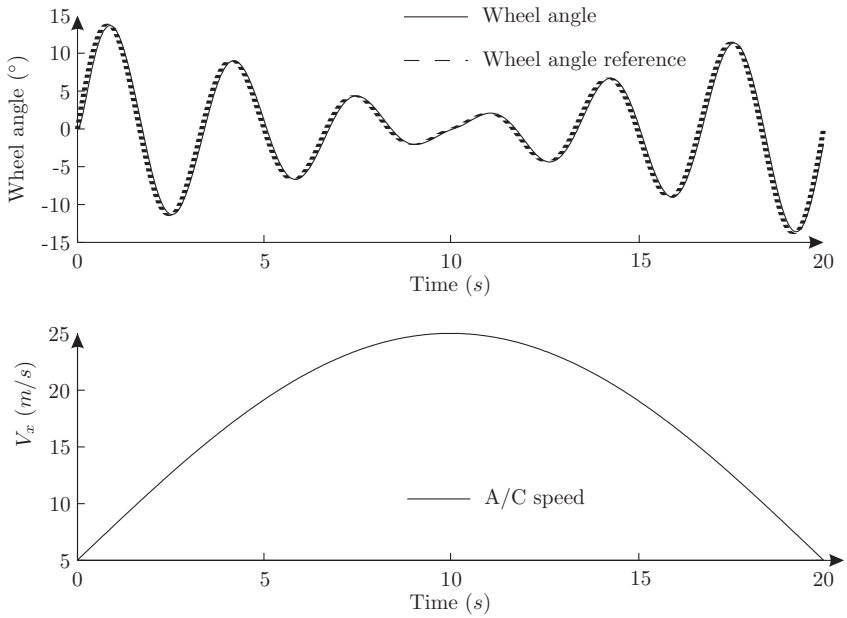

Figure 4.18: Scenario 2 for modern gain scheduling based on the proportional resistive torque model

based on scenario 1, it can be seen that classic gain scheduling synthesized using the A/C model resistive torque estimation gives better results. This may be due to the better identification of the simulation model.

Drawbacks of the classic gains scheduling results

Classic gain scheduling solution is interesting insofar as only the output of the controller is processed and no matrix operations are required (the operations are done directly on the output signals and the state space matrices are in this case not taken into account). Moreover, controllers with different structures may be considered because only the outputs are summed. Thus, the well-known drawback of the $\mathcal{H}_\infty$ solutions which synthesize high order controllers is not important: the different controllers are reduced separately. However, this gain scheduling method presents two main drawbacks. On the one hand, numerous controllers must be synthesized to follow the dynamics of the system correctly. For NLG control, six $\mathcal{H}_\infty$ controllers are interpolated. On the other hand, just a few results concerning the stability of classic gain scheduling are available in the literature and the stability is an important property of the controllers for aeronautical applications. The simulation results show the limit of this control solution insofar as the stability problem of the classic gain scheduling is encountered. Indeed this control solution could not ensure the stability of the control solution for all combinations of the varying parameters.

Discussion about the modern gain scheduling results

Good results are obtained concerning modern gain scheduling based on the polytopic approach. Nevertheless, the controller synthesized with the proportional resistive torque calculation is acceptable, insofar as the responses of scenarios 1 and 2 are better. The response of scenario 1 which slightly goes outside the template is tolerated. The two modern gain scheduling techniques give

different results and this may be explained by the constraints linked to the polytope. Indeed, the choice of the polytope is a compromise between the number of vertices, which is directly linked to the number of $\mathcal{H}_\infty$ controllers and the way in which the polytope includes the parameter varying space: a bad polytope may introduce conservatism or the LMI solver cannot find a solution. For example, the polytope presented in Figure 4.14 is composed of four vertices, but it is not very close to the parameter varying space. The area over the dotted line is quite large. This main drawback may explain that better results are obtained with the controller synthesized with the proportional resistive torque. For this latter, the polytope is closer to the ideal curve of the varying parameter. Even more, the polytope consists of two vertices which coincides with the trajectory of the varying parameter. As a conclusion, an accurate and detailed synthesis model is not the most important goal to reach for control purposes. A compromise must be found between the equation of the synthesis model and the real system and the complexity of the resulting synthesis model. Indeed, a complex synthesis model requires a complex polytope which may increase the conservatism of the LMI formulation.

Improvements of the modern gain scheduling results

To improve the results obtained with modern gain scheduling, less conservative formulation may be taken into account. For example, the formulation which considers the evolution of the varying parameters speed may be interesting [Apkarian and Adams, 1998] [Wu et al., 1996]. In this formulation, the additional hypothesis expressed by $\dot{\rho}_{min} < \dot{\rho} < \dot{\rho}_{max}$ helps to reduce the conservatism by limiting the evolution speed of the varying parameter inside the polytope. This control strategy has been applied with success for the control of the air path system of diesel engine [Wei and del Re, 2007]. Moreover, LMI's formulation based on multiple Lyapunov functions may give good results. In this case, the research of a Lyapunov function for each vertex of the polytope helps to reduce the conservatism [de Oliveira et al., 2004]. As a conclusion, modern gain scheduling based on the polytopic formulation is a powerful tool which helps to consider the non-linearities of the system in the control laws.

$\mathcal{H}_\infty$ control synthesis and feedforward approach

Another interesting point can be underlined regarding the simulation results proposed in this section. As it can be shown in Figure 4.9, a tracking error is observed. This latter, which is approximately of 1° is lower than the maximum allowed value of 2°. Nevertheless, it could be interesting to improve the current solution and take an interest in feedforward tracking controller which may give the possibility to reduce the tracking error [Ohishi et al., 2006].

4.2.5 Controller order reduction

As it is well-known, the main drawback of $\mathcal{H}_\infty$ synthesis is the order of the obtained controller when conventional optimization algorithms are employed to synthesize the controller. Then, different solutions, reducing the controller order can be found in the literature:

- MOR:

Reducing the model order or the controller order with well-known model reduction technique based on the Hankel singular values and presented in details in Section C. This is the solution for a large number of applications ([Hardiansyah et al., 2006]), ([Poussot-Vassal et al., 2008]).

- controller reduction based on γ_∞ constraint:
  Reducing the controller order with the help of an additional optimization algorithm once it has been synthesized with a "conventional" optimization method. The controller structure is first synthesized with a "conventional" method, then a second optimization algorithm tries to find a controller with a closed performance index (γ_∞) and a low order. For example, ([Lee, 2004]) uses a genetic algorithm to find the reduced order controller.

- HIFOO:
  Reducing the controller order, using an optimization algorithm which is able to add some controller structure constraints directly during the synthesis. Such constraints significantly change the optimization algorithm which becomes non-convex and non-smooth. Various tools have been proposed recently to solve this optimization problem ([Apkarian and Noll, 2006]). A toolbox developed on Matlab® called HIFOO (HIFOO: $\mathcal{H}_\infty$ Fixed-Order Optimization) can be used to solve the optimization problem ([Burke et al., 2005]).

Table 4.3 summarizes the advantages and drawbacks of the controller order reduction methods.

4.2.6 Test bench validation

4.2.6.1 Presentation of the test bench

The test bench, developed in the frame of the DRESS project is presented in Figure 4.19.

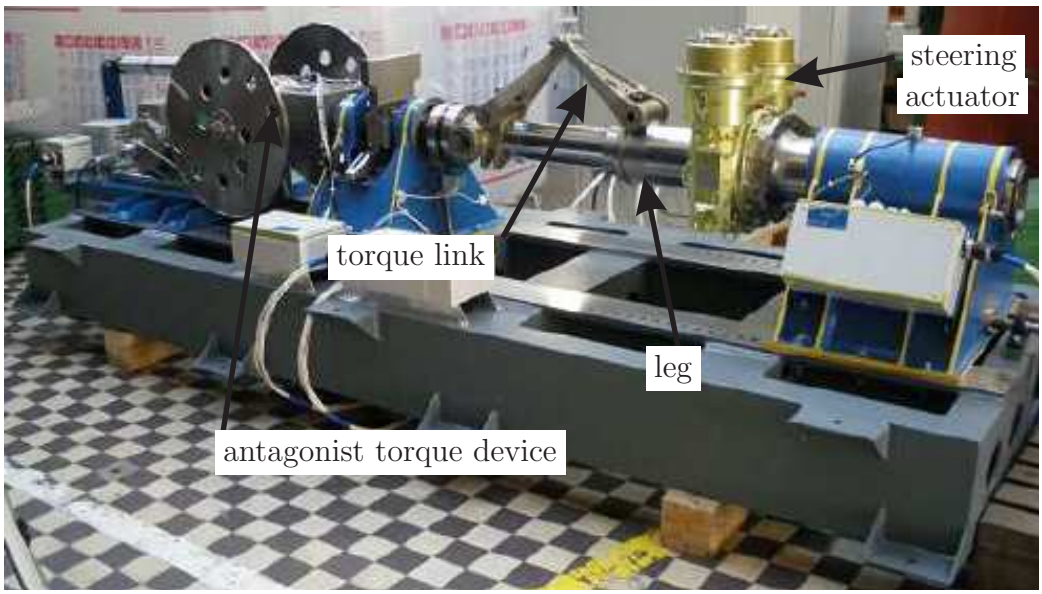

Figure 4.19: Test bench in Messier Bugatti facilities

Method	Advantages	Drawbacks
MOR	• accurate theoretical tool (cf. Section C) • commonly used method	• stability of the reduced controller is not guarantee
controller reduction based on γ_∞ constraint	• the performance index (γ_∞) is kept	• two consecutive optimizations are required
HIFOO	• the structure of the controller is directly fixed • availability of a the HIFOO toolbox	• time required for the controller synthesis is very long, 10 times greater than the classic method of optimization (cf. Section 2.2.2) • optimization based on random initializations

Table 4.3: Advantages and Drawbacks of the controller order reduction methods

The test bench has been designed and manufactured based on a dummy landing gear in order to receive the electromechanical steering actuator. The loading system, used to simulate the load generated at axle level, is based on a hydraulic actuator and a torque control system. This test bench aims at:

- contributing to the validation of the DRESS steering system,
- supporting correlation of modelling activities.

4.2.6.2 Validation of the control solution

Introduction

Previously in this chapter, simulation results based on LPV robust control solutions have been presented. The control algorithms vary as a function of the A/C longitudinal speed. However, the test bench does not take account of the A/C speed. Moreover, the resistive torque is simulated using hydraulic actuators mounted at the bottom of the NLG and it is not possible to validate all the previously presented control solutions. It has thus been decided to test only LTI control solutions, on the test bench. The controller is based on the "usual" 2-input structure and is obtained with the HIFOO optimization solver. This latter gives the possibility to fix the controller order without restriction.

The effectiveness of the HIFOO optimization method has been demonstrated; this solution is used in simulations [Gumussoy et al., 2008]) or for real applications ([Knittel et al., 2007]). The

optimization problem is a hybrid non-convex and non-smooth algorithm which requires two steps (see [Burke et al., 2005] for more details). The algorithm uses a random initialization; in similar conditions (the same synthesis model and the same controller order) different controllers are synthesized. It is difficult to precisely tune the synthesis parameters (that means the weighting parameters) and to obtain the desired response. However, a priori estimate of the controller can be given. It helps to reduce the reliance on random initialization on the one hand, and to lead the study toward a prior solution, on the other hand.

First step of the controller validation

After the first tests on bench, two major improvements on the control solution have been done. Indeed, it has been remarked that the noise on the wheel angle measures provided by redundant sensors was significant, so it is required to take account of this phenomenon in the controller synthesis. First, a new weighting filter W_n has been added, considering the influence of the noise (cf. Figure 4.20). Secondly, the measured signal θ_w is filtered.

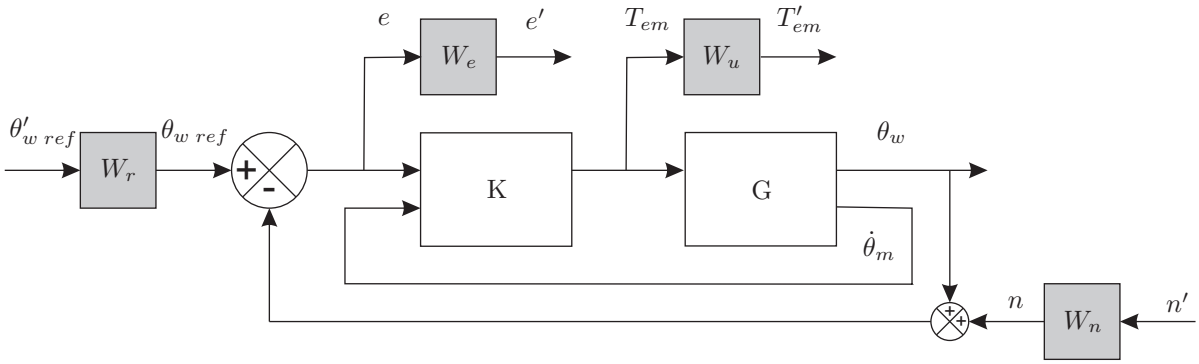

Figure 4.20: Improvement of the model synthesis structure 3

The results of the tests on the bench are presented in Figures 4.21 and 4.22.

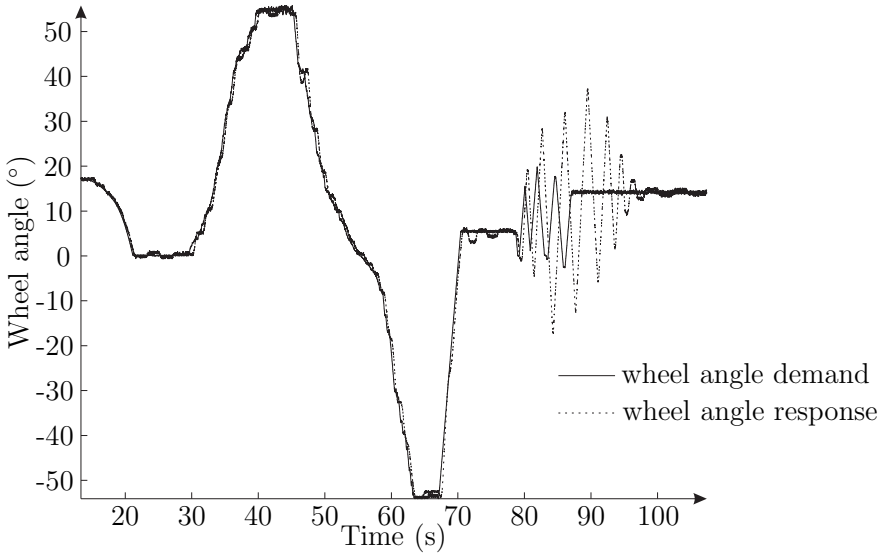

Figure 4.21: Wheel angle response for the first step of the controller validation

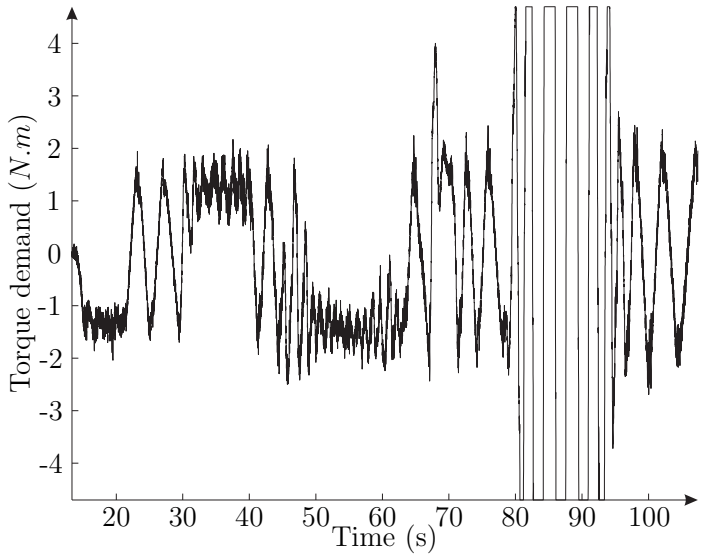

Figure 4.22: Torque required for the first step of the controller validation

It can be seen that the proposed controller gives satisfying results in the first part. Indeed, the wheel angle demand and the wheel angle response are very close. However, at time $t = 80s$, the two signals become different. The wheel angle demand is amplified and the response needs approximately $15s$ to be stabilized. In this case, the response of the system is degraded because the frequency excitation is very high ($\approx 0.5Hz$) and the wheel speed demand is at its maximum ($18°/s$). Figure 4.23 presents a zoom of this particular part of the response. Moreover, it can be seen that the torque demand exceeds the minimum and maximum allowed torque values. Thus, the controller saturates (cf. Figure 4.24).

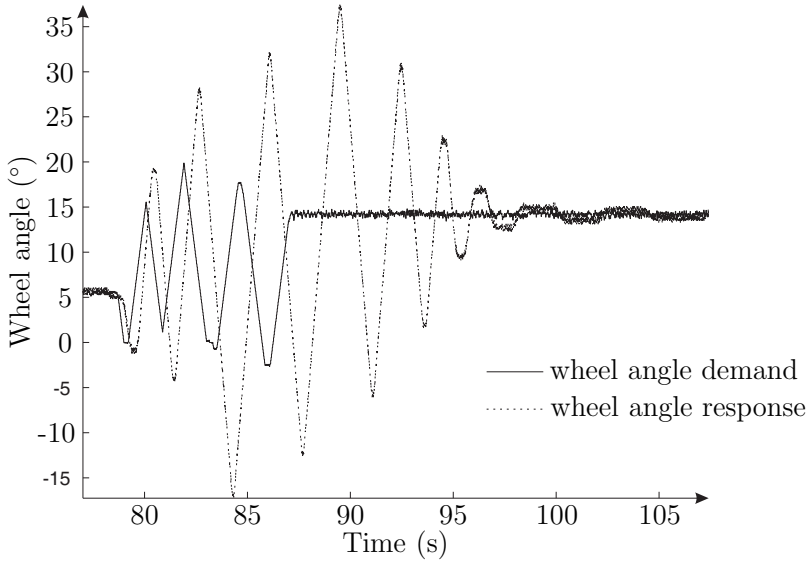

Figure 4.23: Wheel angle response for the first step of the controller validation (ZOOM)

The phenomenon observed at the end of the test is explained with Figure 4.24. It shows two particularities of the motors. On the one hand, they do not have similar behaviours. Indeed, even if the two motors receive similar control signals, the torque response of the first motor (grey

curve) and the torque response of the second motor (dashed grey curve) are not merged. On the other hand, their respective power is not sufficient to follow the required torque. The signals observed on the test bench are different from those obtained with the simulation models. The models of the motors does not sufficiently match with the available motors.

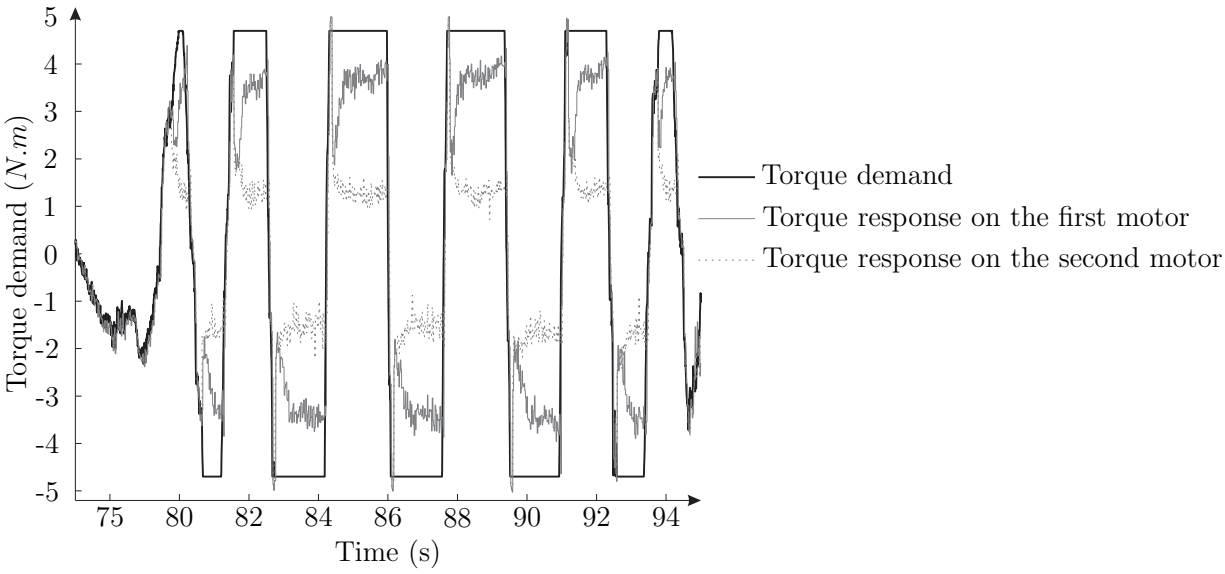

Figure 4.24: Torque required with the motor responses

4.2.7 Conclusions and Perspectives

This section presented the control of the NLG for steering purposes. Firstly, the motivations of the use of robust $\mathcal{H}_\infty$ control theory have been explained (cf. Section 4.2.1). Secondly, a method which gives the possibility to define an optimal structure of the "generalized" model $\mathcal{P}$ and to obtain the definition of the weighting filters has been developed (cf. Section 4.2.2). Thirdly, controllers based on the LTI approach, gain scheduling classic output blending or modern polytopic approach have been synthesized. The simulation results help to conclude on the predilection for modern gain scheduling based on polytopic approach. Indeed, Sections 4.2.4.3 and 4.2.4.4, dedicated to classic gain scheduling approach, have pointed out the fact that instabilities may appear because stability can be assured only locally when a slow variation of the varying parameter is considered. Concerning the synthesis of gain scheduling controller based on the polytopic approach, Sections 4.2.4.5 and 4.2.4.6 present convincing results. Despite closed-loop responses which slightly go outside the template, the gain scheduling controllers based on the polytopic approach are satisfying when they are synthesized with both synthesis models (A/C-based LPV NLG steering model and simple LPV NLG steering model). Nevertheless, better results are obtained with the simple LPV NLG steering model, showing that an accurate and detailed synthesis model is not the most important goal to reach for control purposes. Thus, a compromise must be found between the equation of the synthesis model with the real system and the complexity of the resulting synthesis model. Fourthly, the drawback of $\mathcal{H}_\infty$ control theory which tends to synthesize high order controllers has been mentioned and solutions to deal with this problem

have been suggested (cf. Section 4.2.5). Finally, the control solution has been applied on the real test bench developed in the frame of the DRESS project (cf. Section 4.2.6). For this validation step, it was not possible to implement the modern polytopic gain scheduling controllers, but the simple LTI one has been tested. Indeed, the resistive torque at W/R level, which takes account of the A/C longitudinal speed in the simulation models, is obtained on the test bench by the use of an hydraulic actuator which applies constant torque or torques that corresponds to typical load cases. This is a very important step in the development of a control solution. Based on real test measurements, models have been improved and finally satisfying results are obtained on the test bench.

Concerning the synthesis of the controllers, different improvements have been suggested:

- it could be interesting to introduce a constraint on the evolution speed of the varying parameter ([Apkarian and Adams, 1998] [Wu et al., 1996]),
- the formulation of the polytopic gain scheduling problem could be extended to multiple Lyapunov functions ([de Oliveira et al., 2004]),
- the structure of the controller could integrate a feedforward contribution in order to reduce the tracking error.

Moreover, the LTI controllers which have been tested on the bench are synthesized with the HIFOO toolbox and the LPV NLG steering model based on an A/C model. It could be rewarding to test other controllers based on HIFOO and other synthesis method (cf. Section 4.2.3). Then, the resistive torque applied on the test bench could be improved such that it represents the W/R interface more accurately. This will permit to apply and to validate the gain scheduling approaches.

4.3 Shimmy control

4.3.1 Introduction

In the frame of the DRESS project, the control of the shimmy phenomenon is done through an initiatory study. The objective is to investigate the feasibility of active shimmy damping. Thus, two main points have been studied. On the one hand, a control solution which is able to damp the shimmy oscillations has to be proposed and tested by simulations. On the other hand, the characterization of the control signal has to be determined from the simulation tests. The main reflection deals with the needed dynamics. Indeed, it is well-known that the shimmy frequencies are very high ($\approx 20-30Hz$) and the sizing of the electromechanical shimmy actuator is a critical task.

The first part of the section (cf. Section 4.3.2) aims at presenting the simulation results of the shimmy model through three different test scenarios. Then, three different control solutions, based on fuzzy adaptive control which give the possibility to damp shimmy oscillations are detailed. Firstly, the direct and indirect state feedback solutions are presented in Section 4.3.3. Secondly, in Section 4.3.4, simulation results based on the output feedback control solution are proposed. Finally, a robustness analysis is proposed in Section 4.3.5. This latter aims at studying the behaviour of the control solution when parameters of the model are changing.

The control solutions which are proposed in this section have been done in collaboration with Thai-Hoang Huynh from the Ho Chi Minh University. Particularly, he developed the last solution based on output feedback and for this control solution my contribution consists in tuning the algorithm parameters to be adapted for the considered shimmy model.

4.3.2 Shimmy test scenarios: open loop results

In order to be comparable with previously published works on shimmy analysis, the proposed model (except for the actuator characteristics) has been configured with the parameters presented in [Somieski, 1997] which correspond to the nose landing gear parameters of a commercial civil aircraft. They are summarized in the following table:

Parameter	Value	Unit
V_x	0...80	$m.s^{-1}$
a	0.1	m
e	0.1	m
$c_{F\alpha}$	20	rad^{-1}
δ	5	$^\circ$
$c_{M\alpha}$	-2	$m.rad^{-1}$
α_g	10	$^\circ$
J_a	0.1	$kg.m^2$
J_z	1	$kg.m^2$
B_a	0.1	$N.rad^{-1}.s$
F_z	9000	N
k_s	100000	$N.m.rad^{-1}$
k_d	10	$N.m.rad^{-1}.s$
κ	-270	$N.m^2.rad^{-1}$
σ	0.3	m

To illustrate the performance of the proposed shimmy model, three different test scenarios have been chosen. In the aeronautical domain, they usually help to test the behaviour of the NLG. For all the three proposed cases, the turning tube is kept at zero position and a perturbation is applied directly on the tyre. The case studies that have been selected are:

- Scenario 1: Constant ground speed, pulse disturbance
  The aircraft is supposed to have a forward ground speed of $80m/s$, the disturbance is a torque pulse of $1000N.m$ for $0.1s$ and directly acts on the vertical axis at the wheel level. This test actually corresponds to a tyre damage scenario.

- Scenario 2: Constant ground speed, rough runway
  The purpose of this test is to investigate the effect of the roughness of the runway while the aircraft is running at a maximum speed of $80\,m/s$. This influence is modelled by a random disturbance which is a white noise with zero mean and a standard deviation of $100N.m$.

- Scenario 3: Varying ground speed, rough runway

In this scenario, the same test as in scenario 2 is performed, with a varying forward velocity of the aircraft: v changes from 10 to $80\,m/s$. This test is carried out because of the sensitivity of the shimmy phenomenon to the aircraft forward velocity [Somieski, 1997].

The simulation of scenario 1 is illustrated in Figure 4.25. The disturbance is applied on the tyre at time 0.2s for a duration of 0.1s. As it can be seen in the figure, the NLG starts to oscillate, i.e. shimmy appears, as soon as the perturbation is applied on the tyre. Then, the amplitude of the oscillations starts growing with time and the system becomes unstable.

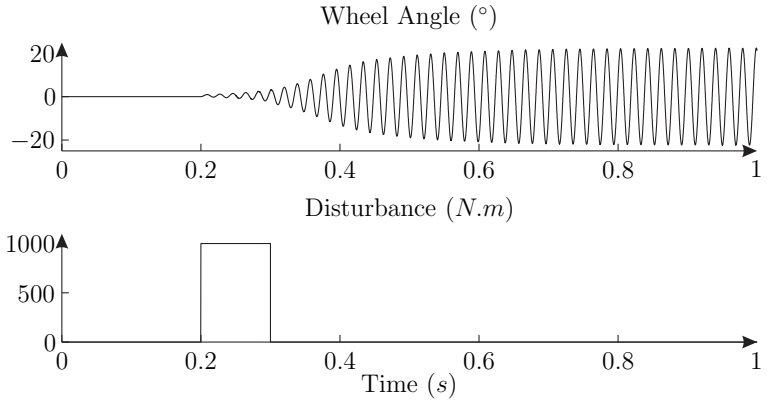

Figure 4.25: Shimmy caused by a tyre damage

Scenario 2 is illustrated in Figure 4.26. The disturbance, representing a high roughness of the runway, is applied on the tyre at the beginning of the simulation and the aircraft runs at $80m/s$. As it can be seen in the figure, the NLG slowly starts to oscillate and after a while, as in scenario 1, becomes unstable in the same way.

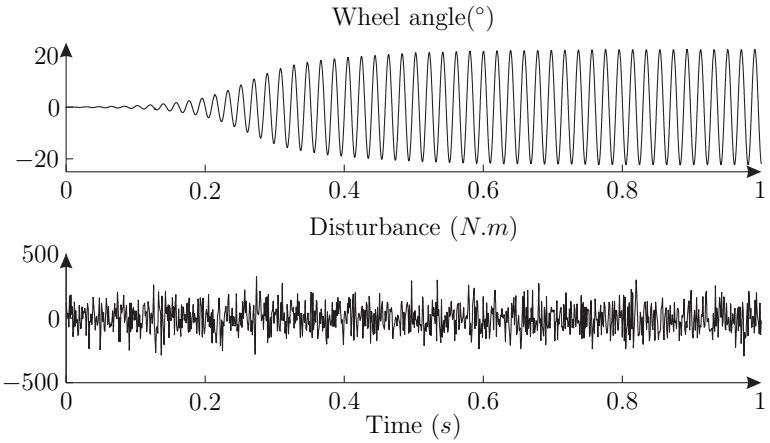

Figure 4.26: Shimmy caused by a rough runway

Concerning these two scenarios, Scenario 1 and Scenario 2, the results are those obtained for a simulation of 1s. For this duration, numerous oscillations with a frequency of $50Hz$ appear, corresponding approximately to the resonance frequency of the shimmy phenomenon.

Scenario 3 is illustrated in Figure 4.27. The aircraft forward velocity is a critical parameter of the shimmy phenomenon and this scenario aims at illustrating this aspect. During landing and take-off, the aircraft ground velocity varies between 0 and $80m/s$ and this scenario shows

the impact of this varying parameter on the behaviour of the NLG; the simulation is performed on $15s$, allowing a speed variation from 0 to $80m/s$. At low speed (under $25m/s$), the system is stable whereas it becomes unstable and shimmy appears when the forward velocity of the aircraft is higher than $25m/s$.

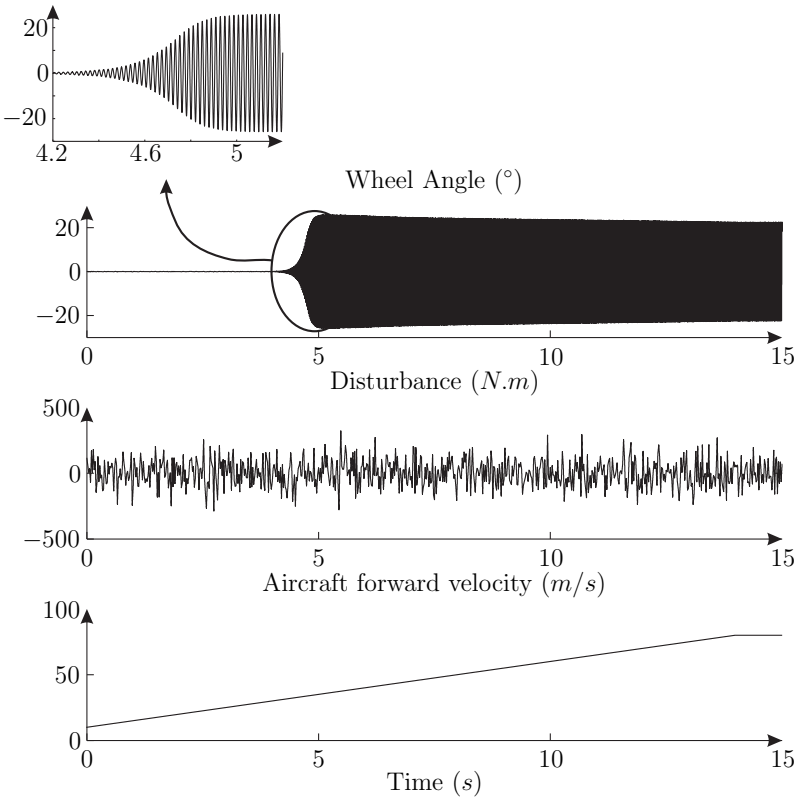

Figure 4.27: Impact of the forward velocity

These 3 scenarios show a shimmy phenomenon characterized by a natural frequency around $50Hz$ and an increasing amplitude up to 20°. These results are in adequacy with the ones which can be found in the literature. It must be underlined that such a situation could generate malfunctioning and/or severe damages of the landing gear. That is why damping solutions are required.

4.3.3 Simulation results based on the state feedback control solutions

4.3.3.1 Controller design

This section describes the design of the parameters used for the indirect and direct fuzzy adaptive controllers respectively presented in Sections 2.3.2.1 and 2.3.2.2.

For the indirect solution, the fuzzy system is constructed with 72 rules such that θ_w and $\dot{\theta}_w$ are defined with three Gaussian membership functions and the other states are defined with two Gaussian membership functions. The membership functions are specified with a "center" c and a "width" σ such that:

$$\mu(x) = \exp\left(-\left(\frac{x-c}{\sigma}\right)^2\right) \tag{4.1}$$

Furthermore, the fuzzy Cartesian product is used to implement the logical "and" operation present in the fuzzy rule such that:

$$\mu_{F_k^1 \times F_l^2 \times \cdots \times F_m^n}(x_1, x_2, \ldots, x_n) = \mu_{F_k^1} \times \cdots \times \mu_{F_m^n} \tag{4.2}$$

Finally, a weighted average method is used for the defuzzification and the output of the fuzzy system obtained is:

$$y = f(x) = \frac{\sum_{i=1}^{p} \theta_i \mu_i}{\sum_{i=1}^{p} \mu_i} = \theta^T \varsigma \tag{4.3}$$

where $\mu_i := \mu_{F_k^1 \times F_l^2 \times \cdots \times F_m^n}(x_1, x_2, \ldots, x_n)$ is the membership function of the ith rule, $\theta^T := [\theta_1, ..., \theta_p]$ and $\varsigma^T := [\mu_1 ... \mu_p]/[\sum_{i=1}^{p} \mu_i]$. Moreover, the membership functions are uniformly distributed in the whole range of each state variable. Concerning the direct solution, the fuzzy system is quite similar with three Gaussian membership functions for state variable θ_w and two for the others. So, the fuzzy system consists of 48 rules. The discourse universe of each state is in the range $(-\overline{x}_i, \overline{x}_i)$ such that $\overline{x}_1 = \pi/10 rad$, $\overline{x}_2 = 10\pi rad.s^{-1}$, $\overline{x}_3 = 0.1m$, $\overline{x}_4 = \pi/10 rad$ and $\overline{x}_5 = 10\pi rad.s^{-1}$. These values were chosen following numerous simulations and correspond to the maximum values of the states obtained with a large disturbance.

The NLG model considered is a 5^{th} order non-linear system with a relative degree of 3. In this case, the tracking error is $e_s(t) = \ddot{e}_0(t) + k_1 \dot{e}_0(t) + k_0 e_0(t)$. The constants chosen for the indirect solution are $k_0 = 25$ and $k_1 = 7$, whereas the constants are equal to $k_0 = 50$ and $k_1 = 15$ for the direct solution. These values were tuned step by step, to obtain the desired response of the system's output. The structure of the two state feedback controllers are not similar that is why the values of the parameters k_0 and k_1 are different.

The particularity of these algorithms is the use of a constant value for the control gain B. This constant, defined by the model parameters k_d, J_a and J_2, is equal to 100. The simulations showed that the maximum value of the estimates $\hat{a}(\mathbf{x})$ is approximately equal to $10,000$; so, for the indirect solution, the error estimation is deliberately bounded by 10% of this maximum value, so $\overline{\delta}_a = 1,000$ is obtained. Concerning the direct solution, $\overline{\delta}_u$ is chosen to be small to limit the chattering phenomenon which may occur in the switching stabilizing control signal.

4.3.3.2 Control solution performances (simulation results)

Scenario 1: constant ground speed, pulse disturbance

As explained in Section 3.3.3, this test corresponds to a tyre damage simulation scenario. Figures 4.28 and 4.29 show the response of the NLG with respectively the direct and the indirect active damping controllers.

It is obvious that no shimmy appears since the oscillations are rapidly and efficiently damped. However, as the figures reveal, there is a small bias angle during the time the disturbance is applied; the wheel only returns to its original zero position when the disturbance disappears. This behaviour of the proposed active damping controllers is quite similar to that of current passive shimmy damping solutions. The main purpose of the designed controllers is not to drive the wheel, but to damp the shimmy oscillation. In fact, it is possible to choose the design

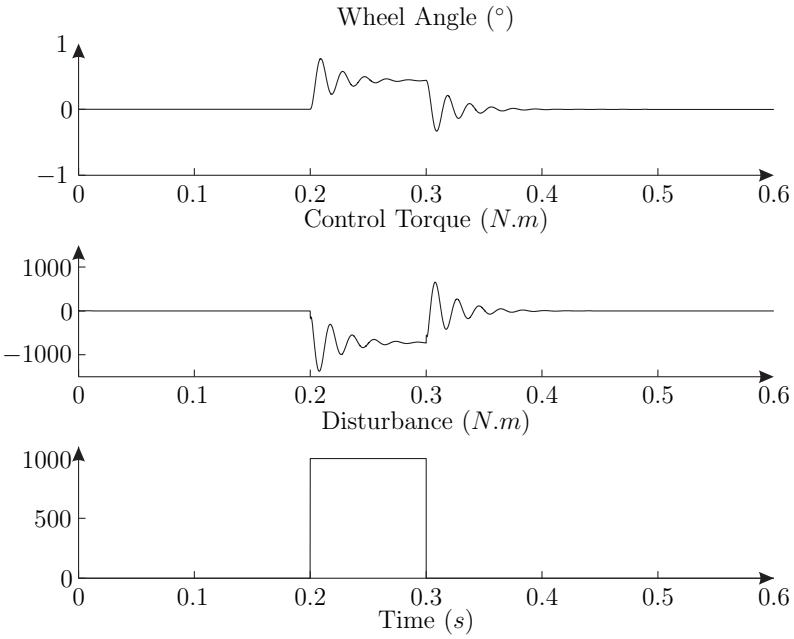

Figure 4.28: Active shimmy damping Scenario 1 (State feedback: Direct solution)

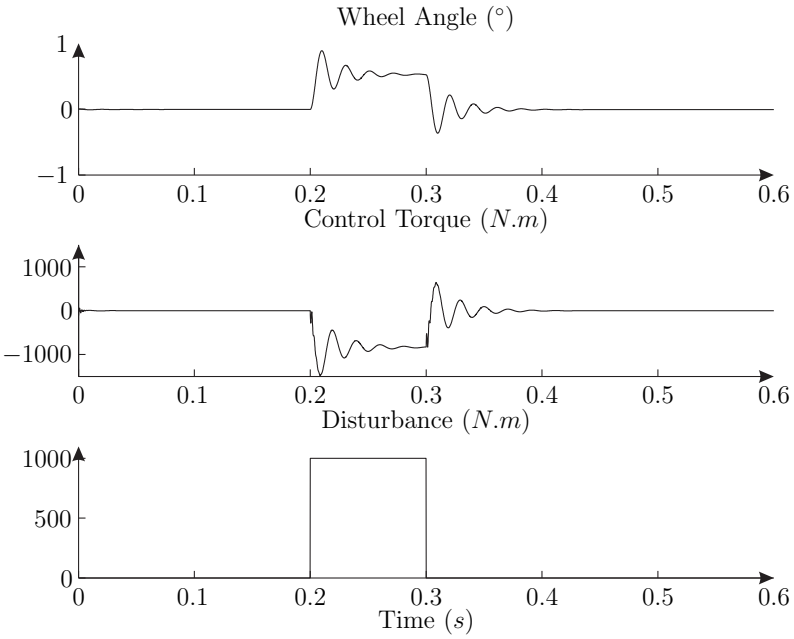

Figure 4.29: Active shimmy damping Scenario 1 (State feedback: Indirect solution)

parameters of the adaptive controllers so that the wheel angle remains close to its initial position (0°) even when the disturbance acts on the system, but in this case the control torque must be larger.

The two solutions give quite similar responses. In both cases, the oscillations are correctly damped and the maximum deviation of the wheel is lower than 1° with a mean value of 0.5°.

Scenario 2: Constant ground speed, rough runway

This scenario is performed to simulate the effects of the roughness of the runway on the NLG at high speed ($80m/s$). The results with the proposed active damping controllers are plotted in Figures 4.30 and 4.31.

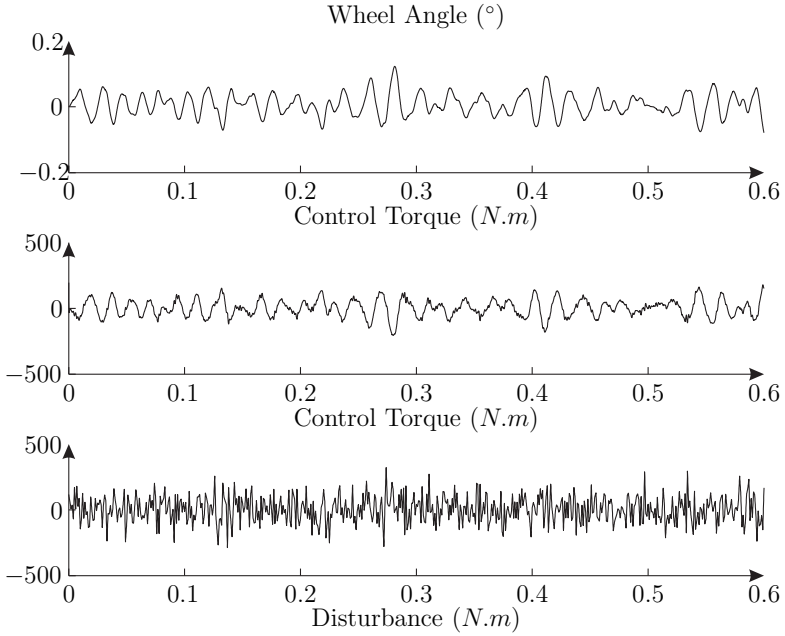

Figure 4.30: Active shimmy damping Scenario 2 (State feedback: Direct solution)

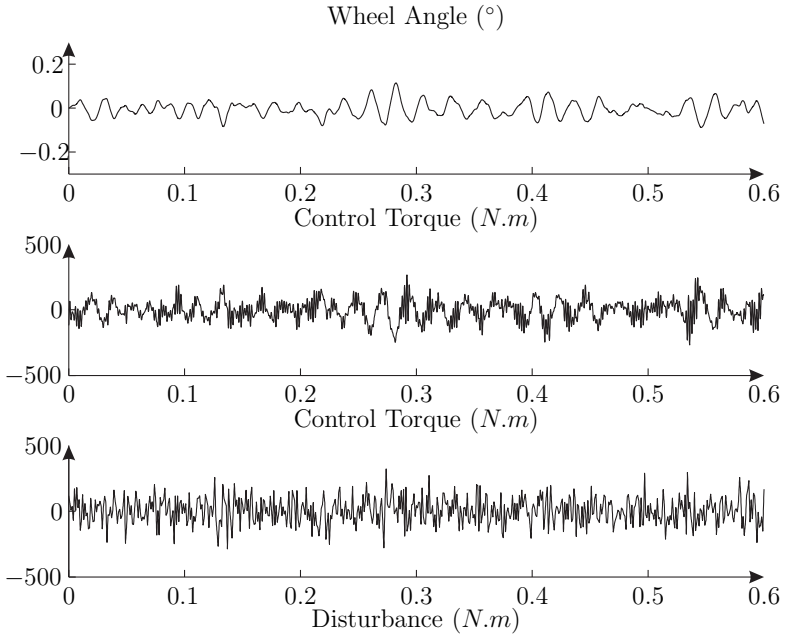

Figure 4.31: Active shimmy damping Scenario 2 (State feedback: Indirect solution)

Even with important random perturbations and at a high forward velocity, shimmy does not occur. Moreover, the variation of the wheel angle due to the high road imperfections, is very small (less than 0.2°). In practice, this small variation cannot cause any damage or malfunction

to the NLG.

Scenario 3: Varying ground speed, rough runway

The aim of this test is to investigate the performance of the damping controllers when the system is under varying speed conditions. The forward velocity is a critical parameter in the shimmy phenomenon: the shimmy oscillations traditionally increase with the increasing velocity. In low speed conditions ($\leq 25m/s$), shimmy does not easily affect the NLG behaviour [Somieski, 1997]. So, this scenario helps to verify that the active controllers do not affect the system stability at low speed and that they damp the oscillations at high speed. Figures 4.32 and 4.33 show the simulation results with the two active shimmy damping controllers in action.

Under the critical forward velocity of the aircraft ($\approx 25m/s$), the two controllers give similar results: shimmy is not observed and the control laws do not destabilize the NLG. Beyond this critical speed, the shimmy oscillations which appear with the non-controlled plant are actually damped.

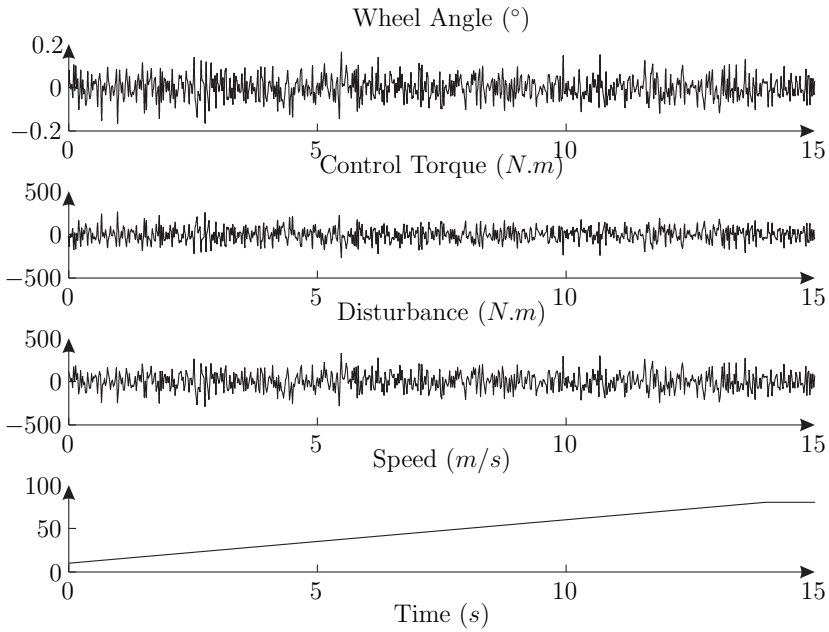

Figure 4.32: Active shimmy damping Scenario 3 (State feedback: Direct solution)

4.3.4 Simulation results based on the output feedback solution

4.3.4.1 Controller design

The design of the fuzzy adaptive output feedback control algorithm presented in Section 2.3.3 is discussed here. On the one hand, the description of the linear dynamic compensator is proposed. On the other hand, the fuzzy system is introduced.

Linear dynamic compensator

The linear dynamic compensator is designed to meet the error dynamic requirements. As discussed in Section 2.3.3, the purpose of v_{ad} is to cancel the unknown approximation error dynamics

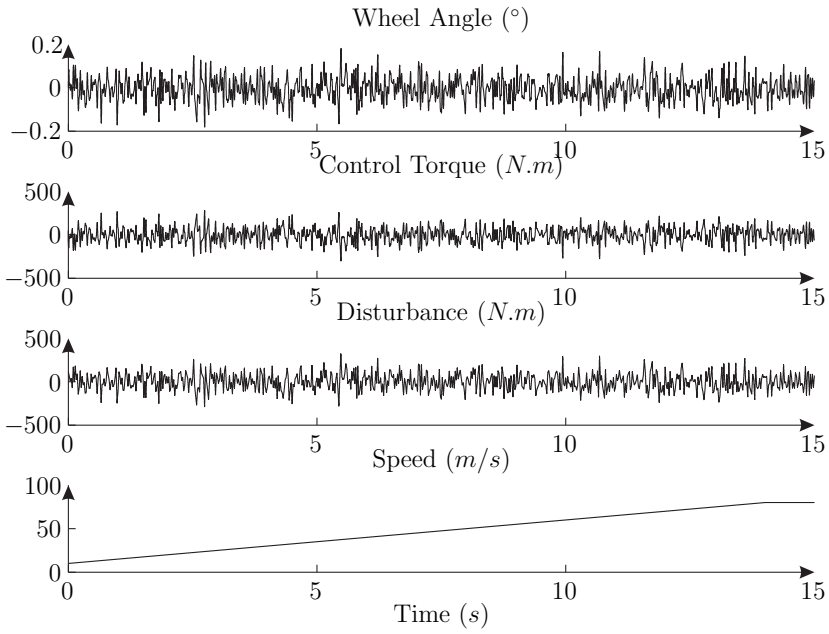

Figure 4.33: Active shimmy damping Scenario 3 (State feedback: Indirect solution)

Δ. In the ideal case, equation (2.46) becomes:

$$s^r \tilde{y}(s) = -v_{dc}(s) \tag{4.4}$$

with r is the relative degree of the system which is equal in the proposed application to 3. Substituting equation (4.4) into equation (2.47) leads to:

$$(s^r D_{dc}(s) + N_{dc}(s))\tilde{y} = 0 \tag{4.5}$$

Equation (4.5) shows that the polynomials $D_{dc}(s)$ and $N_{dc}(s)$ determine the output error dynamics. For this shimmy damping application, the requirement based on the relative degree presented in equation (2.51) becomes:

$$\deg(D_{dc}(s)) \geq \deg(N_{dc}(s)) \geq 2 \tag{4.6}$$

To obtain the control system as simple as possible, choose $D_{dc}(s)$ and $N_{dc}(s)$ as:

$$N_{dc}(s) = b_0 s^2 + b_1 s + b_2 \tag{4.7}$$

$$D_{dc}(s) = s^2 + a_1 s + a_2 \tag{4.8}$$

From equations (4.7) and (4.8), we have

$$s^r D_{dc}(s) + N_{dc} = s^5 + a_1 s^4 + a_2 s^3 + b_0 s^2 + b_1 s + b_2 \tag{4.9}$$

Through an empirical adjustment, the five roots of equation (4.9) are placed at -5, -5, -10, -30, and -35 which leads to

$$D_{dc}(s) = s^2 + a_1 s + a_2 = s^2 + 85s + 2475 \tag{4.10}$$

$$N_{dc}(s) = b_0 s^2 + b_1 s + b_2 = 29375s^2 + 147500s + 262500 \tag{4.11}$$

The transfer function $\bar{G}(s)$ must be strictly positive real, this means $arg(\bar{G}(jw))$ must be in the range $\pm 90°$. The poles of $\bar{G}(s)$ are specified above, it is possible to choose the zeros of $\bar{G}(s)$ interlacing with the poles such that $-90° \leqslant arg(\bar{G}(jw)) \leqslant 90°$, $\forall w$. Particularly, the zeros are placed at -1, -3, -80, -100. Because the numerator of $\bar{G}(s)$ is $N_{ad}(s)$ and $T(s)$ can be determined by assigning the zeros of $\bar{G}(s)$ to them. The low-pass filter $T^{-1}(s)$ should have as wide bandwidth as possible, so the two zeros -80 and -100 are assigned to $T(s)$ and the other zeros are assigned to $N_{ad}(s)$. Moreover, the maximum gain of the filter $T^{-1}(s)$ is chosen to be unity because the purpose of $T^{-1}(s)$ is to make $\bar{G}(s)$ strictly positive real, not to change the dynamics of the basic function of the fuzzy system used in the adaptive part. Finally, the polynomials $N_{ad}(s)$ and $T(s)$ are as follows:

$$N_{ad}(s) = 8000(s+1)(s+3) \tag{4.12}$$

$$T(s) = \frac{(s+80)(s+100)}{8000} \tag{4.13}$$

Fuzzy system

In this work, a fuzzy system is employed to implement the adaptive part of the controller. To satisfy the condition $n_1 \geq n$, it has been chosen to put $n_1 = 5$. The input of the fuzzy system is:

$$\begin{aligned} &\eta(t) = [v(t), v(t-d), y(t), y(t-d), y(t-2d), \\ &y(t-3d), y(t-4d)]^T = [\eta_1(t), ..., \eta_7(t)]^T \end{aligned} \tag{4.14}$$

where time delay $d = 0.0001s$. According to equation (4.14), the fuzzy system has 7 inputs. Two Gaussian membership functions are defined for each input. The membership functions are equally distributed in the range $(-\bar{\eta}_i, \bar{\eta}_i)$ for each input, with $\bar{\eta}_1 = \bar{\eta}_2 = 2000$, $\bar{\eta}_3 = \bar{\eta}_4 = \cdots = \bar{\eta}_7 = 20 \times pi/180$. The fuzzy system consists of 128 rules of the form presented in equation (1.21). The time delay should be small enough and the number of fuzzy rules should be large enough so that the approximation error is small. The parameter vector θ in the conclusion part of the fuzzy system is updated according to equation (2.65) with $F = 10I$ (where I is a 128 identity matrix) and $\lambda_w = 0.001$.

4.3.4.2 Control solution performances (simulation results)

Scenario 1: constant ground speed, pulse disturbance

Figure 4.34 presents the response of the NLG with the output feedback controller.

It is obvious that no shimmy appears and the maximum wheel angle is approximately 5°. The system needs approximately $0.3s$ to damp the oscillations fully. At time $t = 0.6s$, just a small oscillation is still in evidence.

Scenario 2: Constant ground speed, rough runway

The results for the scenario 2, which simulate the effects of the roughness of the runway on the NLG at high speed ($80m/s$), are plotted in Figure 4.35.

Shimmy does not occur and the variation of the wheel angle is very small (less than 0.2°). It can be concluded that at $80m/s$, the control solution is not affected by the roughness of the runway.

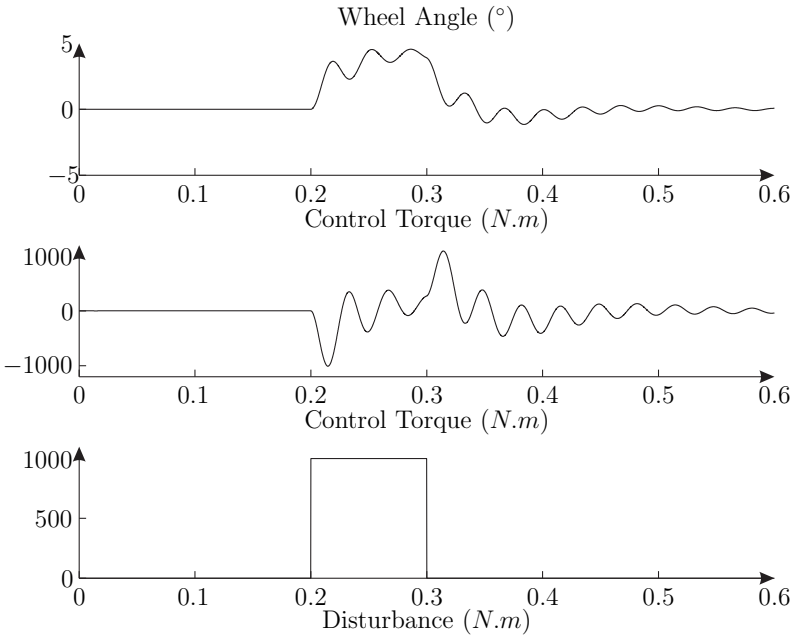

Figure 4.34: Active shimmy damping Scenario 1 (Output feedback)

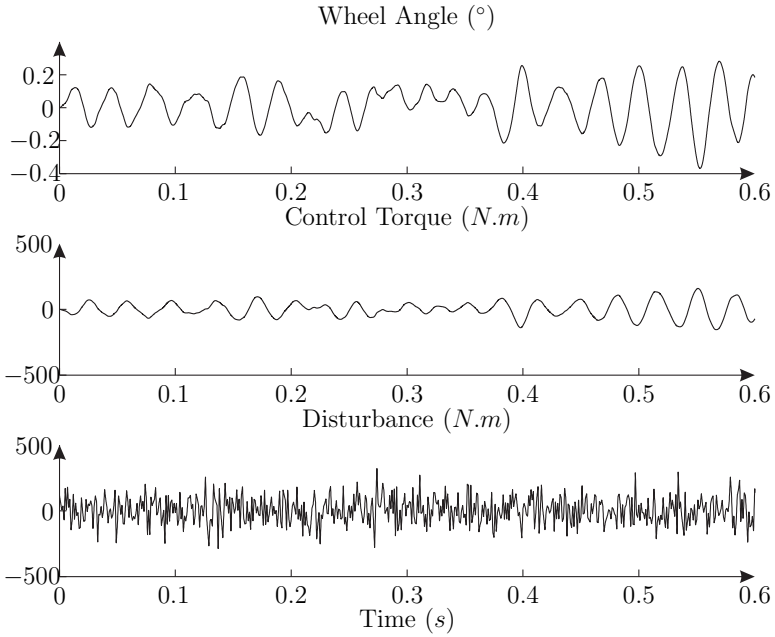

Figure 4.35: Active shimmy damping Scenario 2 (Output feedback)

Scenario 3: Varying ground speed, rough runway

Figure 4.36 shows the simulation results with the output feedback shimmy damping controllers in action for scenario 3. This scenario helps to verify that the controller does not affect the system stability at low speed and that the oscillations are damped at high speed.

The results show that the behaviour of the closed loop system is stable and no shimmy appears.

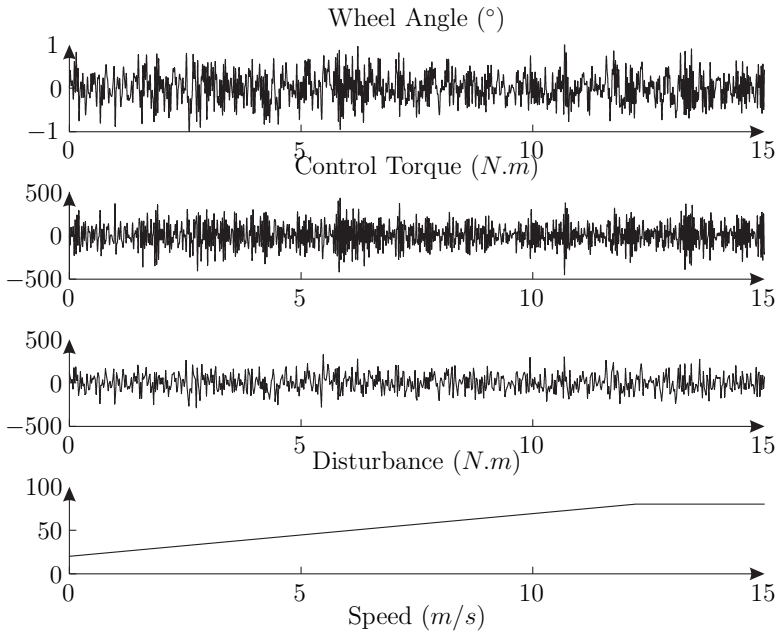

Figure 4.36: Active shimmy damping Scenario 3 (Output feedback)

4.3.5 Robustness analysis of the adaptive control solution

The three proposed control solutions show satisfactory results but the variations of the system parameters are not taken into account during simulation tests. Indeed, the conditions at the W/R interface are not always the same; the runway can be dry or wet. In addition, some components of the NLG varies during the life of the system. Finally, these variations must be taken into account. That is why a robustness study is proposed. This robustness study which is based on the indirect state feedback algorithm, aims at testing the properties of the closed loop system when variations of the parameters are introduced during simulations.

Simulations which correspond to different perturbations that can destabilize the system have been studied (a pulse disturbance acting during 0.1s and a random noise of low amplitude). However, the tuning of the controller has been made by considering a fixed value of the parameters of the landing gear. The robustness of the control solution is not presented here as a theoretical study, but it is rather based on simulations. Different tests are run in order to analyse the performance and the stability of the algorithm when variations of model parameters appear.

The proposed study will take an interest to 4 different aspects affecting the system:

- the tyre,
- the load,
- the speed,
- the NLG stiffness.

The tyre has different behaviours depending on the W/R interface. The generated forces and moments change if the runway is dry, wet or icy [Pacejka, 2006]. Thus, three different forces and moments generated at the W/R interface are included in the study of robustness. These three features called F_y^1/M_z^1, F_y^2/M_z^2 and F_y^3/M_z^3 correspond to a dry, wet or snowy runway.

The load F_z is fixed but this value is not constant during the landing and take off and can vary depending on the load transfer. The robustness study focuses on a variation of ±20% of the nominal load. Thus, F_z^{inf} et F_z^{sup} are the two types of considered loads.

The mechanical characteristics of the NLG are not fixed and the parameters such as the stiffness vary. That is why the study of robustness considers a variation of ±10% of this constant defining k^{inf} and k^{sup}.

The A/C longitudinal speed plays an important role in the outbreak of the shimmy phenomenon. This phenomenon appears beyond $25m/s$ and increases with respect to speed. Thus, simulations are performed considering 3 different speeds $V_x^1 = 20m/s$, $V_x^2 = 50m/s$ and $V_x^3 = 80m/s$.

The combination of all parameter variations is studied. Thus, a total of 36 simulations is conducted to validate the robustness of the algorithm. Table 4.4 presents these simulation cases:

Case	Runway state	Load	speed	Stiffness
1	F_y^1/M_z^1	F_z^{inf}	V_x^1	k^{inf}
2	F_y^1/M_z^1	F_z^{inf}	V_x^1	k^{sup}
3	F_y^1/M_z^1	F_z^{inf}	V_x^2	k^{inf}
4	F_y^1/M_z^1	F_z^{inf}	V_x^2	k^{sup}
5	F_y^1/M_z^1	F_z^{inf}	V_x^3	k^{inf}
6	F_y^3/M_z^3	F_z^{inf}	V_x^3	k^{sup}
7	F_y^1/M_z^1	F_z^{sup}	V_x^1	k^{inf}
8	F_y^1/M_z^1	F_z^{sup}	V_x^1	k^{sup}
9	F_y^1/M_z^1	F_z^{sup}	V_x^2	k^{inf}
10	F_y^1/M_z^1	F_z^{sup}	V_x^2	k^{sup}
11	F_y^1/M_z^1	F_z^{sup}	V_x^3	k^{inf}
12	F_y^1/M_z^1	F_z^{sup}	V_x^3	k^{sup}
13	F_y^2/M_z^2	F_z^{inf}	V_x^1	k^{inf}
14	F_y^2/M_z^2	F_z^{inf}	V_x^1	k^{sup}
15	F_y^2/M_z^2	F_z^{inf}	V_x^2	k^{inf}
16	F_y^2/M_z^2	F_z^{inf}	V_x^2	k^{sup}
17	F_y^2/M_z^2	F_z^{inf}	V_x^3	k^{inf}
18	F_y^2/M_z^2	F_z^{inf}	V_x^3	k^{sup}
19	F_y^2/M_z^2	F_z^{sup}	V_x^1	k^{inf}
20	F_y^2/M_z^2	F_z^{sup}	V_x^1	k^{sup}
21	F_y^2/M_z^2	F_z^{sup}	V_x^2	k^{inf}
22	F_y^2/M_z^2	F_z^{sup}	V_x^2	k^{sup}
23	F_y^2/M_z^2	F_z^{sup}	V_x^3	k^{inf}
24	F_y^2/M_z^2	F_z^{sup}	V_x^3	k^{sup}
25	F_y^3/M_z^3	F_z^{inf}	V_x^1	k^{inf}
26	F_y^3/M_z^3	F_z^{inf}	V_x^1	k^{sup}
27	F_y^3/M_z^3	F_z^{inf}	V_x^2	k^{inf}

Case	Runway state	Load	speed	Stiffness
28	F_y^3/M_z^3	F_z^{inf}	V_x^2	k^{sup}
29	F_y^3/M_z^3	F_z^{inf}	V_x^3	k^{inf}
30	F_y^3/M_z^3	F_z^{inf}	V_x^3	k^{sup}
31	F_y^3/M_z^3	F_z^{sup}	V_x^1	k^{inf}
32	F_y^3/M_z^3	F_z^{sup}	V_x^1	k^{sup}
33	F_y^3/M_z^3	F_z^{sup}	V_x^2	k^{inf}
34	F_y^3/M_z^3	F_z^{sup}	V_x^2	k^{sup}
35	F_y^3/M_z^3	F_z^{sup}	V_x^3	k^{inf}
36	F_y^3/M_z^3	F_z^{sup}	V_x^3	k^{sup}

Table 4.4: Combination of the parameter variations

The validation of the control solution is based on 4 criteria:

1. the maximum wheel angle caused by the perturbation should not exceed 1.5°,
2. the effect of the disturbance should not be in evidence after $0.2s$,
3. the torque required to damp the oscillations should not exceed $2000Nm$,
4. the value of the damping factor d_f.

The damping factor d_f is calculated by considering the amplitude of the successive oscillations a_1 and a_2 such that $d_f = \frac{ln(a_1/a_2)}{\sqrt{4\pi^2 + ln(a_1/a_2)^2}}$.

Simulation results show that criteria 1, 2 and 3 are easily satisfied. When the landing gear parameters vary considering the different cases, the control signal is able to eliminate the shimmy oscillations which appear after the disturbance. Criterion 4 which corresponds to the damping factor is a numerical criterion, evaluating the damping performances of the controller. It allows to compare the results for different simulations. Case 32, presented in Figure 4.37 is the most damped closed-loop system while case 11, presented in Figure 4.38, corresponds to the less damped closed-loop system.

The study of the damping factor shows that the stiffness of the NLG influences the behaviour of the control solution. Indeed, it can be logically noticed that the simulations using the stiffness equal to k^{inf} have more oscillations than the simulations using k^{sup}. In addition, the aircraft speed is also an important factor. An increase of V_x leads to a deterioration of the performances. Simulations done at $20m/s$ help to obtain an important damping while it is lower at $80m/s$.

4.3.6 Discussion

Inadequacy of the PID solution

This section proposes 3 shimmy damping control algorithms. Here, the aim is to compare them, according to different criteria (structure, performance, tuning difficulty, ...). Moreover, a PID controller which is not presented here has been implemented too [Pouly et al., 2009a]. The results of this simple control solution show that the different responses are not satisfactory and in some situations the controller destabilizes the system and generates shimmy before the critical speed.

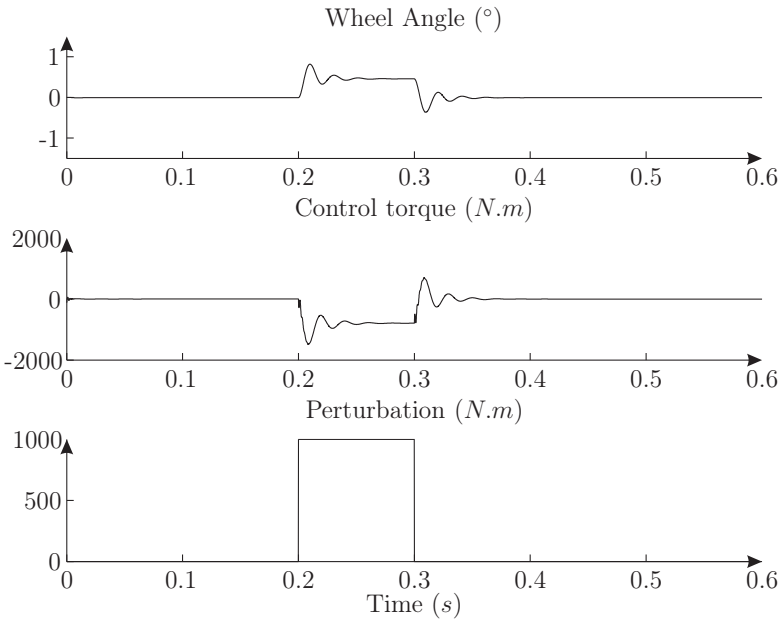

Figure 4.37: Case 32 : system which is the more damped

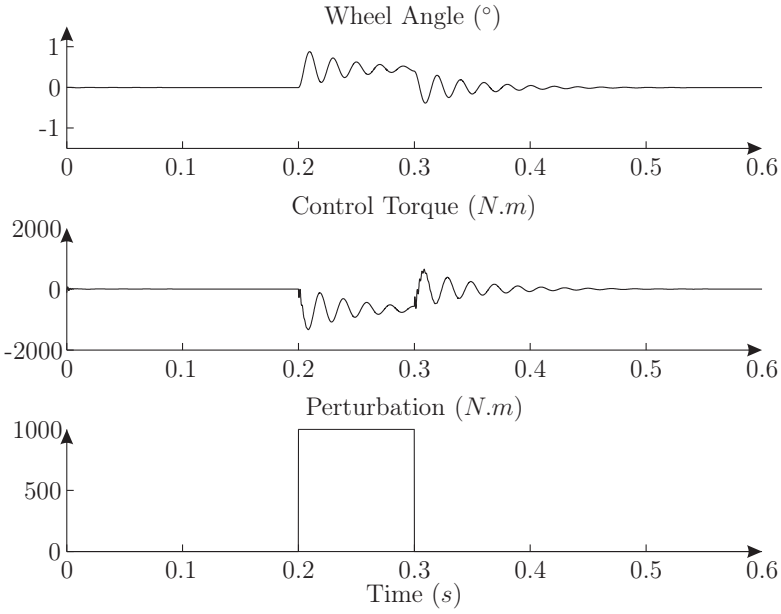

Figure 4.38: Case 11 : system which is the less damped

Results based on the state feedback control solution

For the state feedback indirect adaptive solution, a fuzzy identifier mechanism produces a model of the plant. Then, this model is used to adapt the controller. For the state feedback direct adaptive solution, the model of the plant is not necessary, since the controller parameters are directly identified. Each solution has a specific structure, however, similar components are used in both: a fuzzy identifier, an update law, a feedback linearisation control term and a sliding mode control term. The indirect and direct adaptive solutions require restrictive assumptions (measurement of all the states, bounded errors, ...) and the difference of structure leads to specific assumptions for each solution. Firstly, the direct and indirect solutions differ in the

number of fuzzy identifiers. The direct solution requires only one fuzzy system which allows the identification of the unknown control function. By contrast, the indirect solution generally requires two fuzzy systems which approximate the two functions $a(\mathbf{x})$ and $b(\mathbf{x})$, representative of the unknown non-linear dynamics of the system. This difference is significant in terms of time computation. Secondly, due to the certainty equivalence control term of (2.25), the singularity problem must not appear in the indirect solution. Thus, the fuzzy system must ensure that $\hat{b}(\mathbf{x})$ is bounded away from zero. Thirdly, the direct adaptive solution requires a bounding condition for the derivative of non-linear and smooth functions $b(\mathbf{x})$ of equation (3.41). Nevertheless, the specificities of the system to be controlled lead to particular structures of the indirect and direct solutions. The model of the NLG is specific insofar as the term $b(\mathbf{x})$ of equation (3.41) is independent of the system's states such that $b(\mathbf{x}) = B$. As a consequence, the structure of the algorithms developed here has been simplified. Indeed, a number of drawbacks of the two algorithms disappear. Firstly, the bounding condition of $\dot{b}(\mathbf{x})$ has no meaning because function $b(\mathbf{x})$ is a constant. Secondly, the two solutions require only one fuzzy system (only $a(\mathbf{x})$ is identified in the indirect solution) and thus, time computation for the indirect solution is reduced. Thirdly, the problem of singularity does not exist, considering that B is a constant defined by the structural non-zero parameters of the system. If, in this manuscript, this parameter remains constant, one strategy could be to overcome this assumption. [Ordonez et al., 1997] suggest to overspecify the fuzzy system design and to consider B as a function of the states $\mathbf{x}$. This choice may allow greater adaptation flexibility in particular cases.

Results based on the output feedback control solution

Concerning the output feedback controller, the complexity of the control solution increases. This is obvious because the control solution only measures the system output. This active solution uses a fuzzy logic system approximating the ideal feedback linearisation law by eliminating an approximation error. Then, the control solution consists of an adaptive term, a stabilized term and a feedforward term. The particularity of the fuzzy system is the fact that it has as inputs delayed control terms and outputs. Moreover, it is clear that comparing to the state feedback solutions, the design step is more difficult. At last, due to the aeronautical constraints, as for the two state feedback control solutions, the stability of the algorithm is proved by using the Lyapunov theory.

State feedback and output feedback comparison

As for performances, the manuscript illustrates that the two state feedback adaptive controllers give satisfying and similar results in various test conditions. For scenario 1 (constant ground speed, pulse disturbance), the perturbation is rejected and the oscillations disappear rapidly; the system will not be damaged. For scenarios 2 and 3, the roughness of the runway does not affect the NLG and no shimmy is observed, even above the critical aircraft forward velocity. Concerning the output feedback solution, the response of the closed loop system is satisfying for the different scenarios too. The simulations showed that the amplitude of the wheel angle is slightly greater ($\approx 1^\circ$ for scenario 3) than solutions based on state feedback solutions ($\approx 0.2^\circ$ for scenario 3). The same conclusion can be made for the amplitude of the required torque.

Discussion concerning the fuzzy system

The state feedback control solutions use both a fuzzy system. This latter helps to identify the system dynamics in the case of indirect solution while it permits to directly find the appropriate control law in the case of direct solution. Nevertheless, it could be possible to integrate an a priori knowledge of the system dynamics in the case of indirect solution. Indeed, based on the equation of the system, it could be possible to adjust the input of the fuzzy system. For instance, if the system reveals coupled states, it could be interesting to consider this a priori knowledge. This is only possible for the indirect solution insofar as the dynamics (that means the function $a(x)$ and $b(x)$ could be mathematically defined). On the hand, this addition of supplementary knowledge may improve the performances of the controller. On the other hand, this tends to limit the effectiveness of the universal approximator.

Actuator characteristics

Another aspect of this study is to specify the characteristics (torque required, bandwidth,...) of the electromechanical actuator used for shimmy damping. In Figures 4.30, 4.31 and 4.35, it can be seen that the controllers require the same control torque in terms of amplitude (approximately $1200N.m$). Considering the dynamics of the control signals, the different simulations show that very important dynamics are required. Nowadays, it seems difficult to build an actuator which has the capability to provide such properties with the considered constraints (mass, size, ...).

4.4 Conclusion

This chapter deals with the control of the A/C nose landing gear and two applications are proposed:

- the control of the nose landing gear for steering purposes;
- the damping of the shimmy phenomenon.

The control of the nose landing gear for steering purposes has been detailed in Section 4.2. The proposed $\mathcal{H}_\infty$ control solutions give the possibility to steer the NLG by respecting the specifications. In this section, the attention has been focused on the way of tuning the controller (an optimal methodology which helps to obtain the controller structure and to define the weighting parameters has been proposed, cf. Section 4.2.2) and on the gain scheduling controller (particularly the polytopic approach, cf. Sections 4.2.4.5 and 4.2.4.6). Based on simulation results, the efficiency of gain scheduling $\mathcal{H}_\infty$ controllers that use the polytopic approach has been examined. Moreover, experimental tests, performed on the test bench developed in the DRESS project, have been done (cf. Section 4.2.6). These experiments help to validate the proposed control solutions.

Concerning the damping of the shimmy phenomenon, the proposed study was limited to simulations. After a presentation of the different shimmy test scenarios (cf. Section 4.3.2), three fuzzy adaptive control solutions have been proposed. Firstly, two state feedback control solutions, based on direct and indirect structures have been considered in Section 4.3.3. Then, an output feedback solution which is more adapted for aeronautic constraints has been studied

in Section 4.3.4. The different control solutions, proposed in this section, give the possibility to damp the shimmy oscillations. Yet, because they use the measure of all the states of the systems, the state feedback solutions are more satisfactory from the performance point of view; but the solution based on output feedback is more realistic.

As it can be seen in Figure 3.1 and detailed in Section 3.2, two loops are required for automatic guidance; the low level loop and the high level loop. If Chapter 4 was mainly dedicated to the low level control loop that means the control of the NLG steering actuator, Chapter 5 is devoted to the high level loop. Then, the next chapter will take an interest on the control solutions which helps to automatically drive a rolling system. Based on experimental results of the automotive domain, different control solutions are proposed to control longitudinal and lateral dynamics.

S'il y a tant d'accidents sur les routes, c'est parce que nous avons des voitures de demain, conduites par des hommes d'aujourd'hui sur des routes d'hier.

Pierre-Jean Vaillard

Chapter 5

Automatic guidance of rolling systems

Contents

5.1 Introduction

Automatic guidance of rolling systems is an interesting application which is made possible by the development of accurate positioning devices like Global Positioning System (GPS) for instance. As mentioned in Section 3.2.3, guidance applications are developed for different domains: mobile robots [Peng et al., 2007], car vehicles [Falcone et al., 2007b], agriculture vehicles [Fang et al., 2005] or motorcycle [Rowell et al., 2007]. In the aeronautical domain, automatic guidance is interesting insofar as it would help to facilitate the aircraft on ground displacement and would give the possibility to operate the airports in "all weather" conditions.

This Chapter presents automatic guidance control solutions. The proposed solutions have been tested by simulations considering the A/C models presented in Section 3.3.1. The following takes an interest to the validation of these solutions (longitudinal control and lateral control) through experimental results. The validation of the control solutions is an important step and the test of the control algorithm on a real A/C was not possible. So, it has been decided to adapt the algorithm and to take the advantage of the laboratory experimental resources, which has various equipped vehicles and then apply the control solutions on a passenger car vehicle. Several similarities can be observed between longitudinal and lateral guidance applied on an A/C or a passenger car vehicle:

- Issues are very similar:
  Considering the longitudinal aspect, for both aeronautic and automotive applications, the control of the speed gives the possibility to behave more secure rolling system.

- Models are very similar:

For aeronautic and automotive applications, the "bicycle" model, presented in Section 3.3.1.4 is a well-used model ([Duprez, 2004], [Roos and Biannic, 2006], [Falcone et al., 2007a])

The chapter is organized as follows. First, the high level control loop which includes the longitudinal control and the lateral control is presented in Section 5.2. Then, the instrumentation of the car vehicle which integrates an acquisition system, some sensors and actuators is described. Later, results of the vehicle model identification are given in Section 5.4. On the one hand the identification of a LPV "bicycle" model is performed. On the other hand, based on real measures, two NN are identified. Finally the experimental results, dedicated to longitudinal and lateral control, are described. Concerning the longitudinal aspect, based on a collaboration with different members of the laboratory, an intelligent cruise control is proposed. Concerning the lateral control, different control solutions ("Follow the carrot", LPV MPC and NN MPC) are experimented and a discussion which compares these solutions ends this chapter.

5.2 Longitudinal and lateral control

5.2.1 Choice of the controller strategy

As mentioned in Section 3.2.1, two main control strategies help to control the longitudinal and lateral displacements of a rolling system on the ground. On the one hand, the LoLG structure is considered. This strategy is divided in two different parts; the aim is to decouple the lateral control of the rolling system with the longitudinal control. On the other hand, the LaLG handles the longitudinal controller and the lateral controller at the same same time with a single controller.

In the frame of the vehicle domain, the LoLG strategy is preferred. The fact that the control structure acts on longitudinal and lateral dynamics independently gives the possibility to activate one of the two control possibilities. Indeed, in the automotive domain for example, the longitudinal control or vehicle speed control is nowadays relatively accepted by the drivers and they have a lot of satisfaction to use such a driver assistance system. Concerning the lateral control the driver does not seem willing to let an automatic guidance system steer the vehicle. Moreover, on a control point of view it is easier to implement the strategy that separates the longitudinal and the lateral control.

Nevertheless, even if the two control loops are separated (for the LoLG strategy, one loop is dedicated to the control of the longitudinal behaviour while the other is responsible of the lateral dynamics), dynamics that are considered in the vehicle are entirely coupled. This is clearly felt in the vehicle when a bend is taken at different speeds. Indeed, when the longitudinal speed (V_x) increases, the lateral acceleration (γ_T) becomes more and more significant, resulting in a force that tends to increase with the longitudinal speed augmentation, push the vehicle occupants to the outside of the turn. Thus, considering the modelling and control aspects, the two loops share some data. For example, the lateral control loop uses the longitudinal speed V_x, to adapt the control signal in adequacy with this physical quantity.

5.2.2 Proposed strategy

The chosen solution which is based on the LoLG strategy is presented in Figure 5.1. This strategy clearly corresponds to a LoLG strategy insofar as the two blocks "steering controller" and "speed controller" would combine into one in the case of LaLG strategy. This strategy is

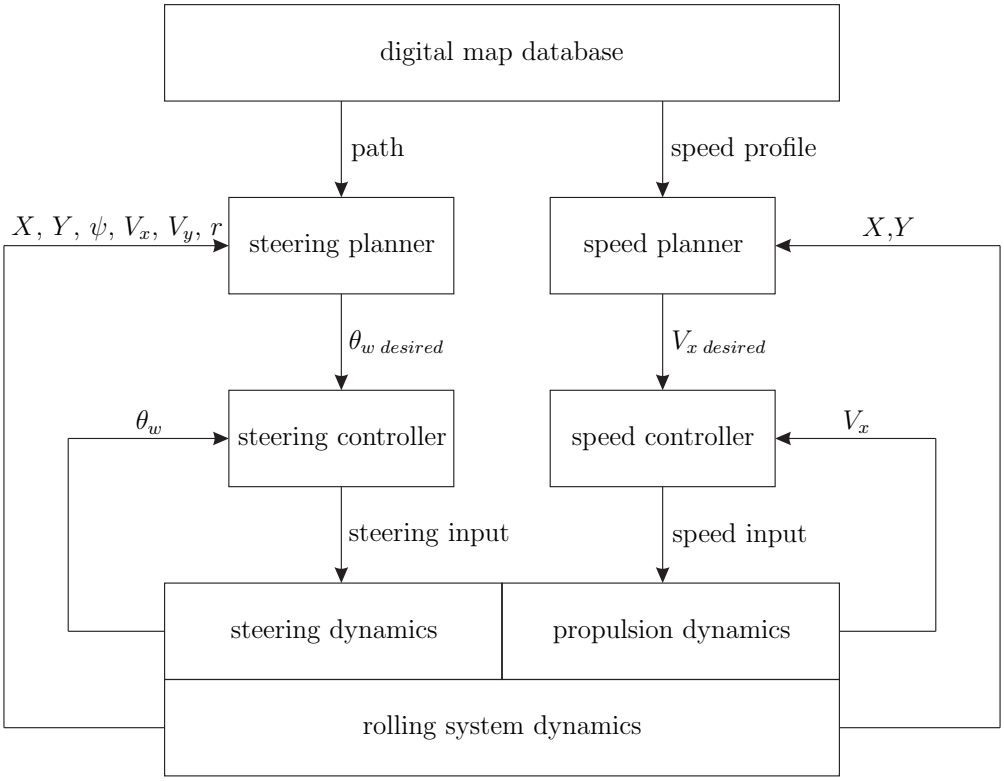

Figure 5.1: LoLG control strategy

based on two parallel loops, the first, on the left, is dedicated to the lateral control while the second on the right aims at providing the appropriate longitudinal speed order. Based on a digital map database of the road network, two data are provided, the path and the speed profile. The path is only a succession of X and Y coordinates that the vehicle must follow. The speed profile is defined based on some information of the digital map database and notably the road curvature. A particular paragraph is dedicated to the achievement of the speed profile in Section 5.5. Regarding to the lateral control loop, the steering planner aims at providing the desired wheel angle. The experimental results of the different proposed control solutions are given in Section 5.6. For the steering controller, in the automotive domain, it is a simple PID loop which controls a steering motor, while in the aeronautic domain the nose wheel is steered by the use of a robust control solution detailed in Section 4.2. With regard to the longitudinal control, the speed planner is based on a Finite State Machine (FSM) detailed in Section 5.5 and a simple PID controls the braking system.

5.3 Instrumentation of the test vehicle

5.3.1 Test vehicle presentation

The laboratory possesses different test vehicles which are fully equipped for modelling, identification, control and diagnostics. Among these vehicles, the Renault Scénic (Figure 5.2), is dedicated to driver assistance systems and particularly systems based on GPS and digital map database.

Figure 5.2: Test vehicle (Renault Scénic)

5.3.2 Acquisition system description

The solution chosen for the data acquisition of all the sensors and the control of all the actuators is an AutoBox® system from dSPACE® which is a standard rapid prototyping system used in automotive industries. It is an hardware and software solution particularly robust and efficient. The AutoBox® is composed of a PowerPC processor and multiple I/O boards. Moreover, it is linked with an industrial computer via an Ethernet network. The industrial computer helps to develop acquisition and control models which are compiled and transferred on the AutoBox®. The input-output boards of the AutoBox® are analog/digital converters, digital signal acquisition board, serial RS232 board, Controller Area Network (CAN) board ...

5.3.3 Sensors descritpion

The main sensors which are installed in the test vehicle and used in the frame of this thesis are:

- an Advanced Driver Assistance Systems Research Platform (ADASRP) navigation system from Navteq®,
- a DGPS receiver,
- a RT3002 inertial unit,
- a steering wheel angle sensor.

5.3.3.1 ADASRP navigation system

The ADASRP provided by Navteq® is an open framework allowing the development of Advanced Driver Assistance Systems (ADAS). It is a global positioning system (GPS) that provides data about the road network ahead of the moving vehicle which can be used for different control applications. The architecture of this system, based on software and hardware components, is presented in Figure 5.3.

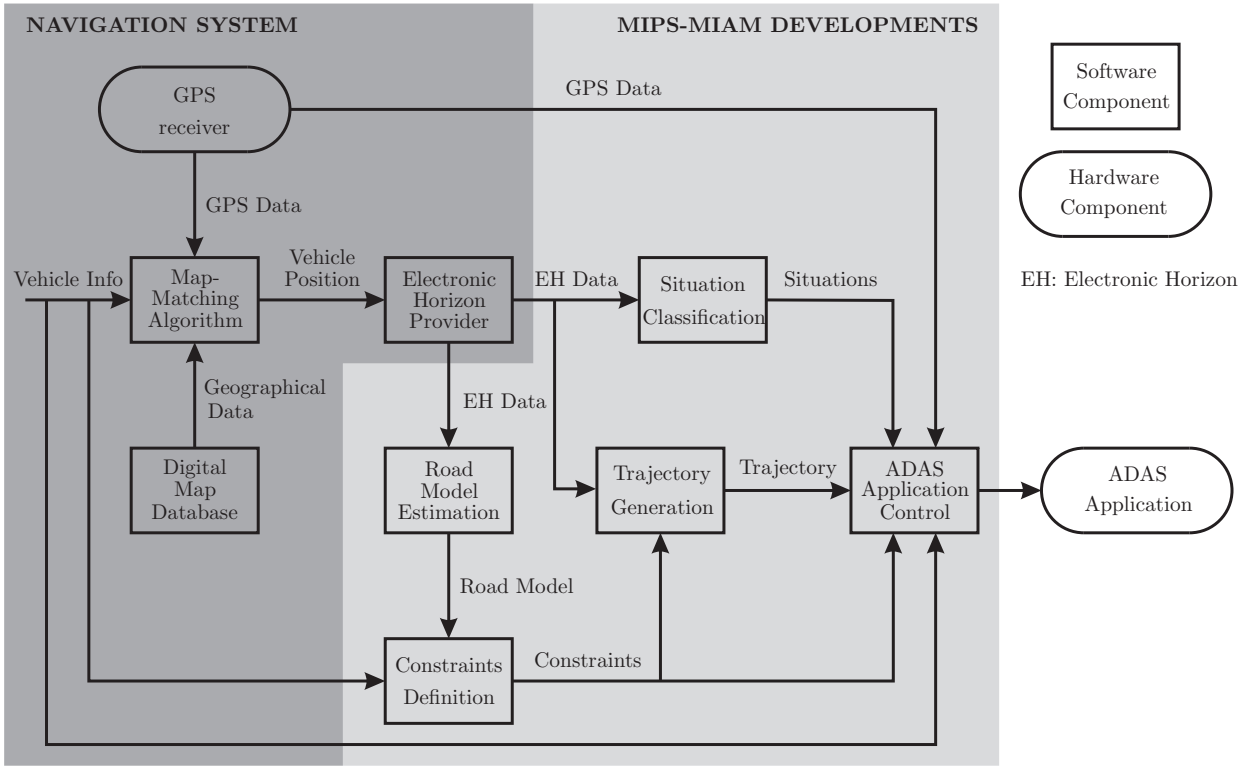

Figure 5.3: ADASRP

It contains a GPS and gyrometer based Sensorbox®, a digital map database, a map-matching algorithm and an electronic horizon provider, which are all available in most standards car navigation systems. The map-matched position is essential for the determination of the current electronic horizon which contains all the road network information about the current and upcoming road context. This information is used to determine road events (bend, intersection, straight line, etc.). From the Electronic Horizon data and the considered constraints, the trajectory is generated. Finally, following the considered ADAS application, informations from the trajectory are collected (for instance the road curvature) and a control signal is provided to the ADAS application. For instance, in the case of Advanced Front Lighting System ([Lauffenburger et al., 2007]), the ADAS Application Control provides the movement of the headlights to the ADAS application.

Considering the characteristics of this system, the positioning accuracy is about 2m and the digital map database accuracy is about 5m in the absolute and 2m in the relative.

5.3.3.2 DGPS receiver

To address the problem of accuracy of the GPS system, some applications require the use of a DGPS (Differential Global Positioning System). It is an enhanced GPS which uses a ground-based reference stations to broadcast the difference between the positions indicated by the satellite systems and the known fixed position. The correction signal is broadcasted over UHF radio signals.

The DGPS system used in the laboratory is composed of a reference station (Scorpio SK6002) and a mobile station (Aquarius MK5002) from Thalès®. The use of DGPS provides a positioning accuracy of 1cm in x, y and 2cm in z.

The acquisition of the DGPS information that means the X and Y position of the vehicle and its heading θ in a Lambert 2 coordinate frame is done by the serial bus at a frequency of 10Hz.

5.3.3.3 RT3002 Inertial Unit

The RT3002 from OXTS® is an inertial and GPS system which includes three angular rate sensors (gyrometers), three servo-grade accelerometers, the GPS receiver and all the required processing for the data integration. In the frame of this thesis, it is mainly used to measure the angular velocity r around the vertical axis z, and longitudinal and lateral speeds (respectively V_x and V_y) of the vehicle.

The RT3002 is controlled by the CAN bus and the acquisition of the information is done at 100Hz. The accuracy of the velocity information is 0.05km/h RMS while the angular rate accuracy is $0.01°/s$.

5.3.4 Actuators presentation

The principal actuators which are installed on the test vehicle and used in the frame of this thesis are:

- a cruise control,
- an electrical braking system,
- a steering motor.

5.3.4.1 Cruise control

The cruise control is a control device that acts directly on the throttle angle regarding the different signals given by the driver via a remote. However to automatically control the vehicle on road, this remote has been replaced by signals coming from the dSPACE® AutoBox® control system. The signals that are sent to the cruise control are:

- **Accelerate**, which increases the throttle angle. A short signal (< 1s) increases the throttle angle by a single step (2-3km/h) and a long signal (> 1s) by gradual steps as long as the signal is active. The final speed is then memorized and maintained by the cruise control.

- **Decelerate**, which decreases the throttle angle. A short impulse signal ($<$ 1s) slightly decreases the vehicle speed (2-3km/h) while a long ($>$ 1s) gradually decreases the vehicle speed. The final speed is then stored and maintained.

- **Cancel** which cancels a maintain phase or another acceleration or deceleration action.

The cruise control is addressed by the CAN bus.

5.3.4.2 Electrical braking system

The braking system is a typical one, composed by a brake pedal, a vacuum booster, brake discs, etc. However, an additional electrical control is available. The latter is used to control the vehicle speed automatically. Anyway, the driver can still use the braking pedal. The electrical braking system is addressed by analogical signals.

5.3.4.3 Steering motor

The steering motor is a multipolar permanent magnets synchronous brushless, three-phases motor SKADDR 148-90 from Motor Power Company® which is directly mounted on the steering column and helps to steer the vehicle wheel. The motor provides a stall torque (the torque which is produced by the motor when the output rotational speed is zero) of $20Nm$ with a maximum rotational speed of $150rad/min$ and is driven by its own servo drive. The performances of this motor are certainly oversized for the considered application and the dimensions of the solution may seem important. However, the specifications that must be reached requires this solution. The motor has been sized to steer the wheel when the vehicle is stopped. The speed performances are required for vehicle identification process when sinusoidal input at high frequency ($\geq 5Hz$) are done. Finally, this motor, presented in Figure 5.4, has no mechanical transmission (no chain and no belt) which is better for security purposes. The steering motor is connected to the CAN bus.

Figure 5.4: Steering motor

5.4 Vehicle model identification

The experimental results of the control solutions presented in Sections 5.5 and 5.6 requires a model of the system to get the control signal based on a MPC approach. Then, LPV MPC and NN MPC control solutions, presented in Section 2.4, require the identification of the model parameters. The two following Sections 5.4.1 and 5.4.2 present the results of model parameters estimation.

5.4.1 Bicycle model identification

5.4.1.1 Identification procedure

As mentioned in Section 1.4, the identification process requires four steps: the definition of the protocol, the cost criteria definition, the parameter estimation and the validation process. These steps will be detailed for the identification of the bicycle model as well as for the two neural network models.

Definition of the protocol

The structure of the model that is identified, is the one presented in Section 3.3.1.4 adapted for the automotive domain:

$$\begin{cases} \dot{V}_y &= \dfrac{-CS_f - CS_r}{M \cdot V_x} V_y + \left(\dfrac{-l_f \cdot CS_f + l_r \cdot CS_r}{M \cdot V_x} - V_x \right) r + \dfrac{CS_f}{M} \theta_w \\ \dot{r} &= \dfrac{-l_f \cdot CS_f + l_r \cdot CS_r}{J_v \cdot V_x} V_y + \left(\dfrac{-l_f^2 \cdot CS_f - l_r^2 \cdot CS_r}{J_v \cdot V_x} - V_x \right) r + \dfrac{l_f \cdot CS_f}{J_v} \theta_w \end{cases} \tag{5.1}$$

As presented in Figure 5.5, the vehicle model is composed of 1 input, the wheel angle θ_w, 1 varying parameter, the longitudinal speed V_x and 2 states, the lateral speed V_y and the yaw rate r. The model requires the knowledge of 6 parameters, the cornering stiffness at the front and rear axles (respectively CS_f and CS_r), the distance between the CG and the front and rear axles (respectively l_f and l_r), the mass M of the vehicle and the inertia J_v.

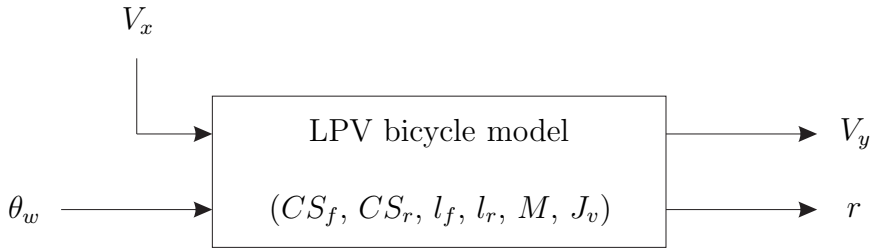

Figure 5.5: Structure of the bicycle model

The lenghts l_f and l_r and the mass M of the vehicle are measured directly and the obtained values are presented in Table 5.1. The values are obtained when two persons are in the vehicle. Then, the parameter estimation process aims at identifying the values of the parameters CS_f, CS_r and J_v. Nevertheless, it is possible to measure the value of J_v [Brossard, 2006]

and [Caroux, 2007] but the estimation process has been preferred due the complexity of the measurement process.

Symbol	Measured value	Unit
l_f	1.12	m
l_r	1.45	m
M	1577	kg

Table 5.1: Values of the measured parameters

Four signals are used for the identification process: the steering wheel angle θ_w, the lateral speed V_y, the yaw rate r and the longitudinal speed V_x. The first is obtained with the steering wheel angle sensor, a constant reduction ratio equal to 17 helps to convert the steering wheel angle into the wheel angle. The measures of V_y, r and V_x are obtained with the RT3002.

The step which consists in recording the different signals has been repeated several times. Thus, the identification procedure can be performed with these different measurements which help to compare the identified parameters. Concerning the input signal, the driver performs sinusoidal steering actions with varying frequencies from approximatively $0.15Hz$ to $2.5Hz$ (chirp signals). The steering wheel angle input signal is presented in Figure 5.6. Moreover, due to

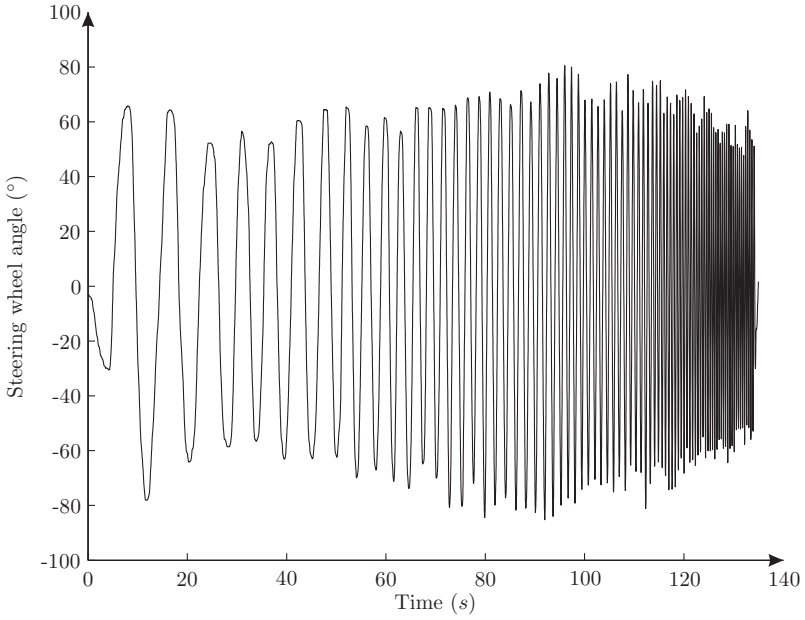

Figure 5.6: Steering wheel angle input signal (identification signal)

the longitudinal speed dependency of the model, different recordings are performed at different constant speed, varying from $5m/s$ to $15m/s$.

Cost criterion definition

As mentioned in Section 1.4 the cost criterion is a quadratic criterion defined by:

$$J = \sum_{t=1}^{N_{samp}} \left(V_{y\ meas}(t) - V_{y\ mod}(t)\right)^T \left(V_{y\ meas}(t) - V_{y\ mod}(t)\right) + \sum_{t=1}^{N_{samp}} \left(r_{\ meas}(t) - r_{\ mod}(t)\right)^T \left(r_{\ meas}(t) - r_{\ mod}(t)\right) \tag{5.2}$$

where N_{samp} corresponds to the number of samples in the signals and the subscript $_{meas}$ and $_{mod}$ corresponds to the signals coming from respectively the measures and the model.

Parameter estimation

The parameter estimation is done with the Levenberg-Marquardt algorithm by the use of the Matlab® System Identification Toolbox function "pem".

Validation process

As soon as the optimization algorithm returns a value of the model parameters (the optimization algorithm ends when the number of increment that has been defined is reached or when the variations of the identified parameter become insignificant), the validation process can be performed. This last step aims at comparing the results of the identified model with the real system by using a different input signal. Thus, the steering wheel angle that is used for the validation procedure is presented in Figure 5.7.

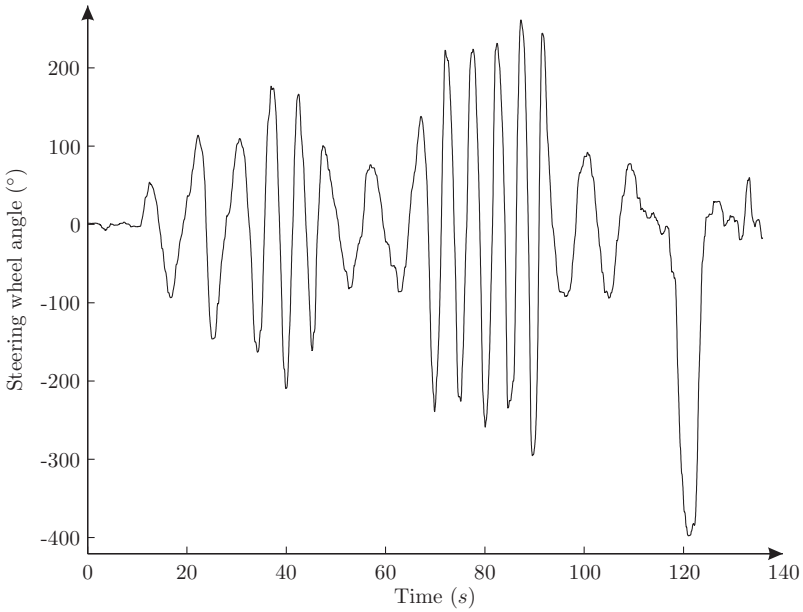

Figure 5.7: Steering wheel angle input signal (validation signal)

5.4.1.2 Results of the identification process

The results of the identification is characterized by the comparison of the validation signal with the signal coming from the model. Figures 5.8 and 5.9 present the comparison for respectively

V_y and r. It can be seen that the validation signal and the signal coming from the model are very close. The fit is 85% for V_y and 80% for r.

The responses V_y and r obtained with the identified model are satisfying for the use in control applications. For the signal r, the response of the model runs over the validation signal. A difference which is approximately equal to $0.08rad/s$ is observed. This phenomenon is less obvious for the signal V_y insofar as both signals (validation signal and response of the model) have similar shape even for the maximal amplitudes. Nevertheless, V_y and r signals show an important error at time $t = 120s$. For V_y, the validation signal goes to $-0.9m/s$ and the response of the model has a larger value with $-1m/s$ while for r, the validation signal is only $-0.9rad/s$ and the response of the model reaches $-1.2rad/s$. This can be explained by the fact that at this time, limits of the bicycle model are reached (the lateral acceleration $gamma_T$ is larger than $3m.s^{-2}$).

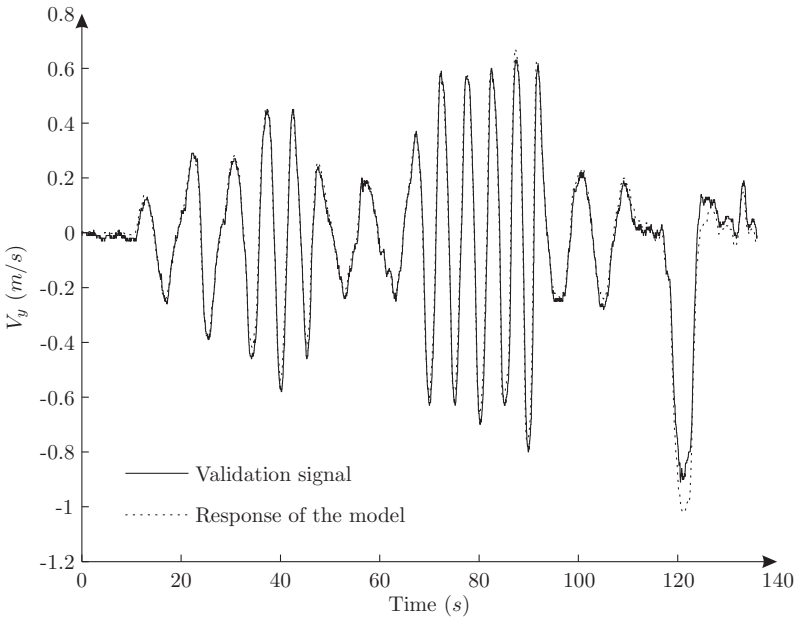

Figure 5.8: Results of the identification for signal V_y

The identification procedure gives the possibility to estimate the values of the 3 parameters. Different estimations have been done with different longitudinal speeds and concerning the parameter J_v an important dispersion has been observed. Indeed, the lower identified value is $J_v = 1756kg.m^2$ while the bigger identified value is $J_v = 3787kg.m^2$. In order to quantify the impact of this important range of values, a sensitivity analysis is proposed. To do this, the 5 other parameters of the bicycle model are fixed ($CS_f = 62829N/rad$, $CS_r = 96702N/rad$, $l_f = 1.12m$, $l_r = 1.45m$, $M = 1577kg$) and the results of the 2 outputs signals with the low and high inertia are compared. The results are proposed in Figures 5.10 and 5.11.

It can be seen on Figures 5.10 and 5.11 that the obtained curves are very close. Indeed, the value of the fit is 99% for V_y and 94% for r. Moreoever, the signal errors which correspond respectively to the difference between the two V_y signals on the one hand and to the difference between the two r signals on the other hand, are low with a maximum amplitude equal to $0.01m/s$ for V_y and equal to $0.08rad/s$ for r. This permits to conclude on the fact that, in the

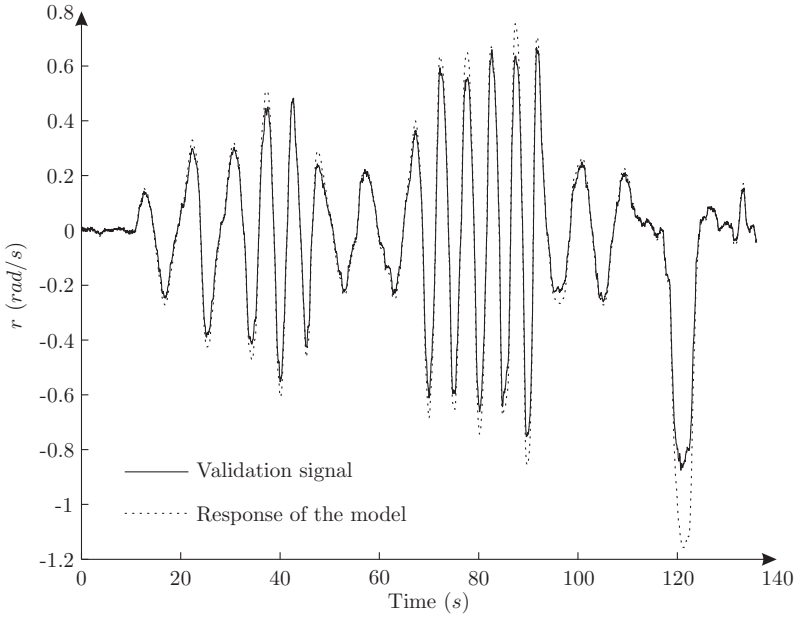

Figure 5.9: Results of the identification for signal r

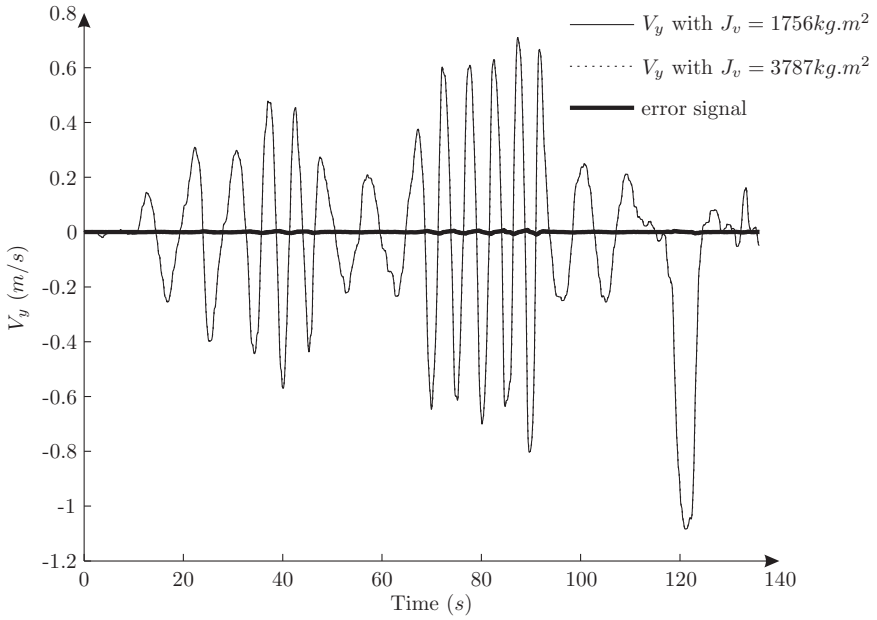

Figure 5.10: Results of sensitivity analysis with signal V_y

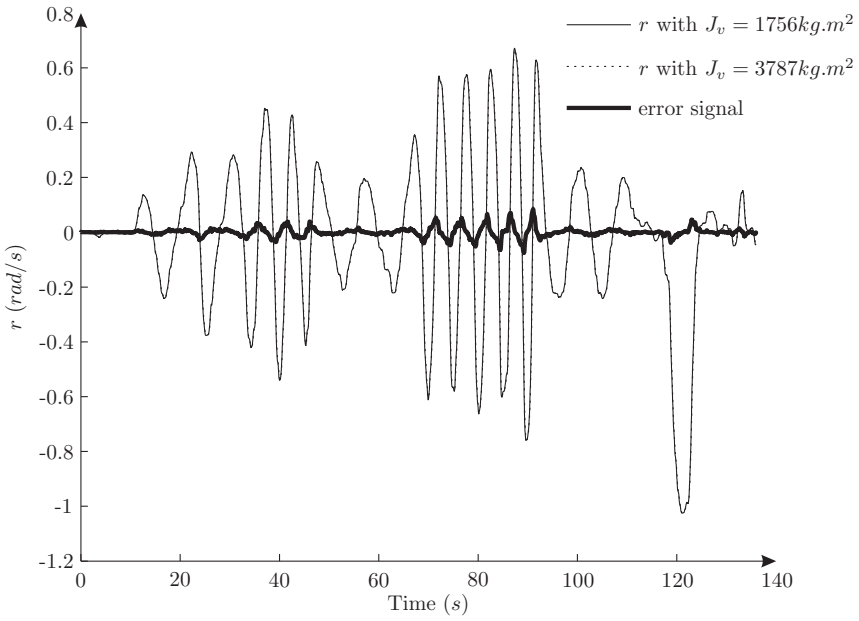

Figure 5.11: Results of sensitivity analysis with signal r

proposed conditions, the influence of the parameter J_v on the behavior of the model is not very important. As a conclusion, the final choice of the parameter is based on a mean value and $J_v = 2659kg.m^2$.

For a "bicycle" model, parameters CS_f and CS_r are very influential and it is known that these parameters vary according to the solicitations. Then, for the estimation of the two parameters CS_f, CS_r, a correlation between these values and the longitudinal speed has been remarked. Figures 5.12 and 5.13 represent the evolution of the stiffnesses as a function of the longitudinal speed. It can be noticed that a second order polynomial permits to fit the cornering stiffness of the front axle CS_f with the longitudinal speed V_x while a first order polynomial gives the possibility to fit the cornering stiffness of the rear axle CS_r with the longitudinal speed V_x. For the parameter CS_f, the chosen fitting function is $CS_f(V_x) = -354V_x^2 + 9979V_x - 1458$ while the relation between CS_r and V_x is $CS_r(V_x) = 7146V_x + 21846$.

5.4.2 Neural network model identification

5.4.2.1 Identification procedure

As done in the previous section, the four steps of the identification process will be presented. Particularly, for the NN identification, the structure of the model is not fixed and this section helps to chose the network configuration (the number of neurons in the hidden layer) and the inputs of the network.

Definition of the protocol

Two different NN structures are presented in this section. The identification process helps to compare the results based on different structures and to choose the most suitable number of neurons of the hidden layer. The first NN structure considers three inputs (the wheel angle θ_w

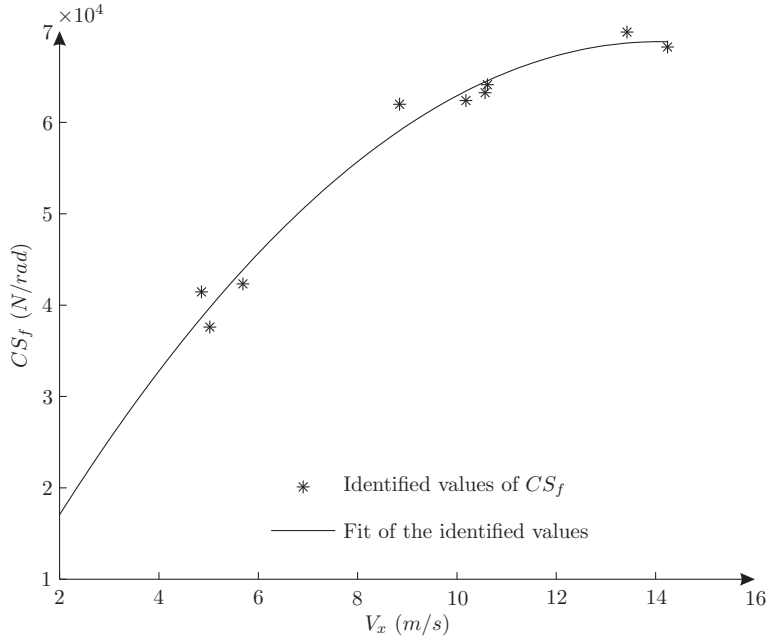

Figure 5.12: Fitting of the estimated values of CS_f

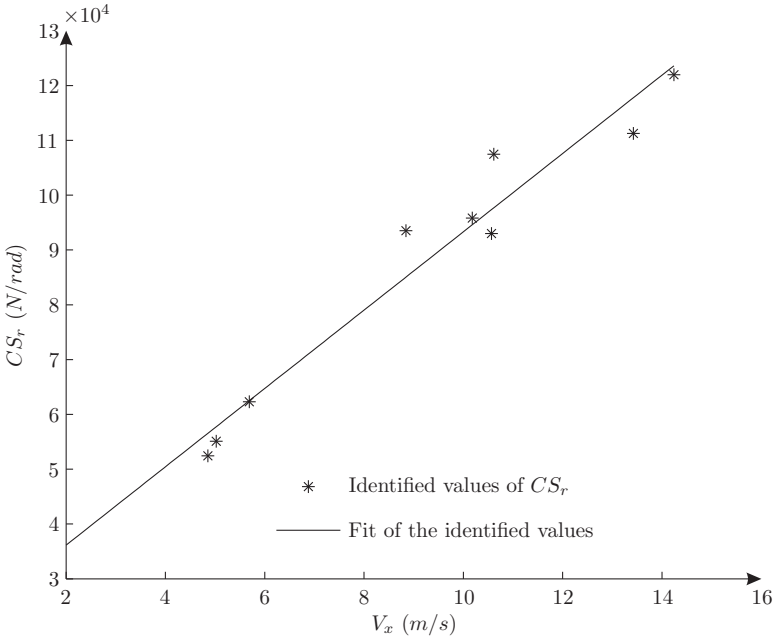

Figure 5.13: Fitting of the estimated values of CS_r

and two delayed inputs $V_y(z^{-1})$ and $r(z^{-1})$) and two outputs (V_y and r). The main drawback of this structure is the fact that the longitudinal speed of the vehicle is not considered. Indeed, it is well-known that this quantity has a major influence on the system dynamics. Then, as mentioned in [Qiang et al., 1999], the second structure includes an additional input V_x. This contribution appears in the structure of the vehicle mathematical model and it is interesting to study the influence of this extra input on the results of the identification. Finally, the two proposed structures are presented in Figures 5.14 and 5.15 where w, w_{bias}, W and W_{bias} are the weights that must be identified. w_{bias} and W_{bias} correspond to the weights of the bias, an additional input for each neuron which helps to reinforce the learning of the network [Abdeslam, 2005].

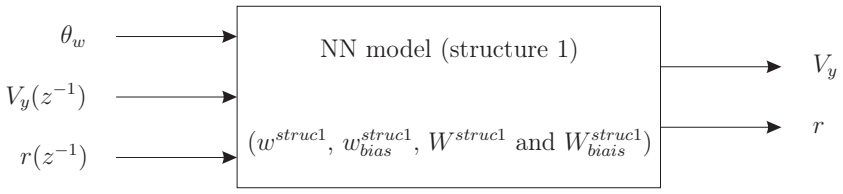

Figure 5.14: Description of the NN (structure 1)

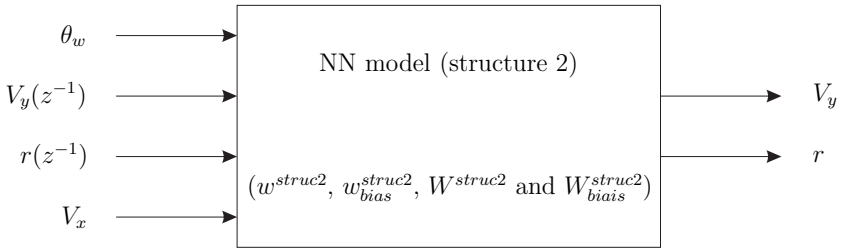

Figure 5.15: Description of the NN (structure 2)

Moreover, the influence of the number of neurons in the hidden layer is studied. The aim of the NN model is to be used as a predictor in the NN MPC control solution. This control algorithm requires an on line optimization, so a low number of neurons will reduce the calculation time.

The identification signal is not similar to those used for the identification of the LPV model insofar as the longitudinal speed must vary. The chosen signals are presented in Figure 5.16.

Cost criterion definition

The cost criterion corresponds to the one used in Section 5.4.1.

Parameter estimation

The parameter estimation is based on the back propagation method presented in Section 1.4.4. The process is computed with the function "batbp" that comes from the toolbox NNSYSID (Neural Network SYstem IDentification) running on Matlab®.

Validation process

The validation signal corresponds to those used in Section 5.4.1.

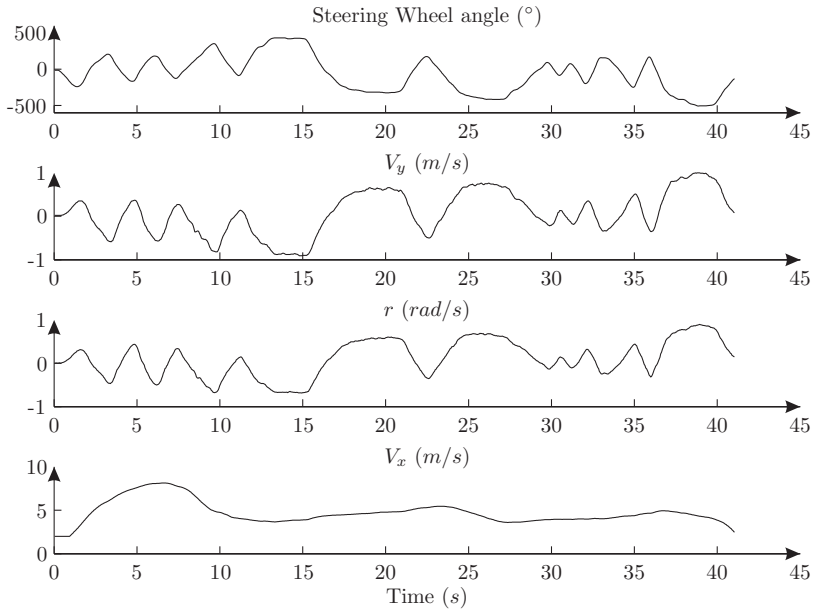

Figure 5.16: Presentation of the NN identification signal

5.4.2.2 Results of the identification process

The table 5.2 presents the NN identification results with both structures considering that the number of neurons in the hidden layer (nCC) varies. The percentages represent the fit between the NN model and the validation signal.

	structure 1		structure 2	
	V_y	r	V_y	r
nCC = 10	61%	71%	74%	75%
nCC = 50	73%	71%	79%	72%
nCC = 100	72%	70%	76%	69%
nCC = 300	72%	68%	73%	68%

Table 5.2: NN identification results

Three main points are deduced from the NN identification results:

- with a limited number of neurons, the NN is not competitive enough because the dynamics of the system are not learned,
- NN with too many neurons reduces the ability of network generalization. The NN tends to learn a particular sequence. This is called over learning,
- results show that the use of an additional input (the longitudinal speed V_x in this case) helps to improve the fit.

Finally, the identification based on the bicycle model gives better results than the identification based on NN model. It can be seen that the bicycle model helps to reach a fit of 85% for V_y and 80% for r, while the best fit with the NN model is only 79% for V_y and 72% for r.

As a conclusion, two models will be used for the prediction of the NN MPC control solution. On the one hand, the NN model with structure 1 and nCC=50. On the other hand, the NN model with structure 2 and nCC=50.

5.5 Longitudinal control: experimental results

5.5.1 Introduction

Nowadays, intelligent transportation systems (ITS) which consist in using synergistic technologies and systems engineering concepts to develop improved transportation systems have an important success. It gives the possibility to enhance safety, security and efficiency by, for instance, designing traffic control systems, collision avoidance systems, etc. Here, attention is focused on a particular ITS system which is the cruise control. This latter aims at controlling the speed of the vehicle following the driver order or other external events. Different cruise controls can be developed:

- common cruise control:
  It consists in maintaining the vehicle speed at a speed pre-set by a driver. These kind of systems are already installed in several usual cars.

- adaptive cruise control:
  It consists in automatically adjusting the speed vehicle by maintaining a fixed distance between two successive vehicles [Naranjo et al., 2003b].

- intelligent cruise control:
  It consists in identifying road characteristics to adapt the speed of the vehicle [Lusetti et al., 2008], [Daniel et al., 2009].

The cruise control application, developed in the frame of this thesis, belongs to the last kind of cruise control (intelligent cruise control) and is a navigation-based longitudinal speed assistance system. This system which has been done in collaboration with other members of the laboratory [Daniel et al., 2009], consists of three main components:

- the maximum longitudinal speed profile generator (it provides $V_{x\,max}$):
  This component aims at interpolating the digital map database points by a trajectory generation process based on parametric cubic spline and providing from the trajectory a continuous curvature which helps to define the maximum longitudinal speed profile (see Section 5.5.2.1),

- the limit speed profile generator (it provides $V_{x\,desired}$):
  This component uses the maximum longitudinal speed profile generator and integrates the vehicle deceleration capability to generate a realistic speed profile (see Section 5.5.2.2),

- the speed controller:
  This components aims at controlling the actuator to follow the desired speed $V_{x\,desired}$ (see Section 5.5.2.3).

5.5.2 Navigation-based longitudinal speed assistance system

5.5.2.1 Maximum longitudinal speed profile generator

Trajectory generation and curvature estimation

In navigation-based applications, the main source of information is the digital map database. Even if they store increasingly more data, their representation of roads is still vectorial: roads are interpreted as a succession of shape points with irregular intervals of several metres. A consequence of this representation is that a limit speed profile cannot be directly calculated from the database information. Therefore, a trajectory generation process based on an interpolation method must be performed. There are several interpolation methods, such as basic polynomial interpolation ([Pauwelussen and Linardatos, 2008]), polar polynomial interpolation, B-Spline interpolation ([Jung-Hoon et al., 2003]), Bi-arc interpolation, or methods based on the combination of straight lines, clothoids and arc circles ([Wang et al., 2008]). Among all the different interpolation methods, the Parametric Cubic Spline interpolation has been adopted ([Boor, 1978]). This mathematical model, mostly used in computer graphics, provides smooth and curvature continuous trajectories. Moreover, parametrization allows a two-dimensional trajectory calculation and this interpolation only needs the coordinates of the shape points to provide a trajectory.

As it is a parametrized method, it is based on the calculation of two cubic Splines: one Spline for the X Cartesian coordinate and the other for the Y Cartesian coordinate. The parametric cubic Spline is then expressed as:

$$\begin{aligned} x_i(t) &= a_{xi}t^3 + b_{xi}t^2 + c_{xi}t + d_{xi} \\ y_i(t) &= a_{yi}t^3 + b_{yi}t^2 + c_{yi}t + d_{yi} \end{aligned} \tag{5.3}$$

To ensure the smoothness of the trajectory and the continuity of the curvature, this method calculates the trajectory under constraints. Each point which is to be interpolated, represents a position constraint as each point must be included in the trajectory. Moreover, continuity conditions on the first and the second derivatives of the trajectory at each point must be provided. A Parametric Cubic Spline example interpolating 4 points is given in Figure 5.17. It shows the continuity conditions on the first and second derivatives ($\dot{f}(t)$ and $\ddot{f}(t)$). As they are located respectively at the beginning and at the end of the Spline, points A and B have fixed second derivative values. These values are called *conditions* in the literature. In this example, they are equal to zero and so correspond to *natural conditions*.

This Parametric Cubic Spline method is used in real time to interpolate the digital map database points located in the upcoming road of the vehicle.

The second step in the trajectory generation process is to extract the curvature from the trajectory:

$$\kappa = \frac{1}{R} = \frac{\ddot{y}(t)\dot{x}(t) - \ddot{x}(t)\dot{y}(t)}{(\dot{x}(t)^2 + \dot{y}(t)^2)^{\frac{3}{2}}} \tag{5.4}$$

Maximum speed profile

In the literature, several methods help to determine the maximum speed profile of a trajectory using different reference speed models ([Glaser et al., 2007]). Here, a simplified model is considered. Firstly, the elevation of the road is not taken into account in the chosen model.

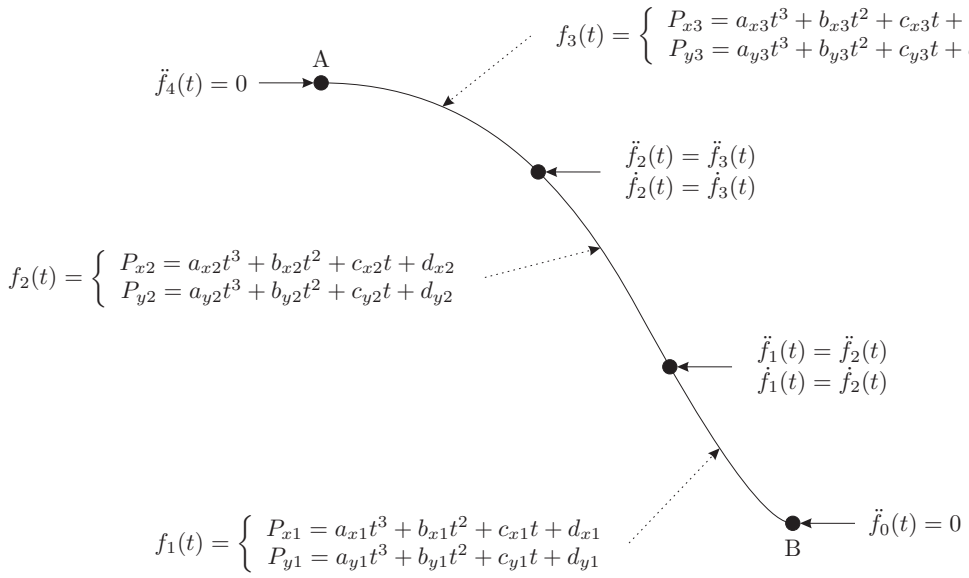

Figure 5.17: A Parametric Cubic Spline example

This information which is not included in the digital map database, has a slight impact on the reference speed. Secondly, the road friction coefficient which characterizes the contact between the tyres and the road is not involved in the computation of the maximum speed profile. The main reasons for this choice are the difficulty to obtain this physical quantity in real-time and the necessity of additional sensors which are costly for current standard vehicles. Thirdly, the general environment of the vehicle is not taken in account: traffic signs, other vehicles, etc, are not involved in the definition of the reference speed model. The driver determines if the used conditions of such a system are adequate (limited traffic, good road visibility, ...) and can control the system insofar as this assistance system can easily be switched off. This is necessary when another vehicle appears or when there is a change in the traffic conditions. Further improvements would be focused on the integration of the vehicle environment in the control system.

The vehicle acceleration, on a planar road, is always composed of two elements: the longitudinal and the lateral acceleration. The accelerations are used by the driver to evaluate his safety and comfort feeling. Considering bend conditions, it is commonly established that the lateral acceleration is bounded by a typical maximum value of $3m/s^2$ ([Gallet et al., 2000]). The second parameter of the simple reference speed model is the curvature which is extracted from the generated trajectory. Using a simple model, the maximum speed profile is defined by:

$$V_{x\,max} = \sqrt{\frac{\gamma_{T_{max}}}{\kappa}} \tag{5.5}$$

with $\gamma_{T_{max}}$ the maximal allowable lateral acceleration and κ the instantaneous road curvature. As the lateral acceleration limitation is a fixed parameter in the reference speed model, only the curvature determines the limit speed profile.

5.5.2.2 Limit speed profile generator

The maximum speed profile $V_{x\,max}$ detailed in Section 5.5.2.1 cannot be directly used for the braking state, insofar as the vehicle deceleration capabilities are not considered in this maximum

speed profile. Indeed, when a sharp bend appears after a straight line, the maximum speed profile changes suddenly without coherence to the braking capabilities. Two major drawbacks imply the necessity of an improved solution which considers the vehicle longitudinal dynamics. On the one hand, the braking action will be very hard. On the other hand, the required control signal may exceed the maximal braking pressure. In this situation, the vehicle will enter the bend with a non-secured speed, greater than the maximum speed and the vehicle passengers could be in danger. To avoid such situation, the braking phase has been improved. The presented solution aims at taking account of the deceleration criterion. The maximum speed profile is combined with a deceleration profile to improve comfort and safety. This solution helps to limit, in real-time, the maximum deceleration, so that the braking system can follow the calculated profile. Moreover, this deceleration profile allows the definition of the deceleration distance. Finally, the chosen deceleration profile reproduces the braking sequence from a common driver performing a smooth braking. The deceleration gradually increases up to a maximum and then decreases back to zero, giving the following triangular deceleration representation (cf. Figure 5.18).

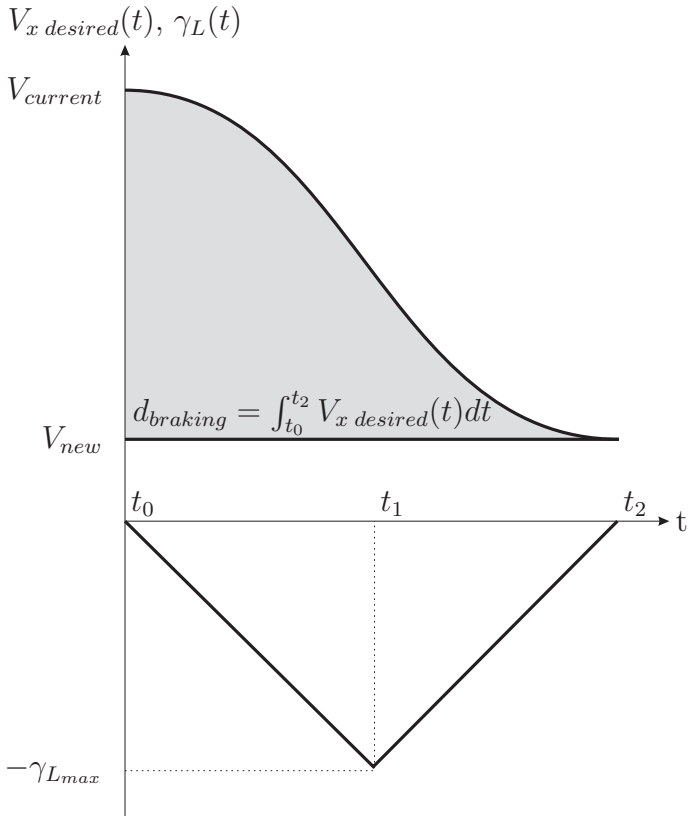

Figure 5.18: Deceleration and speed profile

Based on this deceleration profile and considering the positioning and speed of the vehicle, it is possible to determine if the different speeds ahead of the vehicle defined by the limit speed profile are reachable or not. To test the reachability of the limit speed profile points, the definition of the braking distance ($d_{braking}$) is used:

$$d_{braking} = \frac{3}{\gamma_{L_{max}}}(\Delta V)^2 + 2(2V_{current} - V_{new})\frac{\Delta V}{\gamma_{L_{max}}} \tag{5.6}$$

Considering $\Delta V = V_{new} - V_{current}$ with V_{new} the speed to be reached, the maximum allowable

deceleration of $\gamma_{L_{max}} = 3m/s^2$ and $V_{current}$ the current vehicle speed, the braking distance $d_{braking}$ helps to calculate the distance necessary to reach the speed defined by the limit speed profile. If the different speeds are reachable, in other words, if the distance between the vehicle and the considered point is larger than $d_{braking}$, the vehicle continues to accelerate or to maintain the speed. If not, the vehicle decelerates following the reference profile which is calculated based on the integration of the deceleration profile, so that:

$$\begin{aligned} V_{x\ desired} \text{ for } t \in [t_0, t_1] &= \frac{\gamma_{L_{max}}^2}{2(V_{new} - V_{old})} t^2 + V_{current} \\ V_{x\ desired} \text{ for } t \in [t_1, t_2] &= \frac{\gamma_{L_{max}}^2}{2(V_{new} - V_{old})} t^2 + 2\gamma_{L_{max}} t + 2V_{current} - V_{new} \end{aligned} \tag{5.7}$$

Finally, this limit speed profile which considers the vehicle limitations is safer and more realistic than the maximum speed profile directly obtained from the trajectory. Now, the limit speed profile, called $V_{x\ desired}$ can be used as an input of the speed controller. Here, it is important to insist on the fact that the proposed deceleration profile is used to define in real-time the speed profile. This is possible insofar as no optimization algorithm is used for this task.

5.5.2.3 Speed controller

The speed controller, proposed in this section is an improvement of the solution detailed in [Lauffenburger, 2002]. Here, the control solution is based on a Finite State Machine (FSM). This latter consists of a triplet $(Q, \Sigma, \mathcal{T})$ such that Q is a finite set of states q_i, Σ a finite set of events σ_i and $\mathcal{T}$ the transition functions which specify the set of possible states following a particular event. In the present application, the FSM is defined with $Q = \{$*Accelerating, Maintaining, Braking*$\}$ where:

- *Accelerating* occurs when an increase in speed is requested, when the driver leaves a bend or when the current speed does not correspond to the driver's satisfaction,
- *Maintaining* occurs when the vehicle speed corresponds to the limitation or when it fulfils the driver's satisfaction,
- *Braking* occurs when the speed limitation decreases or when the driver negotiates a bend.

Considering the fact that basic sensors are used (the speed sensor used for this application is available in all usual cars), imprecise and inaccurate measurements must be taken into account. Consequently, the FSM which uses these measurements may be subjected to state oscillations. To cope with the problem, the FSM and particularly the transition conditions of the *Maintaining* state consider a tolerance speed Δ. This latter has been added, so that, for example, the transition conditions between the *Maintaining* state and the *Accelerating* state become $V_x < V_{x\ desired} - \Delta$. The FSM developed for this application is shown in Figure 5.19.

Then, the FSM gives the information to the appropriate actuator, the CC for *Accelerating* and *Maintaining* and the BS for *Braking* to provide u_{CC} and u_{BS} (cf. Figure 5.20).

Finally, an additional constraint has been used. This latter aims at reproducing the behaviour of the driver. Considering common driving conditions, the driver takes account of information

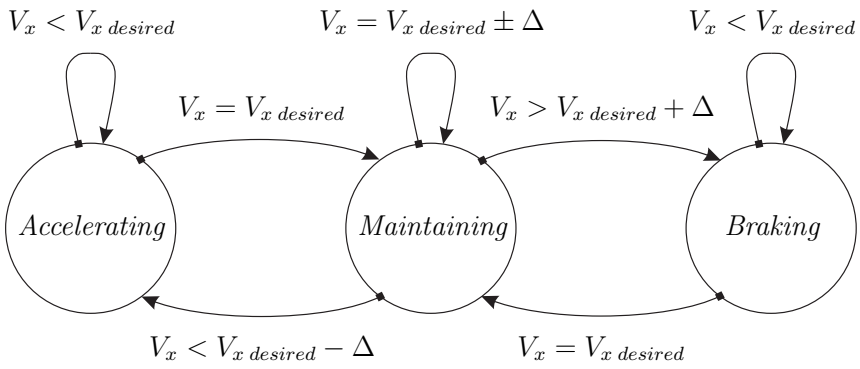

Figure 5.19: Presentation of the FSM

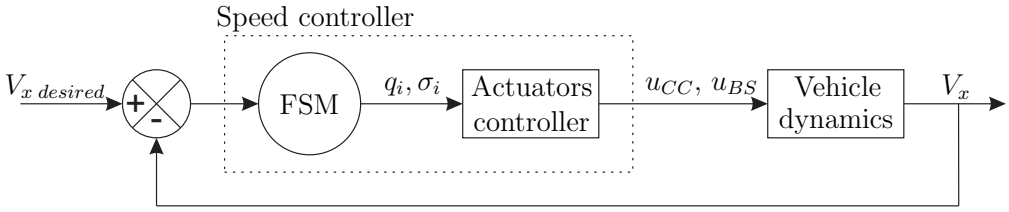

Figure 5.20: Speed control loop

ahead the vehicle to choose an appropriate speed. The same procedure has been implemented in the longitudinal speed controller with the use of a Look Ahead Distance (LAD). This distance helps to consider a reference speed at a further limit speed profile point, thus introducing the driver foreseeing ability. Drivers usually need 1 second to react. With an additional safety margin of 1 second, the control system is also considering a reference speed located at 2 seconds further on the road. The LAD is also defined as: $LAD = 2V(t)$. The braking controller uses an improved definition of the error (LAD dependent), so that:

$$\varepsilon = V_{x\ desired}(X_{LAD}, Y_{LAD}) - V_x(t) \tag{5.8}$$

with $V_{x\ desired}(X_{LAD}, Y_{LAD})$ the reference speed of a trajectory point, situated ahead of the vehicle at a distance d_{LAD}. In other words, the $(X_{LAD}, Y_{LAD})(t)$ trajectory point is defined by solving

$$d_{LAD} = \sqrt{(x(t) - X_{LAD}(t))^2 + (y(t) - Y_{LAD}(t))^2} \tag{5.9}$$

Using this LAD, the system reacts in advance and control is less affected by vehicle response time.

5.5.3 Experimental results

The results obtained with the proposed longitudinal control solution are presented in this section. First, the road that has been taken is presented in Figure 5.21.

It can be seen that the considered driving situation is composed of four bends and some little "oscillations" of the road are observed between the second and the third bend.

Considering this trajectory, the longitudinal controller has been tested and the results are plotted on Figure 5.22.

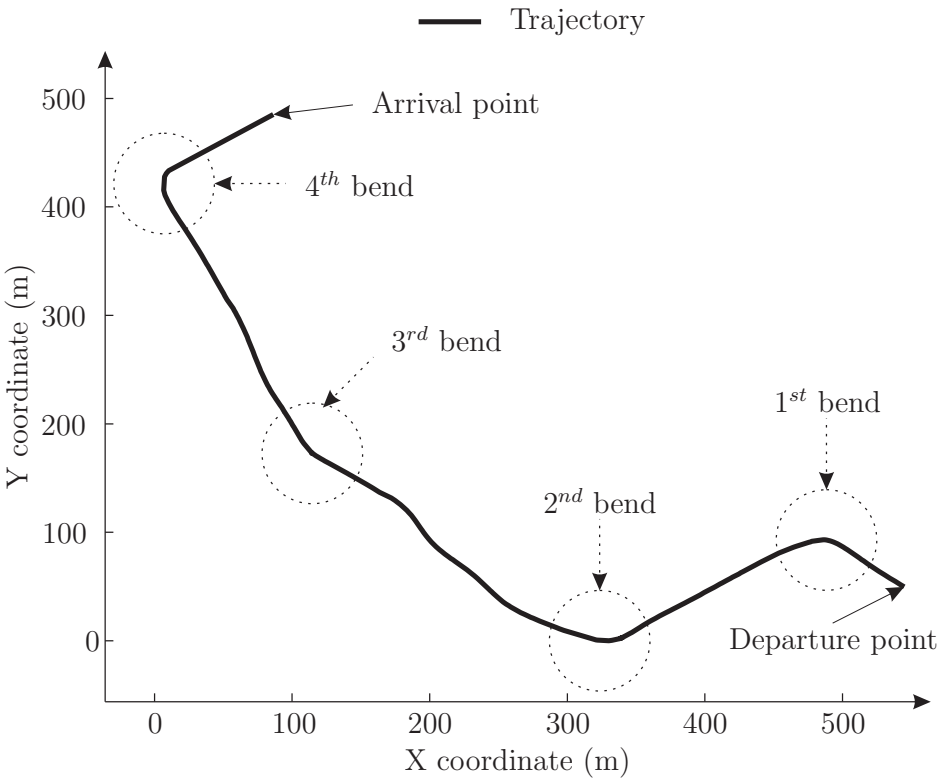

Figure 5.21: Test road

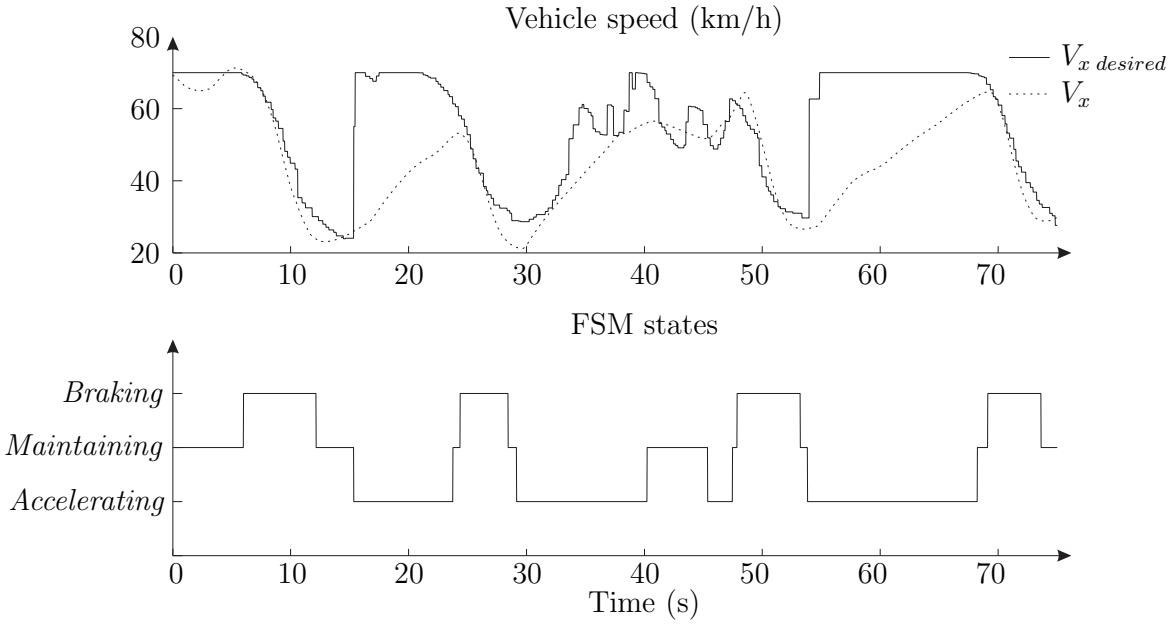

Figure 5.22: Longitudinal control results

On the first plot, the vehicle desired speed $V_{x\ desired}$ and the real vehicle speed V_x are presented. The second plot represents the FSM states changes.

Between the first and second bend (between Time = 15 and 25 seconds) and the third and fourth bend (between Time = 55 and 70 seconds), a large difference can be seen between the desired speed $V_{x\ desired}$ and the real vehicle speed V_x. This is due to the fact that the signal $V_{x\ desired}$ takes account of the vehicle longitudinal dynamics only for the deceleration phase. Here, the vehicle is in a straight line and the speed that the vehicle has to reach corresponds to the maximum allowed speed for this test which is $70km/h$. The proper functioning of the control solution for these periods is seen with the results of the FSM. Indeed, during these two periods (between Time = 15 and 25 seconds and Time = 55 and 70 seconds), $V_{x\ desired}$ is lower than V_x which explains that the FSM is in the *Accelerating* phase.

Between Time = 35 and 50 seconds, two important conclusions have to be done:

- This part of the travel corresponds to the road between the second and the third bend and as said before, some little "oscillations" of the road can be observed. This explains the fact that the signal $V_{x\ desired}$ varies a lot during this period in order to be representative of this succession of little bends.

- Despite a lot of variations of the signal $V_{x\ desired}$, it can be seen that the FSM does not jump from one state to another to follow the desired speed. This has been possible by the introduction of the parameter Δ which gives the possibility to stay in the maintaining step despite the variation of the desired speed. This phenomenon is very pleasant for the vehicle passenger, insofar of the behaviour of the vehicle is very smooth.

Finally, during the braking phase, it can be seen that the vehicle speed is close to the desired speed $V_{x\ desired}$. This is the case between Time = 5 and $15s$, Time = 25 and 30 seconds, Time = 47 and 52 seconds and Time = 70 and 75 seconds. Moreover, as it has been defined in Figure 5.18, it can be shown that the shape of the vehicle speed in Figure 5.22 corresponds to a second order polynomial. Thus, the speed decreases slowly at the beginning. Then, a hard braking is applied, the vehicle speed decreases rapidly. At the end of the braking phase, the speed reaches slowly the desired speed.

5.5.4 Conclusion

This section has presented a longitudinal assistance system based on the use of the basic elements of a standard vehicle: a navigation system, a vehicle speed sensor, a cruise control and a braking system. Using the information provided by the navigation system, a specific trajectory generation process helps to obtain a trajectory. The information contained in this trajectory is fused with a deceleration profile and allows the real-time calculation of the limit speed profile of the upcoming road. The latter is then compared with the vehicle speed to determine the current state of the FSM and appropriate control signals. Dynamic tests with the MIAM test vehicle have shown that the longitudinal assistance system works correctly. Particularly, attention has been focused here in the subjective feel of the passengers. The proposed solution gives the possibility to have a very smooth behaviour. Indeed, the braking phase is very pleasant due to the imposed deceleration

profile. Moreover, the addition of the parameter Δ certainly limits the reactivity of the system, but oscillations between the different states are limited, which increases the passenger comfort.

5.6 Lateral control: experimental results

5.6.1 Introduction

In the literature, different solutions are dedicated to lateral control:

- Lane departure avoidance: this solution aims at keeping the vehicle in the lane [Minoiu et al., 2006],
- Autonomous vehicle: this solution aims at controlling the vehicle lateral dynamics based on GPS information.

This section focuses on the last item dedicated to autonomous vehicles which use GPS information.

Previously, for the longitudinal control, the limit speed profile was given in real-time. Indeed, based on the position of the vehicle, given in real-time by the GPS system, shape points in front of the vehicle were stored and resulted to a trajectory (cf. Section 5.5.2.1) and finally to the limit speed profile (cf. Section 5.5.2.2). For the considered application, more accuracy is required. For this reason, the GPS receiver is replaced by a DGPS receiver. Indeed, for the longitudinal control, a positioning error is not relevant. For instance, if the braking phase begins 5m after the suitable beginning, the vehicle will enter the bend with a largest speed. Nevertheless, for lateral applications, a positioning error leads to undesirable situations insofar as the vehicle may go outside the road.

For the lateral control application presented in this section, the control strategy considers a pre-registered path. Indeed, every test campaign begins with a trajectory registration phase. A path is defined and the vehicle is driven at very low speed and using the DGPS sensor, various points that constitute the path are recorded. This path will be used as an input of the different control strategies developed.

This Section aims at comparing 3 control solutions (FC algorithm, LPV MPC algorithm and NN MPC algorithm) for path following, based on experimental results. Considering a path $\mathcal{P}$ to be followed, defined in the ground-fixed axes $(\vec{X},\vec{Y})$, the aim of the controller is to follow this reference path.

The path which has been chosen to validate the different control algorithms is presented in Figure 5.23. Two successive bends can be shown on the path; the first is turning slowly (that means with a large radius of curvature) while the second is more accentuated (that means with a small radius of curvature). To characterize the capability of the control solution, a plot which represents the distance between the path and each position of the vehicle is given. This distance is called the "error distance". The tests are done for different longitudinal speeds from approximately $4m/s$ to $10m/s$.

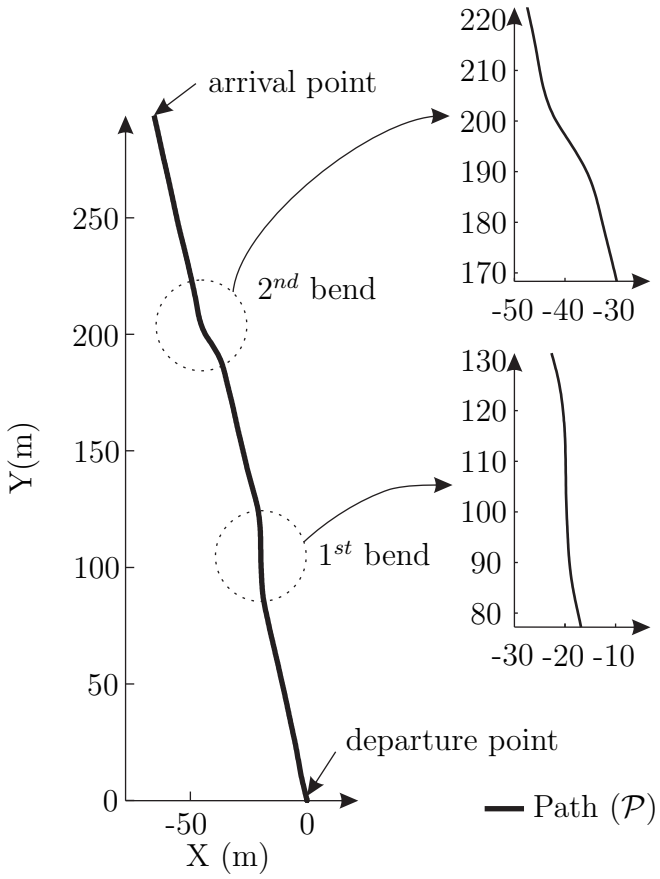

Figure 5.23: Path to be followed

5.6.2 "Follow the Carrot" results

5.6.2.1 Tuning of the control solution

This control method based on a geometric criterion only requires the definition of two parameters as defined in Section 3.2.3.3 (the look ahead distance LAD and the proportional gain k_p). The tuning of the control law, based on an heuristic approach, gave the possibility to obtain the following values: $LAD = 5m$ and $k_p = 0.2$.

5.6.2.2 Experimental results

Figures 5.24 and 5.25 present the experimental results obtained with the FC method. It can be seen that the results are satisfying. At $4m/s$ the maximum error distance is $35cm$ while the maximum is approximately $70cm$ at $8m/s$. However, Figure 5.25 shows that the response is oscillating with large amplitude (the maximum error is $70cm$) from time $t = 26s$ and the vehicle has been stabilized again after. The lateral speed V_y and the yaw rate r have large amplitudes, insofar as the maximum value of V_y is $0.5m/s$ and the maximum value of r is $0.4rad/s$. Likewise, the steering wheel signal changes suddenly from 145° to −110° in 1.2s when time is equal to $29s$; this is a very fast control signal which is not pleasant for the vehicle passengers. Indeed, the control law has some difficulties to provide the good control inputs for the second bend which is more accentuated.

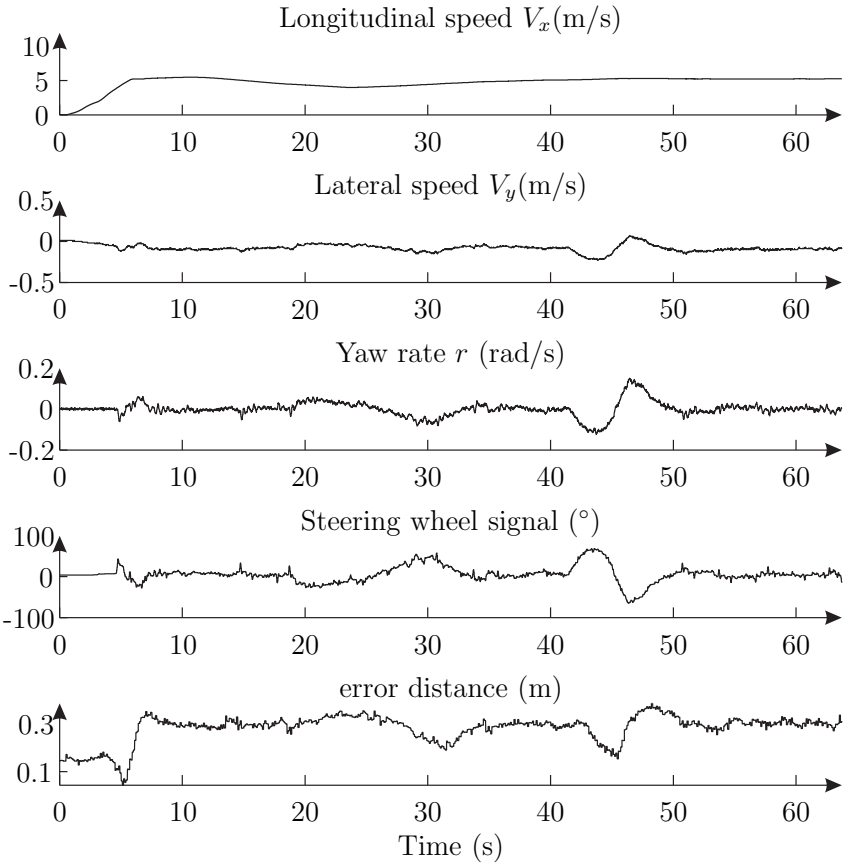

Figure 5.24: Lateral control results with FC at 4m/s

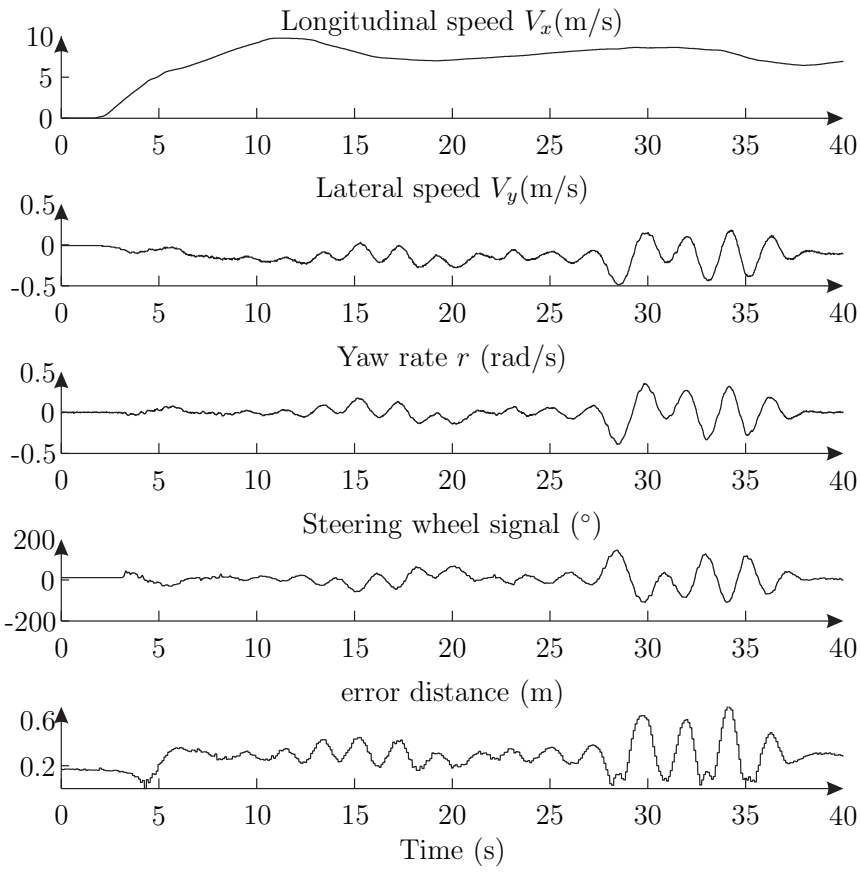

Figure 5.25: Lateral control results with FC at 8m/s

Figure 5.26 shows that this control solution is not able to follow the proposed path at 10m/s. The vehicle is not able to go through the first bend. At time $t = 10s$, when the first bend begins, the vehicle oscillates around the path and leaves it. At time $t = 18s$, the yaw rate reaches an important value equal to $1rad/s$. Then, by making the assumption that the variation of the slip angle is low (less than 0.05 rad/s in this test), the lateral acceleration is approximated by $\gamma_T \approx V_x\dot{\psi}$ and then $\gamma_T \approx 7m/s^2$. This clearly shows that the vehicle is in a critical situation insofar as the lateral acceleration is high.

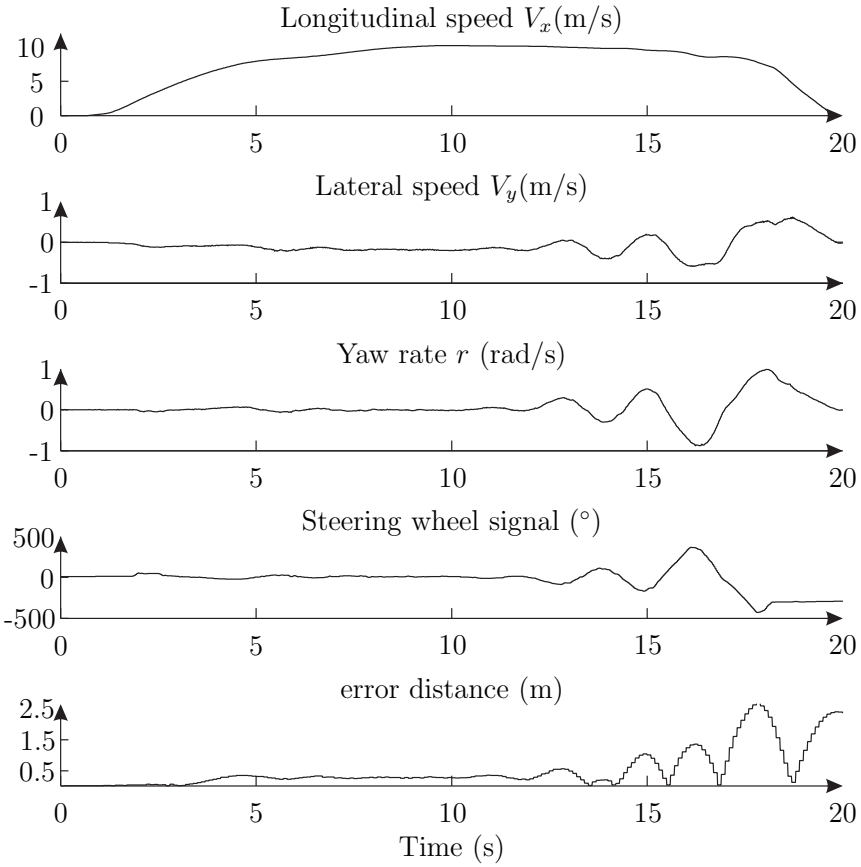

Figure 5.26: Lateral control results with FC at 10m/s

The trajectory which has been taken by the vehicle is proposed in Figure 5.27.

5.6.3 LPV MPC results

5.6.3.1 Presentation of the control solution

Cost criterion of the MPC

To follow the path, the main physical quantity which is taken into account is the lateral displacement of the vehicle, commonly called $y(t)$. The aim of the MPC solution is to find the optimal control signal θ_w which helps to follow the points $y_{ref}(i)$ of the path $\mathcal{P}$. Then, the cost criterion is defined by:

$$J(k) = Q\sum_{n=1}^{Np}\left(\hat{y}(k+n) - y_{ref}(k+n)\right)^2 + R\sum_{n=0}^{Nc}\theta_w(k+n)^2 \tag{5.10}$$

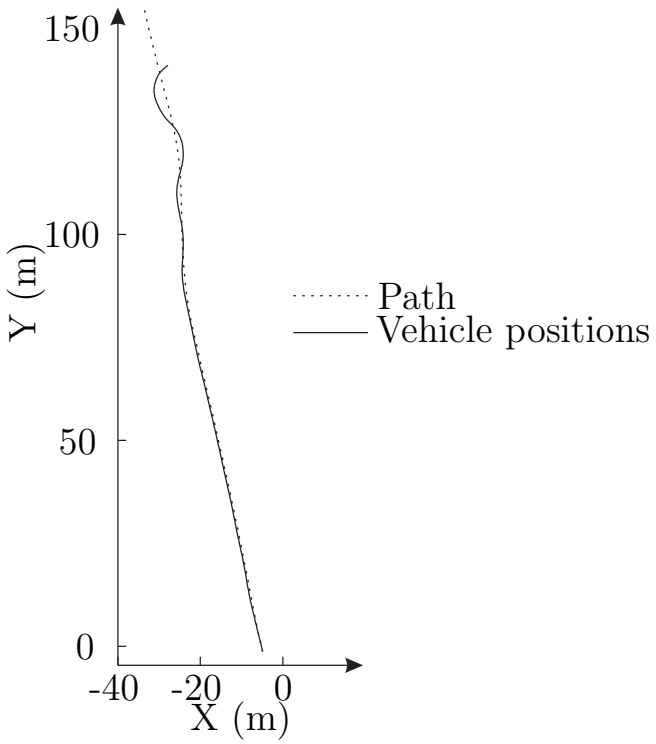

Figure 5.27: Path with FC at 10m/s

The following paragraph 5.6.3.1 presents the method to obtain the vehicle lateral displacement prediction based on the vehicle dynamic prediction and the choice of the reference points $y_{ref(i)}$ of the path.

Prediction of the vehicle positions

The prediction of y on the prediction horizon is based on vehicle dynamic signals and can be expressed as:

$$\dot{y}(t) = V_y(t)cos(\psi(t)) + V_x(t)sin(\psi(t)) \tag{5.11}$$

such that $\psi(t)$ is the heading angle of the vehicle defined by:

$$\dot{\psi}(t) = r(t) \tag{5.12}$$

At each sample time, the path is projected in a local coordinate whose origin is the vehicle CG, the axis $\vec{x}$ coincides with the axis of the vehicle and the axis $\vec{y}$ is defined laterally from the vehicle. The Figure 5.28 presents the path in the ground fixed axes and the new coordinates ($\vec{x}$,$\vec{y}$).

Considering the hypothesis that the heading angle $\psi(t)$ stays relatively small on the prediction horizon, the equation (5.11) is linearised considering usual trigonometric function simplifications:

$$\dot{y}(t) \approx V_y(t) + V_x(t)\psi(t) \tag{5.13}$$

Prediction of the vehicle dynamics

As it can be seen in equations (5.12) and (5.13), the vehicle dynamic signals $r(t)$ and $V_y(t)$ are used to obtain the lateral displacement of the vehicle. The LPV vehicle model, identified in

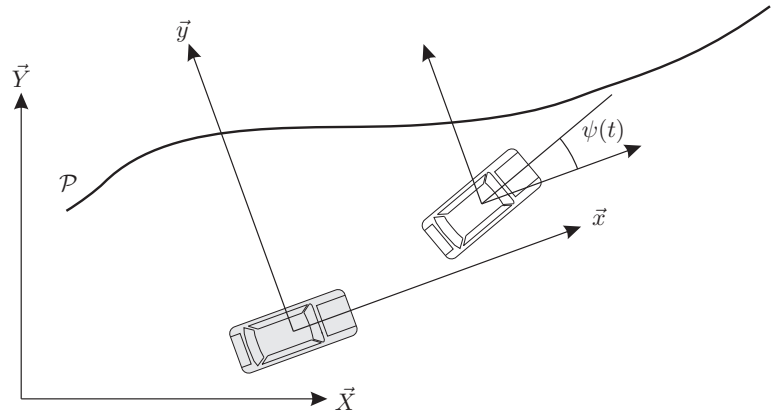

Figure 5.28: Change of coordinates

Section 5.4.1 helps to describe the vehicle dynamics. Finally, the prediction model is a linear LPV model which has 1 input (θ_w), 1 output (y), 4 states (V_y, r , y and ψ) and 1 varying parameter (V_x) such that:

$$\begin{Bmatrix} \dot{V}_y \\ \dot{r} \\ \dot{y} \\ \dot{\psi} \end{Bmatrix} = \begin{bmatrix} \frac{-CS_f(V_x) - CS_r(V_x)}{MV_x} & \frac{-l_f CS_f(V_x) + l_r CS_r(V_x)}{MV_x} - V_x & 0 & 0 \\ \frac{-l_f CS_f(V_x) + l_r CS_r(V_x)}{J_v} & \frac{-l_f^2 CS_f(V_x) - l_r^2 CS_r(V_x)}{J_v V_x} - V_x & 0 & 0 \\ 1 & 0 & 0 & V_x \\ 0 & 0 & 1 & 0 \end{bmatrix} \begin{Bmatrix} V_y \\ r \\ y \\ \psi \end{Bmatrix} + \begin{bmatrix} \frac{CS_f(V_x)}{M} \\ \frac{l_f \cdot CS_f(V_x)}{J_v} \\ 0 \\ 0 \end{bmatrix} \theta_w \tag{5.14}$$

Finally, this model is sampled with a simple first order approximation of the derivative such that:

$$\begin{Bmatrix} V_y(k+1) \\ r(k+1) \\ y(k+1) \\ \psi(k+1) \end{Bmatrix} = A_k \begin{Bmatrix} V_y(k) \\ r(k) \\ y(k) \\ \psi(k) \end{Bmatrix} + B_k \theta_w(k) \tag{5.15}$$

with

$$A_k = \begin{bmatrix} \frac{-CS_f(V_x) - CS_r(V_x)}{MV_x} T_s + 1 & \left(\frac{-l_f CS_f(V_x) + l_r CS_r(V_x)}{MV_x} - V_x \right) T_s & 0 & 0 \\ \frac{-l_f CS_f(V_x) + l_r CS_r(V_x)}{J_v} T_s & \left(\frac{-l_f^2 CS_f(V_x) - l_r^2 CS_r(V_x)}{J_v V_x} - V_x \right) T_s + 1 & 0 & 0 \\ T_s & 0 & 1 & V_x T_s \\ 0 & 0 & T_s & 1 \end{bmatrix}$$

$$B_k = \begin{bmatrix} \frac{CS_f(V_x)}{M} T_s \\ \frac{l_f CS_f(V_x)}{J_v} T_s \\ 0 \\ 0 \end{bmatrix}$$

and T_s the sample time.

Reference point on the path

The cost criterion defined in equation (5.10) requires N_p reference points y_{ref} from the path $\mathcal{P}$. First the point $y_{ref}(0)$, which is not used in the cost criterion is defined. This point is located at the intersection between the path and the $\vec{y}$ axis. It is used to determine the N_p points $y_{ref}(k)$ of the path. Each point is separated by $V_x T_s$ in the direction $\vec{x}$. The Figure 5.29 presents these considered points.

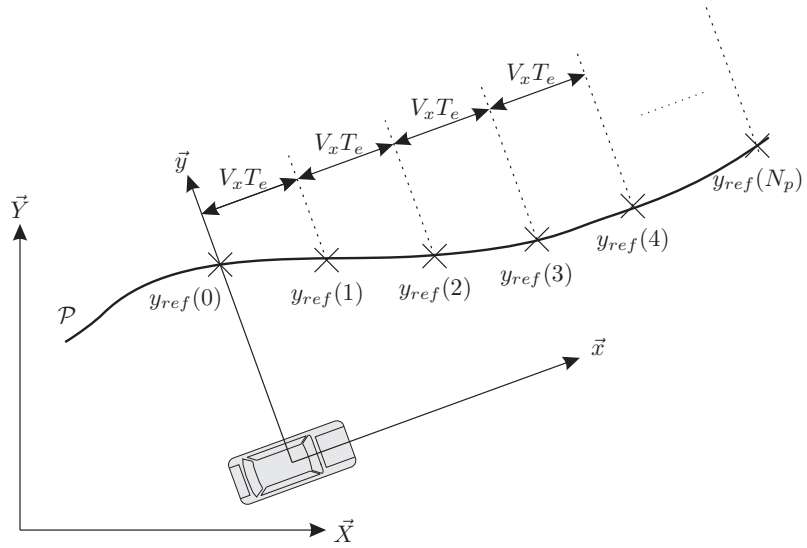

Figure 5.29: Definition of the reference points

5.6.3.2 LPV MPC path following: experimental results

Tuning of the LPV MPC control solution

The controller runs in an AutoBox® system, equipped with a DS1005 processor board with a sample time of 50ms. It is implemented as a C-coded S-Function, using the QP solver routine available in [MathWorks, 2005], based on the publicly available Dantzig-Wolfe's algorithm. The prediction horizon and the control horizon have the same length equal to 15 samples. A constraint is used to limit the maximum steering wheel angle (the maximum hand wheel angle is 350°) and then mechanically protect the steering column.

The tuning of the control solution has shown that the weightings Q and R are of the highest importance. To find the more appropriated values and to facilitate the methodology, Q is considered fixed and R varies. On the one hand, a low value of R generates an aggressive control insofar as the resulting angles and rotational speeds are high. This case is interesting when a

quick reaction is required or when an important input is required to let the vehicle move. However, it has been noticed that oscillations may appear in such conditions. On the other hand, an important value of R allows a smoother control. Here, angles and rotational speeds are low. Such a setting is preferred when a small input leads to a strong reaction of the system. If such a value of R helps to get a satisfying behaviour of the vehicle, the control is applied very late. Indeed, the optimization tries to limit the control without considering the path error.

It is thus reasonable to define different tunings for low speed ($3m/s$) conditions and high speed ($10m/s$) conditions. The driver remarks easily that at low speed, an important hand wheel angle is required to change the vehicle direction. Nevertheless, at high speed, a weak movement of the hand wheel creates a significant lateral movement of the vehicle. As a conclusion, it has been decided to fix Q such that $Q = 2$ and to link the value of R with the longitudinal speed.

Based on this consideration, tests have been done to identify the relationship between R and V_x. These latter have been performed at different forward velocities and for each speed the more suitable value of R is kept. Then, the obtained values of R for the different speeds are used to find a fitting function. Finally, the relation is $R = 2.25 \times V_x^2 - 9.8 \times V_x + 26.8$ has been identified. This tuning helps to reproduce the behaviour of the driver. Namely, at low speed the value of R is small such that the control is able to propose large variations. At high speed, the value of R is high; so the control is weak due to the high sensibility of the vehicle in such driving situations.

Finally, the LPV model of equation (5.14) is transformed into an LTI model at each sample time by considering the vehicle speed constant on the prediction horizon. This assumption is valid, due to the sample time that has been chosen ($50ms$). With a prediction of 15 samples and a sample time of $50ms$, it is considered that the longitudinal speed V_x is constant for a maximum period $0.75s$. This assumption helps to obtain a constrained QP problem.

Experimental results

Figures 5.30, 5.31 and 5.32 present the experimental results obtained with the LPV MPC method.

The experimental results which are obtained with the LPV MPC method are satisfying for the different speeds. At $4m/s$, the error distance is less than $30cm$ excepted at time $t = 42s$, when the vehicle exits the second bend. A similar behaviour is observed at $8m/s$. For this experimental result, the error distance is approximately $30cm$ while a pick of $90cm$ appears at the exit of the second bend. At this instant, the lateral speed reaches $0.25m/s$ and the yaw rate is equal to $0.4rad/s$ but it can be observed that the control is able to reduce immediately the error distance insofar as it is equal to $30cm$ just after the second bend. A similar behaviour is observed at $10m/s$. This time, the error distance is approximately $45cm$ for the first bend. However, the vehicle has some difficulties to exit the second bend. A pick at $1.5m$ is observed, thereafter the vehicle oscillates around the path and the different signals V_y, r and θ_w have an oscillating shape.

For these different experimental results, the behaviour of the vehicle is very pleasant, apart from the oscillations which are felt by the passengers of the vehicle at high speed ($10m/s$). The steering wheel control is smooth and the trajectory followed is regular without hard changes of directions.

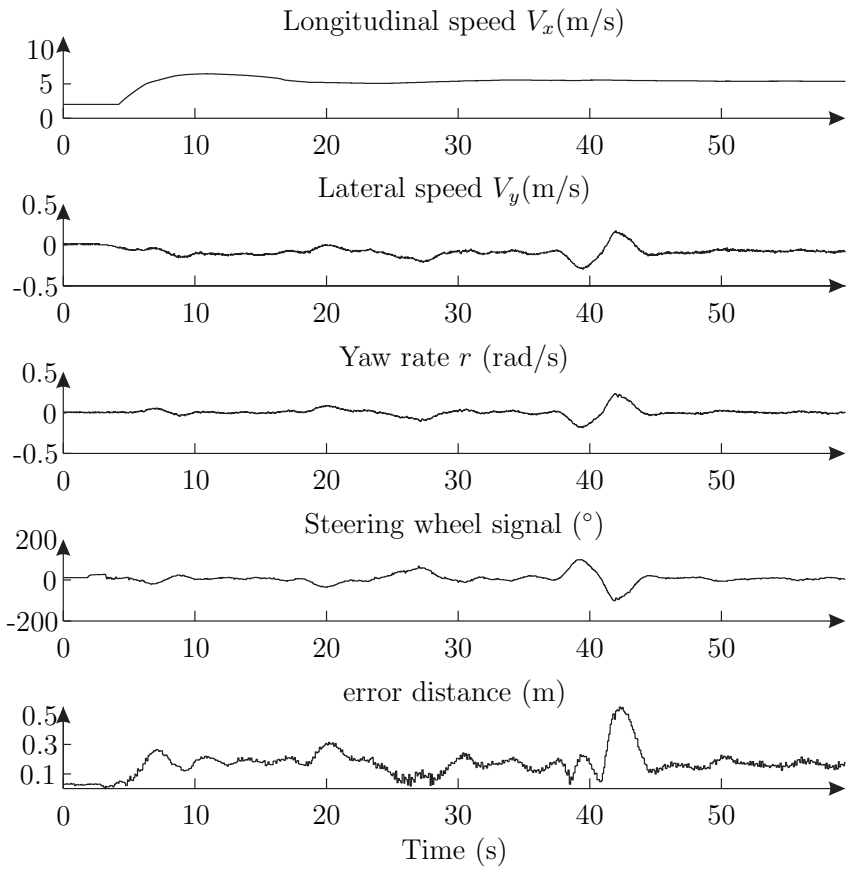

Figure 5.30: Lateral control results with LPV MPC method at 4m/s

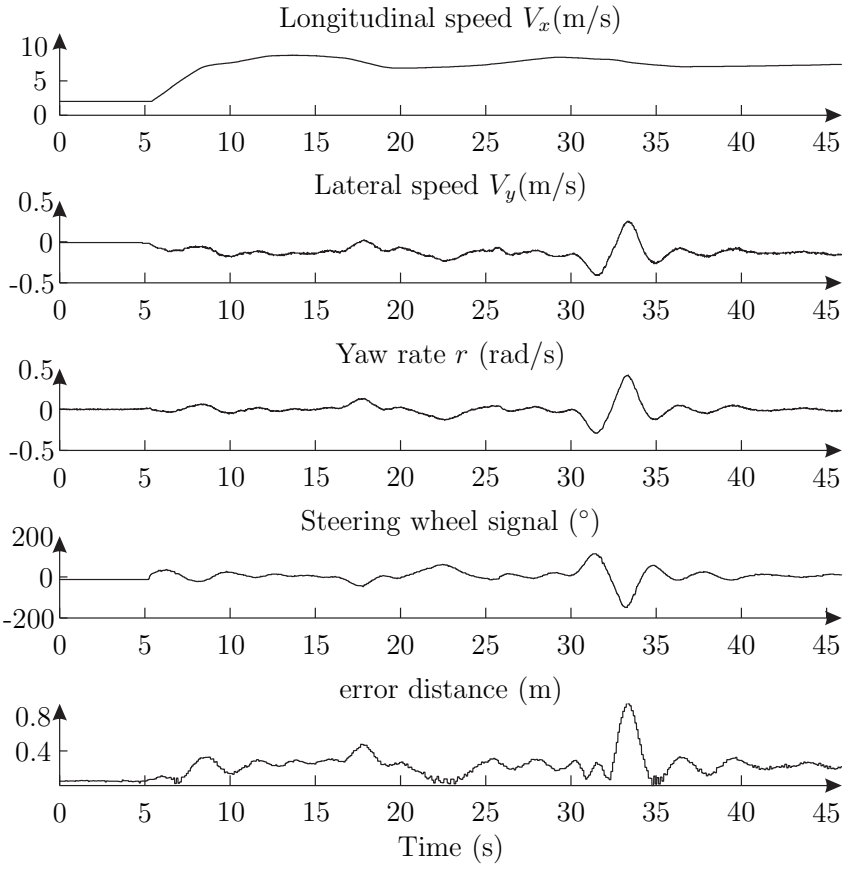

Figure 5.31: Lateral control results with LPV MPC method at 8m/s

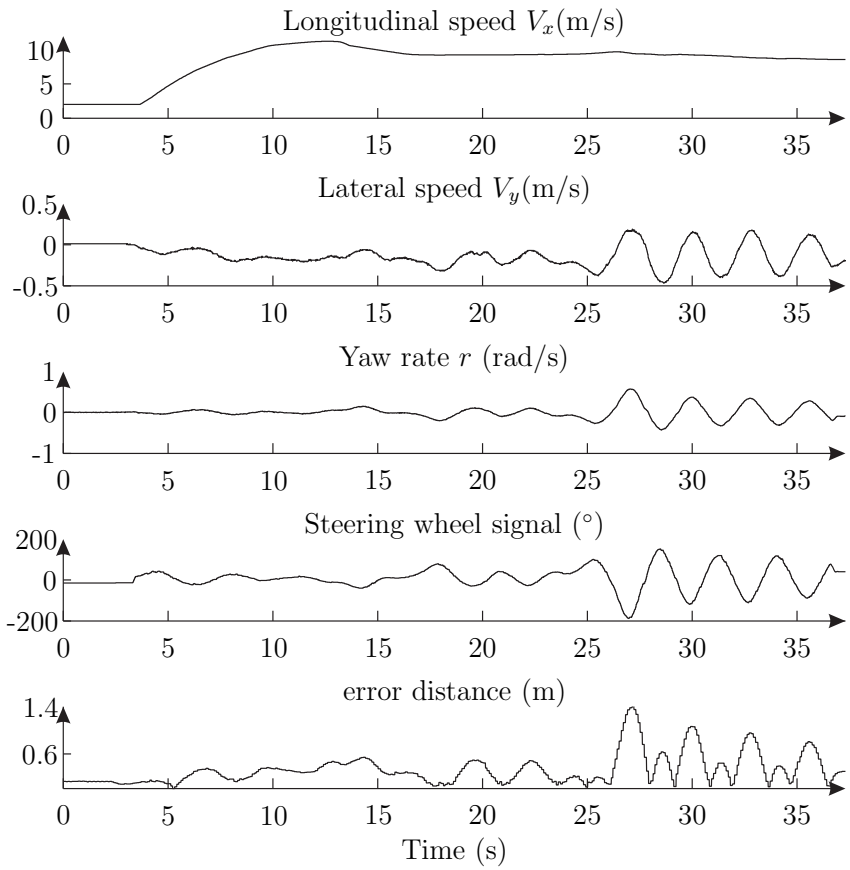

Figure 5.32: Lateral control results with LPV MPC method at 10m/s

5.6.4 NNMPC results

5.6.4.1 Presentation of the control solution

Section 5.6.3.1 presented the different components which help to build the LPV MPC control solution, namely the cost criterion, the vehicle positions prediction, the vehicle dynamics prediction and the path reference point getting. Concerning the NNMPC control solution only the vehicle dynamics prediction is changing. Indeed, the estimated values of the states V_y and r are obtained with the NN presented in Section 5.4.2. For the two NN proposed structures (the NN with three inputs presented in Figure 5.14 and the NN with four inputs presented in Section 5.15), a local linearisation is proposed and as presented in Section 2.4.3.2, the discrete prediction model becomes:

$$\begin{Bmatrix} V_y(k+1) \\ r(k+1) \\ y(k+1) \\ \psi(k+1) \end{Bmatrix} = \begin{bmatrix} b_{0\,11} & b_{0\,12} & 0 & 0 \\ b_{0\,21} & b_{0\,22} & 0 & 0 \\ T_s & 0 & 1 & V_x T_s \\ 0 & T_s & 0 & 1 \end{bmatrix} \begin{Bmatrix} V_y(k) \\ r(k) \\ y(k) \\ \psi(k) \end{Bmatrix} + \begin{bmatrix} c_{0\,1} \\ c_{0\,2} \\ 0 \\ 0 \end{bmatrix} \theta_w + \begin{bmatrix} a_{0\,1} \\ a_{0\,2} \\ 0 \\ 0 \end{bmatrix} \tag{5.16}$$

5.6.4.2 NNMPC path following: experimental results

Tuning of the NNMPC control solution

The tuning of the two control solutions based on NNMPC (with NN structures 1 and 2) are similar to the LPV MPC control solution. Here again, the optimisation algorithm is a C-coded S-Function using the Dantzig-Wolfe's algorithm. Concerning the two horizons (prediction and control) an equivalent tuning is considered insofar as $Np = Nu = 15$. For the weighting Q and R comparable remarks can be done. Numerous tests on the road gave the final tuning ($Q = 2$ and $R = 3.4V_x^2 - 14.7V_x + 49.6$).

Experimental results

Figures 5.33, 5.34 and 5.35 present the experimental results obtained with the NNMPC method with the structure 1 (the NN used for the prediction considers 3 inputs).

The experimental tests with the NNMPC method considering the NN structure 1 give satisfying results for the different speeds. For the two tests at $4m/s$ and $8m/s$, close responses are obtained. The error distance is approximately $40cm$ with picks at the bend level. Contrariwise to other control methods, here the vehicle seems to cut corners. At $10m/s$, the error distance is thin, expect during bend negotiation. Considering the steering wheel angle, these test results give the possibility to show that the control signals are very smooth with low amplitudes (only 60° in the second bend). These tests particularly highlight the difficulties which have been encountered during the tuning phase. Indeed, the value of R has been chosen such that it is V_x depending and several tests are required to find the best value.

Figures 5.36, 5.37 and 5.38 present the experimental results obtained with the NNMPC method with the structure 2 (the NN used for the prediction considers 4 inputs).

The tests with the NNMPC method considering the NN structure 2 help to achieve convincing experimental results. The three plots show that the vehicle is able to follow the road. As for all the other control solutions, the vehicle tends to move away from the road when it enters the

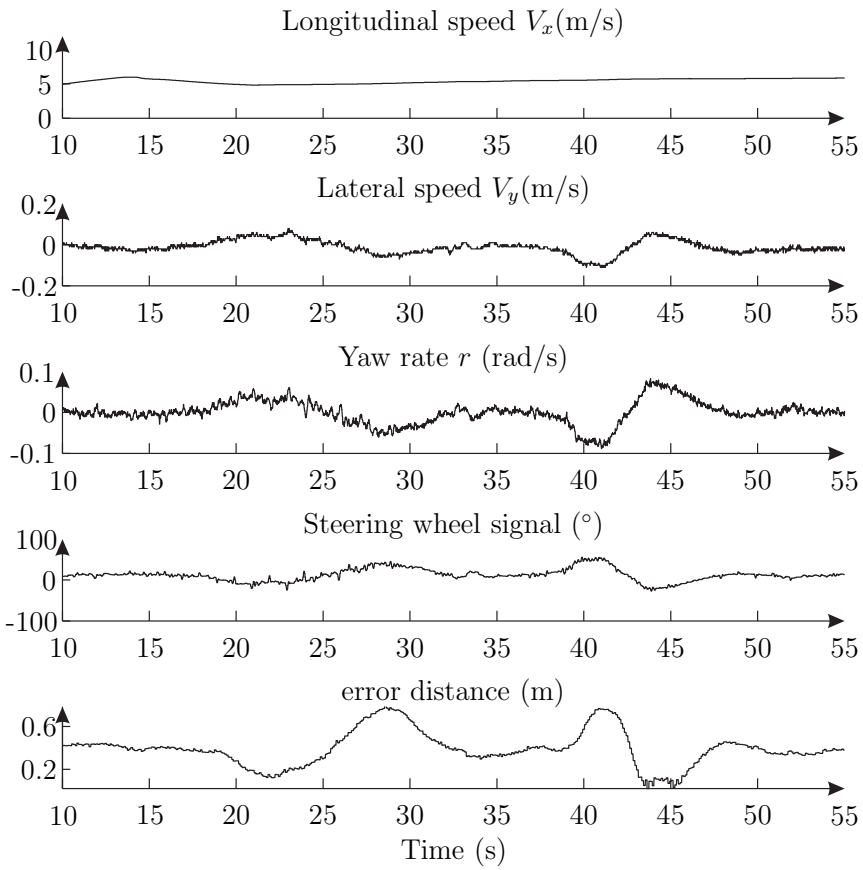

Figure 5.33: Lateral control results with NNMPC method at 4m/s (structure 1)

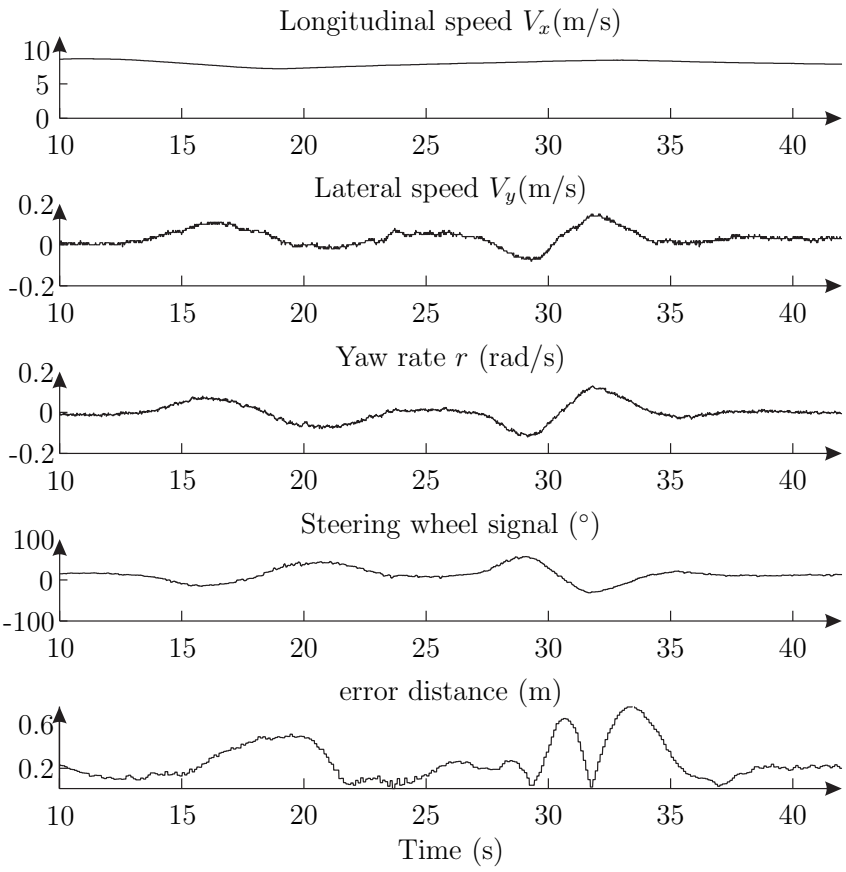

Figure 5.34: Lateral control results with NNMPC method at 8m/s (structure 1)

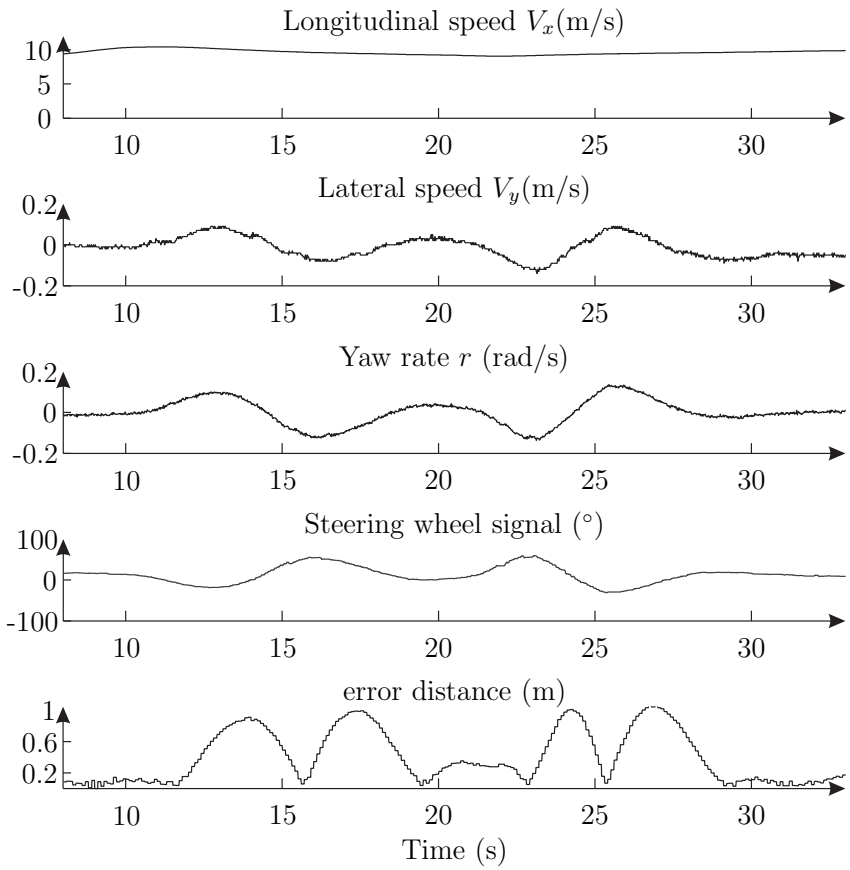

Figure 5.35: Lateral control results with NNMPC method at 10m/s (structure 1)

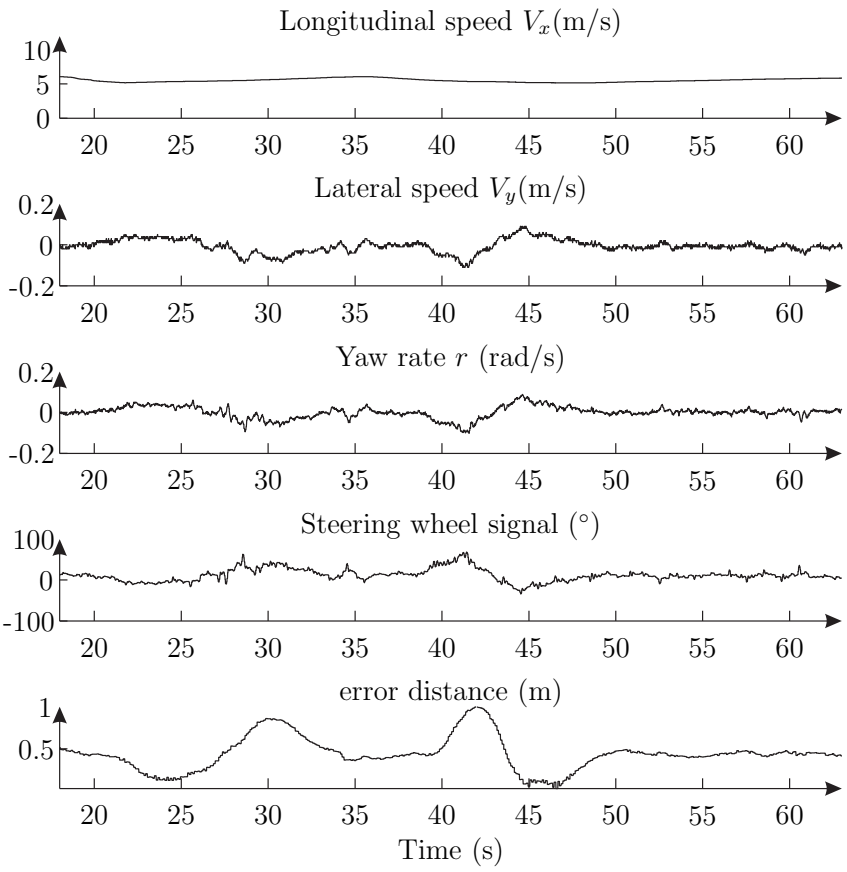

Figure 5.36: Lateral control results with NNMPC method at 4m/s (structure 2)

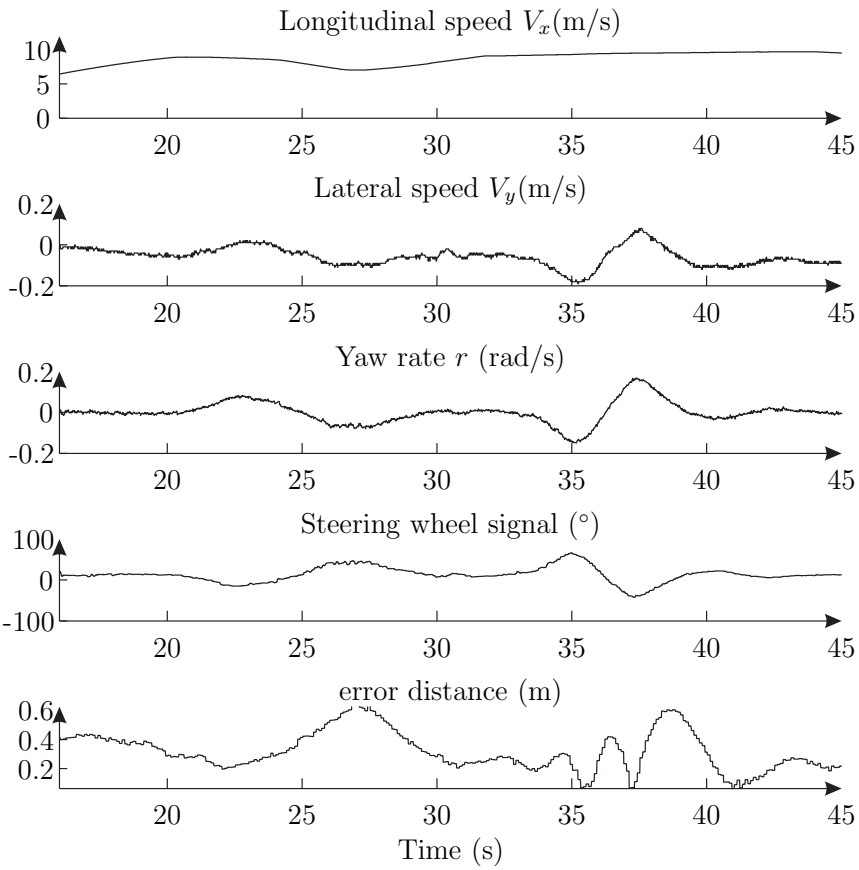

Figure 5.37: Lateral control results with NNMPC method at 8m/s (structure 2)

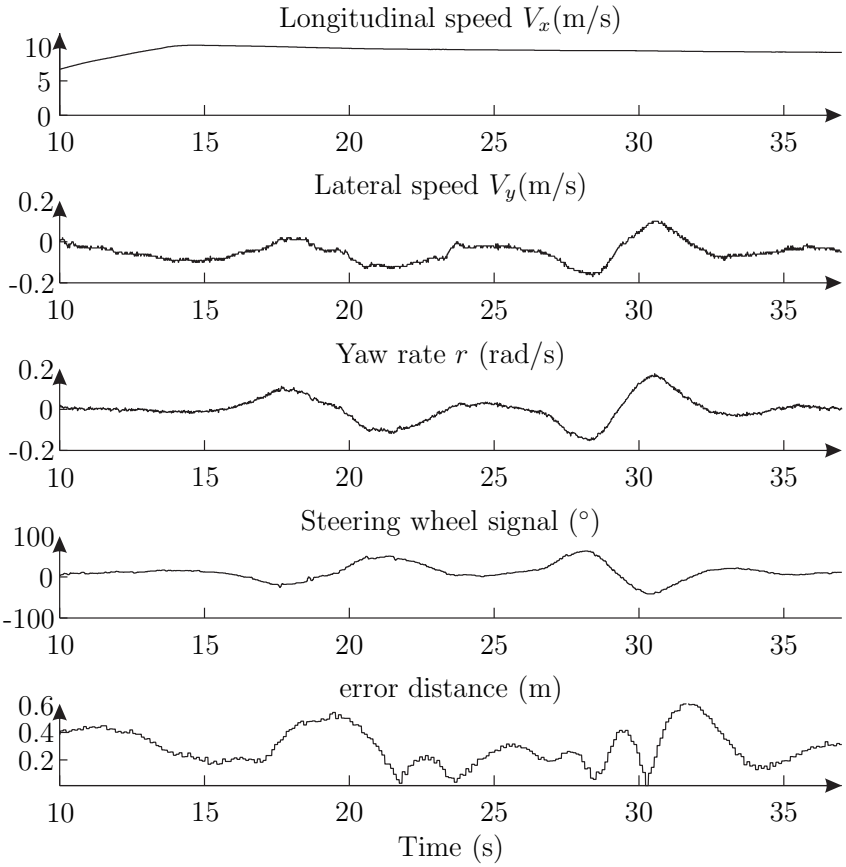

Figure 5.38: Lateral control results with NNMPC method at 10m/s (structure 2)

bend. The results obtained at $8m/s$ and $10m/s$ are the best results. However, the response at $4m/s$ is certainly not optimal. It could be interesting to tune the value of R more precisely.

5.6.5 Remarks on the lateral control solutions

The FC method, based on geometrical concepts, aims at choosing a carrot point in front of the vehicle and comparing the direction of the vehicle with the direction of the carrot point. The control signal is proportional to the error angle, obtained as the difference between the two previous directions. The three other methods are based on MPC which needs 5 steps in its process, the prediction of the system evolution, the definition of the reference trajectory, the definition of the cost criteria, the minimization of the cost criteria and the application of the first term of the optimal solution. The main difference between the three controllers (LPV MPC, NNMPC with structure 1 and NNMPC with structure 2) is the used prediction model. The LPV MPC solution uses a LPV model expressed on the state space form. The two other MPC methods are based on NN predictions. The first based on structure 1 has only three inputs while the second takes into account an additional input which is the longitudinal speed of the vehicle V_x.

The presented results show that the geometrical method gives the less acceptable results insofar as the vehicle cannot be stabilized at high speed. This conclusion seems normal insofar as the geometrical approach considers only one particular point of the path while the other methods take account of 15 points. Nevertheless, it could be possible to improve the results of the control solution by thinking about an evolution of the proposed solution. This could be done with two evolutions. On the one hand, the proportional links between the control and the angle ε_{EO}, the orientation error between the vehicle and the carrot point, may be improved such that the parameter k_p evolves as a function of the longitudinal speed V_x. On the other hand, as proposed in Section 3.2.3.3, it could be interesting to work over the lateral distance between the vehicle and the path. Moreover, the control solutions based on MPC has a satisfying behaviour. The different plots presented in Sections 5.6.3.2 and 5.6.4.2 show that the vehicle behaviour is good insofar as for the different speeds, the error distance is not larger than $1.5m$ expect for LPV MPC solution at $10m/s$. Yet, the presented experimental results highlight the fact that the closed-loop systems are very close. It is difficult to select one of the three solutions. But, due to the very good response of the closed-loop system with the NNMPC solution with structure 2 at $10m/s$, a preference goes towards this solution. The fact that an additional input of the NN is considered may improve the obtained results.

Table 5.3 summarizes the different properties of the implemented control solutions.

To conclude this section, it is important to keep in mind the two following points. On the one hand, the tuning of the control solutions, especially the MPC solutions, is a long and difficult task. It has been remarked that the weightings of the cost criterion have a relationship with the longitudinal speed V_x. But, with the used model, the simulation step does not allow to highlight this relationship. Indeed, excellent results have been found in simulations considering fixed weighting values. In other word, a more accurate simulation model would help the development step and limit the tests on road. On the other hand, it is essential to insist on the main drawback of the MPC solution which is the on-line resolution of the optimization problem.

For the proposed solutions, the optimization is facilitated insofar as the model are linearised. Nevertheless, difficulties have been encountered during the programming step to reach the final solution with a sample time equal to $0.05s$ and a prediction horizon of 15 samples.

5.7 Conclusion

This chapter presented different control solutions which gives the possibility to automatise the movement of a rolling system. It was not possible to apply the proposed algorithm on a real A/C then it has been decided to transpose the solution on a road vehicle. After giving up the two parts of control strategy (one part dedicated to the control of the longitudinal dynamics and the other dedicated to the lateral dynamics), the test vehicle which helps to validate the proposed control solutions was presented. The acquisition system, the actuators and the sensors which gives the possibility to identify the vehicle dynamics and to implement the longitudinal and lateral algorithms were presented in details. An identification procedure has been required insofar as the lateral control solution are based on MPC. Different models have been identified, a LPV state space model and two different NN models. A particularity of the LPV model must be underlined, insofar as a relation between the longitudinal speed and the front and rear cornering stiffnesses has been identified. Next, the experimental results of the longitudinal and the lateral control solutions have been presented. The longitudinal control is based on a finite state machine and a simple PID is used to control the braking actuator. The main particularity of the solution lies in the nature of the reference speed. It is obtained in real-time, through a digital database and an additional step gives the possibility to constrain it. Concerning, the lateral control, four controllers have been implemented and presented (FC, LPV MPC, NNMPC with NN structure 1 and NNMPC with NN structure 2). A path has been pre-registered and the different algorithms have been compared. Finally, the three algorithms based on MPC give the best results. The closed-loop responses are very close but the solution based on NNMPC with structure 2 has been preferred because the response at high speed was the best.

Two major perspectives can be considered. The first will aim at combining the two control loops. In Section 5.5 the control of speed is automated while the driver has to steer the vehicle. In Section 5.6, the lateral dynamics are automatically controlled but the driver has to brake and to accelerate the vehicle. This evolution will give the possibility to let the vehicle move without driver. The second perspective could be to integrate the environment in the control solution. Here, it is considered that the vehicle is alone on the road and that the control is only based on road shape data.

Method	Results	Specificities	Advantages	Drawbacks
FC	does not give satisfying results at high speed	based on geometrical characteristic method where the system to be controlled is not considered	very simple, only 2 tuning parameters	does not allow to reach sufficient performances
LPV MPC	gives the possibility to follow the path	based on model solution which uses a LPV model and QP optimization (at each sample time the varying parameter is fixed on the prediction horizon)	the prediction based on a LPV model helps to provide a good control signal	requires an on line optimization which is problematic for real time implementation
NNMPC with structure 1 and 2	gives the possibility to follow the path	based on model solution which uses a NN model and QP optimization (at each sample time the NN which is non linear, is linearised over the prediction horizon)	the prediction based on a non-linear NN model helps to provide a good control signal	requires an on line optimization which is problematic for real time implementation

Table 5.3: comparison of the lateral control methods

A conclusion is simply the place where someone got tired of thinking.

Arthur Block

Conclusion

The thesis work presented in this manuscript was dedicated to the control of an electromechanical actuator for steering the nose landing gear wheels and thus, giving the possibility to developed algorithms for aircraft automatic guidance based on this more reliable and more redundant actuator. Currently, hydraulic actuators, available on the aircraft, have several drawbacks that the electromechanical actuator, proposed in the DRESS European project, can remedy. Indeed, this latter associated with a new modular architecture based on a digital bus network would allow to:

- reduce the weight of the whole steering system which is an important advantage considering environmental aspects;
- improve safety by the use of a redundant system (two paths mechanical system, digital bus with reconfiguration capabilities);
- reduce maintenance time and costs.

The main contributions of this thesis concern the development of control strategies for the nose landing gear actuator (steering of the nose landing gear wheels and damping of the shimmy phenomenon) and of solutions to achieve automated rolling systems (control of the longitudinal and lateral dynamics). The different solutions that have been proposed are based on common theoretical tools, robust gain scheduling control, non-linear predictive control or non-linear adaptive control. They have given the possibility to reach interesting results validated by experimentations in aeronautic and automotive domains. Indeed, the algorithms developed for the control of the landing gear are corroborated through real tests performed on the DRESS test bench. Moreover, the longitudinal and lateral control solutions detailed in this thesis have been implemented and evaluated thanks to the test vehicle of the MIPS laboratory.

The objective of the manuscript was to introduce the different theoretical tools, to present the application context and to detail the control solutions developed in the aeronautical and automotive domains. Then, this work was presented in five chapters:

- the first chapter entitled “Which model for which system?” defined the concept of “system” and “model”. Then, solutions which helped to find an “appropriate” model based on the knowledge of the system and on the objectives of this model were proposed;
- in the second chapter, control solutions which take account of the specificities of the models, had been detailed. The three control solutions presented aimed at providing the reader the essential information to understand the developed solutions;

- the third chapter gave details concerning the context of the applications. First, the thesis framework was introduced. Then, state-of-art studie was presented. Finally, models required to perform simulations and synthesize controllers are presented;
- the fourth chapter has described the solutions proposed to control the electromechanical nose landing gear steering actuator for both steering and shimmy damping purposes. Particularly, experimental results, performed with the DRESS test bench were included;
- in the fifth chapter, solutions for the control of longitudinal and lateral dynamics of a car vehicle had been described and experimental results had been proposed.

Finally, among different important points, it would be interesting to investigate particular tools that have been just mentioned in this manuscript and to go further in validation of the proposed control solutions.
Chapters 2 and 4 dealt with $\mathcal{H}_\infty$ control solution applied for LPV system. In this field, less conservative formulation would be tested. For example the author proposes to take account of the varying parameters speed or to consider LMI's formulation based on multiple Lyapunov functions.
Considering the control of the nose landing gear, it had been shown that a tracking error persisted with the developed control solution. The author proposes to investigate a feedback-feedforward robust structure, insofar as the feedforward controller is well-known to improve tracking performance.
The tyre characteristics may be expressed by a piecewise linear model as suggested in Appendix A. Then, the author proposes to use such model for the prediction in the predictive control strategy of Chapter 5. This proposition improves the prediction of the system and the control solution presented in Section 2.4.3.3 may give the possibility to obtain the control signal. The author suggests to improve the vehicle lateral dynamics control solution in order to apply it for aeronautic applications. Indeed, the trajectory of an A/C can be controlled by the nose landing gear wheel but also by the use of the rudder, the differential braking or .... The SISO system studied in Chapter 5 could be extended to a MISO system which takes account of many inputs. Moreover, the power consumption of each inputs or their limitation could be considered and taken into account by the constrained optimal control solution.
Finally, the two longitudinal and lateral control solutions proposed in chapter 5, could be coupled in order to obtain a fully automatic vehicle.

Appendix A

Tyre Modelling

A.1 Introduction

The tyre is a very complex system [Pouly et al., 2006] involved in most ground vehicles. It is a key component of vehicles or aircraft insofar as every effort (except aerodynamic forces) applied on the system are generated at the wheel/road interface. It performs three main functions [Gillespie, 1992]:

- supporting the vertical load of the vehicle and recover the ground deformations;
- developing longitudinal forces that accelerate and brake the vehicle;
- developing lateral forces which give the possibility to steer the vehicle.

Moreover, it is made of synthetic and / or metal fibbers and rubber; this results to a system very difficult to model. This appendix proposes the description of some models available in the literature.

As part of this work, the study of the tyre is limited to its lateral behaviour and the longitudinal mechanism which isimportant for braking system is not considered.

A.2 The tyre slip angle

When the tyre is subjected to a transverse force, the surface of the tyre slips on the ground in a direction opposite to the considered effort. The deformation of the contact area creates an angle between the longitudinal axis of the wheel and the direction of the wheel movement. This angle is called the slip angle of the tyre (β). Figure A.1 illustrates this phenomenon.

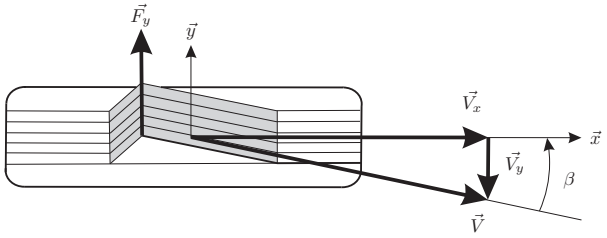

Figure A.1: Presentation of the slip angle

In response to these deformations, the tyre develops a lateral force F_y, function of the slip angle β. This slip angle is defined by:

$$\beta = atan\left(\frac{V_y}{V_x}\right) \tag{A.1}$$

A.3 Available model in the literature

The description of the tyre behaviour can be expressed with simple expressions or more advanced ones, depending on the possibility to determine or to measure the parameters involved or the level of complexity and accuracy required for the purpose. Thus, numerous tyre models have been proposed in the literature (Brush model [Gim, 1988], Fiala model [Fiala, 1954], Sakai model [Sakai, 1969], Pacejka model [Pacejka, 2006],...).

Here, attention is focused on tyre models that are used in this manuscript, that means the linear tyre model, the piecewise linear tyre model and the Pacejka tyre model.

A.3.1 Linear tyre model

The formulation of the F_y contribution based on the linear tyre model is:

$$F_y = CS \times \beta \tag{A.2}$$

with CS the cornering stiffness. This model is very simple but it is limited to a maximum slip angle of approximately 8° (depending on the tyre). However, this model is frequently used for control purposes. Figure A.2 presents this model.

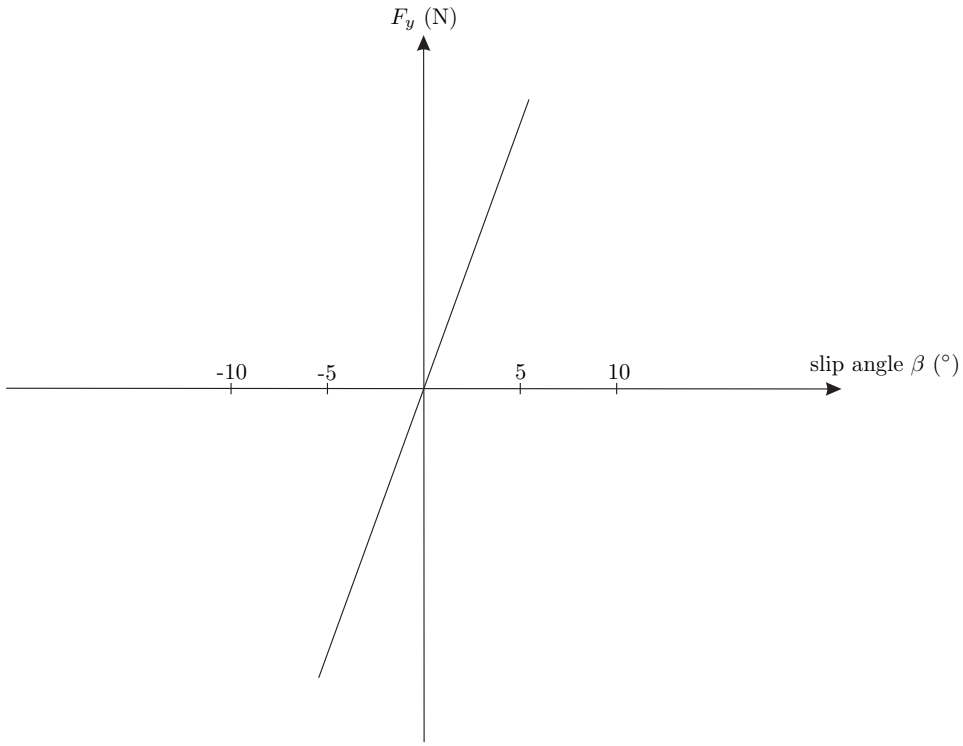

Figure A.2: Presentation of the linear tyre model

A.3.2 Piecewise linear tyre model

The formulation of the F_y contribution based on the piecewise linear tyre model is:

$$F_y = \begin{cases} -a_2\beta - b_2 & \text{if } \beta < -\beta_2 \\ -F_{y\,max} & \text{if } -\beta_2 < \beta < -\beta_1 \\ a_1\beta & \text{if } -\beta_1 < \beta < \beta_1 \\ F_{y\,max} & \text{if } \beta_1 < \beta < \beta_2 \\ a_2\beta + b_2 & \text{if } \beta > \beta_2 \end{cases} \tag{A.3}$$

with a_1, a_2, b_1, b_2 and $F_{y\,max}$ constant parameters and β_1 and β_2 defined in Figure A.3.

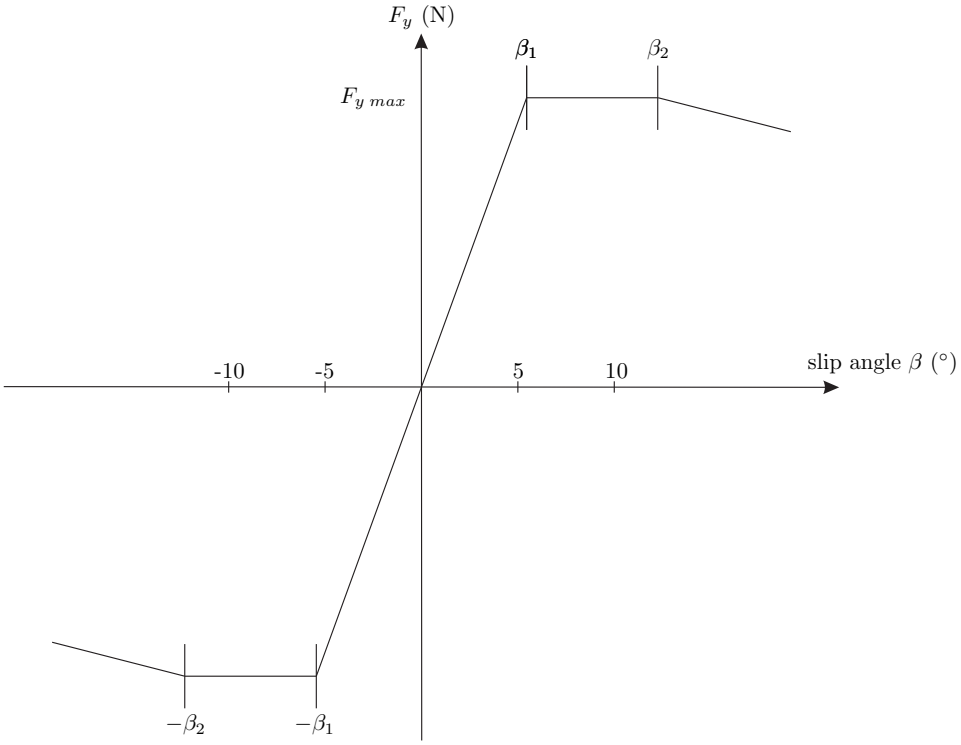

Figure A.3: Presentation of the piecewise linear tyre model

A.3.3 Pacejka tyre model

The formulation of the F_y contribution based on the Pacejka model needs 15 parameters and has the following form:

$$\begin{aligned} F_y \;=\; & D_{F_y} \sin\Bigg[C_{F_y} \arctan\Bigg(B_{F_y}\big((1-E_{F_y})(\beta + SH_{F_y}) \\ & + \frac{E_{F_y}}{B_{F_y}} \arctan(B_{F_y}(\beta + SH_{F_y}))\big)\Bigg)\Bigg] + SV_{F_y} \end{aligned} \tag{A.4}$$

such that:

$$
\begin{aligned}
D_{F_y} &= b_1 F_z^2 + b_2 F_z \\
BCD_{0_{F_y}} &= b_3 \sin(2 \arctan(F_z / b_4)) \\
BCD_{F_y} &= BCD_{0_{F_y}} (1 - b_5 \left|\gamma\right|) \\
C_{F_y} &= b_0 \\
E_{F_y} &= b_6 F_Z + b_7 \\
SH_{0_{F_y}} &= b_9 F_z + b_{10} \\
SH_{F_y} &= SH_{0_{F_y}} + b_8 \gamma \\
SV_{0_{F_y}} &= b_{12} F_z + b_{13} \\
SV_{F_y} &= SV_{0_{F_y}} + (b_{112} F_z^2 + b_{111} F_z) \gamma
\end{aligned}
\tag{A.5}
$$

In this formula ,β is the slip angle of the tyre, γ is the camber angle [Lamy and Basset, 2008] (angle between the vertical axis $\vec{z}$ and the axis of the wheel) which is null and F_z the load on the tyre. This model is presented in Figure A.4.

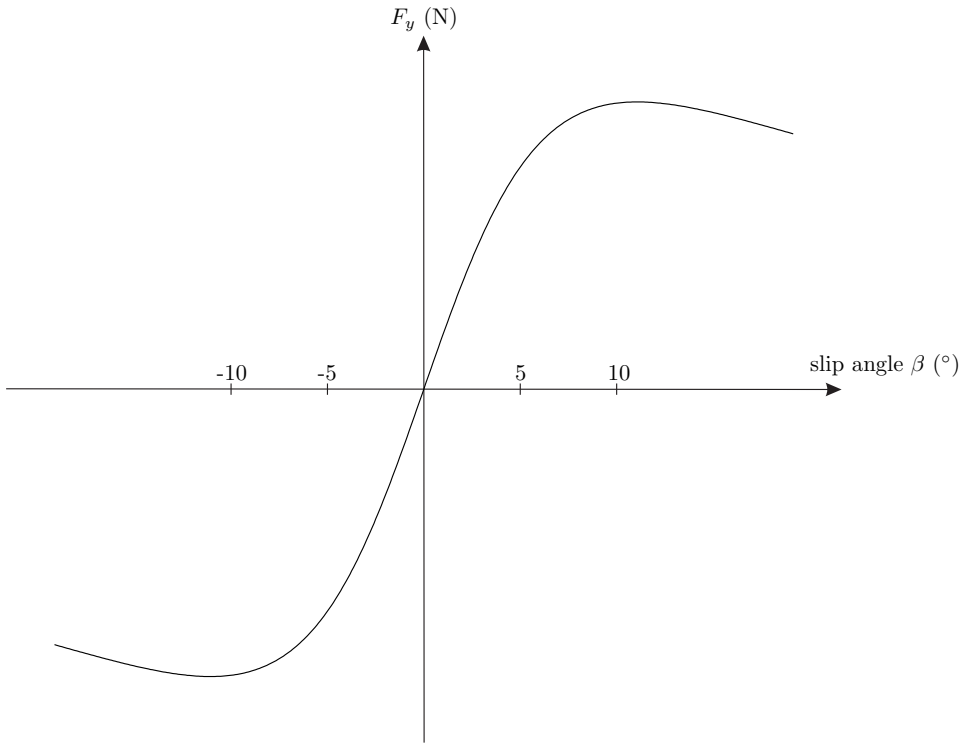

Figure A.4: Presentation of the Pacejka tyre model

Appendix B

Stability proof of the adaptive control algorithms

This appendix aims at presenting the proofs of the theorems that permit to show the stability of fuzzy adaptive control solution.

B.1 State feedback indirect fuzzy adaptive control

This is the proof of the theorem 1 of Section 2.3.2.1.

Proof The *r-derivative* of the output error can be written as:

$$\begin{aligned} e_0^{(r)} &= y_m^{(r)} - y^{(r)} \\ &= y_m^{(r)} - a(\mathbf{x}) - B(u_{ce} + u_{si}) \\ &= -a(\mathbf{x}) + \hat{a}(\mathbf{x}, \theta_a) - \eta e_s - \overline{e}_s - B u_{si} \end{aligned} \tag{B.1}$$

The tracking error equation becomes:

$$\begin{aligned} \dot{e}_s + \eta e_s &= -B u_{si} - a(\mathbf{x}) + \hat{a}(\mathbf{x}, \theta_a) \\ &= -B u_{si} + (\phi_a^T \varsigma_a - \delta_a(\mathbf{x})) \end{aligned} \tag{B.2}$$

Considering the Lyapunov function candidate:

$$V = \frac{1}{2} e_s^2 + \frac{1}{2} \tilde{\theta}_a^T Q_a \tilde{\theta}_a \tag{B.3}$$

where $Q_a \in \Re^{d \times d}$ $(d = dim(\phi_a))$ is a positive definite matrix. Differentiating $V(t)$ with respect to time leads to:

$$\dot{V} = -\eta e_s^2 - B u_{si} e_s + (\hat{a}(\mathbf{x}, \theta_a) - a(\mathbf{x})) e_s + \tilde{\theta}_a^T Q_a \dot{\tilde{\theta}}_a \tag{B.4}$$

Considering equations (2.29) and (2.30), the derivative of the parameter error vector becomes:

$$\dot{\tilde{\theta}}_a = \dot{\theta}_a \tag{B.5}$$

Consequently $\dot{V}$ becomes:

$$\dot{V} = -\eta e_s^2 - B u_{si} e_s + (\hat{a}(\mathbf{x}) - a(\mathbf{x})) e_s - \tilde{\theta}_a^T \varsigma_a e_s \tag{B.6}$$

Equations (2.27) and (2.29) enable the following simplification:

$$\dot{V} = -\eta e_s^2 - B u_{si} e_s + (\tilde{\theta}_a^T \varsigma_a - \delta_a(\mathbf{x})) e_s - \tilde{\theta}_a^T \varsigma_a e_s \tag{B.7}$$

Now the assumption A1 and the definition of u_{si} (equation 2.31) allow to write:

$$\begin{aligned} \dot{V} &= -\eta e_s^2 - \overline{\delta}_a sign(e_s) e_s - \delta_a(\mathbf{x}) e_s \\ &\leq -\eta e_s^2 - \overline{\delta}_a sign(e_s) e_s + |\delta_a(\mathbf{x})|\,|e_s| \\ &\leq -\eta e_s^2 \leq 0 \end{aligned} \tag{B.8}$$

This means that $V \in \mathcal{L}_\infty$. If $V \in \mathcal{L}_\infty$ then $e_s \in \mathcal{L}_\infty$ and $\tilde{\theta}_a \in \mathcal{L}_\infty$ by the definition of V.
If $G_i(s)$ is defined by:

$$G_i(s) = \frac{s^i}{L(s)} \tag{B.9}$$

for $i = 0, \ldots, r-1$, it can be shown that $G_i(s)$ is stable because $L(s)$ has its $r-1$ roots in the open left half plane. Thus, the error becomes:

$$e_0^{(i)} = G_i(s) e_s \tag{B.10}$$

with $e_s \in \mathcal{L}_\infty$.
Then, error $e_0^{(i)}$ is bounded for $i = 0, \ldots, r-1$ and $e_0^{(k)} = y_m^{(k)} - y^{(k)}$, so the conclusion is that $y(t), \ldots, y^{(r-1)}(t)$ are bounded.

As proven above, $\tilde{\theta}_a$ is bounded so the "certainty equivalence" control term is bounded. Moreover, the "sliding mode" control term is bounded. The conclusion is that u is bounded.

If equation (B.8) is used:

$$\int_0^\infty \eta e_s^2 dt \leq -\int_0^\infty \dot{V} dt = V(0) - V(\infty) < \infty \tag{B.11}$$

then $e_s \in \mathcal{L}_2$. Moreover previous considerations show that $\hat{a}(\mathbf{x})$, $\tilde{\theta}_a$, $\delta_a(\mathbf{x}, \theta_a)$ and $\varsigma_a(\mathbf{x})$ are bounded. From (B.2) and the fact that e_s and u_{si} are bounded, it is obvious that $\dot{e}_s$ is bounded. Thus, by Barbalat's Lemma, the tracking error e_s will converge to zero and e_0 will converge to zero.

B.2 State feedback direct fuzzy adaptive control

This is the proof of the theorem 2 of Section 2.3.2.2.

Proof The rth derivative of the output error is:

$$\begin{aligned} \dot{e}_0^{(r)} &= y_m^{(r)} - y^{(r)} = y_m^{(r)} - (a(\mathbf{x}) + Bu) \\ &= y_m^{(r)} - v - B(u - u^*) = -\overline{e}_s - \eta e_s - B(\hat{u} + u_{sd} - u^*) \\ &= -\overline{e}_s - \eta e_s - B\tilde{\theta}_u^T \varsigma_u + B\delta_u - B u_{sd} \end{aligned} \tag{B.12}$$

With $\overline{e}_s = \dot{e}_s - e_0^{(r)}$ the previous equation leads:

$$\dot{e}_s + \eta e_s = -B\tilde{\theta}_u^T \varsigma_u + B\delta_u - B u_{sd} \tag{B.13}$$

Considering the Lyapunov candidate function:

$$V = \frac{1}{2B}e_s^2 + \frac{1}{2}\tilde{\theta}_u^T Q_u \tilde{\theta}_u \tag{B.14}$$

where $Q_u \in \Re^{d\times d}$ $(d = dim(\phi_u))$ is a positive definite matrix. Take the derivative of V with respect to time and notice that $\dot{\tilde{\theta}}_u = \dot{\theta}_u$ implies:

$$\begin{aligned} \dot{V} &= \frac{1}{B}e_s\dot{e}_s + \tilde{\theta}_u^T Q_u \dot{\theta}_u \\ &= \frac{e_s}{B}(-\eta e_s - B\tilde{\theta}_u^T \varsigma_u + B\delta_u - Bu_{sd}) + \tilde{\theta}_u^T Q_u \dot{\theta}_u \\ &= -\frac{\eta e_s^2}{B} - e_s u_{sd} + e_s\delta_u + \tilde{\theta}_u^T(Q_u\dot{\theta}_u - \varsigma_u e_s) \end{aligned} \tag{B.15}$$

The use of equation (2.38) enables to show that:

$$\dot{V} = -\frac{\eta e_s^2}{B} - e_s u_{sd} + e_s\delta_u \tag{B.16}$$

The definition of the sliding control term in equation (2.39) enables to write:

$$\dot{V} \leq -\frac{\eta e_s^2}{B} \leq 0 \tag{B.17}$$

Since V is a quadratic function and $\dot{V} \leq 0$, the control system is proved to be stable. It is clear that $V \in \mathcal{L}_\infty$, which implies $e_s \in \mathcal{L}_\infty$ and $\tilde{\theta}_u \in \mathcal{L}_\infty$. With e_s and u_s bounded, the equation (B.13) gives $\dot{e}_s \in \mathcal{L}_\infty$.
If $G_i(s)$ is defined by:

$$G_i(s) = \frac{s^i}{L(s)} \tag{B.18}$$

for $i = 0, \ldots, r-1$, it can be shown that $G_i(s)$ is stable because $L(s)$ has its $r-1$ roots in the open left half plane. Thus, the error becomes:

$$e_0^{(i)} = G_i(s)e_s \tag{B.19}$$

Then, error $e_0^{(i)}$ is bounded for $i = 0, \ldots, r-1$ and $e_0^{(k)} = y_m^{(k)} - y^{(k)}$, so the conclusion is that $y(t), \ldots, y^{(r-1)}(t)$ are bounded.
From equation (B.16), the following is obtained:

$$\int_0^\infty \eta e_s^2 dt \leq -\int_0^\infty \dot{V} dt = V(0) - V(\infty) < \infty \tag{B.20}$$

which implies that $e_s \in \mathcal{L}_2$. Thus, by Barbalat's Lemma, the tracking error e_s and e_0 will converge to zero.

Appendix C

Solutions to reduce model complexity

C.1 Importance of Model Order Reduction (MOR)

Modelling of complex systems results in most cases in the achievement of complex models that are often used with difficulties in real problems. Then, the approximation of high order systems or high order controllers by models with lower orders is required. An approximation procedure, based on physical considerations or mathematical tools, permits to achieve simpler models. Despite the use of more and more efficient calculation tools, the reduction of the model orders is required and [Fortuna et al., 1992] introduce the main reasons:

- simplify the understanding of a system;
- reduce computation efforts in simulation problems;
- obtain simpler control laws;
- decrease computational effort for the design of controller.

A complex system may be described by a detailed model that considers almost all dynamics and a lot of state variables. This accurate description may render the comprehension of the system impossible. A simplified low order model gives the possibility to focus on the main contributions of the system, that means the most influential dynamics and then facilitates the understanding of its behaviour. This consideration is easily illustrated when a vehicle model is studied. In the literature [Gillespie, 1992], [Gissinger and Le-Fort-Piat., 2002], very accurate descriptions of the vehicle considering for instance the influence of the yaw rate, the pitch rate, the damper or the aerodynamics effects, exist. These models, based on a fine description of the different dynamics, are required for the expert, but the basic understanding of the vehicle dynamic can rely on a simpler description. For example, a low-order model gives the possibility to clearly understand the relation between the longitudinal speed, the steering angle and the resultant lateral acceleration. Then, it is obvious that the simulation of a very detailed model is time consuming. In this case, model reduction helps to decrease the time simulation. For instance, the mechanical modelling often removes the high frequency vibration modes and only keeps the low frequency dynamics. This gives the possibility to increase the sample time of the simulation and then a significant simulation time reduction can be observed. Moreover, the order of the controllers needs to be reduced to permit their real-time implementation. In this

case, a compromise must be done between the required reduction and the performance that must be reached. The obtaining of a high order controller is particularly observed when the controller synthesis is done using the robust $\mathcal{H}_\infty$ theory. Then, the technique of controller order reduction is commonly used. Similarly, the design of controllers based on synthesis models may be restrictive when the order of the synthesis model is too important. In this case, the synthesis of the controller is based on an optimization algorithm and the high order of the initial model may result in an infeasible problem. Then, the reduction of the synthesis model order helps to simplify the optimization problem which results to the feasibility of the control synthesis optimization problem.

Model reduction can be done by several methods. Considering a high order time-invariant model $\mathcal{M}$, the reduction problem aims at finding an approximation $\mathcal{M}_r$ of $\mathcal{M}$ such that $\|\mathcal{M} - \mathcal{M}_r\|_\infty$ is small enough. Here, the balanced realisation-based model order reduction is presented. This method is well-suited because it enables to preserve the majority of the model characteristics. For a complete description of model order reduction techniques, the reader can refer to [Obinata and Anderson, 2001].

C.2 Balanced realisation-based model order reduction

C.2.1 Balanced realisation

A balanced realization is an asymptotically stable and minimal realization in which the observability and controllability gramians are equal and diagonal. The commonly used definition of the balanced realization is:

Definition 25 *Balanced realization*

Considering a realization $A_{bal}, B_{bal}, C_{bal}, D_{bal}$, the realization is a balanced realization if and only if A_{bal} is asymptotically stable and the observability and controllability gramians verify:

$$W_c = W_o = \Sigma = diag(\sigma_1^H, \sigma_2^H, ..., \sigma_n^H) \tag{C.1}$$

such that the σ_i^H are the Hankel singular values and $\sigma_1^H \geq \sigma_2^H \geq ... \geq \sigma_n^H \geq 0$.

The procedure that helps to obtain a balanced realization contains four steps (based on the Moore and Laub algorithm [Laub, 1980]):

- the gramians W_c and W_o for any stable and minimal realization (A, B, C, D) of the system are computed,
- the Cholesky factor R of W_c (which is the unique triangular inferior matrix such that $W_c = RR^T$) is calculated,
- the positive definite matrix W_o is diagonalized such that $R^T W_o R = U\Sigma^2 U^T$ with $U^T U = I$.
- the transformation that helps to obtain the balanced realization is obtained: $T = RU\Sigma^{-1/2}$

Finally, using the transformation, the balanced realization is described by:

$$\begin{cases} A_{bal} = T^{-1}AT \\ B_{bal} = T^{-1}B \\ C_{bal} = CT \\ D_{bal} = D \end{cases} \tag{C.2}$$

C.2.2 Truncation operation

Considering a system $\mathcal{S}$, modelled by a model $\mathcal{M}$ of order n and described by the matrices (A, B, C, D):

$$\mathcal{M} : \begin{cases} \dot{x}(t) &= A\,x(t) + B\,u(t), \\ y(t) &= C\,x(t) + D\,u(t), \end{cases} \tag{C.3}$$

The state $x(t)$ can be divided into two components, one will be the retained component $x_1(t)$ and the other will be the erased component such that

$$x(t) = \begin{bmatrix} x_1(t) \\ x_2(t) \end{bmatrix} \tag{C.4}$$

Then, the matrices A, B and C are separated in different blocks such that:

$$A = \begin{bmatrix} A_{11} & A_{12} \\ A_{21} & A_{22} \end{bmatrix} \tag{C.5}$$

$$B = \begin{bmatrix} B_1 \\ B_2 \end{bmatrix} \tag{C.6}$$

$$C = \begin{bmatrix} C_1 & C_2 \end{bmatrix} \tag{C.7}$$

Finally, the states and dynamics associated to the component $x_2(t)$ are erased and the lower order system using the truncation operator $\mathcal{T}_r(A, B, C, D) = (A_{11}, B_1, C_1, D)$ is obtained:

$$\mathcal{M}_r : \begin{cases} \dot{x}_r(t) &= A_{11}\,x(t) + B_1\,u(t), \\ y_r(t) &= C_1\,x(t) + D\,u(t), \end{cases} \tag{C.8}$$

C.2.3 Balanced truncation

The method of balanced truncation [Moore, 1981] [Pernebo and Silverman, 1982] removes the states of a balanced realization which correspond to the singular values below a certain threshold. Model reduction by balanced truncation simply applies the truncation operation to a balanced realization $A_{bal}, B_{bal}, C_{bal}, D_{bal}$ of a model.

This Section presents the MOR method based on the truncation operation. Some other methods give the possibility to reduce the order of the model based on the balanced realization. For example, the singular perturbation method helps to reduce the order of the model. This last method has the advantage to propose a good approximate model for the low frequencies while the truncation method tends to produce a better approximation for the high frequencies.

C.2.4 Properties of the balanced truncation method

The two main properties of the model reduction based on the balanced truncation method are the stability of the reduced model and the existence of an upper bound of the model reduction error. These properties are summarized in the following theorem:

Theorem 4 *Let $\sigma_1^H \geq \sigma_2^H \geq ... \geq \sigma_n^H \geq 0$ be the ordered set of different Hankel singular values of a stable LTI system $\mathcal{M}$. Let $\mathcal{M}_r$ be the reduced model obtained by removing the states corresponding to singular numbers not larger than σ_k from a balanced realization of $\mathcal{M}$. Then $\mathcal{M}_r$ is stable, and satisfies:*

$$\|\mathcal{M} - \mathcal{M}_r\|_\infty \leq 2 \sum_{i=k}^{n} \sigma_i^H \tag{C.9}$$

Bibliography

[Abdeslam, 2005] Abdeslam, D. O. (2005). *Techniques neuromimétiques pour la commande dans les systèmes électriques : application au filtrage actif parallèle dans les réseaux électriques basse tension*. PhD thesis, Université de Haute-Alsace. 13, 18, 154

[Adamson, 2005] Adamson, P. (2005). A-SMGCS VIS2 - VIS3 transition simulation report. Technical report, EUROCONTROL. 67

[Apkarian and Adams, 1998] Apkarian, P. and Adams, R. (1998). Advanced gain-scheduling techniques for uncertain systems. *IEEE Transactions on Control Systems Technology*, 6:21–32. 30, 115, 121

[Apkarian and Gahinet, 1995] Apkarian, P. and Gahinet, P. (1995). A convex characterization of gain-scheduled $\mathcal{H}_\infty$ controllers. *IEEE Transaction on Automatic Control*, 40 (5):853–864. 22, 27

[Apkarian et al., 1995] Apkarian, P., Gahinet, P., and Beker, G. (1995). Self-scheduled $\mathcal{H}_\infty$ control of linear parameter-varying systems: a design example. *Automatica*, 31:9:1251–1262. 27, 95

[Apkarian and Noll, 2006] Apkarian, P. and Noll, D. (2006). Nonsmooth H_∞ synthesis. *IEEE Transactions on Automatic Control*, 51:71–86. 116

[Astrom and Wittenmark, 1994] Astrom, K. J. and Wittenmark, B. (1994). *Adaptive Control*. Addison-Wesley. 32

[Ballois and Duc, 1996] Ballois, S. L. and Duc, G. (1996). $\mathcal{H}_\infty$ control of a satellite axis: loop-shaping, controller reduction and μ-analysis. *Control Engineering Practice*, 4 (7):1001–1007. 23

[Beji and Bestaoui, 2001] Beji, L. and Bestaoui, Y. (2001). An adaptive control method of automated vehicles with integrated longitudinal and lateral dynamics in road following. *Second Workshop on Robot Motion and Control*. 73

[Beji and Bestaoui, 2005] Beji, L. and Bestaoui, Y. (2005). Motion generation and adaptive control method of automated guided vehicles in road following. *IEEE Transactions on Intelligent Transportation Systems*, 6:113–123. 55, 73

[Bemporad et al., 2003] Bemporad, A., Garulli, A., Paoletti, S., and Vicino, A. (2003). *A Greedy Approach to Identification of Piecewise Affine Models*. Springer Berlin / Heidelberg. 17

[Bemporad and Morari, 1999] Bemporad, A. and Morari, M. (1999). Control of systems integrating logic, dynamics, and constraints. *Automatica*, 35 (3):407–427. 49

[Besselink, 2000] Besselink, I. J. M. (2000). *Shimmy of aircraft main landing gears.* PhD thesis, Delft University of Technology. 54, 63, 64, 65

[Biannic, 1996] Biannic, J.-M. (1996). *Commande robuste des systèmes à paramètres variables: Applications à l'aéronautique.* PhD thesis, Centre d'Étude et de Recherche de Toulouse. 9

[Björck, 1996] Björck, A. (1996). Numerical methods for least squares problems. *SIAM Journal on Control.* 17

[Black, 1982] Black, R. (1982). Application of ture dynamics to aircaft landing gear design analysis. *NASA Tire modellingWorkshop.* 64

[Boor, 1978] Boor, D. (1978). *A practical guide to spline.* New York: Springer-Verlag. 157

[Borrelli et al., 2005] Borrelli, F., Falcone, P., Keviczky, T., Asgari, J., and Hrovat, D. (2005). MPC-based approach to active steering for autonomous vehicle system. *International Journal of Vehicle Autonomous Systems*, 3. 45, 75

[Boyd et al., 1994] Boyd, S., Ghaoui, L., Feron, E., and Balakrishnan, V. (1994). *Linear matrix inequalities in system and control theory.* Studies in applied mathematics. Philadelphia, PA: Society for Industrial and Applied Mathematics. 25

[Brossard, 2006] Brossard, J.-P. (2006). *Dynamique du véhicule.* Presses Polytechniques et Universitaires Romandes (PPUR). 147

[Burke et al., 2005] Burke, J., Henrion, D., Lewis, A., and Overton, M. (2005). HIFOO - A MATLAB package for fixed-order controller design and H_∞ optimization. *IFAC Symposium on Robust Control Design.* 95, 116, 118

[Calise et al., 2001] Calise, A. J., Hovakimyan, N., and Idan, M. (2001). Adaptive output feedback control of nonlinear systems using neural networks. *Automatica*, 37:1201–1211. 22, 32, 37, 38, 40, 50

[Caroux, 2007] Caroux, J. (2007). *Modélisation, identification et observation de la dynamique transversale d'un véhicule.* PhD thesis, Université de Haute Alsace. 16, 81, 148

[Chaib et al., 2004] Chaib, S., Netto, M. S., and Mammar, S. (2004). H_∞, adaptive, PID and fuzzy control: a comparison of controllers for vehicle lane keeping. *IEEE Intelligent Vehicles Symposium.* 54, 77

[Chen et al., 2007a] Chen, B., Liu, X., and Tong, S. (2007a). Adaptive fuzzy output tracking control of MIMO nonlinear systems by backstepping approach. *IEEE Transactions on Fuzzy Systems*, 15 (2):287–300. 32

[Chen et al., 2007b] Chen, B., Tong, S., and Liu, X. (2007b). Fuzzy approximate disturbance decoupling of MIMO nonlinear systems by backstepping approach. *Fuzzy Sets and Systems*, 158:1097–1125. 32

[Cole et al., 2006] Cole, D. J., Pick, A. J., and Odhams, A. M. C. (2006). Predictive and linear quadratic methods for potential application to modelling driver steering control. *Vehicle System Dynamics*, 44:259–284. 4, 54, 74

[Colin et al., 2007] Colin, G., Chamaillard, Y., Bloch, G., and Corde, G. (2007). Neural control of fast nonlinear systems application to a turbocharged SI engine with VCT. *IEEE Transactions on Neural Networks*, 18(4):1101–1114. 45

[Coulter, 1990] Coulter, R. C. (1990). Implementation of the pure pursuit path tracking algorithm. Technical report, Robotics Institute Camegie Mellon University Pittsburgh, Pennsylvania. 69

[Cuvillon et al., 2005] Cuvillon, L., Laroche, E., Gangloff, J., and Mathelin, M. D. (2005). GPC versus $\mathcal{H}_\infty$ control for fast visual servoing of a medical manipulator including flexibilities. *IEEE International Conference on Robotics and Automation, Spain, Barcelona, April 2005*. 23

[Daniel et al., 2009] Daniel, J., Pouly, G., Birouche, A., Lauffenburger, J.-P., and Basset, M. (2009). Navigation-based speed profile generation for an open road speed assistant. *12th IFAC Symposium on Control in Transportation Systems (CTS)*. 156

[Dantzig, 1963] Dantzig, G. B. (1963). *Linear Programming and Extensions*. Princeton, NJ: Princeton University Press. 17

[de Oliveira et al., 2004] de Oliveira, P., Oliveira, R., Leite, V., Montagner, V., and Peres, P. (2004). $\mathcal{H}_\infty$ guaranteed cost computation by means of parameter-dependent lyapunov functions. *Automatica*, 40:1053–1061. 115, 121

[Doyle et al., 1990] Doyle, J., Francis, B., and Tannenbaum, A. (1990). *Feedback Control Theory*. Dover Publications. 22

[Doyle et al., 1989] Doyle, J., Glover, K., Khargonekar, P., and Francis, B. (1989). State-space solution to standard $\mathcal{H}_2$-$\mathcal{H}_\infty$ control problems. *IEEE Transactions on Automatic Control*, 34:831–847. 25

[Duprez, 2004] Duprez, J. (2004). *Automatisation du pilotage au sol pour la navigation aéroportuaire*. PhD thesis, Université Toulouse III. 67, 80, 81, 141

[Duprez et al., 2004] Duprez, J., Mora-Camino, F., and Villaurn6, F. (2004). Control of the aircraft-on-ground lateral motion during low speed roll and manoeuvers. *IEEE Proceedings of Aerospace Conference*. 67

[Eberhart and Kennedy, 1995] Eberhart, R. and Kennedy, J. (1995). A new optimizer using particle swarm theory. *Sixth International Symposium on Micro Machine and Human Science, Nagoya, Japan*, pages 39–43. 97

[Egerstedt et al., 2001] Egerstedt, M., Hu, X., and Stotsky, A. (2001). Control of mobile platforms using a virtual vehicle approach. *IEEE Transaction on Automatic Control*, 46:1777–1782. 70, 71

[Falcone et al., 2007a] Falcone, P., Borelli, F., Asgari, J., Tseng, H., and Hrovat, D. (2007a). Linear time varying model predictive control and its application to active steering systems stability analysis and experimental validation. *International Journal of Robust and Nonlinear Control*. 75, 141

[Falcone et al., 2007b] Falcone, P., Borelli, F., Asgari, J., Tseng, H., and Hrovat, D. (2007b). Predictive active steering control for autonomous vehicle systems. *IEEE Transaction on Control System Technology*, 15:566–580. 4, 54, 75, 140

[Falcone et al., 2007c] Falcone, P., Borrelli, F., Tseng, H. E., Asgari, J., and Hrovat, D. (2007c). Integrated braking and steering model predictive control approach in autonomous vehicles. *Fifth IFAC Symposium on Advances of Automotive Control, Seascape Resort, USA, 20-22 Aug, 2007*. 75

[Falcone et al., 2007d] Falcone, P., Tufo, M., Borelli, F., Asgari, J., and Tseng, H. (2007d). Predictive autonomous vehicles: a linear time varying model predictive control approach. Technical report, Department of Engineering University of Sannio. 75

[Fallah et al., 2008] Fallah, M. S., Long, S. H., Xie, W. F., and Bhat, R. (2008). Robust model predictive control of shimmy vibration in aircraft landing gears. *Journal of Aircraft*, 45. 54, 66

[Fang et al., 2006] Fang, H., Fan, R., Thuilot, B., and Martinet, P. (2006). Trajectory tracking control of farm vehicles in presence of sliding. *Robotics and Autonomous Systems*, 54:828–839. 72, 73

[Fang et al., 2005] Fang, H., Lenain, R., Thuilot, B., and Martinet, P. (2005). Trajectory tracking control of farm vehicles in presence of sliding. *IEEE/RSJ International Conference on Intelligent Robots and Systems (IROS 2005)*, pages 58–63. 54, 72, 140

[Fausett, 1994] Fausett, L. (1994). *Fundamentals of neural networks: architectures, algorithms, and applications*. Prentice-Hall, Inc. 12, 13

[Ferrari-Trecate et al., 2003] Ferrari-Trecate, G., Muselli, M., Liberati, D., and Morari, M. (2003). A clustering technique for the identification of piecewise affine systems. *Automatica*, 39:205–217. 17

[Fiala, 1954] Fiala, E. (1954). Lateral forces on rolling pneumatic tires. *Zeitschrift V.D.I*, 29. 190

[Fortuna et al., 1992] Fortuna, L., Nunnari, G., and Gallo, G. (1992). *Model order reduction techniques with applications in electrical engineering*. Springer Verlag. 197

[Fuller, 1995] Fuller, R. (1995). *Neural Fuzzy Systems*. 12, 13

[Gahinet and Apkarian, 1994] Gahinet, P. and Apkarian, P. (1994). A linear matrix inequality approach to $\mathcal{H}_\infty$ control. *International Journal on Robust and Nonlinear Control*, 4:421–448. 25, 94

[Gallet et al., 2000] Gallet, A., Spigai, M., and Hamidi, M. (2000). Use of vehicle navigation in driver assistance systems. *Proceedings of Intelligent Vehicles*, pages 492–497. 158

[Garcia and Morari, 1989] Garcia, C. and Morari, D. P. M. (1989). Model predictive control: theory and practice. *Automatica*, 25:335–348. 22

[Gilbert, 1963] Gilbert, E. (1963). Controllability and observability in multi-variable control systems. *SIAM Journal on Control*, 1:128–151. 5

[Gillespie, 1992] Gillespie, T. D. (1992). *Fundamentals of Vehicle Dynamics*. Society of Automotive Engineers. 189, 197

[Gim, 1988] Gim, G. (1988). *Vehicle dynamic simulation with a comprehensive model for pneumatic tires*. PhD thesis, University of Arizona, Tucson , Arizona. 190

[Gissinger and Le-Fort-Piat., 2002] Gissinger, G. and Le-Fort-Piat., N. (2002). *Contrôle-commande de la voiture*. Traité IC2, série Systèmes automatisés), Lavoisier, Paris. 197

[Glaser et al., 2007] Glaser, S., Nouvelière, L., and Lusetti, B. (2007). Speed limitation based on advanced curve warning system. *Proceedings of Intelligent Vehicle Symposium, Istanbul, Turkey*. 157

[Goldberg, 1989] Goldberg, D. (1989). *Genetic Algorithms in Search, Optimization and Machine Learning*. Addison-Wesley Longman Publishing Co., Inc. 94, 98

[Goodwine and Stépán, 2000] Goodwine, B. and Stépán, G. (2000). Controlling unstable rolling phenomena. *Journal of Vibration and Control*, 6:137–158. 54, 64, 66

[Gu and Hu, 2002] Gu, D. and Hu, H. (2002). Neural predictive control for a car-like mobile robot. *Robotics and Autonomous systems*, 39:73–86. 55, 75

[Gumussoy et al., 2008] Gumussoy, S., Millstone, M., and Overton, M. (2008). H_∞ strong stabilization via HIFOO, a package for fixed-order controller design. *47th IEEE Conference on Decision and Control*. 117

[Hajjaji and Bentalba, 2003] Hajjaji, A. E. and Bentalba, S. (2003). Fuzzy path tracking control for automatic steering of vehicles. *Robotics and autonomous systems*, 43:203–213. 73, 74

[Han et al., 2006] Han, K., Zhao, J., and Qian, J. (2006). A novel robust tuning strategy for model predictive control. *Proceedinds of the 6th World Congress on Intelligent Control and Automation,*. 44

[Hardiansyah et al., 2006] Hardiansyah, Furuya, S., and Irisawa, J. (2006). A robust H_∞ power system stabilizer design using reduced-order models. *Electrical Power and Energy Systems*, 28:21–28. 116

[Hellström and Ringdahl, 2006] Hellström, T. and Ringdahl, T. J. O. (2006). *Development of an Autonomous Forest Machine for Path Tracking*. Springer Berlin / Heidelberg. 68

[Hermann and Krener, 1977] Hermann, R. and Krener, A. (1977). Nonlinear controllability and observability. *IEEE Transaction on Automatic Control*, 22:728–740. 12

[Herrmann et al., 2005] Herrmann, G., Turner, M. ., and Postlethwaite, I. (2005). *Linear Matrix Inequalities in Control*. Springer Berlin / Heidelberg. 25

[Hu et al., 2000] Hu, J., Bohn, C., and Wu, H. (2000). Systematic $\mathcal{H}_\infty$ weighting function selection and its application to the real time control of a vertical take-off aircraft. *Control Engineering Practice*, 8:241–252. 94, 97

[Huynh et al., 2008] Huynh, T.-H., Pouly, G., Lauffenburger, J.-P., and Basset, M. (2008). Active shimmy damping using direct adaptive fuzzy control. *17th IFAC World Congress*. 95

[Jacquet, 2008] Jacquet, A. (2008). *Nouveau concept de lois de commandes intégrées pour un système de freinage d'avion*. PhD thesis, Université de Haute Alsace. 80

[Jeanneau, 2007] Jeanneau, M. (2007). *Nonlinear analysis and synthesis techniques for aircraft control*, chapter The Airbus on-ground transport aircraft benchmark, pages 3–24. Springer-Verlag. 78

[Jung-Hoon et al., 2003] Jung-Hoon, H., Ronald, C., and Dong-Soo, K. (2003). Mobile robots at your fingertip: Bezier curve on-line trajectory generation for supervisory control. *International Conference on Intelligent Robots and Systems*. 157

[Kalman, 1963] Kalman, R. (1963). Mathematical description of linear dynamical systems. *SIAM Journal on Control*, 2:152–192. 5

[Kalman and Bucy, 1961] Kalman, R. and Bucy, B. (1961). New results in linear filtering and prediction. *Journal of Basic Engineering (ASME)*, 83 (D):98–108. 7

[Kawai et al., 2007] Kawai, F., Ito, H., Nakazawa, C., Matsui, T., Fukuyama, Y., Suzuki, R., and Aiyoshi, E. (2007). Automatic tuning for model predictive control: Can particle swarm optimization find a better parameter? *22nd IEEE International Symposium on Intelligent Control Part of IEEE Multi-conference on Systems and Control*. 44

[Khalil, 2002] Khalil, H. K. (2002). *Nonlinear Systems*. Prentice Hall. 22, 34

[Knittel et al., 2007] Knittel, D., Henrion, D., Millstone, M., and Vedrines, M. (2007). Fixed-order and structure $\mathcal{H}_\infty$ control with model based feedforward for elastic web winding systems. *Proceedings of the IFAC/IFORS/IMACS/IFIP Symposium on Large Scale Systems (LSS), Gdansk, Poland*. 23, 117

[Kosko, 1993] Kosko, B. (1993). Fuzzy logi. *Scientific American*, 269 (1):76–81. 14

[Kosko, 1994] Kosko, B. (1994). Fuzzy systems as universal approximators. *IEEE transactions on Computers*, 43:1329–1333. 34

[Lamy and Basset, 2008] Lamy, C. and Basset, M. (2008). Vision-based determination of wheel camber angle and tire deflection. *Proceedings of the 17th World Congress The International Federation of Automatic Control Seoul, Korea, July 6-11, 2008*. 192

[Landau and Besançon-Voda, 2001] Landau, I. and Besançon-Voda, A. (2001). *Identification des systèmes*. Hermès. 15

[Laub, 1980] Laub, A. (1980). Computation of balancing transformation. *JACC, FA8-E*. 198

[Lauffenburger, 2002] Lauffenburger, J. (2002). *Contribution à la surveillance temps-réel du système "Conducteur - Véhicule - Environnement" élaboration d'un système intelligent d'aide à la conduite*. PhD thesis, Université de Haute Alsace. 160

[Lauffenburger et al., 2007] Lauffenburger, J. P., Bradai, B., Herbin, A., and Basset, M. (2007). Navigation as a virtual sensor for enhanced lighting preview control. *IEEE Intelligent Vehicles Symposium Istanbul, Turkey, June 13-15, 2007*. 144

[Lavergne et al., 2004] Lavergne, F., Camino, F. M., Villaumé, F., and Jeanneau, M. (2004). Neural networks contribution to modeling for flight control. *Proceedings of the World Aviation Congress, Reno, USA*. 79

[Lee, 2004] Lee, C.-H. (2004). Low order robust controller design for preserving H_∞ performance: Genetic algorithm approach. *ISA Transactions*, 43:539–547. 116

[Lemay, 2008] Lemay, D. (2008). A320 tricycle model. Technical report, Messier-Bugatti. 80

[Levenberg, 1944] Levenberg, K. (1944). A method for the solution of certain non-linear problems in least squares. *The Quarterly of Applied Mathematics*, 2:164–168. 17

[Li and Tong, 2003] Li, H.-X. and Tong, S. (2003). A hybrid adaptive fuzzy control for a class of nonlinear MIMO systems. *IEEE Transaction on Fuzzy Systems*, 11:24–34. 32

[Liberzon and Morse, 1999] Liberzon, D. and Morse, S. (1999). Basic problems in stability and design of switched systems. *IEEE Control Systems Magazine*, 19(5):59–70. 109

[Liu et al., 2003] Liu, C.-C. L. R.-F., Yang, C.-D., and Chang, Y.-H. (2003). Helicopter $\mathcal{H}_\infty$ control design with robust flying quality. *Aerospace Science and Technology*, 7:159–169. 23

[Ljung, 1999] Ljung, L. (1999). *System Identification:Theory for the User*. Prentice Hall. 3, 5

[Ljung, 2008] Ljung, L. (2008). Perspectives on system identification. *Proceedings of the 17th IFAC World Congress, Seoul, Korea, July 6-11, 2008*. 17

[Lusetti et al., 2008] Lusetti, B., L.Nouvelière, Glaser, S., and Mammar, S. (2008). Experimental strategy for a system based curve warning system for a safe governed speed of a vehicle. *IEEE Intelligent Vehicles Symposium Eindhoven University of Technology Eindhoven, The Netherlands, June 4-6, 2008*. 156

[Lyapunov, 1992] Lyapunov, A. M. (1992). *General Problem of the Stability of Motion*. CRC. 12

[Maalouf et al., 2006] Maalouf, E., Saad, M., and Saliah, H. (2006). A higher level path tracking controller for a four-wheel differentially steered mobile robot. *Robotics and Autonomous Systems*, 54:23–33. 55, 73, 74

[Maciejowski, 2000] Maciejowski, J. (2000). *Predictive control: with constraints*. Prentice Hall. 22, 43

[MathWorks, 2005] MathWorks, T. (2005). Model predictive control toolbox. Technical report. 171

[Minoiu et al., 2006] Minoiu, N., Netto, M., Mammar, S., and Glaser, S. (2006). A new strategy for lane departure avoidance. *Proceedings of the IEEE International Conference on Control Applications, Munich, Germany, October 4-6, 2006*. 164

[Moore, 1981] Moore, B. (1981). Principal component analysis in linear systems: Controllability, observability, and model reduction. *IEEE Transactions on Automatic Control*, 26 (1):17–32. 199

[Moreland, 1954] Moreland, W. J. (1954). The story of shimmy. *Journal of the aerospace sciences*. 64

[Naranjo et al., 2005] Naranjo, J. E., Gonzales, C., Garcia, R., de Pedro, T., and Haber, R. E. (2005). Power-steering control architecture for automatic driving. *IEEE Transactions on Intelligent Transportation Systems*, 6:406–415. 73

[Naranjo et al., 2003a] Naranjo, J. E., Gonzalez, C., Garcia, R., de Pedro, T., Revuelto, J., and Reviejo, J. (2003a). Fuzzy logic based lateral control for GPS map tracking. *IEEE Intelligent Vehicles Symposium, Parma, Italy, June 14-17, 2004*. 73

[Naranjo et al., 2003b] Naranjo, J. E., Gonzalez, C., Reviejo, J., Garcia, R., and de Pedro, T. (2003b). Adaptive fuzzy control for inter-vehicle gap keeping. *IEEE Transactions on Intelligent Transportation Systems*, 4:132–142. 73, 156

[Narendra and Balakrishnan, 1997] Narendra, K. and Balakrishnan, J. (1997). Adaptive control using multiple models. *IEEE Transactions on Automatic Control*, 42 (2):171–187. 109

[Nemani et al., 1995] Nemani, M., Ravikanth, R., and Bamieh, B. (1995). Identification of linear parametrically varying systems. *Proceedings of the 34th IEEE Control and Decision Conference, New Orleans, LA, USA, Dec13-15, 1995*, 3:2990–2995. 17

[Netto et al., 2004] Netto, M. S., Chaib, S., and Mammar, S. (2004). Lateral adaptive control for vehicle lane keeping. *American Control Conference, Boston, Massachusetts, 30 June-2 July 2004*. 73

[Norgaard et al., 1999] Norgaard, M., O. Ravn, N. K. P., and Hansen, L. K. (1999). *Neural Networks for Modelling and Control of Dynamic Systems*. Springer. 22

[Obinata and Anderson, 2001] Obinata, G. and Anderson, B. (2001). *Model Reduction For Control System Design*. Springer. 198

[Ohishi et al., 2006] Ohishi, K., Miyazaki, T., Inomata, K., Koide, D., and Tokumaru, H. (2006). Robust feedforward control system considering sudden disturbance for optical disk recording system. *Electrical Engineering in Japan*, 156 (4):60–68. 115

[Ordonez et al., 1997] Ordonez, R., andJ. T. Spooner, J. Z., and Passino, K. M. (1997). Adaptive fuzzy control: Experiments and comparative analysis. *IEEE Transactions on Fuzzy Systems*, 5:167–188. 136

[Ortega and Rubio, 2004] Ortega, M. and Rubio, F. (2004). Systematic design of weighting matrices for the $\mathcal{H}_\infty$ mixed sensitivity problem. *Journal of Process Control*, 14:89–98. 94, 97

[Pacejka, 2006] Pacejka, H. B. (2006). *Tyre and Vehicle Dynamics*. Butterworth Heinemann. 11, 80, 84, 132, 190

[Packard, 1994] Packard, A. (1994). Gain scheduling via linear fractional transformations. *Systems & Control Letters*, 22:79–92. 27

[Palladino et al., 2006] Palladino, L., Duc, G., and Pothin, R. (2006). Contrôleur LPV dédié au freinage en virage avec braquage et carrossage actifs. *CIFA, Bordeaux, France, 30 may-1 June, 2006*. 23

[Passino and Yurkovich, 1998] Passino, K. and Yurkovich, S. (1998). *Fuzzy control*. Boston: Addison-Wesley. 14

[Pauwelussen and Linardatos, 2008] Pauwelussen, J. and Linardatos, D. (2008). Predict the road to prevent roll-over, using the navigation database. *IEEE Intelligent Vehicle Symposium (IV2008). Eindhoven, Netherlands*. 157

[Pena et al., 2005] Pena, M., Camacho, E., Pinón, S., and Ricardo, R. C. (2005). Model predictive controller for piecewise affine system. *16th IFAC World Congress, Prague*. 45, 49

[Peng et al., 2007] Peng, J., Wang, Y., and Sun, W. (2007). Trajectory-tracking control for mobile robot using recurrent fuzzy cerebellar model. *Neural Information Processing - Letters and reviews*, 11:15–23. 54, 72, 140

[Pernebo and Silverman, 1982] Pernebo, L. and Silverman, L. (1982). Model reduction via balanced state space representations. *IEEE Transactions onAutomatic Control*, 27 (2):382–387. 199

[Pouly et al., 2008a] Pouly, G., Huynh, T.-H., Lauffenburger, J.-P., and Basset, M. (2008a). Active shimmy damping using fuzzy adaptive output feedback control. *10th International Conference on Control, Automation, Robotics and Vision (ICARCV), Hanoi, Vietnam, December 17-20, 2008*. 95

[Pouly et al., 2008b] Pouly, G., Huynh, T.-H., Lauffenburger, J.-P., and Basset, M. (2008b). Indirect fuzzy adaptive control for active shimmy damping. *17th IFAC World Congress*. 95

[Pouly et al., 2009a] Pouly, G., Huynh, T.-H., Lauffenburger, J.-P., and Basset, M. (2009a). State feedback fuzzy adaptive control for active shimmy damping. *European Journal of Control (submitted, under review)*. 95, 134

[Pouly et al., 2009b] Pouly, G., Lauffenburger, J., Birouche, A., and Basset, M. (2009b). Gain scheduling $\mathcal{H}_\infty$ controllers for aircraft nose landing gear steering using LPV techniques. *IEEE Transactions on Control Systems Technology (submitted, under review)*. 94

[Pouly et al., 2009c] Pouly, G., Lauffenburger, J.-P., and Basset, M. (2009c). Procédé de gestion de la commande d'orientation d'un atterrisseur d'aéronef. 94

[Pouly et al., 2009d] Pouly, G., Lauffenburger, J.-P., and Basset, M. (2009d). Reduced order $\mathcal{H}_\infty$ control design of a nose landing gear steering system. *12th IFAC Symposium on Control in Transportation Systems, Redondo Beach, California, USA, September 2-4, 2009*. 94

[Pouly et al., 2008c] Pouly, G., Lauffenburger, J.-P., Basset, M., and Abdeslam, D. O. (2008c). Etude de robustesse d'une commande adaptative floue pour le contrôle de shimmy. *5ème Conférence Internationale Francophone d'Automatique (CIFA), Bucarest, Roumania, September 3-5, 2008*. 95

[Pouly et al., 2006] Pouly, G., Lauffenburger, J.-P., Basset, M., and Wissart, T. (2006). Correlation between objective tire parameters and subjective test driver evaluation. *5th IFAC Symposium on Advances in Automotive Control (AAC), Seascape resort, USA, August 20-22, 2006*. 189

[Poussot-Vassal et al., 2008] Poussot-Vassal, C., Sename, O., Dugard, L., Gáspár, P., Szabó, Z., and Bokor, J. (2008). A new semi-active suspension control strategy through LPV technique. *Control Engineering Practice*, 16:1519–1534. 50, 116

[Previdi and Lovera, 1999] Previdi, F. and Lovera, M. (1999). Identification of a class of linear models with nonlinearly varying parameters. *Proceedings of the 5th European Control Conference, Karlsruhe, Germany, 31 August -3 September 1999*. 17

[Pronzato, 2005] Pronzato, L. (2005). Parameter estimation and model structures. *Eurotherm Winter School,*. 3

[Putney, 2006] Putney, J. S. (2006). Reactive navigation of an autonomous ground vehicle using dynamic expanding zones. Technical report, Master Thesis report, faculty of the Virginia Polytechnic Institute. 69

[Qiang et al., 1999] Qiang, L., Huiyi, W., and Konghui, G. (1999). Identification and control of four-wheel-steering vehicles based on neural network. *Proceedings of the IEEE International Vehicle Electronics Conference, 1999. (IVEC '99)*. 154

[Qin and Badgwell, 2000] Qin, S. and Badgwell, T. (2000). An overview of nonlinear model predictive control applications. In *Nonlinear Predictive Control*. 45

[Qin and Badgwell, 2003] Qin, S. and Badgwell, T. (2003). A survey of industrial model predictive control technology. *Control Engineering Practice*, 11:733–764. 45

[Richalet, 1991] Richalet, J. (1991). *Pratique de l'identification*. Hermès Paris, ISBN 2-86601-287-9. 5

[Robert and Douglas, 2007] Robert, L. and Douglas, A. (2007). *Linear State-Space Control Systems*. John Wiley & Sons. 7

[Roos, 2007] Roos, C. (2007). *Contribution à la commande des systèmes saturés en présence d'incertitudes et de variations paramétriques: application au pilotage de l'avion au sol.* PhD thesis, Université de Toulouse. 78

[Roos and Biannic, 2006] Roos, C. and Biannic, J. (2006). Aircraft-on-ground lateral control by an adaptive lft-based anti-windup approach. *IEEE International Conference on Control Applications.* 67, 141

[Rowell et al., 2007] Rowell, S., Popov, A. A., and Meijaard, J. P. (2007). Model predictive control techniques for motorcycle rider control. *Fifth IFAC Symposium on Advances of Automotive Control, Seascape Resort, USA, 20-22 Aug, 2007.* 54, 74, 140

[Rugh and Shamma, 2000] Rugh, W. J. and Shamma, J. S. (2000). Research on gain scheduling. *Automatica*, 36:1401–1425. 26, 109

[Ruiz-Velázqueza et al., 2004] Ruiz-Velázqueza, E., Fematb, R., and Campos-Delgado, D. (2004). Blood glucose control for type i diabetes mellitus: A robust $\mathcal{H}_\infty$ tracking problem. *Control Engineering Practice*, 12:1179–1195. 23

[Sakai, 1969] Sakai, H. (1969). Theoretical study of the effect of tractive and braking forces on cornering characteristics of cires. *Safety Research Tour Paper, Stability and Control Committee, Society of Automotive Engineers of Japan*, 4. 190

[Sandou et al., 2008] Sandou, G., Duc, G., and Beauvois, D. (2008). Optimisation par essaim particulaire du réglage d'un correcteur $\mathcal{H}_\infty$. *CIFA, Bucarest, Roumanie, 3-5 september, 2008.* 97

[Santos et al., 2001] Santos, L. O., Afonso, P., Castro, J., Oliveira, N., and Biegler, L. (2001). On-line implementation of nonlinear MPC: an experimental case study. *Control Engineering Practice*, 9:847–857. 45

[Sastry and Bodson, 1989] Sastry, S. and Bodson, M. (1989). *Adaptive Control Stability, Convergence and Robustness.* Prentice HAll. 32, 33

[Scherer, 1990] Scherer, C. (1990). *The Riccati Inequality and State-Space$\mathcal{H}_\infty$-Optimal Control.* PhD thesis, University Würsburg, Germany. 25

[Scherer et al., 1997] Scherer, C., Gahinet, P., and Chilali, M. (1997). Multi-objective output-feedback control via LMI optimization. *IEEE Transactions on Automatic Control*, 42:896 – 911. 25, 26, 30, 50, 94

[Schlippe and Dietrich, 1954] Schlippe, B. V. and Dietrich, R. (1954). Shimmying of a pneumatic wheel. *NACA TM 1365.* 64

[Schmitt, 1999] Schmitt, C. (1999). *Contribution à l'identification des paramètres physiques des systèmes complexes.* PhD thesis, Université de Haute Alsace. 5

[Schutter and Boom, 2004] Schutter, B. D. and Boom, T. V. D. (2004). MPC for continuous piecewise affine systems. *Systems & Control Letters*, 52:179–192. 45

[Seyr and Jakubek, 2005] Seyr, M. and Jakubek, S. (2005). Mobile robot predictive trajectory tracking. *2 nd International Conference on Informatics in Control, Automation and Robotics, Barcelona, Spain, 14-17 September 2005.* 75

[Seyr et al., 2005] Seyr, M., Jakubek, S., and Novak, G. (2005). Neural network predictive trajectory tracking of an autonomous two-wheeled mobile robot. *IFAC World Congress, Prague, Czech Republic.* 75

[Smiley, 1957] Smiley, R. (1957). Correlation, evaluation, and extension of linearized theories for tire motion and wheel shimmy. *NACA 1299.* 64

[Smiley and Horne, 1960] Smiley, R. and Horne, W. (1960). Mechanical properties of pneumatic tires with special reference to modern aircraft tires. *NACA TR-R-64.* 64

[Snyman, 2005] Snyman, J. (2005). *Practical Mathematical Optimization: An Introduction to Basic Optimization Theory and Classical and New Gradient-Based Algorithms.* Springer Publishing. ISBN 0-387-24348-8. 17

[Somieski, 1997] Somieski, G. (1997). Shimmy analysis of a simple aircraft nose landing gear model using different mathematical methods. *Aerospace Science and Technology*, 87:545–555. 63, 64, 65, 87, 88, 122, 123, 128

[Sonntag, 1998] Sonntag, E. (1998). *Mathematical control theory, deterministic finite dimensional systems.* Springer. 33

[Spooner and Passino, 1996] Spooner, J. T. and Passino, K. M. (1996). Stable adaptive control using fuzzy systems and neural networks. *IEEE Transactions on Fuzzy Systems*, 4:339–359. 22, 32, 33, 35, 36, 37

[Sura and Suryanarayan, 2004] Sura, N. and Suryanarayan, S. (2004). Stability and response studies on simplified models of nose-wheel landing gear with hard tires. *Aerospace Engineering*, 85:29–36. 64

[Sweriduk et al., 1998] Sweriduk, G. D., Menon, P. K., and Stienberg, M. L. (1998). Robust command augmentation system design using genetic methods. *G. D. Sweriduk; P. K. Menon; M. L. Stienberg;.* 97, 98

[Takagi and Sugeno, 1985] Takagi, T. and Sugeno, M. (1985). Fuzzy identification of systems and its applications to modeling and control. *IEEE Transactions on Systems, Man, and Cybernetics*, 15 (1):116–132. 14

[Theodoulis, 2008] Theodoulis, S. (2008). *Robust Control in a Nonlinear Context for Large Operating Domains.* PhD thesis, Supélec Faculté des Sciences d'Orsay. 27, 50, 95

[Thota et al., 2008] Thota, P., Krauskopf, B., and Lowenberg, M. (2008). Interaction of torsion and lateral bending in aircraft nose landing gear shimmy. *Springer Netherlands.* 64, 65

[Vandenberghet and Boyd, 1996] Vandenberghet, L. and Boyd, S. (1996). Semi-definite programming. *Society for Industrial and Applied Mathematics*, 38 (1):49–95. 25

[Villaumé, 2002] Villaumé, F. (2002). *Contribution à la commande des systèmes complexes: application à l'automatisation du pilotage au sol des avions de transport*. PhD thesis, Université de Toulouse. 67, 78

[Wang et al., 2008] Wang, C., Hu, Z., and Uchimura, K. (2008). Precise curvature estimation by cooperating with digital road map. *IEEE Intelligent Vehicles Symposium*, pages 859–864. 157

[Wang et al., 1995] Wang, H., Harris, G. L. C., and Brown, M. (1995). *Advanced adaptive control*. Pergamon. 32

[Wang et al., 2007] Wang, J., Zolotas, A., and Wilson, D. (2007). Active suspensions: A reduced-order $\mathcal{H}_\infty$ control design study. *Mediterranean Conference on Control & Automation, 2007. MED '07*. 23

[Wang et al., 2003] Wang, Q., Spronck, P., and Tracht, R. (2003). An overview of genetic algorithms applied to control engineering problems. *Proceedings of the Second International Conference on Machine Learning and Cybernetics, Xi'an, 2-5 November 2003*. 94, 98

[Wei and del Re, 2007] Wei, X. and del Re, L. (2007). Gain scheduled $\mathcal{H}_\infty$ control for air path systems of diesel engines using lpv techniques. *IEEE Transactions on Control Systems Technology,*, 15:406–415. 115

[Wit, 2000] Wit, J. (2000). *Vector pursuit path tracking for autonomous ground vehicles*. PhD thesis, University of Florida. 71

[Wu et al., 1996] Wu, F., Yang, X., Packard, A., and Becker, G. (1996). Induced $\mathcal{L}_2$ norm control for lpv systems with bounded parameter variation rates. *International Journal of Robust and Nonlinear Control*, 6:983–998. 115, 121

[Yamane et al., 1997] Yamane, H., Takahara, Y., and Oyobe, T. (1997). Aspects of aircraft engine control systems R&D. *Control Engineering Practice*, 5 (5):595–602. 80

[Yang et al., 2004] Yang, Y. S., Feng, G., and Ren, J. (2004). A combined backstepping and small-gain approach to robust adaptive fuzzy control for strict-feedback nonlinear systems. *IEEE Transactions on Systems, Man, and Cybernetics-Part A: Systems and Humans*, 34(3):406–420. 32

[Zadeh, 1965] Zadeh, L. (1965). Fuzzy sets. *Information and Contro*, 8 (3):338–353. 14

[Zin, 2005] Zin, A. (2005). *Sur la commane robuste de suspensions automobiles en vue du contrôle global de chassis*. PhD thesis, Institut National Polytechnique de Grenoble. 25